THE GEOCHEMISTRY AND PETROGENESIS OF RAROTONGA, AN OCEAN ISLAND IN THE SOUTH PACIFIC.

GARY M. THOMPSON

INFORMATION TO USERS

This manuscript has been reproduced from the microfilm master. UMI films the text directly from the original or copy submitted. Thus, some thesis and dissertation copies are in typewriter face, while others may be from any type of computer printer.

The quality of this reproduction is dependent upon the quality of the copy submitted. Broken or indistinct print, colored or poor quality illustrations and photographs, print bleedthrough, substandard margins, and improper alignment can adversely affect reproduction.

In the unlikely event that the author did not send UMI a complete manuscript and there are missing pages, these will be noted. Also, if unauthorized copyright material had to be removed, a note will indicate the deletion.

Oversize materials (e.g., maps, drawings, charts) are reproduced by sectioning the original, beginning at the upper left-hand corner and continuing from left to right in equal sections with small overlaps. Each original is also photographed in one exposure and is included in reduced form at the back of the book.

Photographs included in the original manuscript have been reproduced xerographically in this copy. Higher quality 6" x 9" black and white photographic prints are available for any photographs or illustrations appearing in this copy for an additional charge. Contact UMI directly to order.

UMI

A Bell & Howell Information Company
300 North Zeeb Road, Ann Arbor MI 48106-1346 USA
313/761-4700 800/521-0600

The Geochemistry and Petrogenesis of Rarotonga, an Ocean Island in the South Pacific.

by

©Gary M. Thompson, B.Sc., M.Sc.

A thesis submitted to the School of Graduate studies
in partial fulfillment of the requirements for the degree of Doctor of Philosophy

Department of Earth Sciences
Memorial University of Newfoundland

October 1998

St. John's Newfoundland

Frontispiece: Aerial view of Rarotonga taken from the east

ABSTRACT

Rarotonga is the emergent summit of a Plio-Pliestocene volcanic complex built by effusive and pyroclastic eruptions of mainly mafic magma. Petrographically the mafic rock types are ankaramite and basalt. Phenocryst assemblages provide the basis for recognizing two types of ankaramites and basalt, one with a relatively simple equilibrium assemblage of olivine , titanaugite and magnetite (type I), and one with olivine, diopside-augite and titanaugite in which phenocrysts show dis-equilibrium textures (type II) The final stages of volcanism on Rarotonga witnessed the pyroclastic eruption of phonolites and the effusive eruption of foidal phonolites.

Chemically the two mafic types are divided on silica content with, the type I rocks generally have lower silica content than the type II rocks. The remaining elements (both major and trace) having similar concentrations in both types. Although some of the mafic rocks have primitive compositions they probably do not represent primary compositions due to the presence of accumulated minerals. Both type I and type II rocks are enriched in incompatible trace elements compared to primitive mantle. On Bowen diagrams the foidal phonolites and phonolites plot as extensions of the trends defined by the mafic rocks. There is, however, a compositional gap between the mafic rocks and the felsic rocks.

Distribution coefficients determined on mafic rocks from Rarotonga show high concentrations of most of the incompatible trace elements (*e.g.*, Sr, Th, Y, REE etc.) in the pyroxenes relative to the other phases suggesting that fractionation of pyroxenes

dominated trace element distributions during crystal fractionation. In such cases, the highly incompatible elements (Kd < 0.001) are the LFSE Ba and Cs, and the HFSE. Elements that could also be classified as strongly incompatible are Nb and Ta (Kd < 0.1). The remaining trace elements have Kd values that range from ~0.1 (La) up to ~0.8 (Yb). Magnetite incorporates higher amounts of Nb and Ta compared to the titanaugites, and any significant fractionation of magnetite will effect the bulk distribution of Nb and Ta. The LREE have lower Kd values than MREE and HREE with the HREE having Kd values close to unity. Consequently, the separation of titanaugite produces an overall enrichment of REE in the residual liquid with an increase in the La/Yb ratio.

Most of the bulk compositional variation observed in the Rarotonga lavas is due to crystal fractionation processes. Rayleigh fractional crystallization is preferred to equilibrium crystallization on account of the abundance of zoned phenocrysts in many of the Rarotonga rocks. Olivine and clinopyroxene were the two phases controlling crystal fractionation of the mafic rocks. In the type II magmas, the first clinopyroxenes to crystallize had diopside-augite compositions while later clinopyroxenes had titanaugite compositions. As the magma fractionated towards more intermediate compositions kaersutite began to crystallize. Due to slight differences in silica saturation the type I magmas fractionated toward a foidal phonolite end-member forming a low silica suite. The type II magmas fractionated towards phonolite forming a high silica suite.

Viscosity increased during fractionation of the magma chambers inhibiting eruption of the intermediate compositions. A late stage fluid (probably formed during pneumatolysis) was concentrated in the fractionating magma chambers (Na_2O, Th and Y,

etc.). This fluid along with continued increase of alkalis decreased the overall viscosity of the magma to a point where eruptions could start again. The phonolite magmas, which only formed pyroclastic eruptions, were slightly more viscous than the foidal phonolites which erupted as flows.

Whereas much of the compositional variability observed amongst Rarotonga lavas can be attributed to fractional crystallization, important differences in incompatible element ratios and bulk composition of primitive Rarotonga lavas must have been inherited from processes occurring in their mantle source regions. Quantitative modeling shows that the primary magmas which produced the lavas on Rarotonga were produced by low degrees of partial melting (<5%) of a (garnet-free) spinel lherzolite source. The mantle source also contained either an amphibole or a mica phase and was enriched relative to primitive mantle in the highly incompatible elements. The type I magmas were probably produced slightly deeper in the mantle than the type II magmas.

ACKNOWLEDGMENTS

I wish to thank my supervisor, Dr. J. Malpas for his supervision and hospitality throughout this project and for the opportunity to immerse myself in Newfoundland culture. I would also like to acknowledge Drs. G. Jenner and I.E.M. Smith who provided productive criticism and discussion.

I would like to thank the people of Rarotonga especially Tony Utanga for making my stay in Rarotonga both successful and enjoyable. The technicians of both Memorial University and Auckland University (New Zealand) are thanked for preparing thin sections, for major and trace whole rock analysis and for ensuring that machines operated to the best of their potential.

I am indebted to the following people for making my stay in Newfoundland memorable and helping me cope with Newfie culture (the bits I can remember anyway) Chris Lee, the lizard Ladies Bonnie Campbell and Lisa Gardener, Richard Cox, Jeff Saunders, Detlef Gunther, Paul and Dawn Lamswood and finally George Street, Old Sam and Old Stock.

My parents Ian and Maxi have provided support and encouragement. during my absence from New Zealand. I would especially like to thank my wife Sarah for her love and help and for putting up with endless "...I'll be finished in just another couple of months/weeks" for the last two years.

Financial support was provided by NSERC operating grants to Drs. J Malpas and G. Jenner and by Memorial University of Newfoundland (Graduate student fellowships). SOPAC also provided financial support for a field assistant

Table of Contents

Geochemistry

Distribution Coefficients

Petrogenesis of the Mafic Rocks

Petrogenesis of Felsic Rocks

Petrogenesis of Rarotonga and Underlying Mantle

LIST OF FIGURES

List of Tables

Chapter One

Introduction

"Ocean islands....volcanoes from nowhere- pimples on plates far removed from where the action is (plate edges, or boundaries)."

(Morton, 1996)

1.1 Opening Statement

Since the general acceptance of the plate tectonic theory to explain lithospheric features, we have been able to develop a better understanding of the kinematics of plate motion for the last 200 million years. However, it is the dynamics of plate motion that still remain an enigma. The dynamics of plate motion are obviously intrinsically related to mantle kinematics. To enable an understanding of mantle kinematics and dynamics it is important that we understand the physical and chemical properties of the mantle.

It is generally regarded that the igneous rocks which make up ocean islands formed from magmas which originated within the mantle. Ocean islands are therefore a source of a large amount of information about mantle composition and of the processes which operate in the mantle in the absence of continental crust. An understanding of the processes occurring during the petrogenesis of ocean island basalts

will help reveal the physical nature of the underlying mantle. The magmas, however, are generated by complex melting processes and on their rise to the surface are affected by assimilation and crystal fractionation through which their chemical compositions are modified. Therefore, before trace elements and to a certain extent radiogenic isotopes can be used to identify mantle source regions, we have to be aware of any modifications to these geochemical tracers during the ascent of the primary magmas to the Earth's surface.

It is therefore necessary that we more fully understand the petrogenesis of ocean islands. Wilson's and Morgan's hypotheses of hotspots and plumes go a long way towards linking these surface features (principally the Hawaiian islands) with the underlying mantle. Their hypotheses should be supported by the following observations: the linearity of island chains; the asymmetric but systematic age-distance relationship between islands within an individual chain; the parallelism of various island chains situated on the same lithosphere plate; and the reconstructions of the change in direction of plate motions (*e.g.*, Christofferson, 1968; Jarrard and Clague, 1977).

A closer examination of discrete islands within some ocean island chains of the South Pacific show that there are discrepancies that cannot solely be explained by the hotspot theory as it is understood today. The Cook-Austral chain is one of the best examples of a chain that clearly does not fit the hotspot model. It is not a single linear chain and does not show a systematic increasing age relationship between islands with

distance from the proposed position of the mantle plume, which is manifested by active volcanism at the Macdonald seamount at the south eastern end of the chain. The Cook-Austral chain deviates so much from what is expected of an ocean island chain formed by oceanic plates moving over a stationary mantle plume that it led Okal and Batiza (1987) to state:

"*. . . one starts wondering whether the hotspot theory would have emerged as it did, had more cases of the Austral-type chains been documented (especially if located in more accessible regions) early in the game.*"

It is therefore important that these apparently anomalous ocean island chains be examined in more detail, particularly those islands in the chains that clearly counter the hotspot model. These islands should then be compared with islands and island chains that conform to the present hotspot model to determine if the differences are significant and the nature of modification to the hypothesis that must be made.

1.2 Ocean Islands

Much of our knowledge of the volcanic and petrologic evolution of ocean islands is based on extensive studies on the islands of the Hawaiian group (*e.g.*, Macdonald and Katsura, 1964; McDougall, 1964; Murata and Richter, 1966; White, 1966; Jackson, 1968; McDougall and Swanson, 1972; Moore et al., 1982; *etc.*). This

early work showed a common pattern for the evolution of the islands within this group, with four distinct stages of volcanic growth, summarized below:

Stage 1. The initial period of ocean island growth appears to consist of alkaline volcanism, *e.g.*, Loihi seamount. These early alkali lavas are totally enveloped by the second stage of ocean island growth.

Stage 2. The growth of massive basalt shield volcanoes whose volumes range from 3000 (Kauai) to 40,000 km^3 (Mauna Loa) occurs in this stage. Many of the islands are formed by multiple overlapping shield volcanoes; *e.g.*, on the youngest island, Hawaii, there are five overlapping shields all younger than 500 000 years. The bulk of the exposed lava that erupted during the shield building stage is tholeiitic basalt. It should be noted, however, that the composition of the tholeiites is not uniform, and varies from one volcano to another (*c.f.* Mauna Loa, Mauna Kea and Hualalai on Hawaii). For example, historic Lilauea lavas and Mauna Loa lavas overlap in abundances of Al_2O_3 and Na_2O, but historic Kilauea lavas have higher CaO, TiO_2 and K_2O contents and lower SiO_2 contents than Mauna Loa lavas (Frey and Rhoden, 1987).

Stage 3. The stage following the building of the shield is highly variable. Collapse of the summit occurs on some volcanoes, with continuing eruption of lava from these volcanoes filling and overflowing the resulting caldera. The stage of volcanism that caps the younger shield building stage accounts for less than one percent of the total bulk of the island. The change in eruptive pattern is always accompanied by a change

in magma composition, with the late lavas being more alkali than the shield building lavas.

Stage 4. Following a period of extensive erosion (a hiatus of approximately 1 to 2 m.y.) on four of the islands (Kauai, Niihau, Oahu and western Maui), highly alkaline mafic lavas (nephelinites, melilite basalts and basanites) erupted. This period of volcanism is referred to as the post-erosional stage. The eruption of highly alkali lava after a hiatus, in which the island should have moved beyond the influence of the active plume, is still not fully understood. Within the Hawaiian chain the production of these lavas is attributed to adiabatic melting during the passage of an island over the flexural bulge associated with coeval edifice construction (Jackson and Wright, 1970; Clague and Dalrymple, 1987). However, this relationship between the flexural bulge and the initiation of post erosional magmatism is not as clear on other island chains, *e.g.*, the Canary Islands, leading to the suggestion that post erosional magmatism could be due to episodic reduction of mid-plate compression (Vogt, 1988).

The above scenario is often considered to represent the typical evolution of an ocean island. However, recent research on islands of the South Pacific has shown that there are important differences between the islands of this region and the well-studied ocean islands of the Hawaiian chain. South Pacific ocean islands are generally smaller in volume than those of the Hawaiian chain. The duration of volcanic activity on a single South Pacific island is comparable with that of Hawaiian islands, although exceptions do exist where the span of volcanism exceeds several million years (Jarrad

and Clague, 1977). Tholeiitic basalts are conspicuously absent on nearly all of the ocean islands in the South Pacific, with the oldest exposed rocks being alkali basalts. Only one island group, the Marquesas, has exposed quartz-normative tholeiites (Duncan et al., 1986). The relative volume of the eruptive stages described above is not strictly followed on some of the South Pacific islands. For example, the bulk of the exposed lavas on the Western Samoan islands appears to belong to what is described above as the post erosional stage (stage 4; Wright, 1986).

1.3 Area of Study

As discussed by Okal and Batiza (1987), the Cook-Austral chain appears to be a clear maverick within the hotspot/plume theory. It is therefore important that we explain the existence of those islands within the chain that question the chain's formation from a single mantle plume. In the case of the Cook-Austral chain, Rarotonga appears to be the most unusual, having an anomalous age compared to a predicted age using a hotspot/plume model; a different mantle chemical signature to the other islands in the chain; and in being spatially offset from the other islands in the chain.

1.3.1 Cook-Austral Chain

The Cook and Austral islands form ≥ 1500 km long northeast-southwest trending chain, from about 29°S and 140°W to about 20°S and 155°W (Figure 1.1). The chain is sub-parallel to other island chains of the Pacific (*e.g.*, the Society and the Tuamotu islands). Except for an active submarine volcano, MacDonald seamount (Norris and Johnson, 1969) at the south-eastern extension of the chain, all of the islands are extinct volcanoes rising more than 5000 m from a sea-floor of Paleocene age (Pitman et al., 1974). The islands do not actually form a single linear chain, but two overlapping parallel chains (Figure 1.1). In addition, radiometric dating of individual islands has shown that there is not a simple linear relationship between time and distance of individual islands from the proposed mantle plume, manifested today by active volcanism at the MacDonald seamount. Three islands do not follow the age/distance relationship (Rarotonga, Aitutaki and Atiu) and both Rurutu and Tubuai islands have extended periods of volcanic activity spanning several million years (Turner and Jarrard, 1982).

Available dates for Rarotonga suggest that volcanism was initiated approximately three million years ago and lasted for one to two million years. In a single hotspot model with the active hotspot now located under MacDonald seamount to the south east, Rarotonga should be at least 20 million years old (Figure 1.1). Aitutaki and Atiu both have young exposed volcanic rocks with radiometric ages of

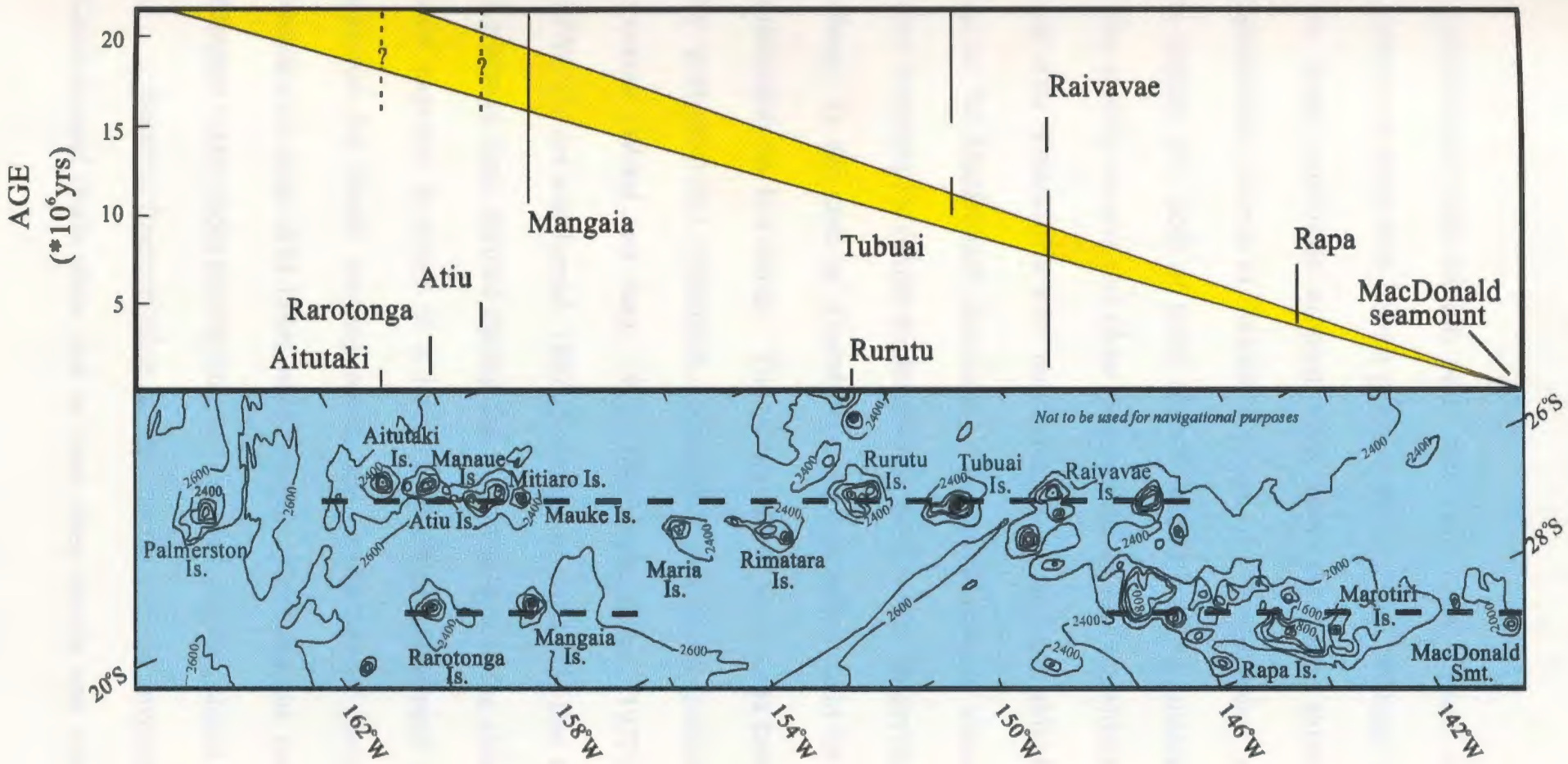

Figure 1.1: Location map of Rarotonga in the Cook/Austral chain in the south Pacific, showing the ages of volcanic edifices on the chain and their age-distance relationship with respect to active volcanism now manifested at MacDonald seamount. The ages of the islands are all based on radiogenic dating except for the two dashed lines for Atiu and Aitutaki that show the possible age of the shield building stage of these islands based on geomorphic critera. The yellow region is the predicted age for the volcanic effects if volcanism was due to the Pacific plate moving over a stationary plume located underneath the MacDonald seamount (After Darymple et al., 1975).

approximately one million years and three million years respectively. The extent of erosion on these two islands prior to the eruption of these younger rocks suggests that the latest volcanoes erupted long after the main shield building stage. Using geomorphic criteria as indicators of age of volcanic cones, as outlined by Kear (1957), it appears that both of these islands' shield building phases occurred in the Miocene. This poorly constrained older geomorphic age of the shield building stage of Aitutaki and Atiu is consistent with the formation of the main shield at a single hotspot located under the MacDonald seamount. The re-initiation of volcanism on these two islands may therefore be similar to the evolutionary model observed on islands in the Hawaiian chain. In the case of Aitutaki the flexural bulge could be due to the loading on the lithosphere by Rarotonga. The young age of Rarotonga cannot be as readily explained by post-erosional volcanism, because it has been generally accepted by previous workers (Wood and Hay, 1970; Dalrymple et al., 1975; Duncan and McDougall, 1976; Turner and Jarrad, 1982; Staudigel et al., 1991) that the exposed mafic rocks on Rarotonga were formed during the main shield building phase. However, if the rocks now exposed is result of a late period of post-erosional volcanism that has totally covered the shield forming rocks, the young age of Rarotonga is explained. The absence of deep drill holes on Rarotonga precludes the confirmation of whether the exposed mafic rocks overlie an older, eroded volcanic shield.

Isotopic fingerprinting of the mantle sources involved in the formation of the Cook-Austral chain show that at least three mantle end members are involved in the

formation of the chain. Two islands, Mangaia and Tubuai, have a pure HIMU component as defined by Staudigel et al. (1991). The remaining islands lie on a mixing line between HIMU and EMII, with Rarotonga having an additional EMI component (Staudigel et al., 1991).

1.3.2 Rarotonga

Rarotonga, the largest of the Cook Island Group, is one of the southern-most islands in the archipelago located near the northern end of the Cook-Austral island chain (Figure 1.1). It is elliptical in shape, 11km EW and 8km NS, and represents the upper 650 m. of an oceanic volcano that rises a total of 5000 m above the surrounding sea floor. A coastal fringe of lowland consisting of raised reef material borders the densely forested mountainous interior comprising a deeply dissected volcanic edifice. Erosion of the remnant volcano has left a deeply dissected terrain that bears little trace of its original form, apart from the felsic lava flows which erupted from vents on the flanks of the main volcano and still show their primary morphology. The almost exclusive volcanic nature of the rock units making up the island suggests that the present level of exposure lies in the upper part of the original volcanic edifice and the radial distribution of the drainage system is inherited from the original volcanic form of the island.

The island was first described by Marshall (1930) and subsequently mapped by Wood and Hay (1970). They formulated a geologic history based on the rocks they found, using the typical sequence of events recorded on the Hawaiian islands (Table 1.1). Only two studies have provided any significant systematic radiometric dating of Rarotonga rocks (both used K-Ar methods); Dalrymple et al., 1 975 and Turner and Jarrard, 1982. In both these studies a relatively limited selection of rocks was dated: Dalrymple et al. (1975), dated four basalts and two phonolites (a flow and a clast from a breccia), the exact location and stratigraphic position of these samples being unknown as they misplaced their field notes; while Turner and Jarrard, (1982), analyzed four phonolites (two flows and clasts from two breccias) and 14 basalts. These results are summarized in Table 1.2. The dates show that the activity that built the volcano took place in Late Pliocene and Early Pleistocene times.

Subsequent work on Rarotonga has focused on the isotopic fingerprinting of the volcanic rocks forming the island as part of regional studies determining mantle heterogeneity in the South Pacific (Palacz and Saunders, 1986; Nakamura and Tatsumoto, 1988; Staudigel et al., 1991).

Table 1.1

Stratigraphic column of Wood and Hay 1970

Unit Names	Rock Descriptions
Intra-Caldera	
Manureva Flows	dark green phonolite with sodalite, aegirine, nepheline, and zeolite-filled vesicles
Tuakata flows	dark green flow banded nepheline phonolite
Extra-Caldera	
Muri Flows	dark green to gray dense phonolite with sodalite, aegirine, analcime, and zeolite-filled vesicles
Raemaru Flows	light olive green-gray fined grained phonolite
Intra-Caldera	
Maungatea Breccia	roughly stratified breccia of angular basaltic and phonolitic rocks with beds of pale-gray phonolitic primary tuff and ash
Extra-Caldera	
Maungaatapu Breccia	light brown to light gray phonolitic-basaltic breccia; sub-horizontal bedding, with thin beds of fine vitric tuff
Te Kou Complex	weathered phonolitic and trachytic flows and pyroclastics, yellow brown cinders and tuff forming residual cinder cone
	erosional episode
Avatiu Caldera Complex	gray to black basalt, oceanite, ankaramite in flows, dykes, breccia, scoria, and ash.
	caldera formation
Te Manga Group	gray to black basalt, ankaramite, limburgite in flows, dykes, and pyroclastics dipping generally seaward comprising the bulk of the primitive volcano.
Pue Ash	yellow-brown ash, approximately 50ft thick, passing up to about 500ft of sub-aerial cross-bedded gray cinder, ash and fine breccia. Deposits of an early eruption on the flank of a primitive volcano.

Table 1.2

Summary of radiometric dates from Dalrymple et al. (1975) and Turner and Jarrad (1982).

Rock type	Location	Method	Calculated age
	Dalrymple et al (1975)		
phonolite flow	?	K-Ar	1.21±0.21
phonolite (trachyte)	?	K-Ar	1.24±0.24
basalt	?	K-Ar	1.19±0.04
basalt	?	K-Ar	1.30±0.06
basalt	?	K-Ar	1.83±0.3
ankaramite	?	K-Ar	1.75±0.12
	Turner and Jararrd (1982)		
phonolite	Muri flows	K-Ar	1.1±0.04
phonolite	Raemaru flows	K-Ar	1.36±0.05
phonolite	Maungatea	K-Ar	1.24±0.04
(trachyte)	Breccia		1.26±0.04
phonolite	Te Kou	K-Ar	1.16±0.04
(trachyte)			1.29±0.04
ankaramite	Paupa stream	K-Ar	1.55±0.05
			1.60±0.05
alkali basalt	Pue stream	K-Ar	1.44±0.05
			1.75±0.05
alkali basalt	Pue stream	K-Ar	1.66±0.06
			1.65±0.06
alkali basalt	Tupapa stream	K-Ar	1.63±0.25
alkali basalt	Rutaki stream	K-Ar	1.97±0.12
			2.31±0.14
ankaramite	Avana stream	K-Ar	1.2±0.03
alkali basalt	Avana stream	K-Ar	1.39±0.04
alkali basalt	Avana stream	K-Ar	1.41±0.04
alkali basalt	Avana stream	K-Ar	1.68±0.05
alkali basalt	Avana stream	K-Ar	1.79±0.05
alkali basalt	Avana stream	K-Ar	1.94±0.06
alkali basalt	Avana stream	K-Ar	2.14±0.06
			3.64±0.15
alkali basalt	Avana stream	K-Ar	2.27±0.08

1.4 Aim of This Study

The aim of this study was to test the thesis that, although Rarotonga in the Cook/Austral chain does not exactly fit with the Wilson/Morgon hotspot model, its presence does not invalidate this model. To test this Rarotonga was examined in detail to understand its petrogenesis. In order to do this the following procedure was followed:

i. describe the rock types found on the island and their distribution;

ii. determine their geochemistry;

iii. identify the process which have modified these rocks since the production of primary magmas;

iv. determine primary magma compositions and their source characteristics; and

v. compare the evolution of the island with that of typical hotspot models.

1.5 Format of Thesis

This thesis has a further seven chapters following the introduction. The contents of each are as follows:

Chapter two

The Mantle. A Review

A review on the geochemistry and structure of the mantle.

Chapter three

Geology of Rarotonga:

A brief description of the geology of Rarotonga including field relationships and petrography of the mafic and felsic rocks.

Chapter four

Geochemistry

A summary of the whole rock (major and trace elements and some radiogenic isotopes of selected rocks) and mineral (major and trace element) geochemistry.

Chapter five

Distribution Coefficients

The distribution coefficients to be used in petrologic modeling in subsequent chapters are calculated in this chapter.

Chapter six

Petrogenesis of the Mafic rocks:

Using the data from chapters two through four, the petrogenesis of the mafic rocks is discussed including an evaluation of the mantle source region and the generation of the primary magmas from this source.

Chapter seven

Petrogenesis of the Felsic rocks.

The genesis of the felsic rocks and the absence of rocks with compositions intermediate to the mafic and felsic rocks are discussed.

Chapter eight

Summary.

A model for the formation of Rarotonga using all of the information available is given, including a comparison with other ocean islands.

4.5.1 Conventions

The systematics for sample numbers are as follows: rock samples, R-XX, where XX is a unique number for that sample; phenocrysts from which geochemical analyses were obtained have the following identifiers, RXX-AAXX-B, where RXX identifies the rock sample from which the phenocryst came, AA the type of phenocryst, *i.e.*, Ol, Px, Ox for olivine, pyroxene and oxide respectively, XX the unique number for that phenocryst, B- where on the crystal the analysis was made, i.e. C, R, I for core, rim, and an intermediate position between the core and rim. In some samples, the intermediate position may have an additional number where several analyses were made from core to rim. These analyses are numbered sequentially from core to rim.

A list of the common acronyms and abbreviations used in this thesis is given in Table 1.3.

Table 1.3

List of acronyms used in this thesis

Ab	Albite
An	Anorthite
apsf	Atoms per structural formula
BVSP	Basaltic Volcanism Study Project
cpx	Clinopyroxene
D	Bulk distribution coefficient
D.I.	Differentiation index
Di	Diopside
DMM	Depleted MORB mantle
EMI	Enriched mantle source I
EMII	Enriched mantle source II
En	Enstatite
Fo	Forsterite
Fs	Ferrosilite
HFSE	High field strength elements
HIMU	Mantle source high in μ; $\mu = {}^{238}U/{}^{204}Pb$
HREE	Heavy rare earth element
ICP-MS	Inductively coupled plasma mass spectrometer
Kd	Distribution coefficient
LAM-ICP-MS	Laser ablation microprobe-ICP-MS
LFSE	Low field strength elements
LREE	Light rare earth element
Mg#	Magnesium number $Mg/(Mg+Fe^{2+})*100$
MORB	Mid ocean ridge basalt
MREE	Middle rare earth element
mt	Magnetite
Neph	Nepheline
OIB	Ocean island basalt
ol	Olivine
Or	Orthoclase
plag	Plagioclase
ppm	Parts per million
px	Pyroxene
REE	Rare earth element
Wo	Wollastonite
WPB	Within plate basalt
wt. %	Weight percent

Chapter Two

The Mantle, A Review

"...a fierce and vehement fire certainly burned within the entrails of the great spheroid."

(A Journey to the center of the Earth, Jules Verne, 1872)

2.1 Introduction

What we understand of mantle structure is based on geophysical evidence, while mineralogical and chemical composition are inferred from petrological studies of igneous rocks found on the earth's surface and from the rare samples of the mantle occurring, for example, as inclusions in volcanic rocks.

Direct sampling of the mantle is limited to xenoliths (mantle nodules carried to the surface from depths no greater than 200 km), ophiolites (*e.g.*, Troodos, Cyprus; Bay of Islands, Newfoundland, Canada; *etc.*) and ocean drilling (*e.g.*, Hess deep, East-Eq. Pacific, ODP Leg 147). Because of their limited exposure and size, such direct

samples can offer only a spatially restricted understanding of mantle composition. Further evidence can be gained from the geochemistry of mantle-derived magmas such as mid ocean ridge basalts (MORB; *e.g.* Mid Atlantic Ridge and the East Pacific Rise) and within plate basalts (WPB; *e.g.*, ocean islands and flood basalts, *etc.*). These are found throughout the geologic record, have a world wide distribution, and are therefore likely to have formed from a wide variety of mantle source regions. Oceanic magmas (MORB and WPB) are the preferred rocks to study for information about the mantle because they have had limited interaction with continental crust unlike continental within plate basalts (Deccan traps, Columbia river basalts *etc.*), or a subducting oceanic slab in the way that oceanic volcanic arc or back arc basin basalts (Tonga-Kermadec islands; Fiji, *etc.*) have.

2.2 Mantle Structure and Dynamics

Geophysical modeling of mantle structure involves the interpretation of gravity and magnetic anomalies, heat flux and the propagation of seismic waves. A simplified model of Earth, PREM (Preliminary Reference Earth Model) developed from seismic studies is given in Figure 2.1. This model can be used as a first approximation of the Earth's internal structure (for a comprehensive review see Peltier, 1989). It is generally accepted that large scale convection must occur in the mantle, but debate still continues on the nature of this convection: *i.e.*, does whole mantle convection exist or

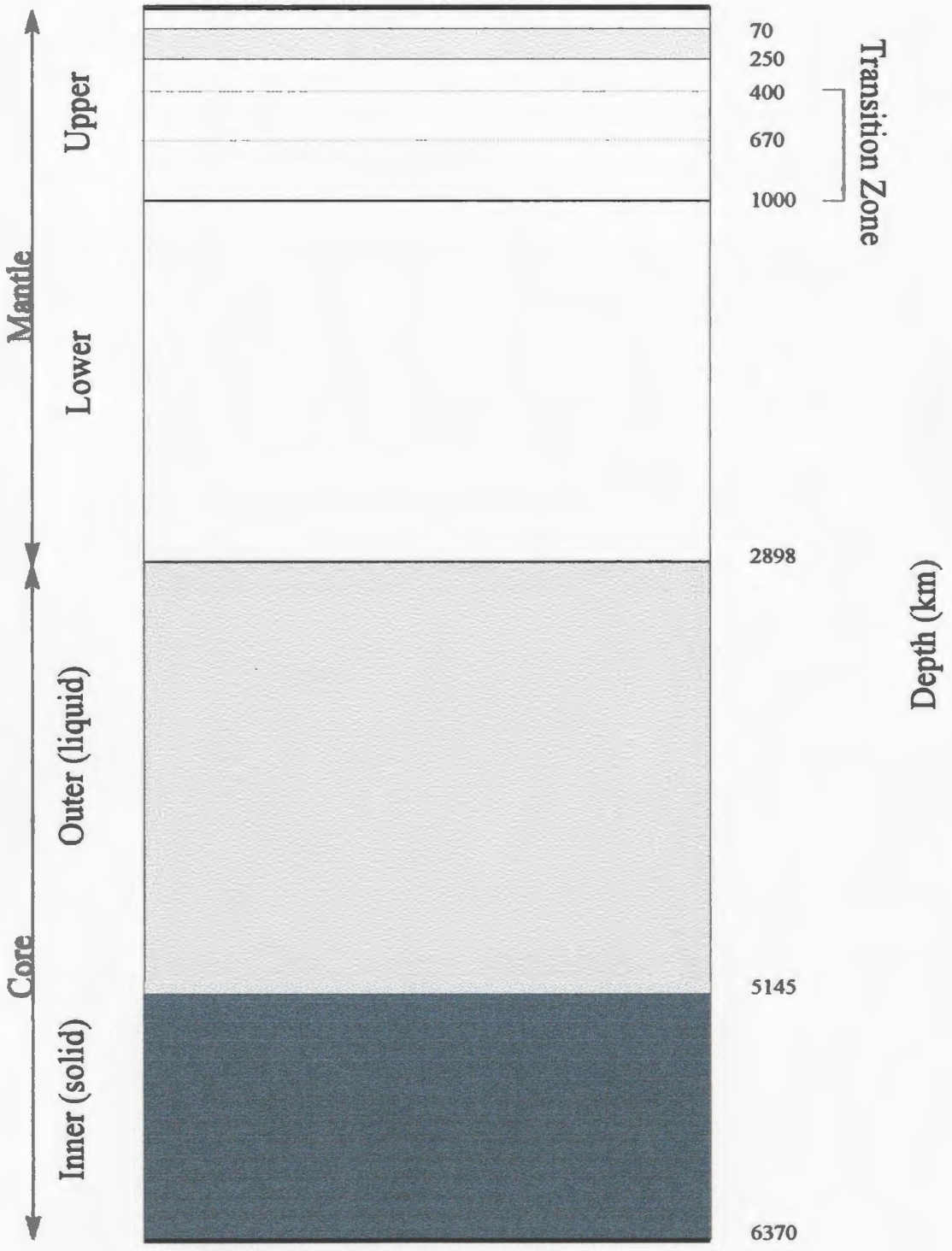

Figure 2.1: Major divisions of the Earth based on seismic data. Note that at this scale the thickness of the crust (ca. 40 km for continental and ca. 11 km for oceanic) is represented by only the outer black line. The major transitions in the mantle occur at 400 km where olivine is transformed to a spinel structure and at 670 km where the conversion of most of the silicates to a perovskite structure takes place. The zone of low seismic velocities in the upper mantle is indicated by the shaded band (after Philpotts, 1990).

does the upper and lower mantle exist as two distinct convecting regions? The regional geometry of mantle circulation is difficult to determine, partly because the thickness of lithospheric plates suppresses the surface expression of the convective flow and partly because it is difficult to detect or image rising and sinking mantle material, as is apparent from numerical experiments (White and McKenzie, 1995).

In 1963 Wilson published one of the first papers in which ocean island volcanism was linked to convection of the underlying mantle. Subsequently, Morgan (1971 and 1972) refined Wilson's model by proposing that such regions of magma production were the result of mantle plumes originating from the core/mantle boundary. Morgan also suggested that plumes are fixed in space with respect to one another, an observation which has since been corroborated by Minister and Jordan (1978). White and McKenzie (1995) suggested that the assumption that rising regions of the mantle consist of deeply rooted axis-symmetric plumes is unlikely to be correct, but went on to suggest that axis-symmetric models may provide a reasonable representation of the thermal structure of the mantle in the region immediately beneath the lithosphere, where most melts are generated.

McNutt and Fisher (1987) recognized the following features of the ocean floor in the South Pacific in the area of French Polynesia (Figure 2.2):

i. The ocean floor is shallower than ocean floor of comparable age in the North Pacific and Atlantic;

Figure 2.2: Sketch map showing location of the South Pacfic Superswell (shown in yellow) and the DUPAL anomaly (shown in pink).

ii. The flexural strength of the lithosphere in this region is weaker than that of the ocean lithosphere in the North Pacific and Atlantic;

iii. Seismic velocities in the upper mantle are lower than expected;

iv. The region has a negative geode anomaly; and 30% of the heat flux from all hotspots in the world is released from this region, which constitutes only 3% of the Earth's surface.

This region has been referred to as the South Pacific Superswell by McNutt and Judge (1990).

Seismic tomography studies suggest that the South Pacific Superswell is the lithospheric expression of an upper mantle phenomenon, and that there exists an antipodal superswell in the Afar region (Cazenave and Thoravel, 1994). The South Pacific Superswell appears to be not simply a recent phenomenon and its possible presence can be traced back to the Cretaceous (Smith et al., 1989; McNutt et al., 1990). Superswells may be the surface expression of superplumes which originate in the upper mantle, possibly at the base of the Low Velocity Zone (LVZ), in the Transition Zone (Cazenavae and Thoravel, 1994), or in the lower mantle (Fukao, 1992; Hart et al., 1992; Coffin and Eldholm, 1993).

2.3 Mantle Chemical Heterogeneity

The diversity of chemical compositions in materials derived from the mantle show that it is chemically and isotopically complex. The importance of some oceanic basalts to understanding the chemical composition of the mantle has already been mentioned in section 2.1. Oceanic igneous rocks can be divided into two groups, those formed at mid ocean ridges and those formed on discrete ocean islands at some distance from these ridges. Ocean island (within plate) basalts (OIB) are enriched in the light rare earth elements (LREE) and other incompatible elements (Tatsumoto et al., 1965; Schilling and Winchester, 1967; Schilling, 1971, 1973; DePaolo 1979; Schilling et al., 1983; Zindler et al., 1984) when compared to MORB. Early models of the mantle postulated a two-component layered mantle with the depleted MORB source overlying a primitive mantle from which OIB were formed. Subsequent work (Sun, 1982; White and Hoffman, 1982; Zindler et al., 1984) showed that this two-component mantle model is not adequate to explain the chemical variation observed in all oceanic basalts. At least four hypothetical source components (Figure 2.3) are needed to account for the chemical and isotopic diversity (Staudigel et al., 1984; White, 1985; Zindler and Hart, 1986, Weaver, 1991).

The reservoirs defined by isotopic signatures are:

i) a depleted MORB mantle source (DMM): high $^{143}Nd/^{144}Nd$, low $^{87}Sr/^{86}Sr$, depleted in light rare earth elements (LREE);

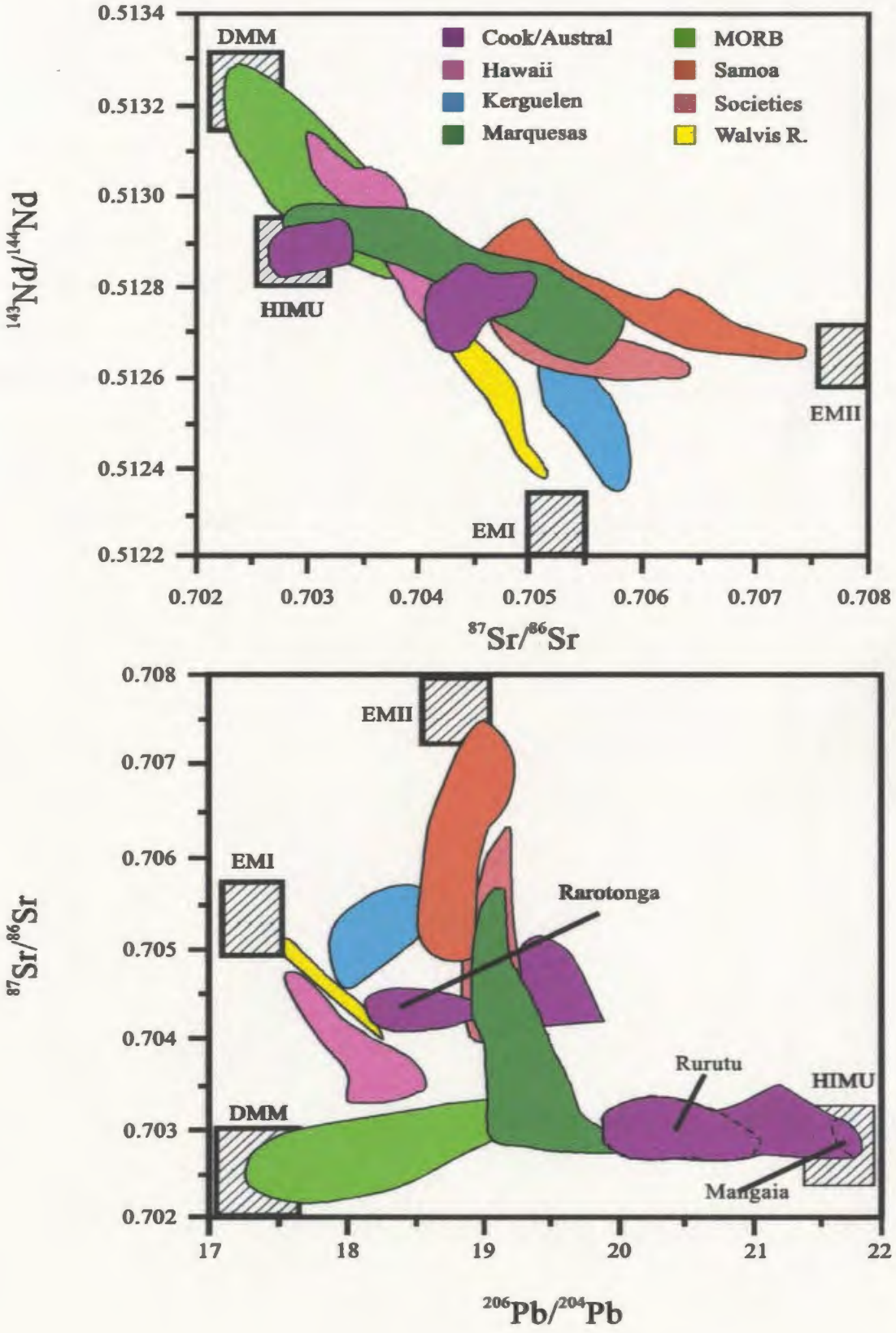

Figure 2.3: Isotopic variations for oceanic basalts in the South Pacific. Hypothetical mantle end-members are shown for reference (after Staudigel et al., 1984).

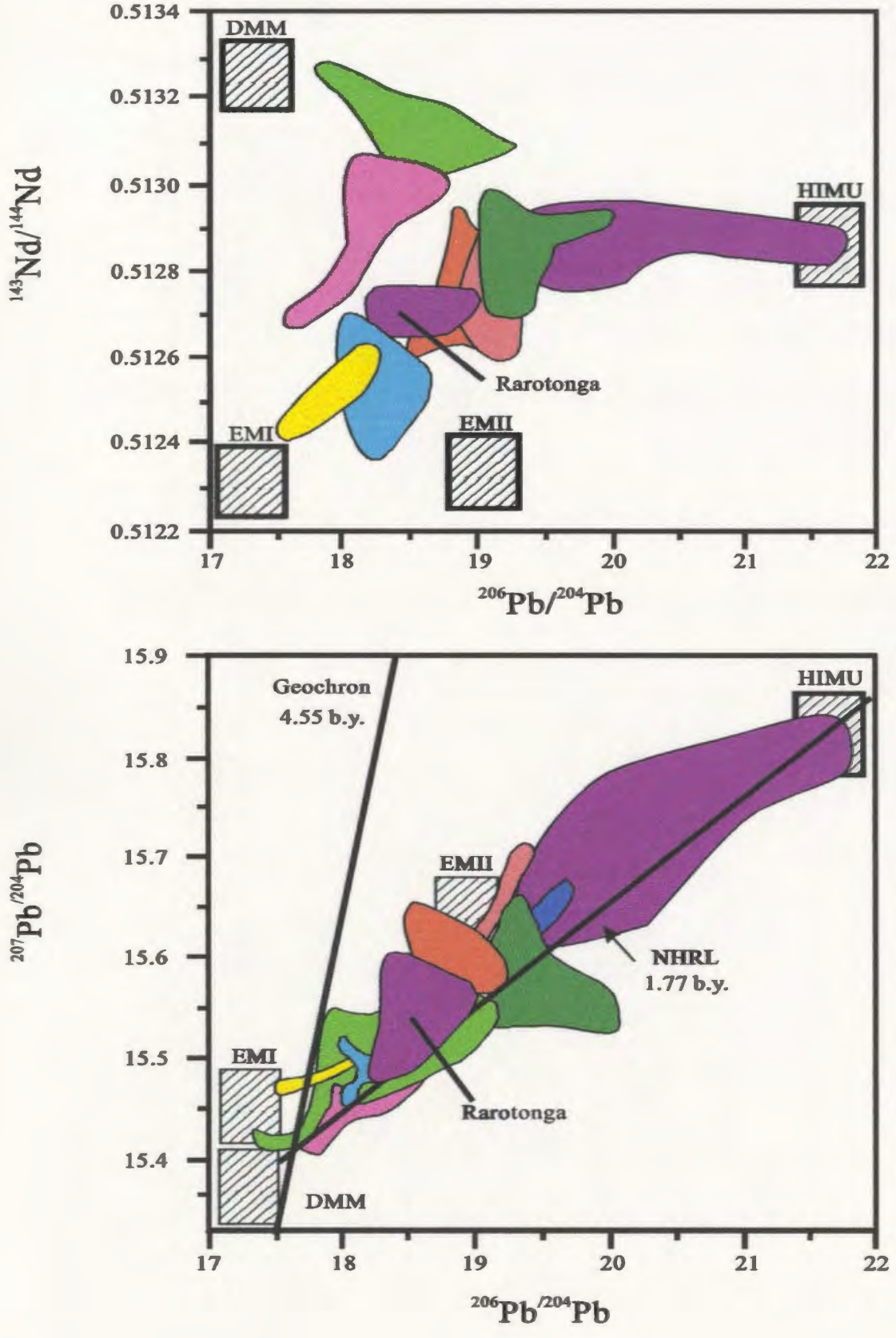

Figure 2.3: (continued).

ii) a mantle source high in $^{238}U/^{204}Pb$ (HIMU): high $^{206}Pb/^{204}Pb$, intermediate $^{143}Nd/^{144}Nd$, low low $^{87}Sr/^{86}Sr$;

iii) an enriched mantle (EMI): low $^{143}Nd/^{144}Nd$, intermediate $^{87}Sr/^{86}Sr$, low $^{206}Pb/^{204}Pb$ and $^{208}Pb/^{204}Pb$ with $^{207}Pb/^{204}Pb$ > MORB

iv) an enriched mantle (EMII): low $^{143}Nd/^{144}Nd$, high $^{7}Sr/^{86}Sr$, intermediate $^{206}Pb/^{204}Pb$ and $^{208}Pb/^{204}Pb$;

In order to further constrain the chemical characteristics of the mantle reservoirs workers have compared their trace element compositions (*e.g.*, Saunders et al., 1988 and Weaver, 1991; Table 2.1). The difference between trace element compositions in these mantle reservoirs is more subtle reflecting, in part, the use of radiogenic isotopes as the principle criteria on which the reservoirs were first identified.

The scale of heterogeneity within the mantle is extremely variable ranging from truly global down to a scale of less than tens of kilometers. Dupre and Allegre (1983) observed that ocean island basalts from a large area of the Indian Ocean have anomalous Sr, Nd and Pb isotopic mantle source signatures, equivalent to that of the EMII end member. Hart (1984) then traced this anomaly, which he called the DUPAL anomaly, almost continuously around the southern hemisphere between 60°S and the Equator (Figure 2.2). Staudigel et al. (1984) observed that mantle isotopic signatures of ocean island basalts in the South Pacific Superswell lie on a hypothetical mixing line between the HIMU mantle end-member and the EMII end-member (Figure 2.3) with

Table 2.1

Incompatible trace element ratios in mantle reservoirs (from compilations by Saunders et al., 1988, Weaver, 1991)

	Zr/Nb	La/Nb	Ba/Nb	Ba/Th	Rb/Nb	K/Nb	Th/Nb	Th/La	Ba/La
DMM	14.8	0.94	9.0	77	0.91	323	0.117	0.125	9.6
HIMU	3.2-5.0	0.66-0.77	4.9-6.9	49-77	0.35-0.38	77-179	0.078-0.101	0.107-0.333	6.8-8.7
EMI	4.2-11.5	0.86-1.19	11.4-17.8	103-154	0.88-1.17	213-432	0.105-0.122	0.107-0.128	13.2-16.9
EMII	4.5-7.3	0.89-1.09	7.3-13.3	67-84	0.59-0.85	248-378	0.111-0.157	0.122-0.163	8.3-11.3

two exceptions; Pitcairn Island and Rarotonga. Both Pitcairn and Rarotonga have an EMI component in their mantle signature. Not only does it seem apparent that islands within a single group (*c.f.*, Rarotonga and Pitcairn with the other islands in their respective chains) are tapping different mantle sources, but studies (Dupre et al., 1982; Barling and Goldstien, 1990) have shown that mantle heterogeneity can be observed within a single island.

How these different mantle source regions are related is still debatable:

- Is the mantle a stratified body with each of the end-members, discussed above, representing a single layer?
- Does the mantle consist of chemically distinct regions of various sizes distributed like plums in a pudding (Carlson, 1988)?
- Is the mantle similar in appearance to a marble cake in which mantle convection stirs and mixes chemically distinct regions (Allegre and Turcotte, 1986; Kellog and Turcotte, 1990)?

It is clear from the chemical characteristics of oceanic basalts that mixing of the DMM, HIMU, EMI and EMII end-members does occur, but the nature of mixing is speculative with various models being proposed:

i. Solid-solid mixing to produce either a veined mantle (Tarney et al. 1980), a streaky mantle (Zindler et al., 1984; Fitton and James, 1986), or a marble-cake mantle (Allegre and Turcotte, 1986);

ii. Fluid-solid mixing resulting in mantle metasomatism (Stolz and Davies, 1988).

These models differ in the location of the OIB reservoirs, *i.e.*, whether they are at the base of the upper mantle (Ringwood, 1985), in the lower mantle (Dupre and Allegre, 1983; Saunders et al., 1988), or intimately mixed with the depleted reservoir (DMM) in the upper mantle (Zindler et al., 1984).

Chapter Three

Field Relations and Petrography

3.1 Introduction

The purpose of this chapter is to describe and document the various rock types found on Rarotonga. The first section is dedicated to presenting a general overview of the geology of Rarotonga, while the remainder of the chapter provides a detailed description of the igneous rocks. The petrographical descriptions are generalised for. there are wide variations in modal composition within a given rock type (Appendix 1). The classification scheme used for naming the rocks is that of the IUGS Sub-commission on the Systematics of Igneous Rocks (Le Maitre, 1989).

3.2 Overview of the Geology of Rarotonga

The morphology of Rarotonga is controlled by two processes, the initial formation of the island by volcanic activity and subsequent modifications to the volcanic edifice by erosion. Erosion has all but obscured the original volcanic form of the island, leaving its interior as a series of steep razor-backed ridges separating deep valleys (Frontispiece and

Figure. 3.1). This style of relief is characteristic of many tropical and subtropical islands in the South Pacific. It can also be seen in subtropical terrains that are not volcanic, *e.g.*, the Urewera district of the North Island, New Zealand. In Rarotonga it can be argued that the large eastern valley which has a semi-circular appearance, is formed by the drainage of the central highlands by the Avatiu and Takuvaine rivers. Both of these valleys display over-steepened slopes at their heads, a feature which can be observed in all head waters of streams draining the central mountains, reflecting a residual mountain stage or early planeze stage of erosion.

The products of two compositionally distinct phases of volcanic growth are presently exposed on Rarotonga; an initial stage of mafic volcanism, followed by the eruption of more fractionated rocks. At least three distinctive styles of volcanism include high-level dykes, lava flows and pyroclastic eruptions.

Geological mapping of the island (Figure. 3.2; map pocket) shows that mafic dykes are ubiquitous on the island, *i.e.*, there is no localised area of emplacement. The felsic flows are all found on the flanks of the island, while felsic breccia is concentrated in the centre. Radiometric ages of rocks on Rarotonga (see Chapter one) suggest that the exposed rocks represent an essentially continuous single phase of volcano growth without any significant periods of volcanic quiescence.

The mafic rocks were erupted over a period of approximately 2 million years from at least two main volcanic vents in the approximate centre of the island. During this stage, the formation of parasitic cinder cones was also a significant component of shield growth. There is no evidence for extensive faulting or disruption of units within any

Figure 3.1: View of interior of Rarotonga showing steep relief. Taken from Te Kou looking west.

single area of the island. Following this period of mafic volcanism, eruption of the felsic rocks occurred as outpourings of lavas on the flanks of the volcanic cone, and blanketing of the central part of the island by dominantly felsic pyroclastic ejecta.

3.2.1 Mafic Rocks

Fresh exposures of the mafic rocks are virtually limited to the bottom few metres of the river valleys. This restricted exposure in conjunction with the character of ocean island volcanism, *i.e.*, sporadic eruptions both temporally and spatially, limits the lateral comparison of outcrops, consequently preventing the accurate determination of the temporal relationships between mafic rocks.

Mafic Dykes

Mafic dykes are generally radial to the centre of the island, ubiquitous, with no concentration of exposed dykes within any one particular area. The dykes range in width from 0.3m to 1m and are vertical or steeply dipping. However, by extrapolating the strike directions of the dykes, two volcanic centres can be identified. One is located on the eastern wall of the Tukavaine valley and the second is found at the head of the Avatiu stream (Figure 3.2). Near the location of the volcanic centre in the Avatiu stream several steeply dipping dykes (Figure 3.3) intrude in a parallel fashion and are chilled against each other. This type of dyke emplacement is commonly observed in areas of extension,

Figure 3.3: Several steeply dipping dykes intruded in a parallel fashion and chilled against each other, Avatiu stream. The location from which the photograph was taken is shown below.

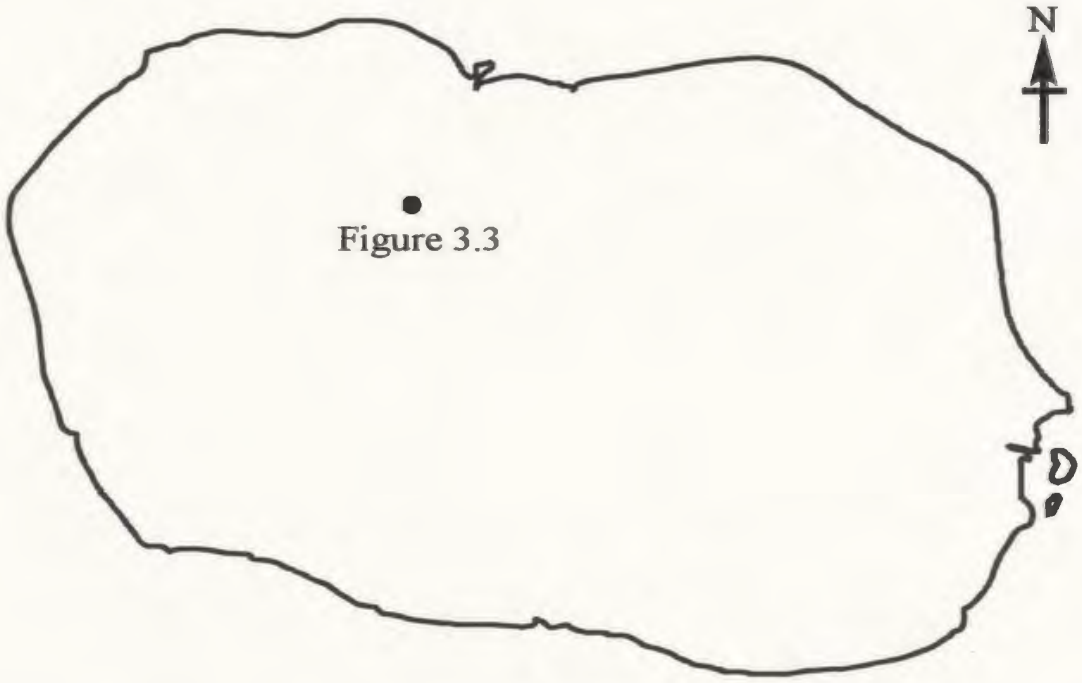

e.g., ophiolite sequences, where they are referred to as "sheeted dykes". Although they are found on some other ocean islands, *e.g.*, Gran Canaria (Stillman, 1986) where they have been similarly interpreted as evidence for extension, in Rarotonga there is no evidence for any substantial extension and this sequence of sheeted dykes probably represents a primary conduit of a volcanic centre, where multiple eruptions occurred over a prolonged period of time.

Mafic Lava Flows

The exposed lava flows all formed by sub-aerial eruption and are generally less than five metres and usually only one to two metres, thick. Lava flows dip seaward at angles between 5 and 20 degrees. However, this is extremely variable as the flow of lava was to a large extent controlled by the pre-existing topography. Due to the limited exposure it is impossible to determine if flows erupted from the summit or from the flanks of the volcano. Dissected lava flows show a typical structure of an oxidised blocky *aa* flow top grading down into dense massive basalt. Some of the thicker flows display columnar jointing, underlain by fracturing parallel to the base of the flow (Figure 3.4).

Mafic Pyroclastics

Pyroclastic eruptions resulted in the formation of thick-bedded layers of volcanic breccia, thin layers of volcanic ash, and cinder cones. Volcanic breccia is volumetrically

Figure 3.4: A basaltic flow displaying columnar jointing, underlain by fracturing parallel to the base of the flow. Quarry behind the hospital on the western side of Rarotonga. The location that the photograph was taken is shown below.

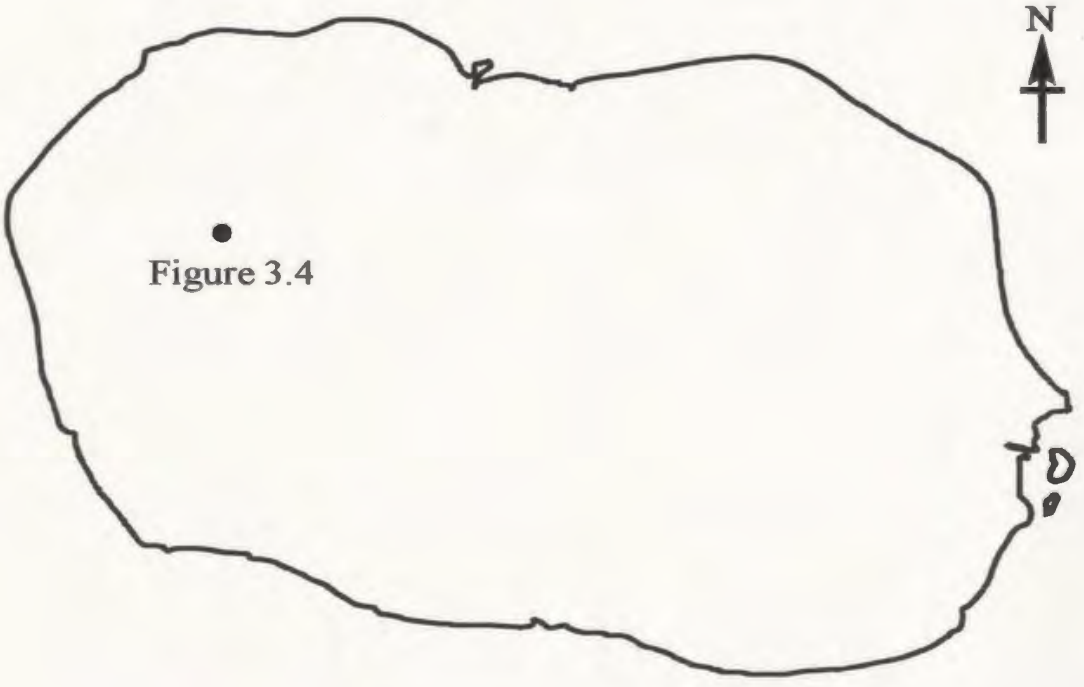

the dominant lithology of the mafic pyroclastics, forming many steep cliffs and ridges overlooking the Tukavaine and Avatiu valleys. These breccia units represent periods of violent volcanism and are generally one of the earlier eruptive sequences exposed on Rarotonga. However, pyroclastic eruptions occurred throughout the mafic phase of igneous activity. The clasts in the volcanic breccias comprise compositions which encompass the entire spectrum of mafic lithologies found on the island and range from 1cm up to 20cm in diameter.

Not all the breccia outcrops are of primary volcanic origin. Some breccias are formed by the reworking of pre-existent breccia units. This is shown by the dominance of clasts within these units that have weathered rims and a lower degree of angularity than those seen in the primary pyroclastic breccia units. These sedimentary breccia units inter-finger with the lava flows and pyroclastic beds.

In rare localities, thin deposits of volcanic ash are observed (Figure 3.5). These consist of several thin layers of a fine yellow ash, which invariably overlie lava flows and are in turn covered by subsequent flows of mafic lava. The ash beds are only found on the south-eastern side of the island. If the ash was erupted from the summit of the volcano this would suggest that the wind direction was from the north west at the time of eruption. This may indicate the direction of the then prevailing winds, but a significant number of ash beds would have to be recorded and examined in detail before a reliable assumption could be made.

The third type of pyroclastic unit found on Rarotonga is derived from a more localised eruptive style which resulted in the formation of small parasitic cones on the

Figure 3.5: Ash beds (light coloured unit) sandwiched between a lava flow and upper breccia unit. The location from which the photograph was taken is shown below.

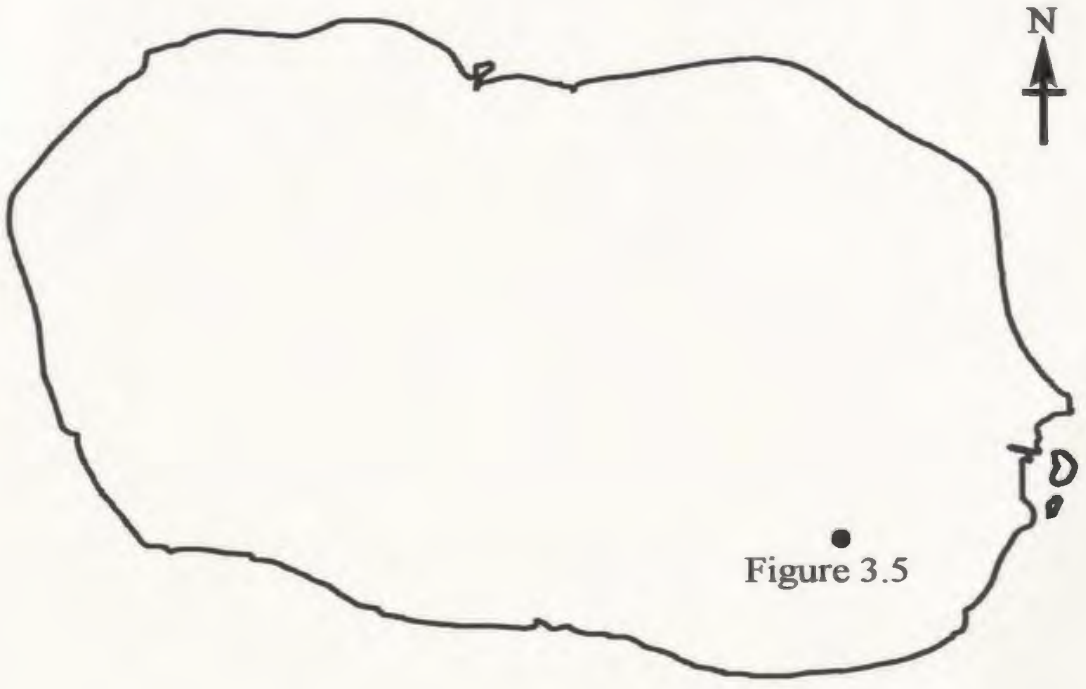

flanks of the main volcano. The best preserved example of such a parasitic cone is found in the head waters of Pue stream (Pue ash; Wood and Hay 1970). This cone displays all the features typical of a Strombolian cinder cone. It consists of spherical scoria bombs up to 5cm in diameter, in a matrix of fine grey ash. The eruptive centre of the cone is characterised by a lack of bedding and the occurrence of numerous dykes. On the flanks of the cone, further to the east of the centre, rough bedding becomes more prominent and dips seaward at approximately 15°E.

3.2.2 Felsic Rocks

Two styles of eruption of the more fractionated rocks are noted, that which formed a thick breccia that blanketed the earlier mafic eruptives, and relatively tranquil out-pourings of felsic lavas. There is no direct evidence for the temporal relationship between these pyroclastics and flows.

Felsic Pyroclastics

Felsic pyroclastic rocks are best represented by the breccia unit that forms the Maungatea Bluff in the central part of the island. This breccia is also found on the adjacent Maungatapu ridge where it forms narrow aiguilles up to 20 m high. It is light brown to grey in colour, and is made up of angular clasts up to 0.5 m in size of both felsic and mafic compsoitions (Figure 3.6). A rough horizontal stratification is caused by the

Figure 3.6: Felsic breccia with clasts of angular phonolite and basalt. The triangular coin has sides approximately 1 cm sides.. The location from which the photograph was taken is shown below.

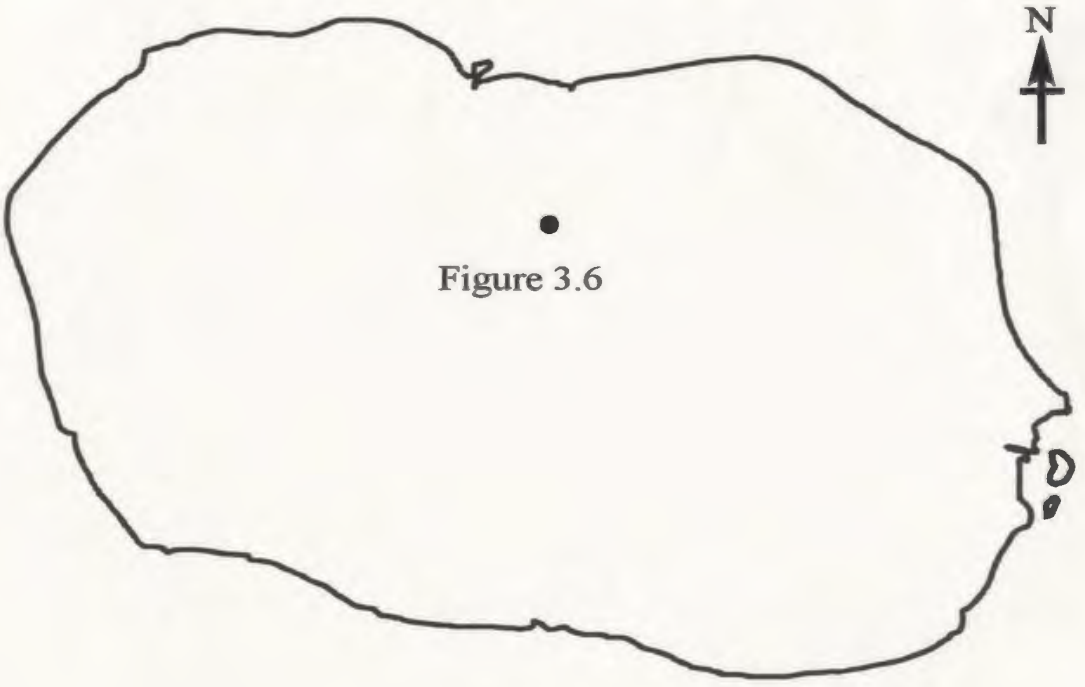

Figure 3.6

interbedding of breccia beds (up to 3m thick) and thin (less than 1m thick) beds of grey tuff. Individual beds are poorly sorted. The beds forming Maungatea bluff dip north between 5° and 10°, whereas along the Maungatapu ridge the beds are nearly horizontal and erosion patterns in the breccia appear to be controlled by vertical jointing; this results in spalling, which has reduced this once extensive unit to a few remnant pinnacles (Figure 3.7). Differential weathering of beds has produced irregular ledges along the cliff faces. The breccia overlies weathered basaltic breccia near the base of the Maungatapu ridge along a basal contact which is sharp and irregular.

Felsic Lava flows

The outcrop pattern of the phonolite lavas indicates that their lateral extent is limited and that they are located in four main areas; Muri Beach, Raemaru, Black Rock and Tuakata, and each of these is interpreted as a descrete flow event. At least one (Raemaru) exhibits multiple eruptions. The lavas are a dark green colour and flow banding occurs locally and is well developed within the Tuakata flow. The Tuakata flow overlies weathered mafic breccia units, but there is no evidence for the development of a paleosol. The two eruptive centres near the coast (Muri Beach and Black Rock) have flows which extend past the present shoreline.

The phonolite lavas appear to have erupted after the shield building stage was virtually complete. There is some evidence (see Chapter one) that there was a slight temporal overlap with the waning stages of mafic volcanism. However, there is abundant evidence that some of the flows erupted after a brief hiatus. The eruption of the Muri

Figure 3.7: Remnant pinnacles along Maungatapu Ridge. The upper photograph is taken from the south looking north, Ikurangi can be seen in the distance. The lower photograph is a close up of Youngs tooth.

flows on the south-east coast of the island diverted the middle section of the Avana stream from a normal radial south-east direction to the north-east. The Tuakata flow overlying weathered basaltic breccia also provides evidence for a hiatus after the eruption of the mafic rocks, although this could just be a local feature. Although both features suggest that the effects of erosional processes were well developed by the time of initiation of the phonolitic flows, it is impossible to assess the length of time necessary for the weathering of fresh basaltic rocks and the development of a radial stream pattern on the island because of uncertainties involved with rates of erosion in tropical climates.

3.3 Petrography of the Mafic Rocks

The mafic rocks that constitute most of the exposure on Rarotonga can be divided by their petrographic characteristics into ankaramites and basalts.

3.3.1 Ankaramites

The ankaramites are coarse grained porphyritic rocks containing large phenocrysts of pyroxene (>20% of total rock volume) with smaller subordinate olivine phenocrysts. The groundmass consists of prisms of pyroxene and laths of plagioclase, olivine, and magnetite. These phases are generally poikilitically enclosed by anhedral pink pyroxene. Using mineralogical characteristics, the ankaramites can be further

subdivided into two groups which will be referred to as type I and type II ankaramites.

Type I Ankaramites

The mineralogy of the type I ankaramites is relatively simple: titanaugites generally comprise approximately 30% of the total rock volume; olivine phenocryst abundances range from 3 to 11%; magnetite phenocrysts from 2 to 7%; and the groundmass ranges between 50 and 65% of the total rock volume (Figure 3.8 and Figure 3.9).

Titanaugites form large (up to 15mm) euhedral zoned phenocrysts. Titanaugite is characteristically pleochroic with α=β=pale brown and γ=violet; optical zoning is defined by a deepening of the pleochroic colours from core to rim. Accompanying this optical zoning is the occurrence of small magnetite crystals in the phenocryst margins that are arranged in clusters parallel to crystal growth (Figure 3.10). Crystal faces are generally well developed and the phenocrysts appear to be in equilibrium with the groundmass.

Olivine is the second major phenocryst phase. The crystals are smaller than the titanaugite phenocrysts, with a maximum size of 5mm. The larger phenocrysts are generally euhedral and do not exhibit any signs of alteration (Figure 3.11). In only one sample (R83) of the type I ankaramites is there extensive serpentinization of olivine (Figure 3.12).

Magnetite is the third phenocryst phase in the type I ankaramites. In some samples, magnetite can constitute as much as 7% of total rock volume (Figure 3.13).

Figure 3.8: Type I ankaramite sample. Coin has approximately 1cm sides.

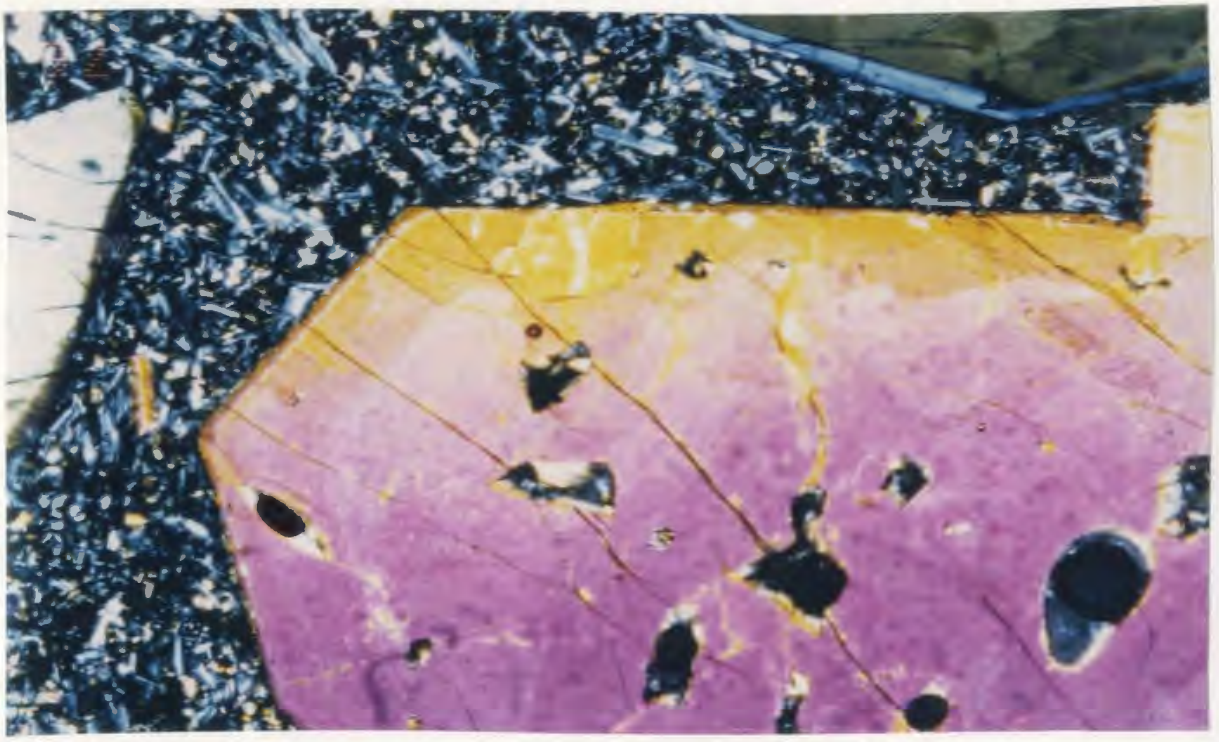

Figure 3.9: Euhedral pyroxene from the above sample under crossed nicols. Field of view is 2mm.

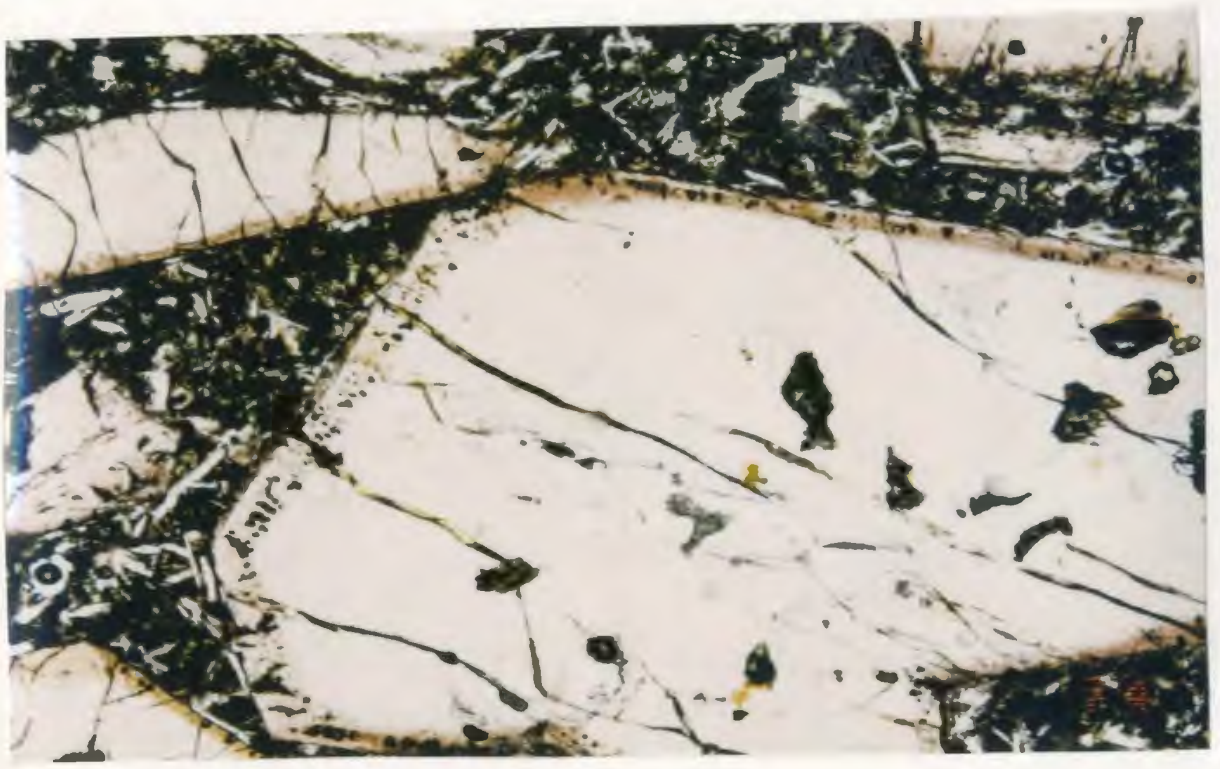

Figure 3.10: Titanaugite with magnetite intergrowths arranged in clusters parallel to crystal growth (R120). Plane polarized light. Field of view is 2mm.

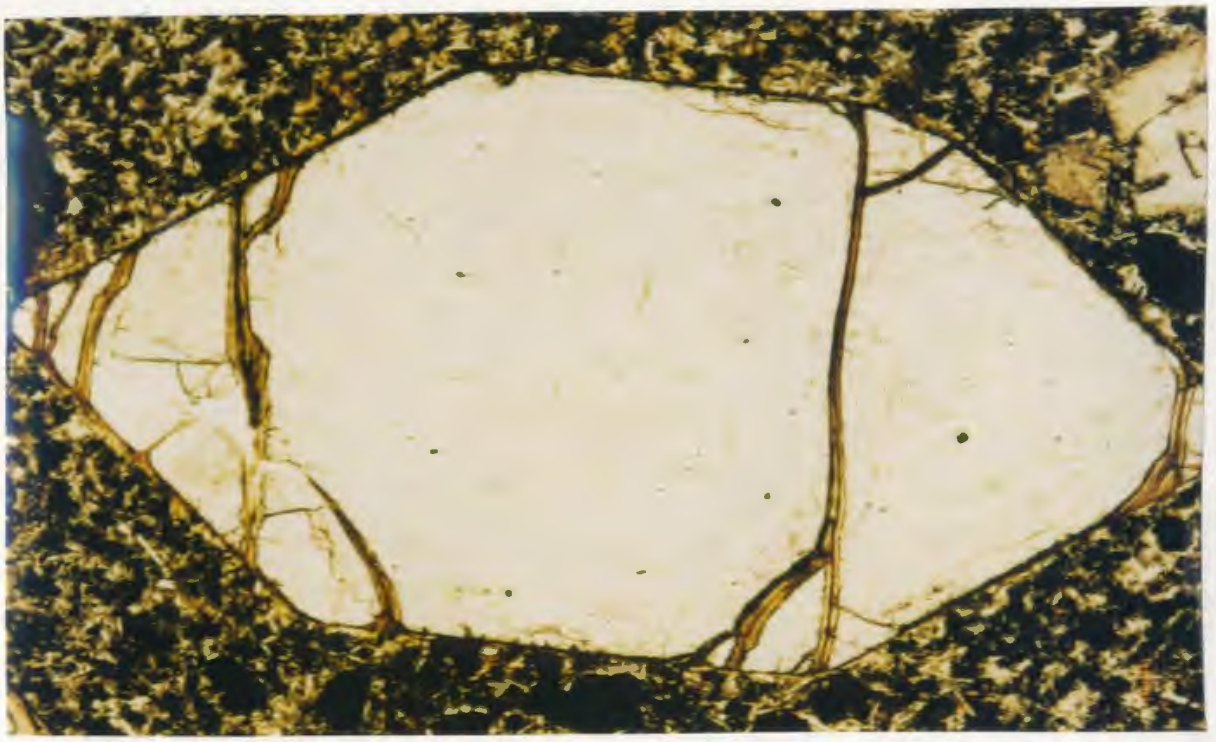

Figure 3.11: Euhedral olivine phenocryst. Plane polarized light (R82). Field of view is 2mm.

Figure 3.12: Olivine showing extensive serpentinization (R83). Crossed nicols. Field of view is 2mm

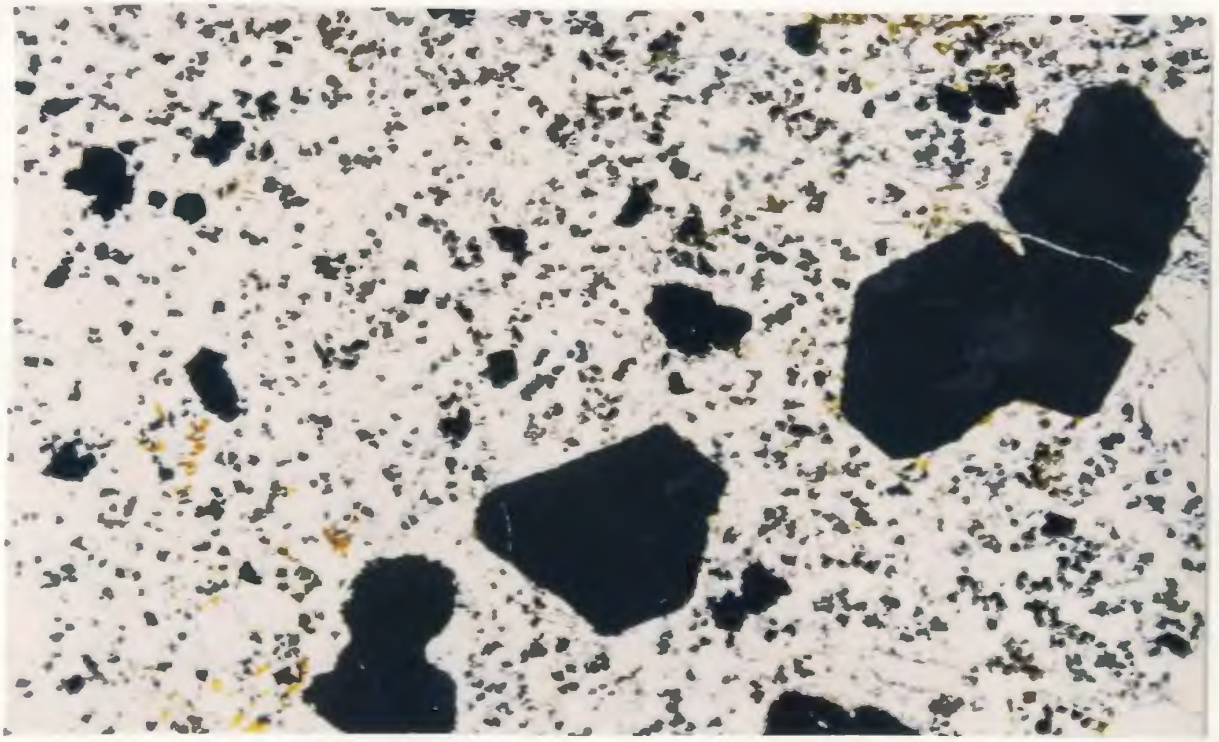

Figure 3.13: Abundant oxide phenocrysts in sample R35. Plane polarized light. Field of view is 2mm

Magnetites occur mainly as skeletal grains up to 2mm in size; they also occur as inclusions in pyroxene and olivine phenocrysts.

The groundmass in type I ankaramites consists of the above three phases along with small laths of feldspar. These phases are poikilitically enclosed by anhedral titanaugite which is similar to the rims of the larger pyroxene phenocrysts in having a dark pink colour. The groundmass shows no visible evidence of alteration. Even in sample (R83) with extensive serpentinization of the olivine phenocrysts, the groundmass is relatively unaltered.

Type II Ankaramites

Type II ankaramites have a similar texture and grain size to the type I ankaramites. The features that distinguish type II ankaramites from the type I ankaramites are: pyroxene composition and morphology; the degree of olivine alteration; the relative abundance of magnetite phenocrysts. Another notable feature of the type II ankaramites is the occurrence of rare xenoliths. Lherzolite dominates the xenolith assemblage, being composed of olivine, clinopyroxene and/or orthopyroxene and rare spinel. This mineralogy suggests that the xenoliths are derived from the mantle.

Two types of pyroxenes are present in the type II ankaramites, strongly pleochroic titanaugites (α=β=pale brown and γ=violet), and pale greenish diopside-augites. The titanaugites and diopside-augites are similar in size to the titanaugites of type I ankaramites and are evenly distributed. However, unlike in the titanaugites of the type I ankaramites, the pyroxenes in this group exhibit irregular margins (Figure 3.14)

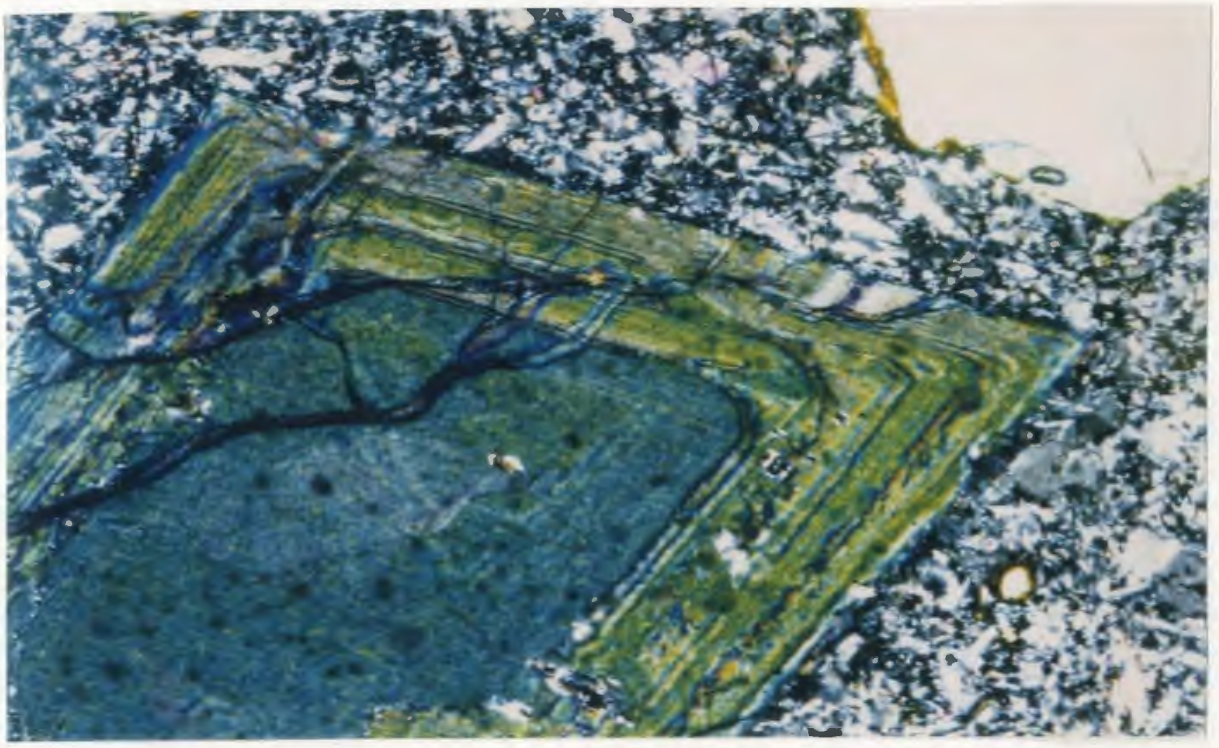

Figure 3.16: Pyroxene phenocryst with diopside-augite core mantled by zoned titanaugite (R94). Plane polarized light. Field of view is 2mm.

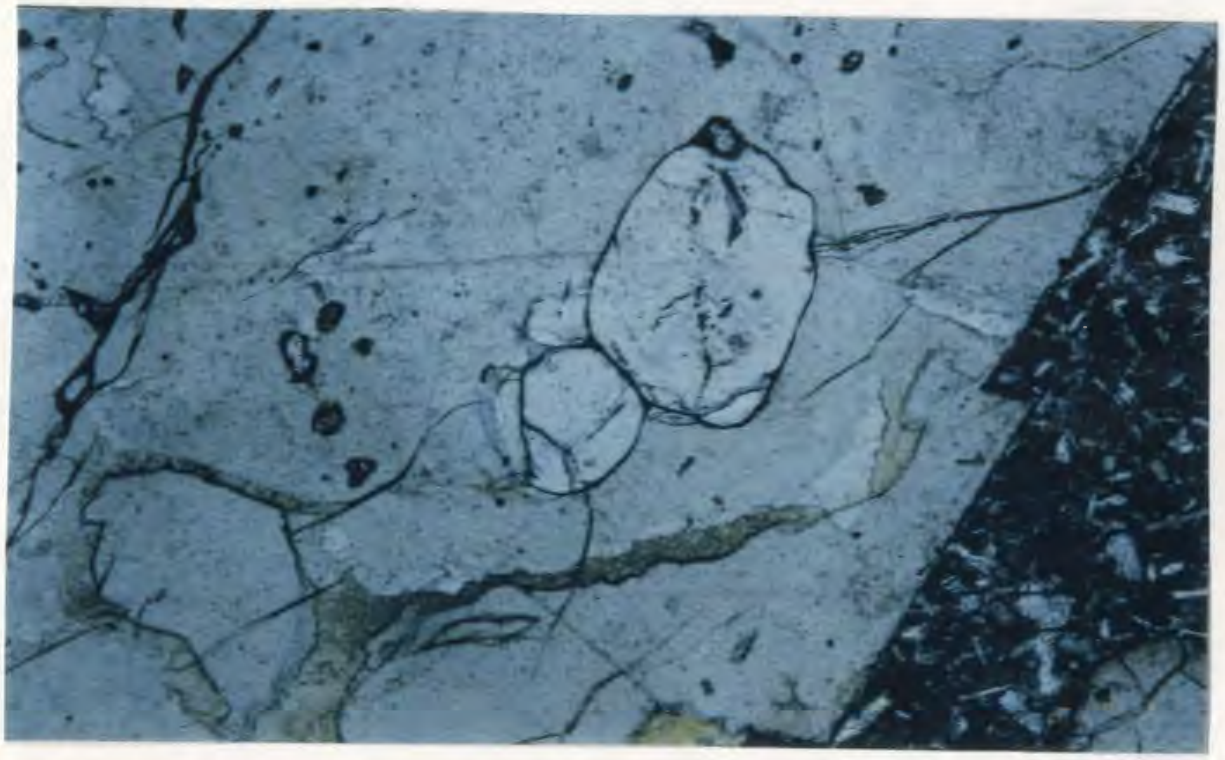

Figure 3.17: Photomicrograph of anhedral olivines in pyroxene phenocryst (R40) Plane polarized light. Field of view is 1mm.

and some phenocrysts have a sponge-like texture (Figure 3.15) which is attributed to resorption.

There is a rare third group of pyroxene phenocrysts, *i.e.*, those with diopside-augite cores mantled by titanaugite rims (Figure 3.16). The rims do not appear to be quench features as regular optical zoning can be observed, a feature that is unlikely to occur during quenching. The cores of these phenocrysts are generally rounded to angular, suggesting that a variety of histories may be revealed

Olivine occurs as 3-5mm subhedral phenocrysts and as small anhedral grains in the cores of some large clinopyroxene crystals (Figure 3.17). As with the pyroxene phenocrysts, olivines display irregular crystal faces (Figure 3.18) and have sponge-like textures. Replacement of olivine by iddingsite is more prevalent within this type of ankaramites. In some instances total replacement of all the olivine phenocrysts within an individual sample has occurred..

Unlike its occurrence in type I ankaramites, magnetite only occurs as a minor groundmass phase, not a major phenocryst phase.

3.3.2 Basalts

The basalts are generally finer grained than the ankaramites and contain abundant feldspar laths, together with augite and olivine phenocrysts. They have similar mineral assemblages to the ankaramites (Figure 3.19) but are texturally and modally distinct. They are dominated by feldspar laths (< 1mm) with subordinate pyroxene phenocrysts (<

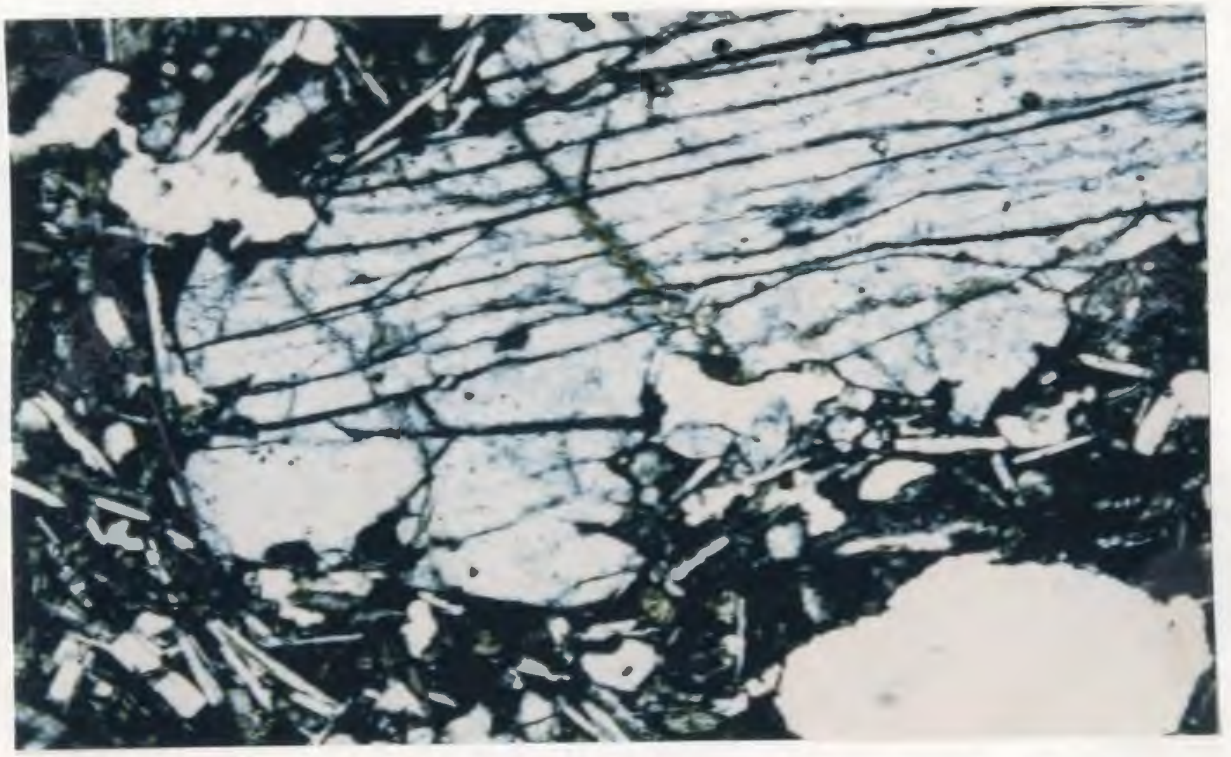

Figure 3.14: Pyroxene phenocryst with irregular margins (R42). Plane polarized light. Field of view is 2mm.

Figure 3.15: Photomicrograph of pyroxene with spong-like texture (R102). Plane polarized light. Field of view is 1mm.

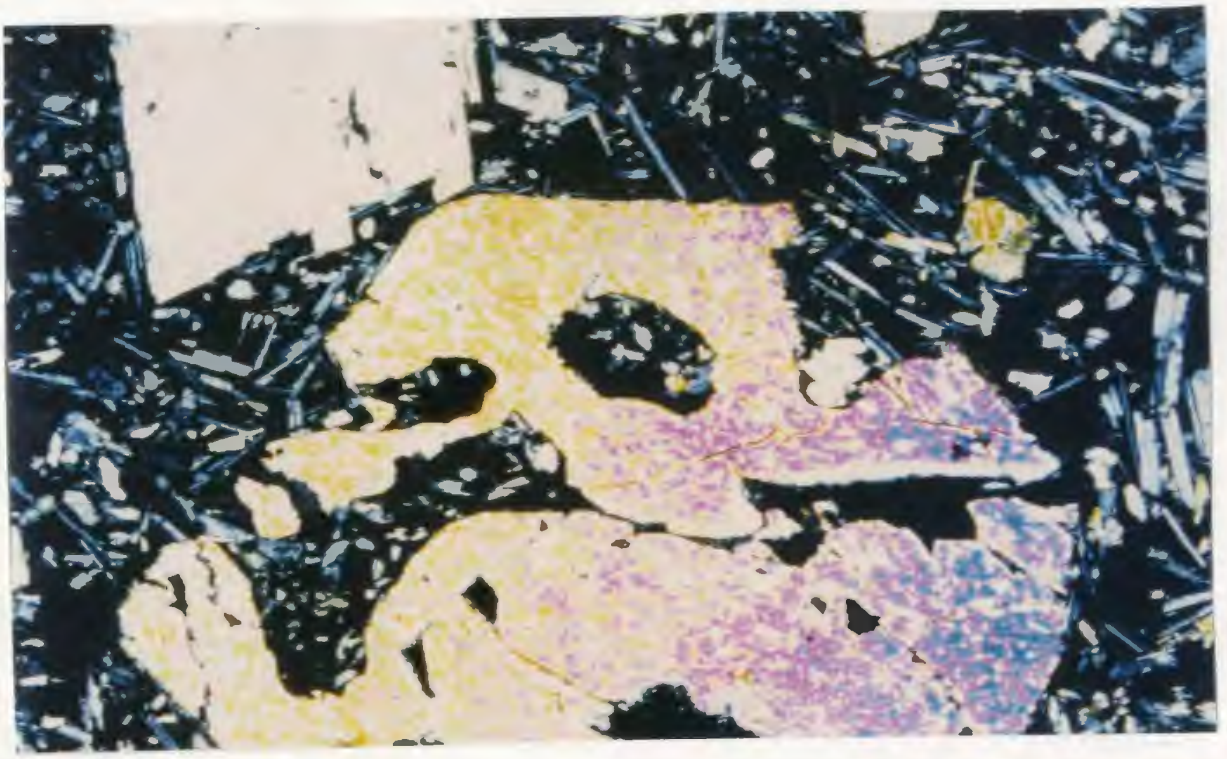

Figure 3.18: Photomicrograph of olivine phenocryst with irregular margins (R42). Crossed nicols. Field of view is 2mm

Figure 3.19: Photomicrograph of basalt (R78). Crossed nicols. Field of view is 2mm.

2mm) and rare olivine micro-phenocrysts. The alignment of plagioclase laths gives these rocks a predominant trachytic texture.

The division of the basalts into two types based on the composition of their pyroxene phenocrysts is more equivocal than the division of the ankaramites; this is in part due to the paucity of phenocrysts within the basalts. Titanaugite is the most common pyroxene phase within the basalts. However, in some basalts, titanaugites and diopside-augites can be identified, suggesting that they can be divided along similar lines to the ankaramites.

Olivine is a rare phenocryst phase in the basalts, but one sample can be classed petrographically as an oceanite with olivine the only phenocryst phase as well as a major phase within the groundmass assemblage. Magnetite can be abundant as both phenocrysts and as a groundmass phase. In sample R-56, brown pleochroic kaersutite crystals occur (Figures 3.20 and 3.21). These are found as small euhedral crystals in the groundmass (< 0.5mm) or larger phenocrysts which are typically greater than 1mm in size.

Glomerocrysts are present in most basalts and can be quite common in some samples. The glomerocrysts range in size from a few millimetres up to 10mm. In a few samples high abundances of large glomerocrysts result in basalts that have a similar appearance in hand sample to the ankaramites. The glomerocrysts are composed principally of titanaugite laths (up to 3mm), and plagioclase laths (1-2mm). Small anhedral olivine grains can also be found within the augites in glomerocrysts. In many

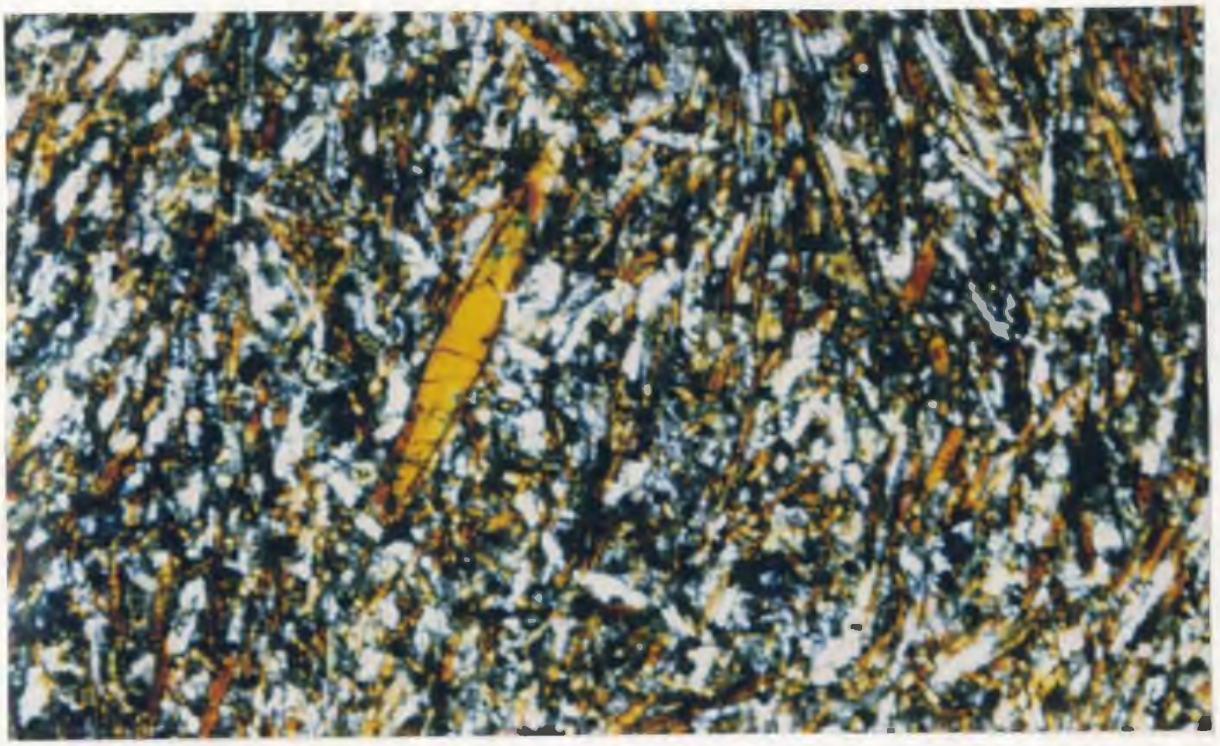

Figure 3.20: Abundant kaersutite phenocrysts in sample R56. Crossed nicols. Field of view is 1mm.

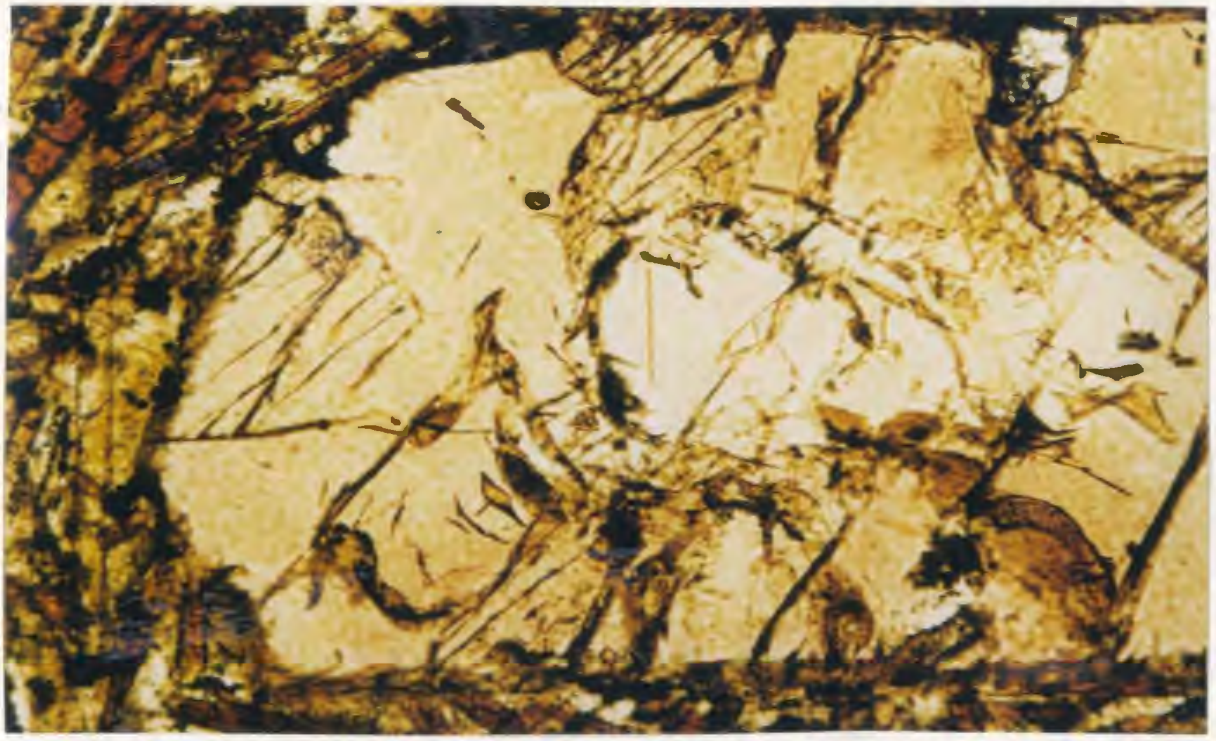

Figure 3.21: Pyroxene phenocryst in a basalt with a diopside-augite core mantled by titanaugite (R56). Plane polarized light. Field of view is 2mm.

instances the trachytic texture of the groundmass bends around the glomerocrysts.

The groundmass of the basalts is generally microcrystalline to cryptocrystalline. Where mineral phases can be identified, they are generally feldspars, titanaugites and opaques.

3.4 Petrography of the Felsic Rocks

There are two types of felsic rock found on Rarotonga; a light grey medium-grained trachytic rock found as clasts in breccia beds and a dark green fine-grained rock which forms lava flows.

3.4.1 Felsic Breccias

The felsic clasts in the breccias are all fine- to medium-grained ranging from microcrystalline to slightly porphyritic (Figures 3.22 and 3.23). They have a distinctive trachytic texture formed by abundant sub-parallel laths of anorthoclase. Minor amounts of green aegirine phenocrysts and euhedral oxides are ubiquitous. Rare phenocrysts of nepheline and sodalite can also be found. The felsic clasts within the breccia unit are thus classified as phonolites (Figure 3.24).

Anorthoclase phenocrysts dominate the mineral assemblage of these rocks. In the coarser samples two populations of anorthoclase crystals occur, phenocrysts that are greater than 0.5mm and microcrysts less than 0.1mm. Many larger feldspar phenocrysts

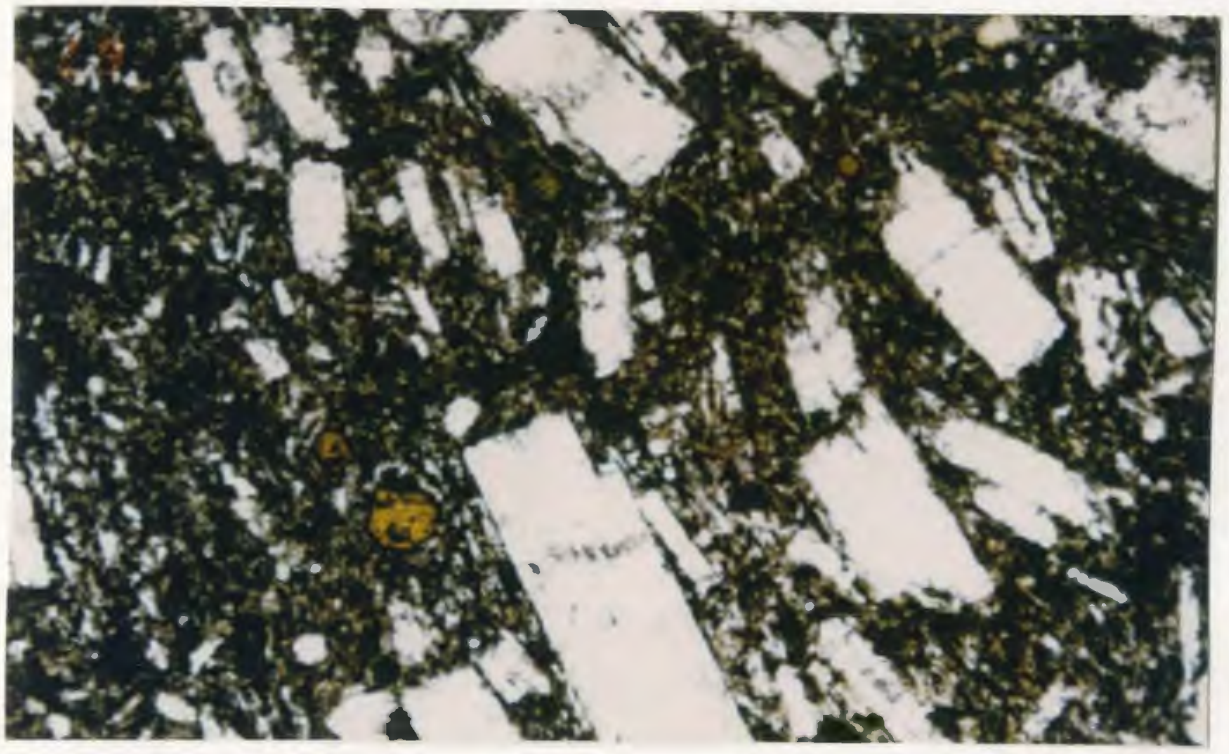

Figure 3.22: Phonolite clast from breccia (R122). Plane polarized light. Field of view is 2mm.

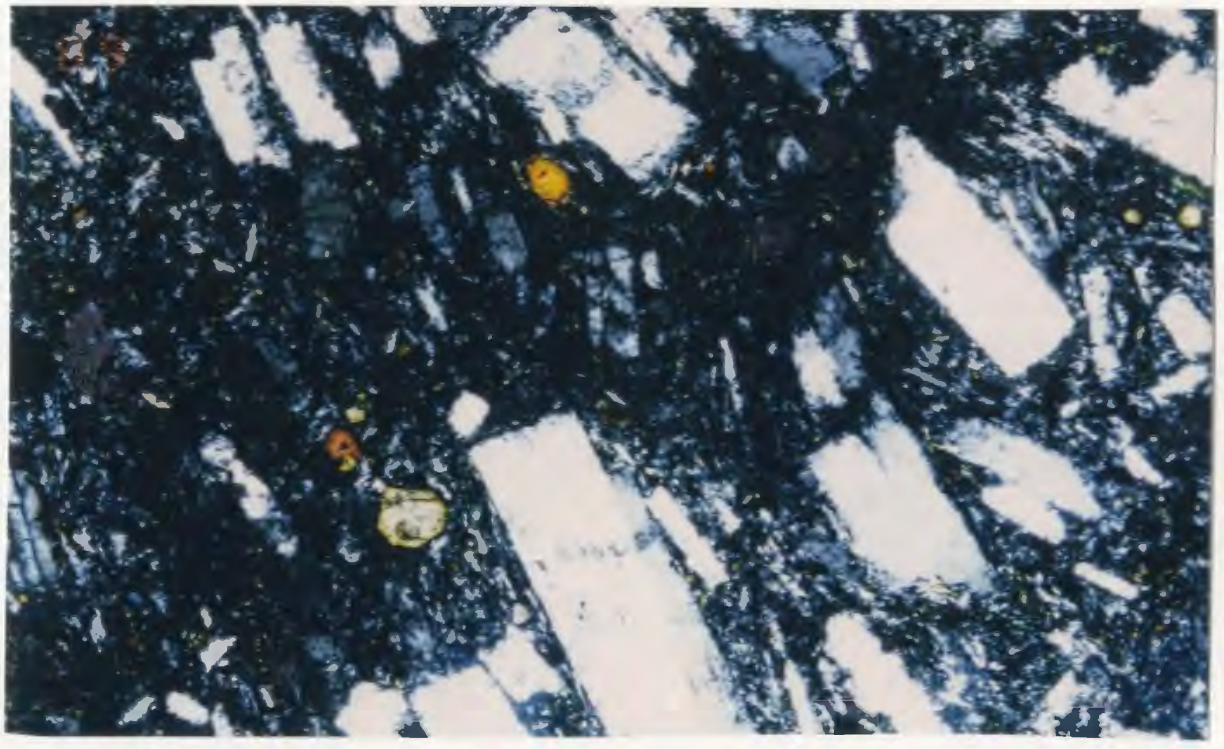

Figure 3.23: The above sample but under crossed nicols. Field of view is 2mm.

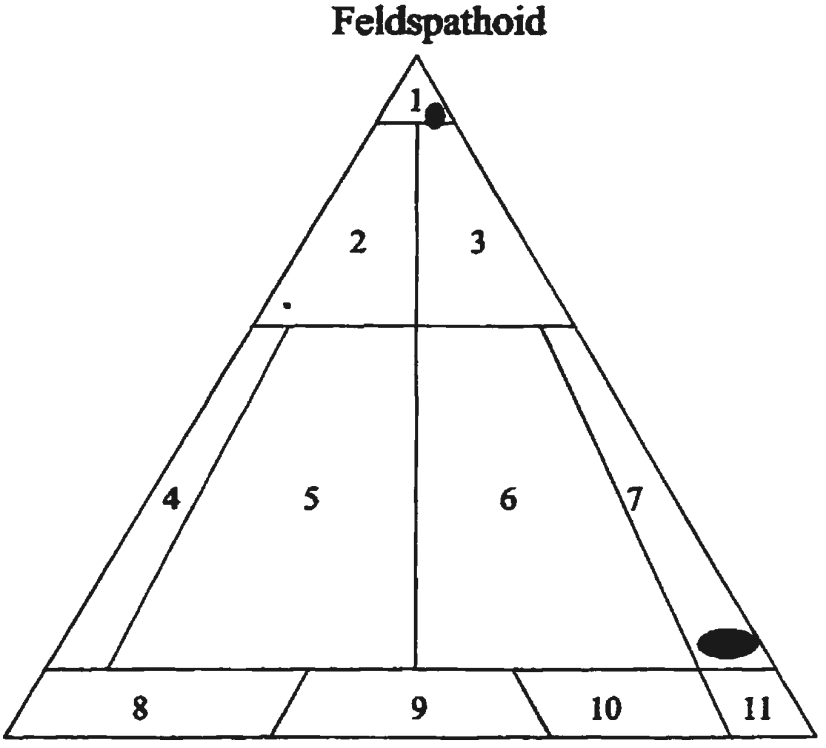

1. Foidite
2. tephritic foidite
3. phonolitic foidite
4. basanite (ol> 10%), tephrite (ol < 10%)
5. phonolitic basanite (ol > 10%), phonolitic tephrite (ol < 10%)
6. tephritic phonolite
7. phonolite
8. basalt andesite
9. foid-bearing latite
10. foid-bearing trachyte
11. foid-bearing alkali feldspar trachyte

Figure 3.24: Classification and nomenclature of volcanic rocks containing modal plagioclase, alkali feldspar and feldspathoids based on the IUGS Sub-commission on the Systematics of Igneous rocks (1989). Estimated modal abundances of breccias shown by blue field, lavas by red field.

have cores of corroded oligoclase mantled by alkali feldspar (Figure 3.25). When these phenocrysts are examined using back scattered electron imaging, multiple growth stages can be observed (Figure 3.26). The outer zones display fine laminae and are bounded by sharp crystal faces. The inner zones, differentiated by their contrast in atomic mass on the back scattered electron image, lack the fine scale concentric laminations observed in the last stage of phenocryst growth and have irregular boundaries.

3.4.2 Felsic Lava Flows

These rocks can be classified as foidal phonolites (Figure 3.24). The flows are all fine-grained, characterised by the presence of abundant nepheline and sodalite phenocrysts (Figures 3.27 and Figure 3.28). These phenocrysts are < 0.2mm in size. In addition, rare dark green aegirine phenocrysts (0.5mm) are found in varying abundance in all the flows. The phenocrysts are surrounded by a groundmass of microcrystalline aegirine, alkali feldspars, sodalite, nepheline and interstitial analcime.

The nepheline generally occurs as euhedral hexagonal crystals. Microlite aegirine needles are commonly found poikilitically enclosed by the nepheline phenocrysts. Some of the larger nepheline phenocrysts have sodalite cores.

There is a sympathetic decrease in modal aegirine as the modal abundance of nepheline and sodalite increases. The Raemaru and Black Rock flows have the highest concentrations of nepheline and sodalite, while the Tuakata flows have the lowest modal amounts of these minerals and the highest modal amounts of aegirine.

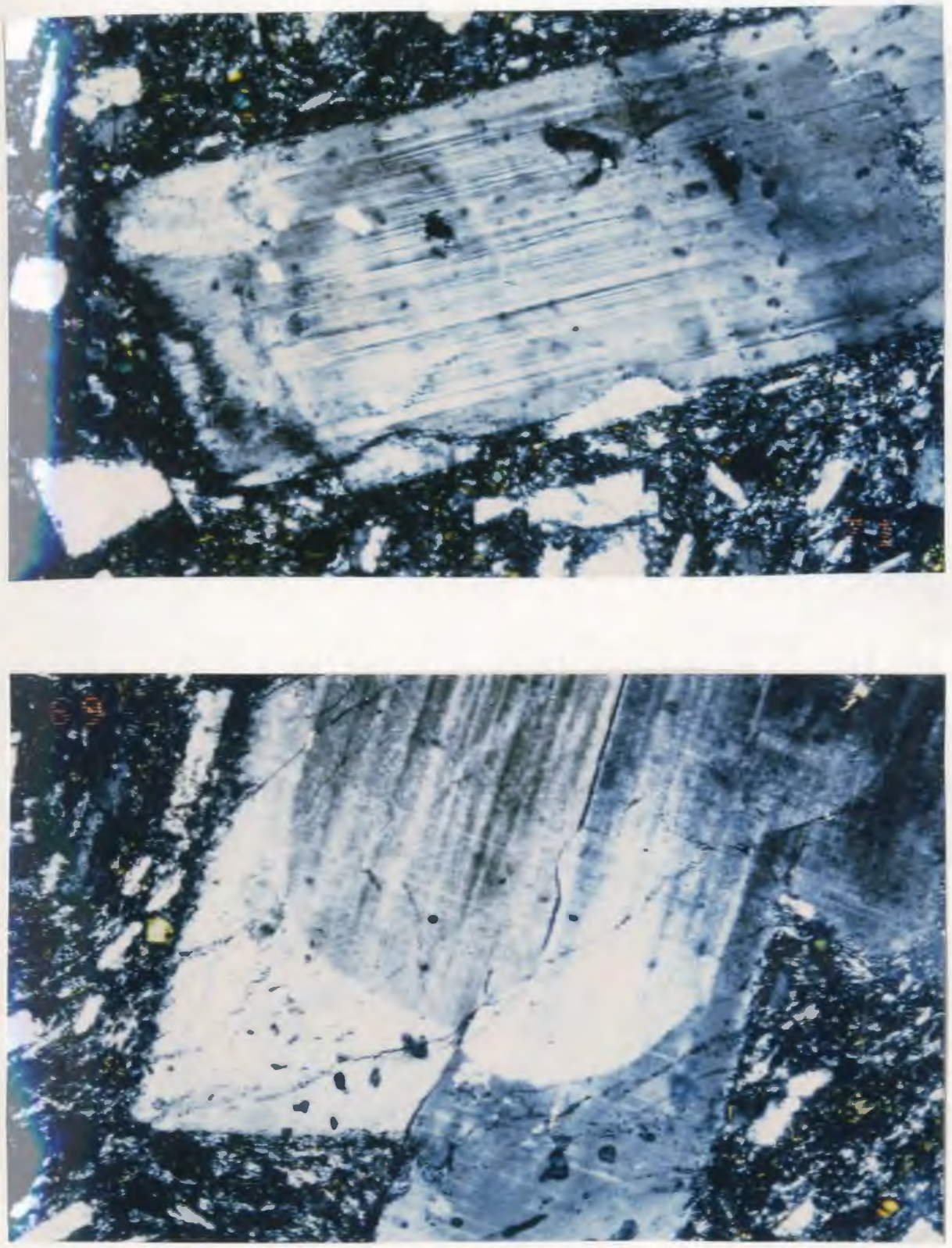

Figure 3.25: Feldspar phenocryst with an oligioclase core mantled by anorthoclase (R122). Crossed Nicols. Field of view is 2mm.

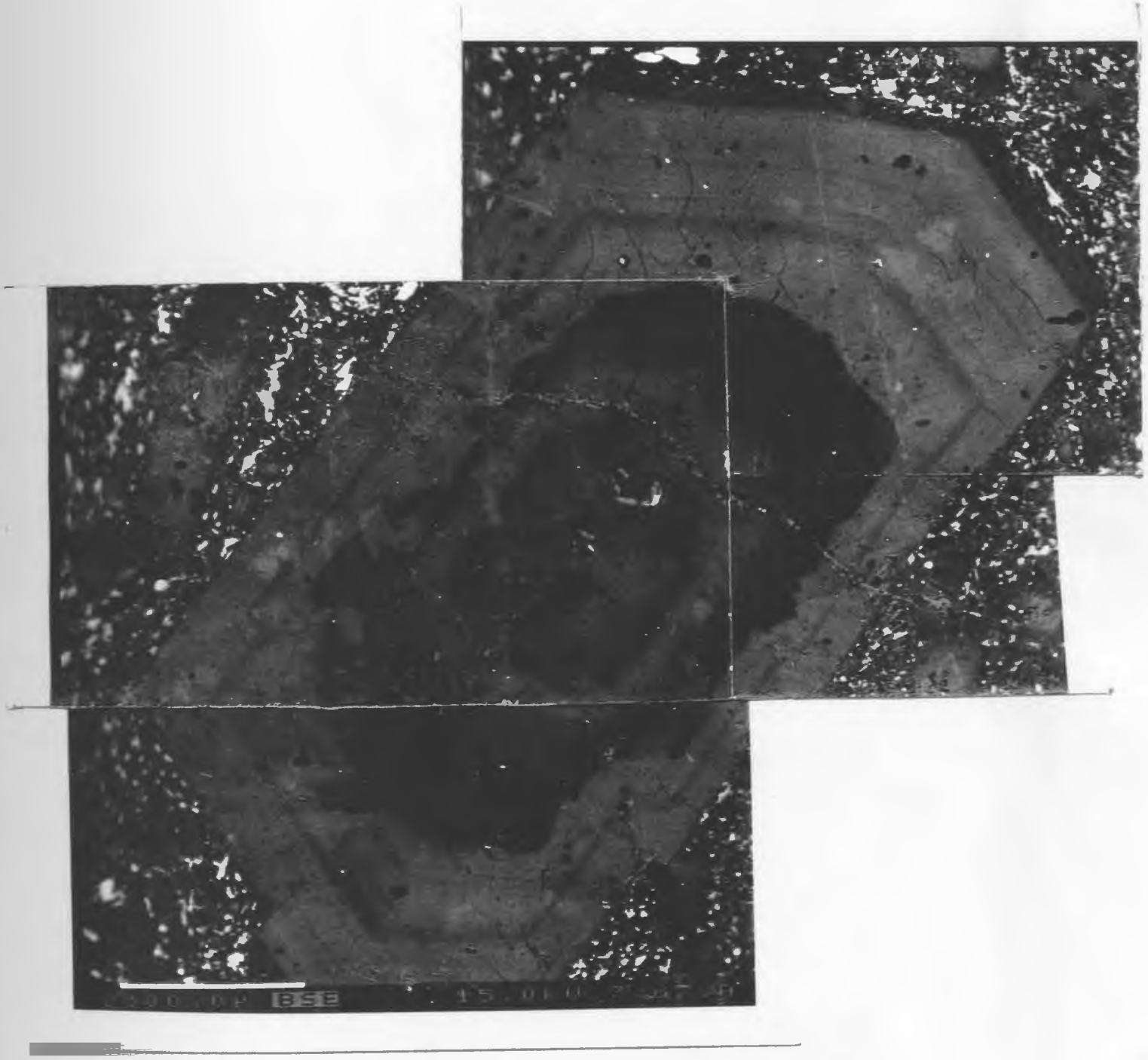

Figure 3.26: Back scattered electron image of a feldspar phenocryst in sample R107. The white bar is 500 microns.

Figure 3.27: Phenocryst poor foidal phonolite (R25). Crossed nicols. Field of view is 2mm

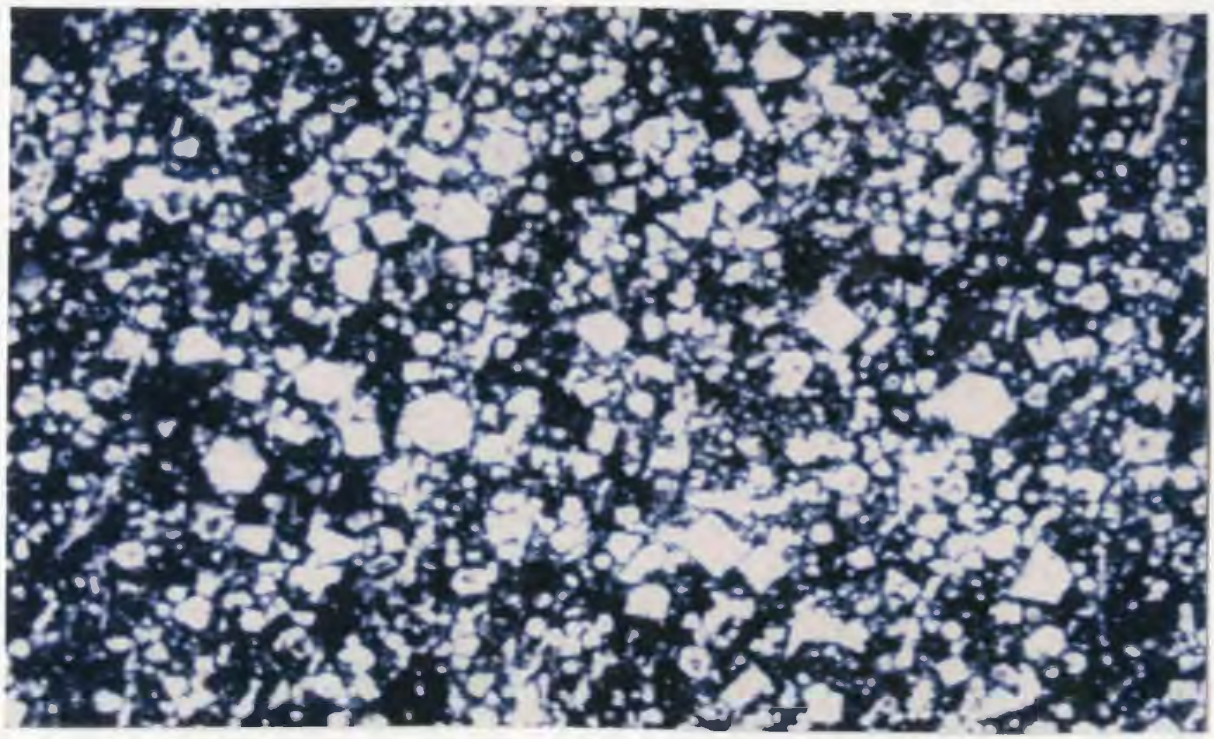

Figure 3.28: Relitively phenocryst rich foidal phonolite (R38). Crossed nicols. Field of view 2mm.

3.5 Interpretation

Mafic rocks

The petrography suggests that at least two distinct parental magmas were present during the formation of Rarotonga that resulted in the eruption of two petrographically distinct types of lava. The type I ankaramites formed from a magma in which titanaugite was crystallising, while the type II ankaramites also contain diopside-augite phenocrysts.

The abundance of phenocryst phases in some ankaramites leads to the suggestion that these rocks may have formed by the partial accumulation of crystals. Petrographic evidence therefore suggests that olivine and pyroxene accumulation dominated crystal fractionation processes. Within the type I ankaramites the crystallisation of magnetite was also an important facet of the petrogenesis of daughter magmas. In both groups, as the magmas evolved, kaersutite began to crystallise.

The irregular crystal faces and sponge-like texture of the olivine and pyroxene phenocrysts in the ankaramites are interpreted as the result of resorption due to disequilibrium. The corroded cores of some pyroxene phenocrysts suggest that there was a stage in which they were not in equilibrium with the melt and were partially resorbed before a second stage of pyroxene growth occurred. This second stage of pyroxene crystallisation has a titanaugite composition.

There are three possibilities for the occurrence of the two types of pyroxene, titanaugites and diopside-augites, in the type II ankaramites:

i. one of the pyroxenes represents xenocrysts derived from the wall rock traversed by the host magma of the second; or

ii. each type was derived from a different magma, which subsequently mixed; or

iii. the two types of pyroxene are cognate but formed under different pressure-temperature regimes or in a chemically stratified magma chamber.

Petrologically there is no difference between i. and ii. which essentially represent assimilation and magma mixing respectively. However, if one of the pyroxene phases occurs as xenocrysts derived from the wall rocks traversed by the host magma, it would be expected that polymineralic xenoliths would be more common and this is not the case. In only rare instances are polymineralic xenoliths found and these are invariably ultramafic xenoliths derived from the mantle and have no similarities to the mineralogy of the mafic rocks found on Rarotonga. If the features observed in the mafic rocks were the result of magma mixing, this leads to the concept of two contemporaneous chemically distinct magmas. The question arises: are these two magmas formed from the same primary magma and, therefore, represent periodic replenishment processes, or do the magmas represent two separate fractionation lineages from different primary magmas?

In case iii., for the two pyroxenes to be cognate requires a model in which the chemical and/or physical conditions of the magma change. This can be achieved through several possible processes. The chemical change could be due to a change in oxygen fugacity caused by simultaneous precipitation of magnetite. Crystal fractionation will also affect the overall chemistry and physical properties of the magma. *i.e.*, temperature

increases due to latent heat of crystallisation. The temperature and chemistry of the magma can also be modified by magma recharge.

Another possibility is a compositionally zoned magma chamber or a magma chamber in which large temperature gradients existed. In such a model the titanaugites and diopside-augites crystallise in separate parts of the same magma chamber. The disequilibrium features would, therefore, be caused by the movement of phenocrysts between these two environments, either by crystal settling or by convection within the magma chamber. If convection was at such a scale as to mobilise phenocryst phases, it is hard to envisage chemical or physical gradients remaining as convection would homogenise the magma chamber. Therefore, crystal settling is the only possible mechanism available to transport phenocrysts from one part of the magma chamber to another. To account for the corroded cores of some phenocrysts, it could be suggested that these phenocrysts passed through a section of the magma chamber in which they underwent a period of resorption before resuming a second stage of growth. This seems a highly implausible situation, as the two sections of a magma chamber that are within the stability field for pyroxene need to be separated by a zone in which the magma is above the pyroxene liquidus.

A third possibility for the resorption of the cores is rapid upward movement resulting in the magma being temporally above the pyroxene liquidus at low pressures. At this stage resorption of the pyroxene phenocrysts occurred resulting in the irregular corroded outline of the cores. As the magma cooled at these higher levels the magma dropped below the pyroxene liquidus and further crystallisation of radially zoned

pyroxene occurred.

Given the available petrographic evidence it is not possible to discount any of the above magma chamber models. The chemical composition of these pyroxene phases may help to support or discount assimilation or magma mixing. This will be examined in the next chapter.

Felsic rocks

The close spatial and temporal relationship between the mafic rocks and felsic rocks leads to the suggestion that they may be petrologically related. However, this relationship is not entirely unequivocal due the absence of rocks of intermediate composition. The foidal phonolites and phonolites each have distinctive mineralogies that suggest that they formed from different parental magmas. They also have radically different styles of eruption that suggest that the rheological properties of these two felsic magmas were dissimilar. This could be due to a number of differences between the two magmas which can result in different viscosity: chemical *e.g.*, differences in major compositions (*e.g.*, SiO_2, Al_2O_3 and/or alkalis) or volatiles (*e.g.*, H_2O, CO_2 etc.); or physical properties *e.g.*, pressure, temperature or degree of crystallinity.

The presence of optical zoning in feldspar phenocrysts of the phonolite breccia, with the interior zones exhibiting corroded margins, indicates that these phenocrysts formed in a dynamic system in which cyclic growth and resorption occurred. Counting the major zones shows that there are at least six stages of phenocryst growth (Figure 3.26). Each period of growth was followed by a period of resorption that resulted in the

irregular corroded outlines of the inner zones. These inner zones do not have the fine scale radial zoning observed in the outermost zone (the latest stage of growth), which suggests that during resorption the fine scale growth zones were destroyed.

3.6 Conclusions

From the field relationships and petrography of the igneous rocks found on Rarotonga the following conclusions can be drawn:

i. The topography of Rarotonga is controlled by two processes, the initial formation of the island by volcanic activity and subsequent modifications to the volcanic edifice by erosion;

ii. There are four major igneous rock types found on Rarotonga: two mafic types (containing both ankaramites and basalts), felsic lavas (foidal phonolites) and felsic breccias (phonolites);

iii. The two mafic types are distinguished by the presence of diopside-augites phenocrysts, poly-phase pyroxene phenocrysts (POPPs) and a greater degree of alteration of olivine phenocrysts in the type II mafic rocks;

iv. No temporal or spatial difference exists between the two types of mafic rocks with both types being ubiquitous over the entire island;

v. The felsic rocks appear to be the youngest rocks, with the foidal phonolite lavas occurring on the flanks of the island, while the phonolite breccia is concentrated in the centre.

Four important questions remain about the petrogenesis of Rarotonga, that cannot be resolved from the field relations and petrography of the rocks exposed on the island at present. These can be listed as follows:

i. The relationship between the diopside-augites and titanaugites in the type II ankaramites: *e.g.*, are the diopside-augite and titanaugite pyroxene phases crystallised from the same magma? If so, are they the result of processes internal to a stationary magma chamber or the result of upward movement of the magma through the mantle and crust? If the diopside-augites and titanaugites are not crystallised from the same magma, were the primary magmas that eventually produced the pyroxenes chemically distinct?

ii. The chemical characteristics of the type I and type II mafic rocks: *e.g.*, what is the relationship between the type I and type II ankaramites? Are petrographical differences reflected in the chemistry of the mafic rocks? What is the composition of their primary magmas? What processes were involved in their formation and how did crystal fractionation and possibly magma mixing affect their petrologic line of descent?

iii. The relationship between the felsic rocks and the mafic rocks: *e.g.*, how are the two suites of felsic rocks, the phonolites and foidal phonolites, related and what is their relationship to the mafic rocks? and

iv. Finally, what is the nature of the underlying mantle that produced the primary

magma(s)?

These questions will be addressed in the following chapters, where the chemistry of the mineral phases and the whole rock chemistry will be examined in detail.

Chapter Four

Geochemistry

"Measure what can be measured, and make measurable what cannot be measured."

Galileo Galilei (1564-1642)

4.1 Introduction

The aim of this chapter is to document the whole rock and mineral chemistry of the igneous rocks from Rarotonga. Each data set will be described quantitatively and then subjected to a more interpretative and qualitative discussion. The whole rock chemistry will be summarised first, followed by the mineral chemistry. Whole rock chemical analyses are presented in Appendices 2. Mineral chemical analyses are presented in Appendices 3 and 4 respectively.

4.2 Whole-Rock Chemistry

Major elements and some trace elements (Ba, Rb, Sr, Pb, Th, U, Zr, Nb, Y, La, Ce, Sc, V, Cr, Ni, Cu, Zn, Ga) were analysed by X-ray fluorescence spectrometry. Other

trace elements (Cs, Li, Nb, Hf) and REE were analysed by ICP-MS. Radiogenic isotope ratios ($^{143}Nd/^{144}Nd$ and $^{87}Sr/^{86}Sr$) were determined by thermal ionisation mass spectrometry on selected samples of the mafic rocks, phonolites and foidal phonolites. The procedures for sample preparation, precision, accuracy and sensitivity of the different analytical methods used are given in Appendix 2.

4.2.1 Geochemical Classification of Rocks

All the Rarotonga rocks lie along a strongly undersaturated compositional trend on an alkali versus silica diagram (Figure 4.1). The rocks are classified according to the total alkali-silica (TAS) classification of Le Bas et al. (1986), in which the cone-building basaltic rocks are picritic basalts, basalts and basanites (Figure 4.1), and the felsic rocks are chemically classified as foidial phonolites and phonolites. The evolved rocks (phonolites and foidal phonolites) lie on an extension of the trend exhibited by the mafic rocks on this diagram.

The mafic rocks can be divided into two types based on silica content; a low silica (< 45 wt. %) and a high silica type (Figure 4.1). The low silica type corresponds to the type I rocks described in Chapter two. In the relatively high silica type (SiO_2 > 45 wt. %), both titanaugites and diopside-augite phenocrysts occur. These are the type II rocks described in Chapter two. The low silica rocks are all nepheline normative (~2.5 to 35 % Ne) and the more fractionated type I are leucite normative (~1 to 16 % Lc). The high silica rocks are not as undersaturated with respect to silica, having normative

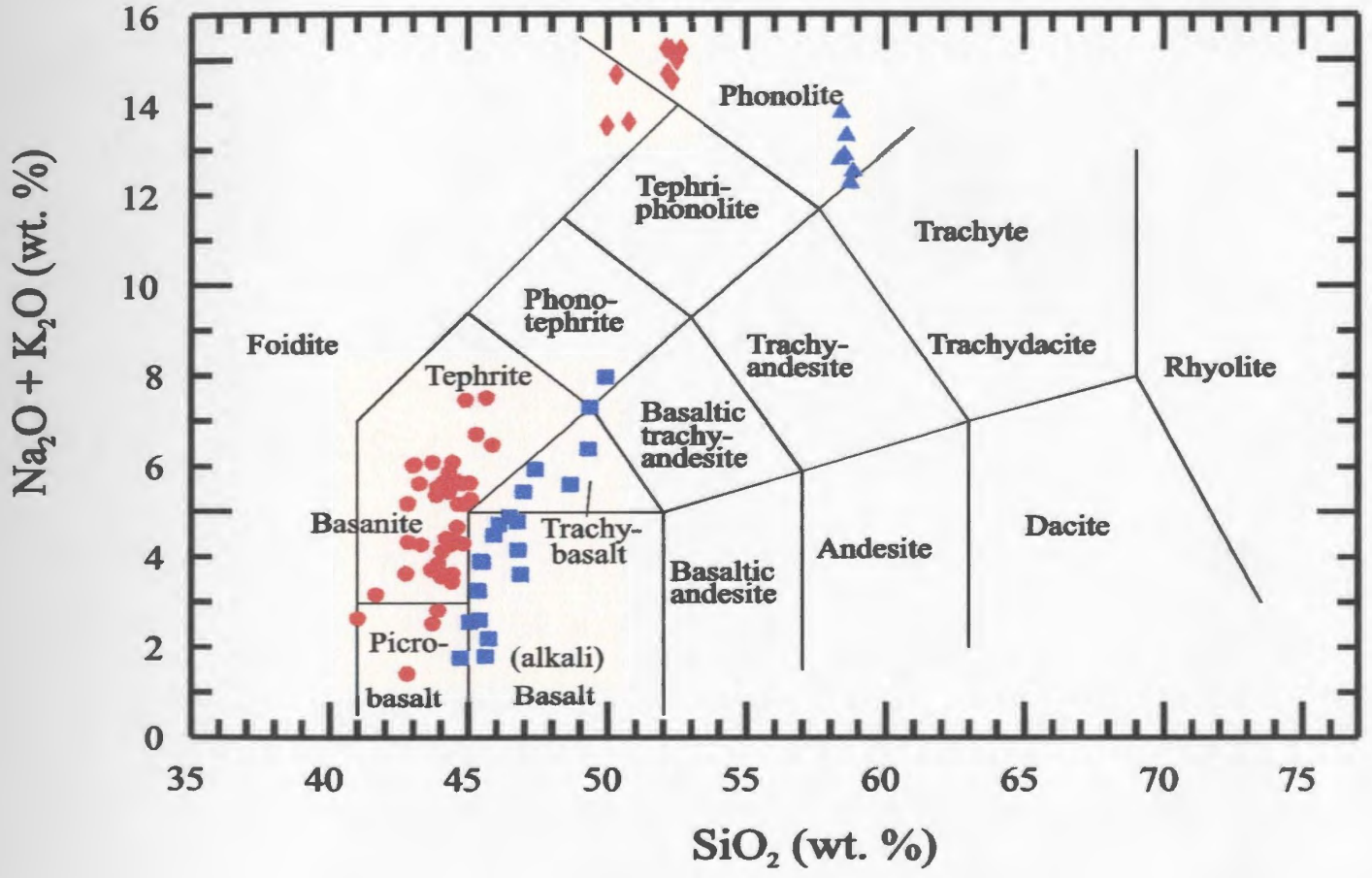

Figure 4.1: The chemical classification and nomenclature of volcanic rocks on Rarotonga using the total alkalis versus silica (TAS) diagram of Le Bas et al. (1986). Red circles - type I rocks; blue squares - type II rocks; red diamonds - foidal phonolite rocks; blue triangles - phonolites

nepheline ranging from 0 to ~9 %. Using the amount of normative nepheline, the type I rocks are classified as nephelinites (>15% Ne), basanites (5 %< Ne <15 %) alkali basalts (<5 % Ne), while the type II rocks are alkali basalts.

4.2.2 Major and Selected Trace Elements

Mafic Rocks

When the major elements are compared with MgO (Figure 4.2) the division of the two mafic types described above is not apparent. However, the type I suite has a slightly more limited range of MgO values than the type II suite (17.5 to ~5 wt. % and 18 to ~3 wt. % respectively). With decreasing MgO the SiO_2 concentrations remain relatively constant (~44 wt. % in the type I rocks and ~45 wt. % in the type II rocks until MgO reaches about 6 wt. % when the SiO_2 increases from *ca* 44 to 46 wt. % in the type I rocks and from *ca* 45 to 50 wt. % in the type II rocks. As MgO decreases in both types there is an increase in Al_2O_3 (type I ~8.6 to 16.5 wt. %; type II ~8.4 to ~19 wt. %), P_2O_5 (type I ~0.5 to 1.5 wt. %; type II ~0.5 to 1.3 wt. %), and the alkalis (Na_2O+K_2O; type I ~3 to 8 wt. %; type II ~2 to 9 wt. %). Titanium displays a similar trend increasing from *ca.* 2.7 to a maximum of 4.5 wt. % in type I, and *ca.* 2.5 to a maximum of 4 wt. % in type II, with decreasing MgO. However, there is an abrupt change of slope at *ca.* 6 wt. % MgO, where TiO_2 concentrations decrease to a minimum of *ca.* 3.5 wt. % in the type I rocks and ~2.9 wt. % in the type II rocks. CaO and FeO^t remain relatively constant (~ 12 wt. % for both oxides) as MgO decreases to approximately 6 wt. % where both CaO and FeO

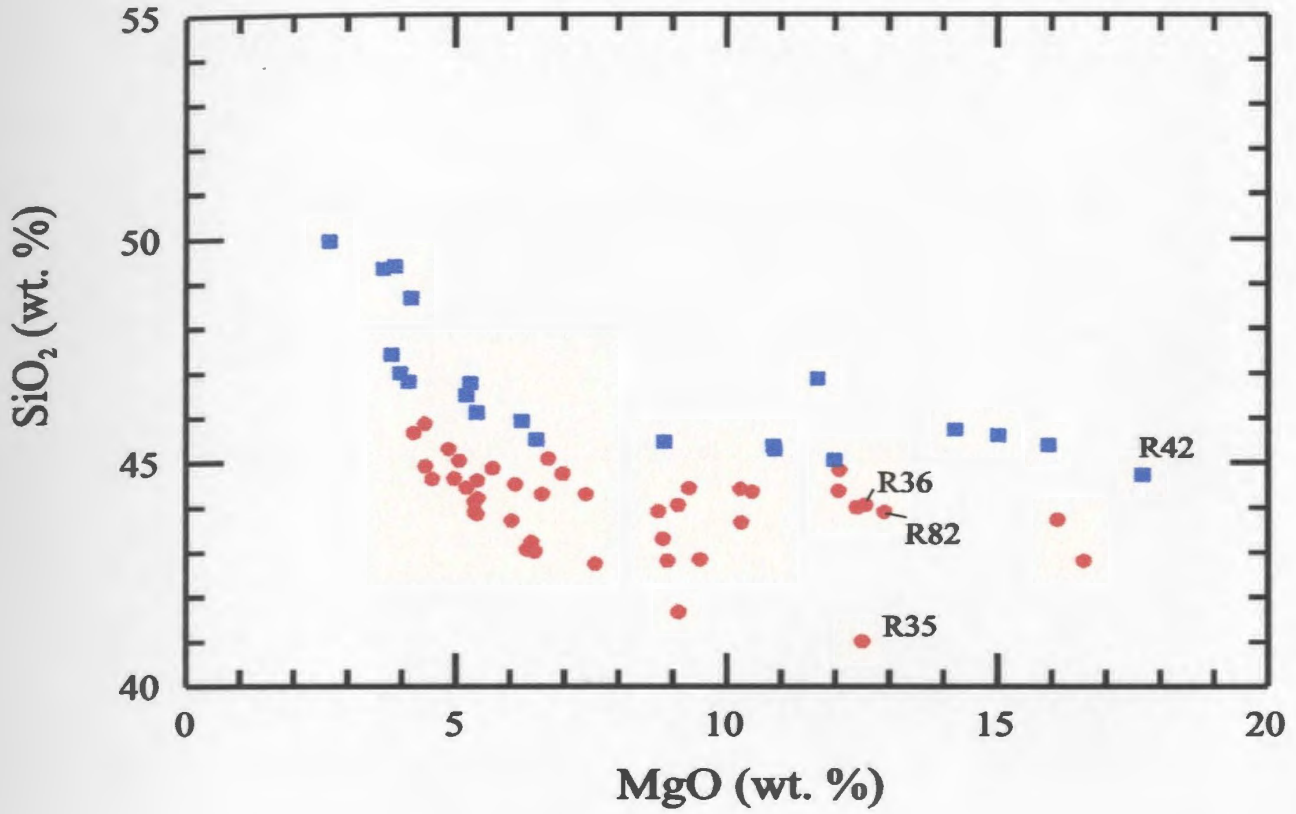

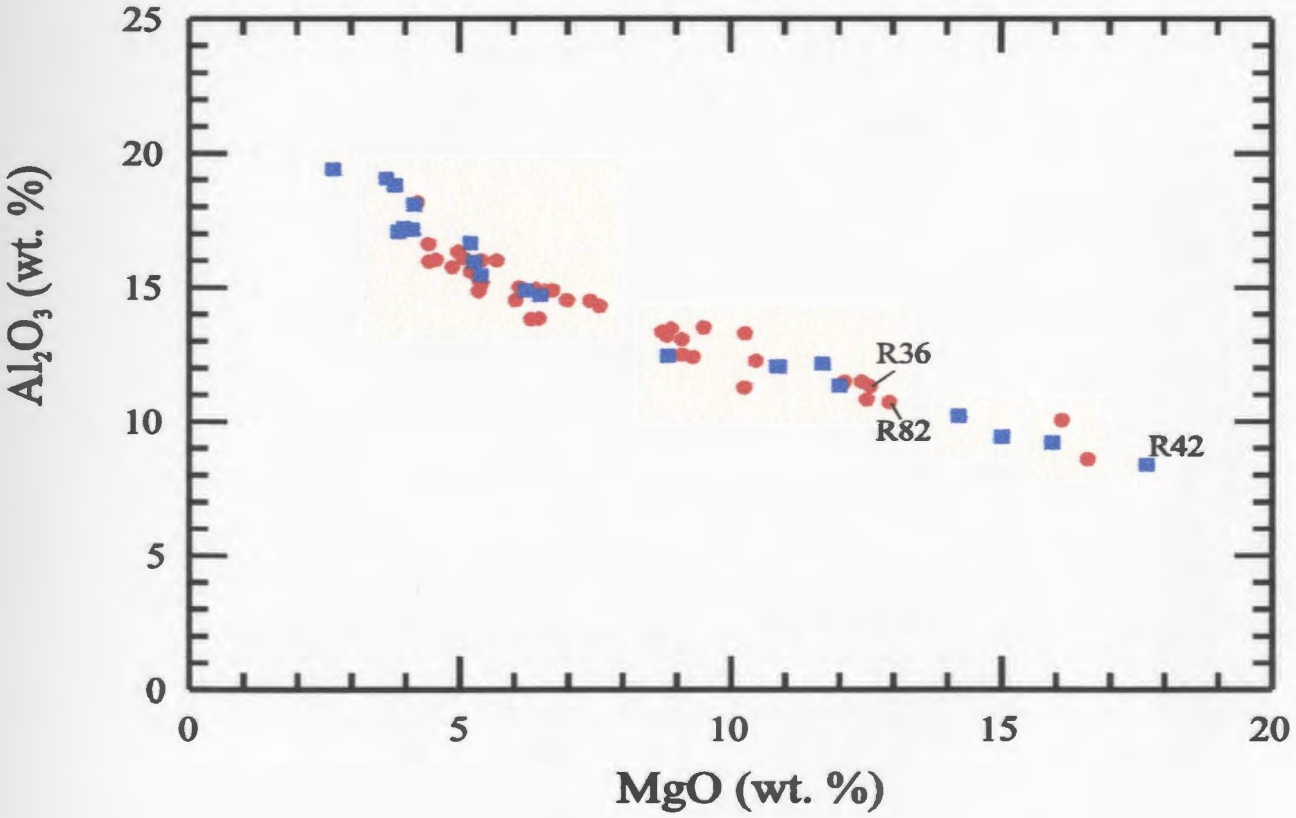

Figure 4.2: MgO variation plots for major elements (all in wt. %). Symbols are the same as Figure 4.1.

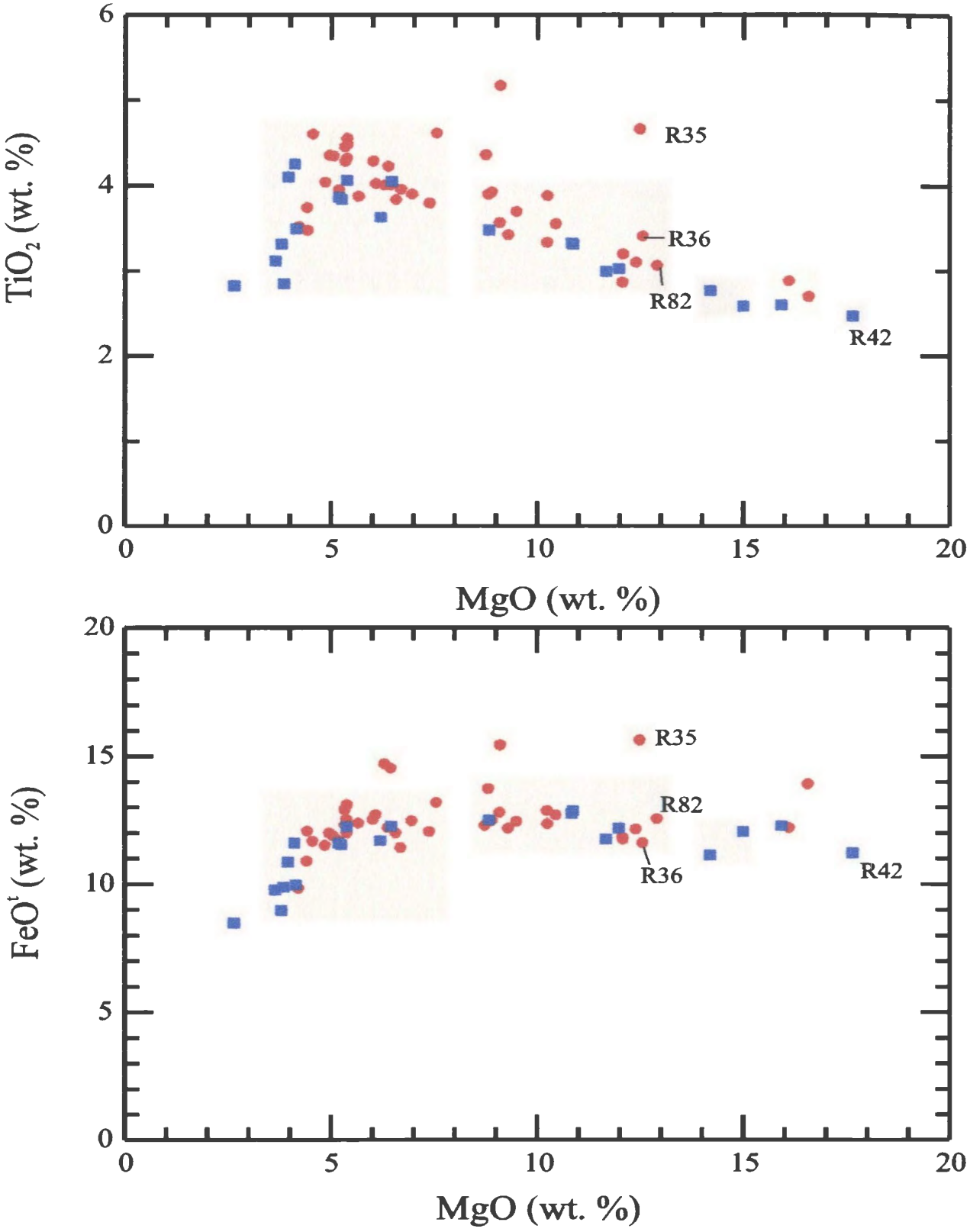

Figure 4.2: Continued

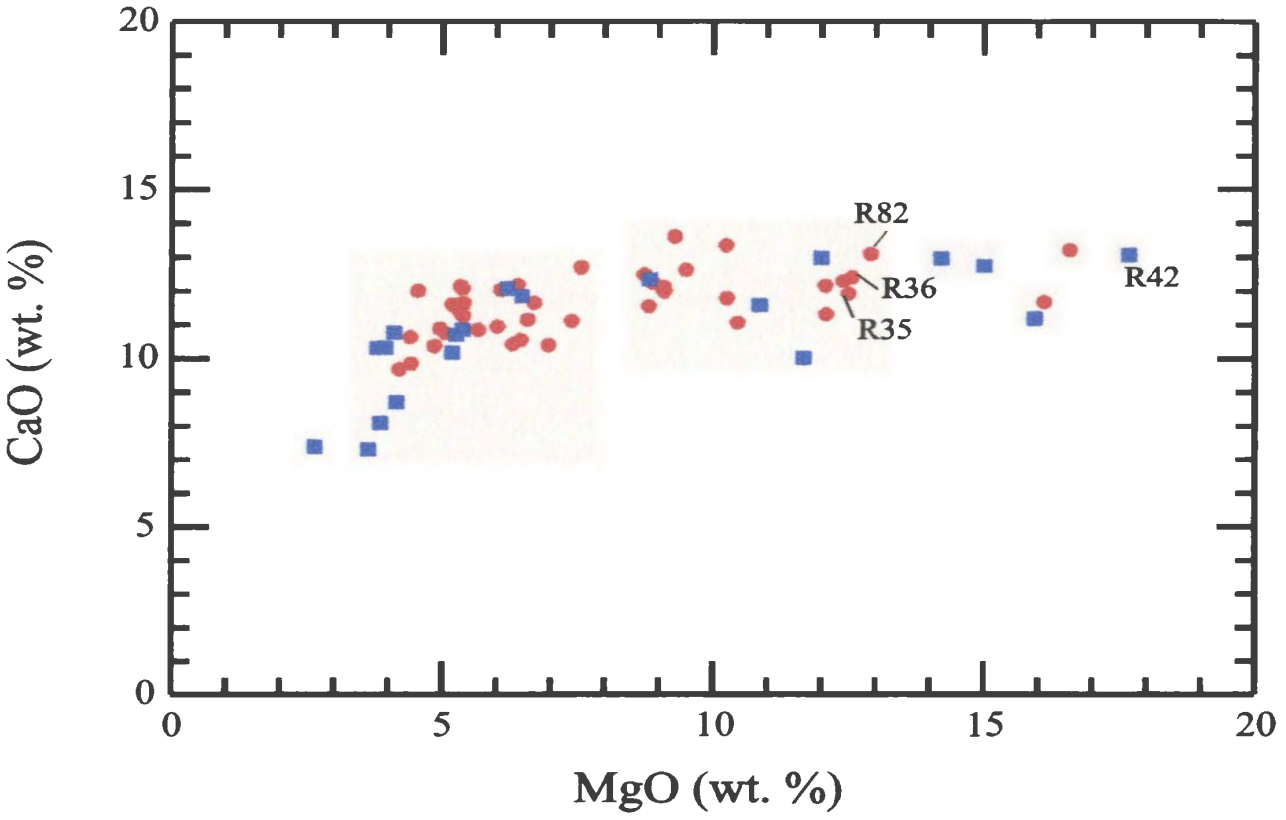

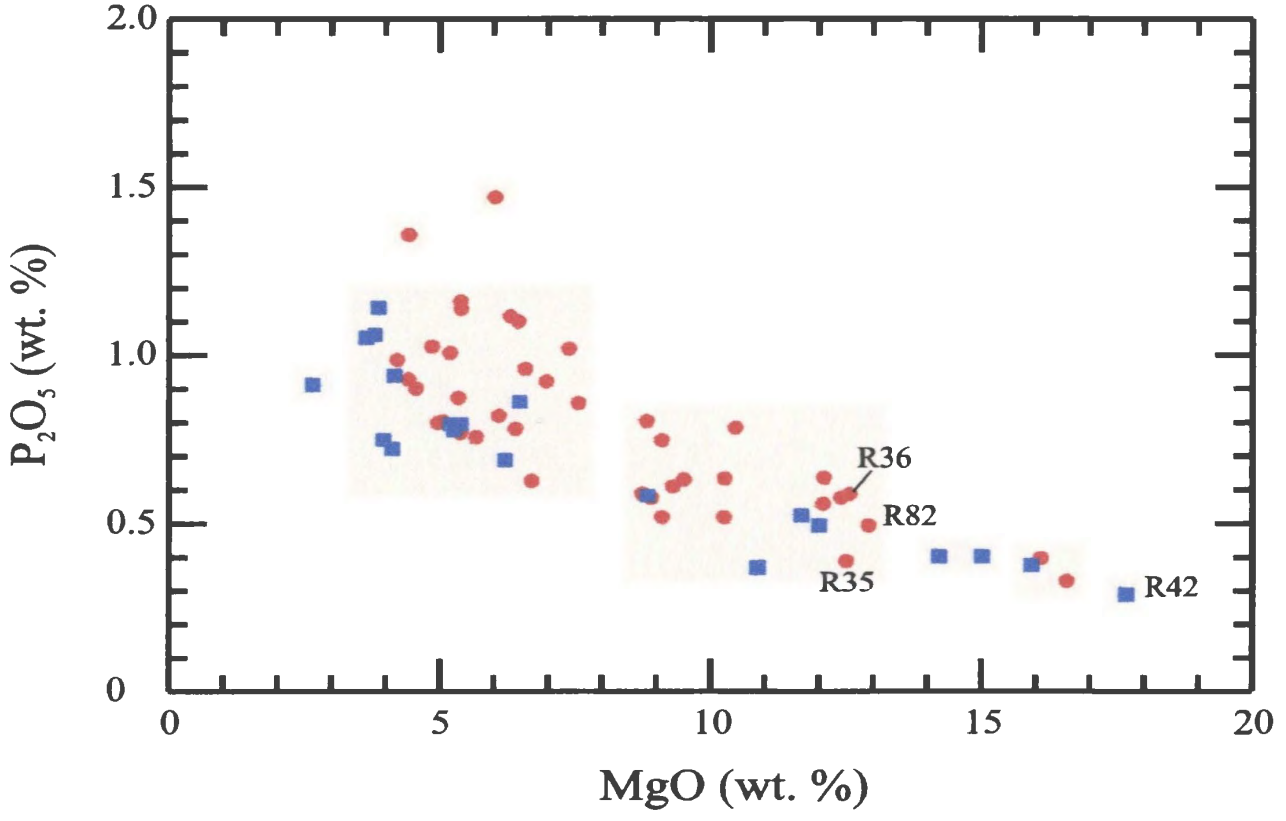

Figure 4.2: Continued

decrease in concentration, to *ca.* 9 wt. % in the type I rocks and *ca.* 7.5 wt. %, for the type II rocks.

The Rarotonga rocks display a wide range in trace element composition, as shown by the variation of selected elements relative to Zr in Figure 4.3. Similar correlations are obtained if SiO_2 or MgO are used as the abscissa.

Zr (type I ~200-500 ppm; type II~200-600 ppm), Nb (type I ~40-140 ppm; type II ~40-160 ppm), Y (type I ~20-34 ppm; type II ~20-42 ppm) and Rb (type I ~20-100 ppm; type II ~20-160 ppm) appear to behave as incompatible elements and describe similar, fairly well constrained, positive correlation throughout the mafic suites.

The ferromagnesian trace elements, Ni, Sc, and Cr in the type I rocks show a depletion in concentration (Ni ~400-8 ppm, Sc ~30-10 ppm Figure 3.3; Cr~900-7 ppm) with increasing Zr concentration. In the type II rocks, R128 and R102 have high Ni and Cr, *ca.* 400 ppm and 900 ppm respectively, while the remaining basalts in this group have Ni concentrations ranging from ~120 ppm to 10 ppm and Cr ranging from ~140 to 10 ppm. Scandium shows a more uniform distribution decreasing from ~30ppm to 10 ppm with increasing Zr. Vanadium in both types does not show any significant correlation with Zr, remaining relatively constant (200-350 ppm) except for two samples (R56 and R78) in type II rocks which have lower V (~100 ppm) and higher Zr.

Normalising the trace elements to primitive mantle compositions (Figure 4.4) shows that the Rarotongan rocks have Rb, Ba, Th, Nb and Zr concentrations between 20 and 100 times that of primitive mantle, while Y is about three times the concentration in primitive mantle. There appear to be both a slightly positive Nb anomaly and negative K

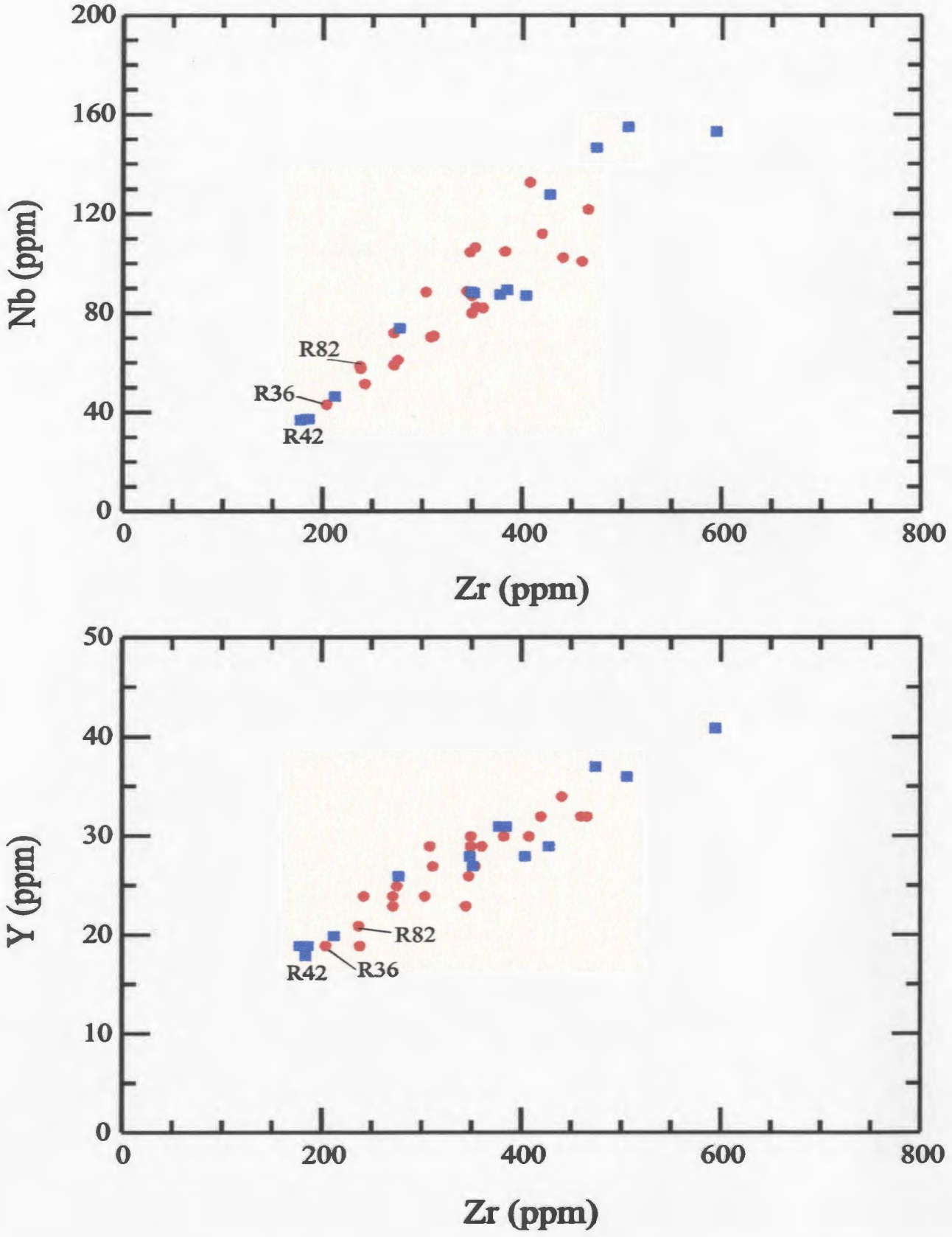

Figure 4.3: Zr variation plots for selected trace elements (all in ppm). Symbols are the same as Figure 4.1.

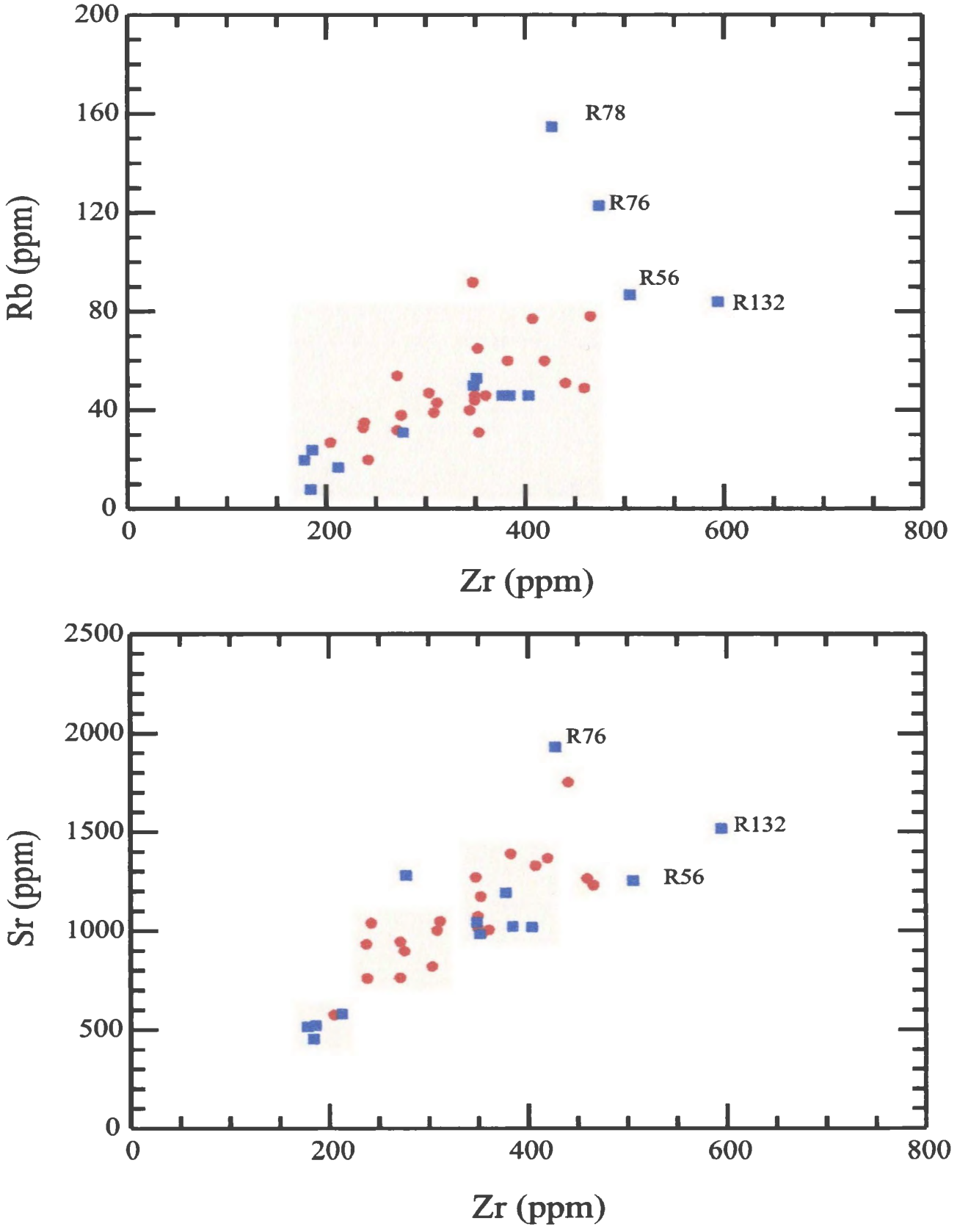

Figure 4.3: Continued

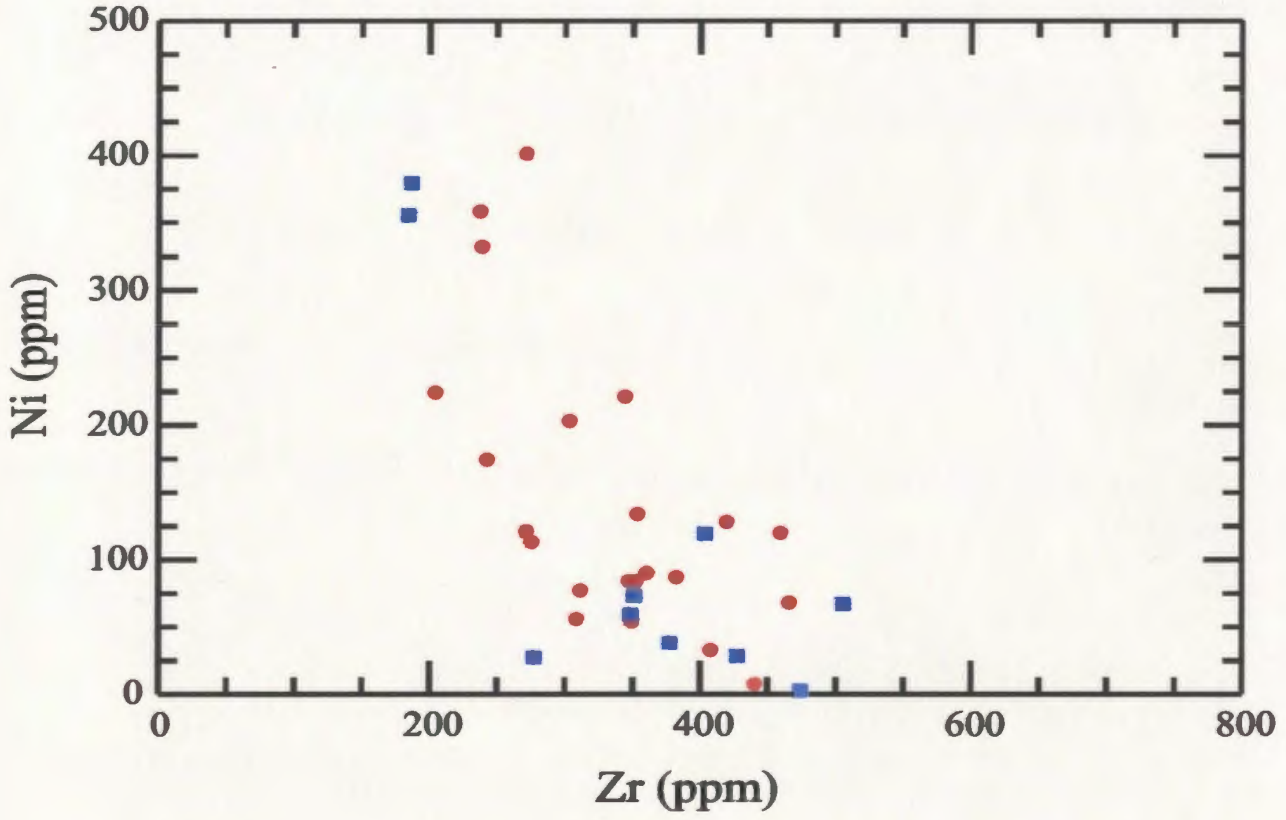

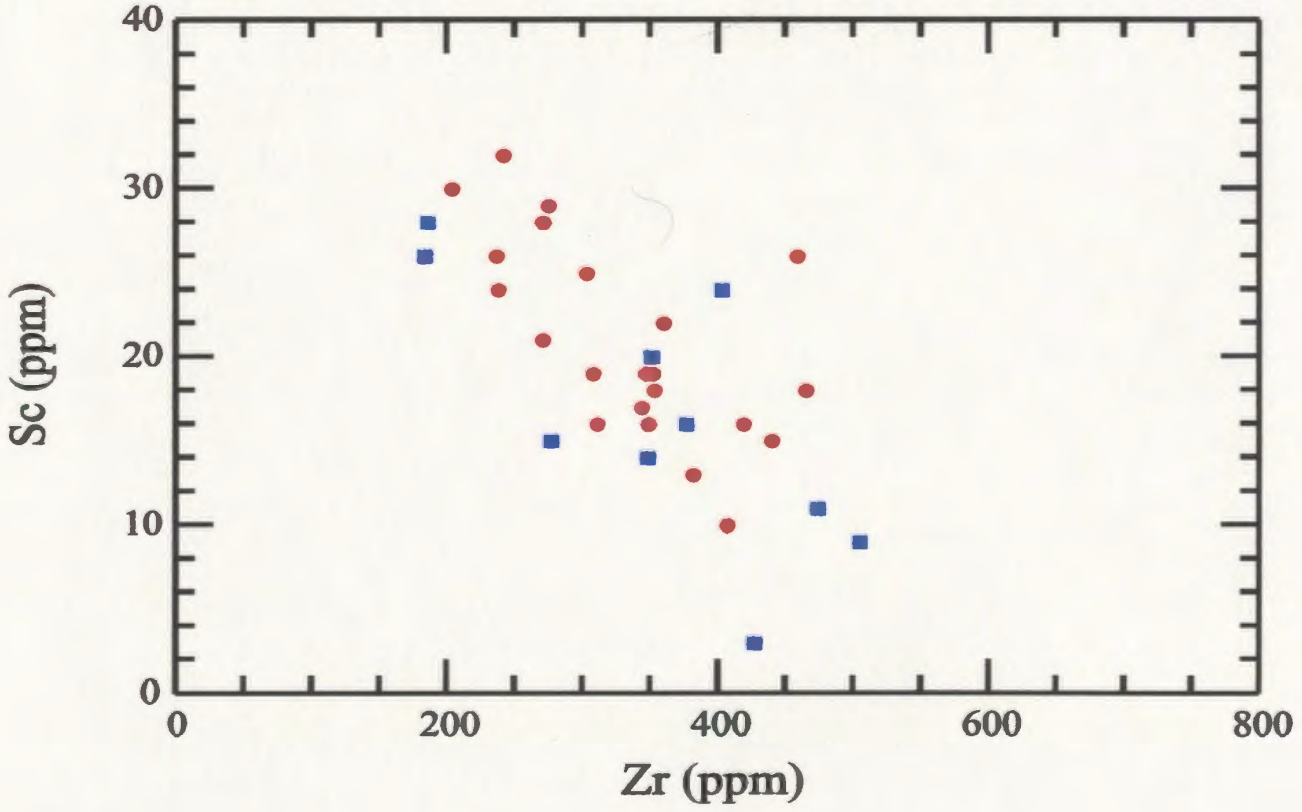

Figure 4.3: Continued

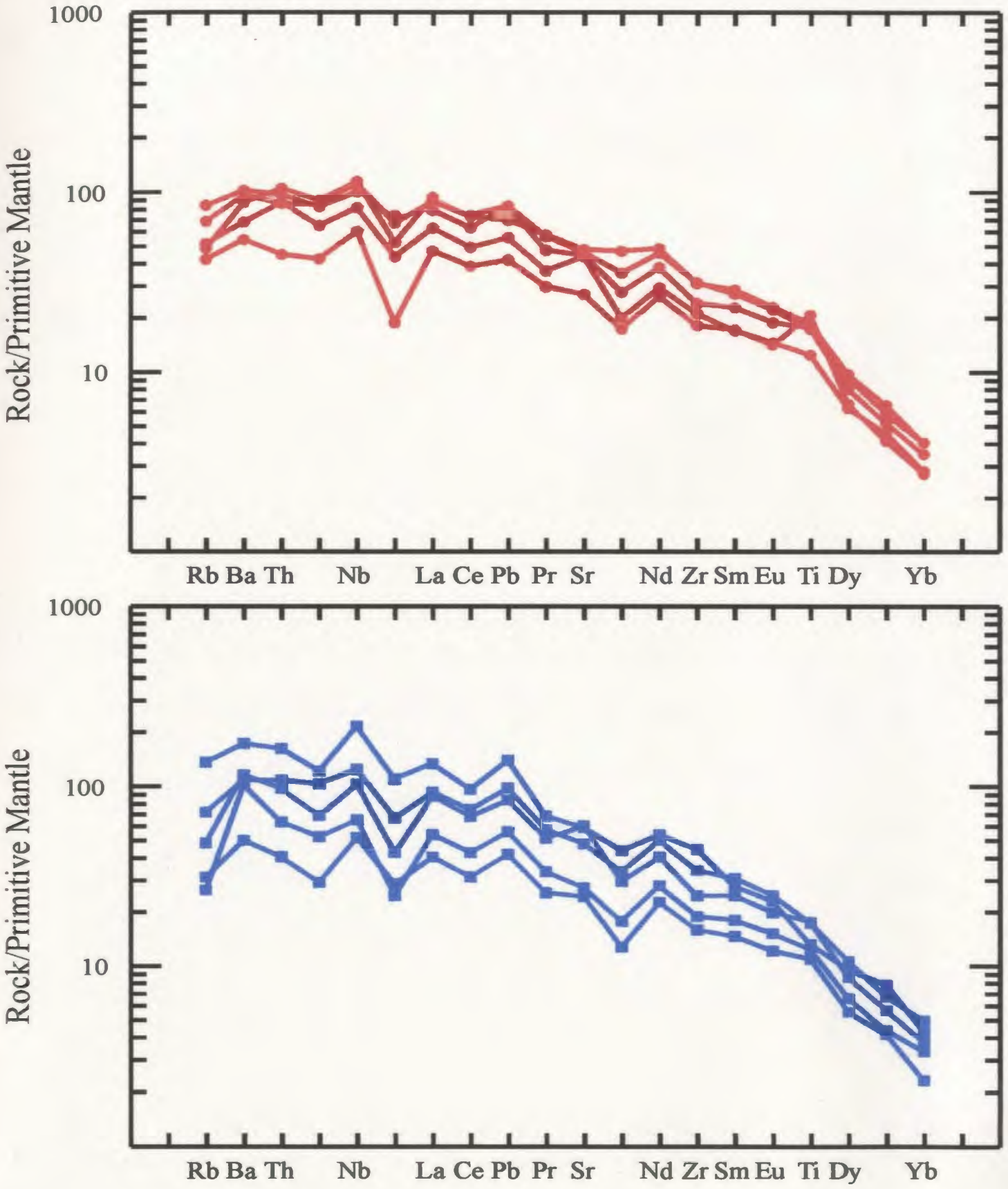

Figure 4.4: Primitive mantle (Sun and McDonough, 1989) normalised trace element plots of selected mafic samples. Symbols are the same as Figure 4.1.

and Rb anomalies. The REE will be discussed in more detail below. The type II rocks display a slightly wider range of trace element concentrations.

Felsic Rocks

As can be seen from Figure 4.1 (TAS) the felsic rocks plot as extensions of the trends defined by the mafic rocks. To show the variation in the elements in the felsic rock the various oxides were plotted against the differentiation index (D.I.) of Thornton and Tuttle (1960)-Figure 4.5. This index extends the abscissa compared with the restricted range of MgO or SiO_2 wt. %.

Although the foidal phonolites are extremely fractionated, with Mg# between 15 and 30 and D.I. between *ca.*, 75 and 85, they have low SiO_2 concentrations (50-53 wt. %). Aluminium (~18-21 wt. %) displays a positive correlation with D.I. Potassium (~4-5.5 wt. %) and silica also exhibit positive correlation, although both trends show some scatter. Sodium contents do not appear to show any correlation with D.I. The remaining oxides all display a negative correlation with D.I. (FeO^t ~7-4 wt. %; CaO ~6-3 wt. %; MgO ~1.5-0.5 wt. %; TiO_2 ~1.5-0.5 wt. %).

The phonolites have higher SiO_2 concentrations with a more restricted range than the foidal phonolites, with all of these samples having approximately 58 wt. % SiO_2. The phonolites have relatively restricted variation in major elements and it is difficult to ascertain if trends exist with respect to D.I. Sodium (~6-8 wt. %) however, exhibits a well defined positive correlation with D.I., while CaO (~3.5-2 wt. %) displays a slightly less well defined negative correlation.

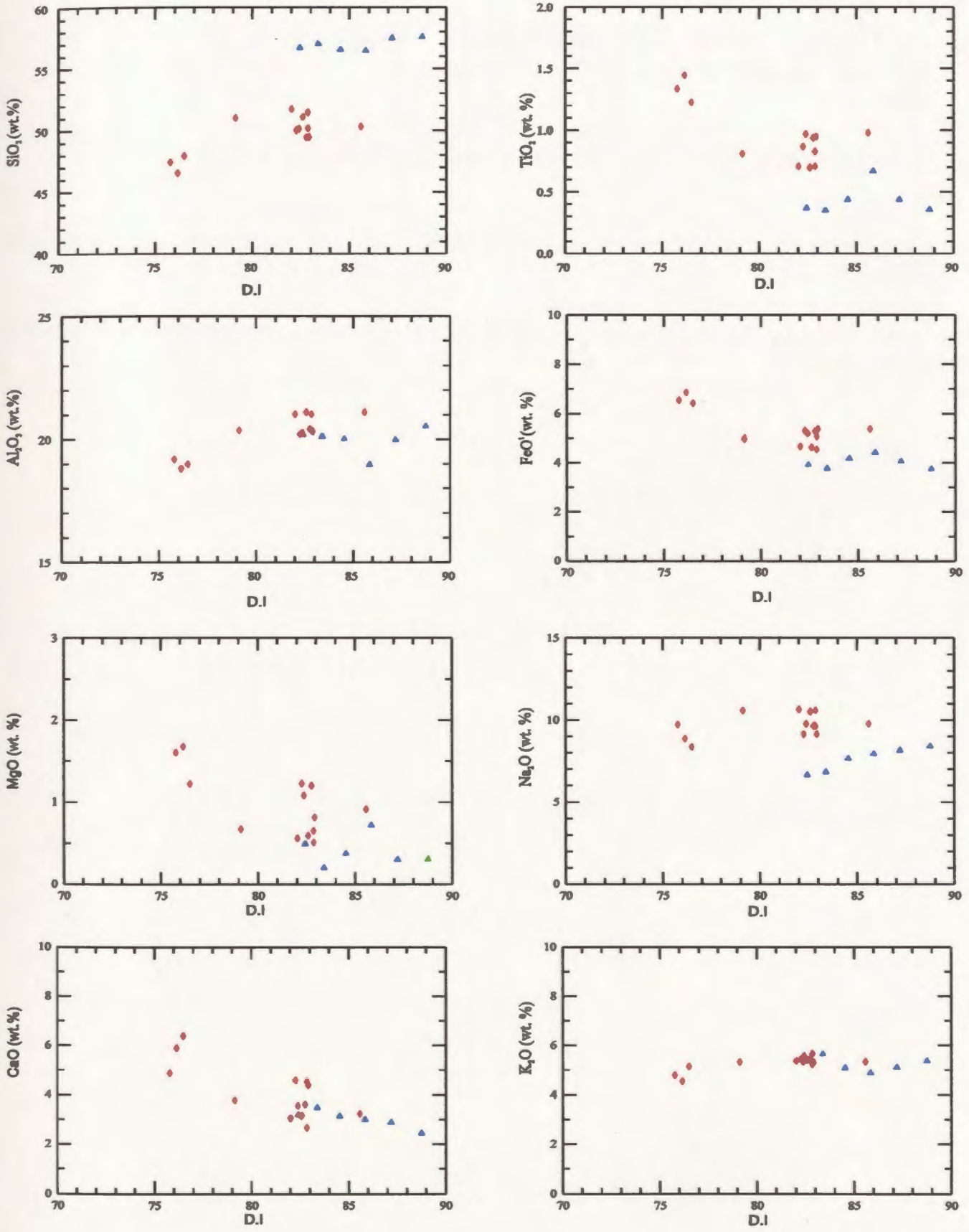

Figure 4.5: Variation plots for major elements vs. differentiation index (D.I.; Thornton and Tuttle, 1960). Symbols are the same as Figure 4.1.

Trace elements in the foidal phonolites do not show any obvious correlation between concentration and D.I. However, when MgO wt. % is used on the abscissa, Y (~28-40 ppm) and Sr (~3000-2000 ppm) exhibit slight positive correlation (Figure 4.6). There is an inflection in the Rb trend, with concentrations increasing (~100-180 ppm) with decreasing MgO until about ~1 wt. % MgO at which point the Rb concentration decreases.

The only trace elements in the phonolites that exhibit any clear relationship with D.I. are Hf, Sr and Y, all of which display a positive correlation. Barium, although showing no correlation with D.I., does show a positive correlation with MgO wt. %; decreasing from ~2000 ppm to 1500ppm with decreasing MgO. Zirconium (~850 ppm), Th (~25 ppm) and Nb (~180ppm) all have a restricted range in concentrations and do not vary with increasing D.I or MgO wt. %.

The foidal phonolites have significantly higher concentrations of Nb, Zr and Th, while Y and Sr are slightly higher in the more fractionated foidal phonolites (high D.I, low Mg#) than the phonolites with a similar D.I.

4.2.3 Rare Earth Elements

Mafic rocks

The REE of the two types of mafic rocks are plotted in Figure 4.7 where the REE are normalised to chondrite values. All the basalts are strongly enriched in light REE (LREE) over heavy REE (HREE). In the type I rocks the LREE are 100-120 times more

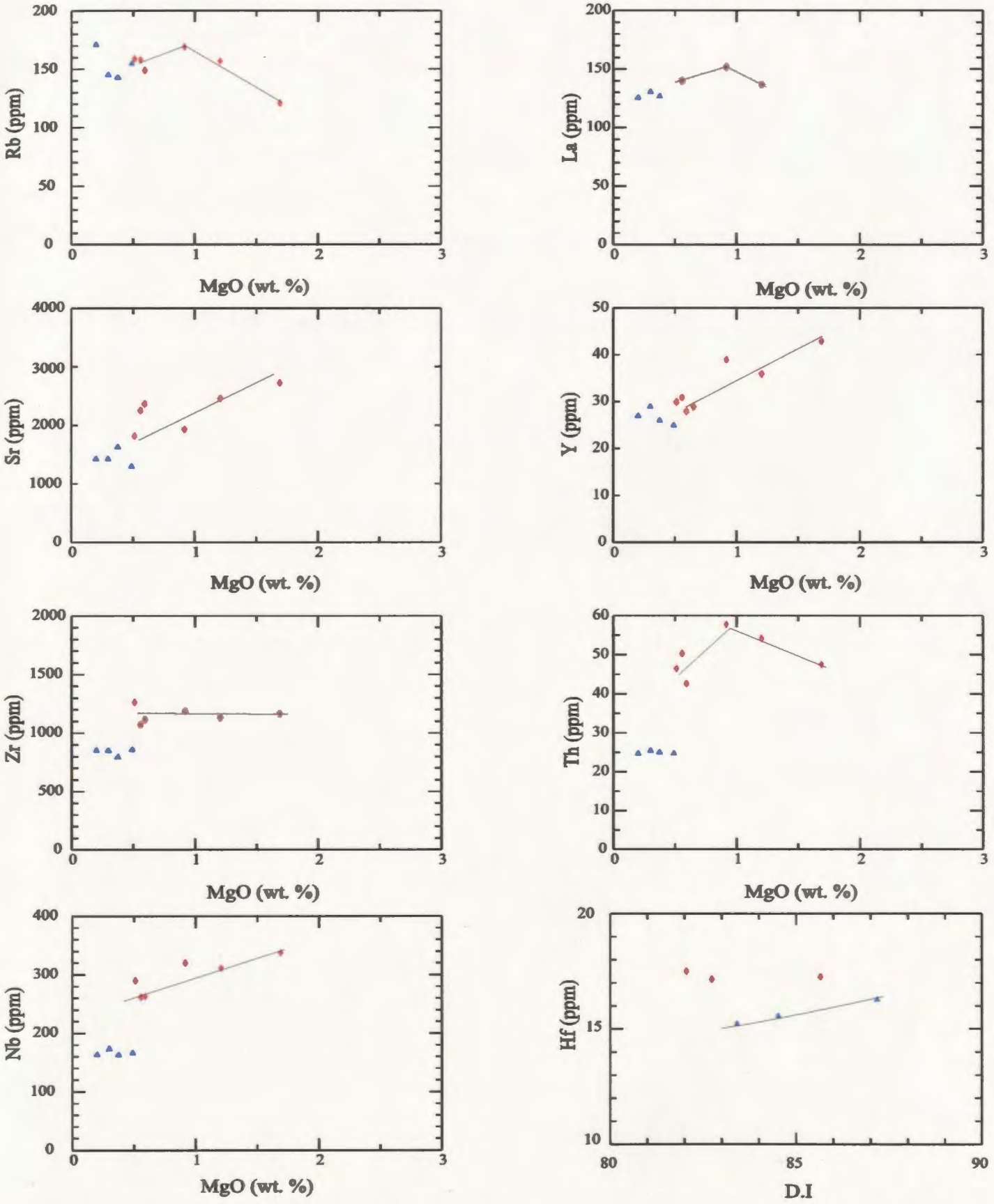

Figure 4.6: Variation plots for selected trace elements (ppm) vs MgO (wt. %) and D.I. Trends discussed in the text are shown for reference. Symbols are the same as Figure 4.1.

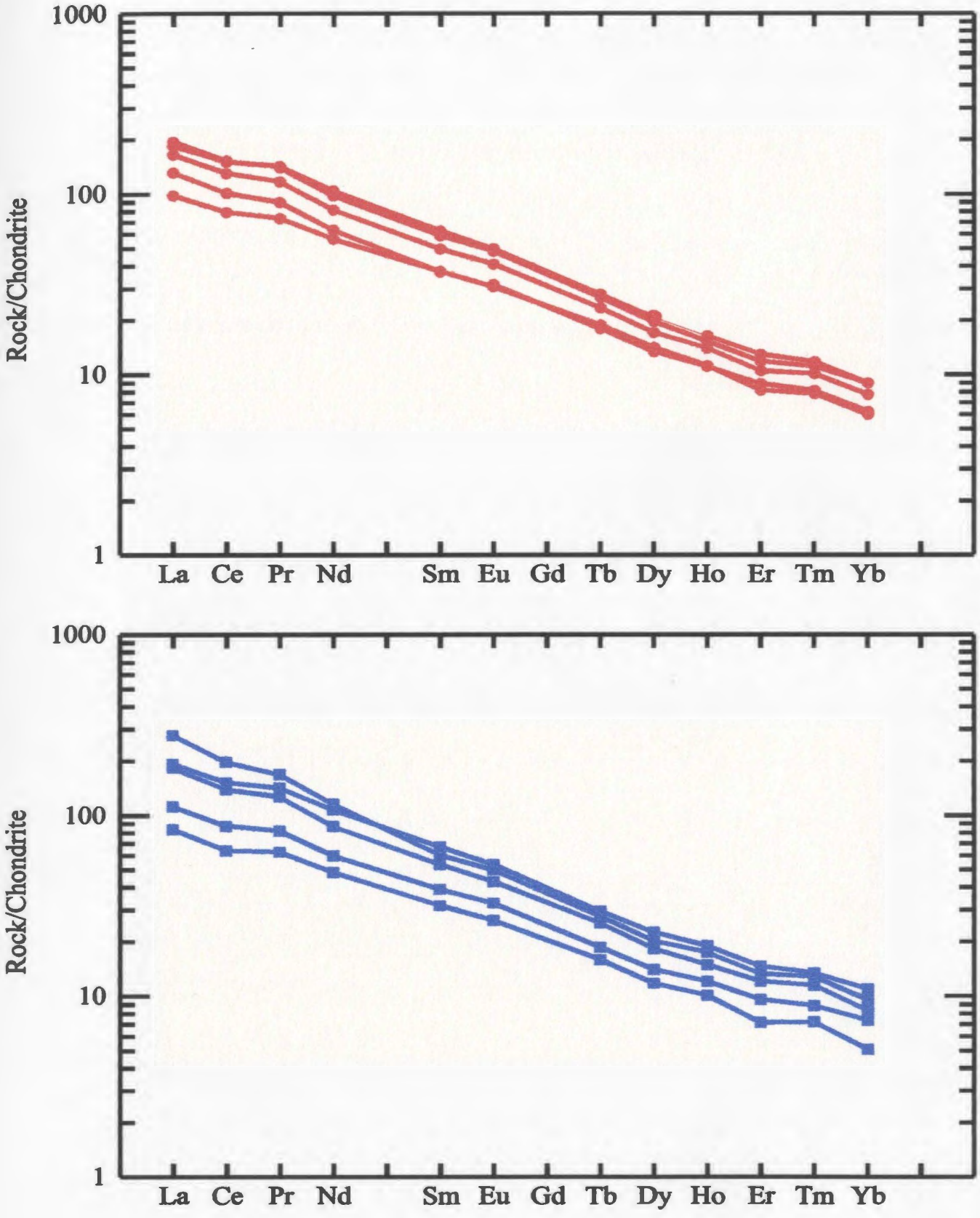

Figure 4.7: Chrondrite normalised (Nakamura, 1974) REE plots of selected mafic rocks. Symbols are the same as Figure 4.1

enriched and the HREE 6-9 times more enriched than chondrite concentrations. In the type II rocks LREE are 90 to 130 times and HREE 5 to 10 times chondrite concentration.

REE concentrations increase with increasing SiO_2 and decreasing MgO concentrations. There is no apparent relationship between the ratio of the LREE:HREE with MgO in the type I rocks (Figure 4.8), with La/Yb ratios range between 22 and 31, where the type II rocks with the highest La/Yb ratios have the lowest MgO concentration with ratios ranging from 20 up to 44 (Figure 4.8). When the La/Yb ratios are compared to HFSE a positive correlation is observed for both type I and II samples (Figure 4.9).

Felsic rocks

The felsic rocks are all enriched in REE when compared to chondrite REE concentrations (Figure 4.10). LREE are 100-600 times and HREE approximately 10 times chondrite. The REE patterns are slightly concave with relative depletion in the middle ranges (Nd-Dy). Both groups show extreme LREE enrichment over HREE ($La_N/Yb_N \sim 35$). This ratio remains relatively constant with increasing MgO and HFSE concentrations. The phonolites have a slight positive Eu anomaly.

4.2.4 Isotopes

Type I and type II rocks appear to have slightly different radiogenic isotopic signatures (Figure 4.11). Type I mafic rocks have a generally restricted range of $^{143}Nd/^{144}Nd$ and $^{87}Sr/^{86}Sr$ ratios, 0.51270 to 0.51275 and 0.7040 to 0.7044 respectively,

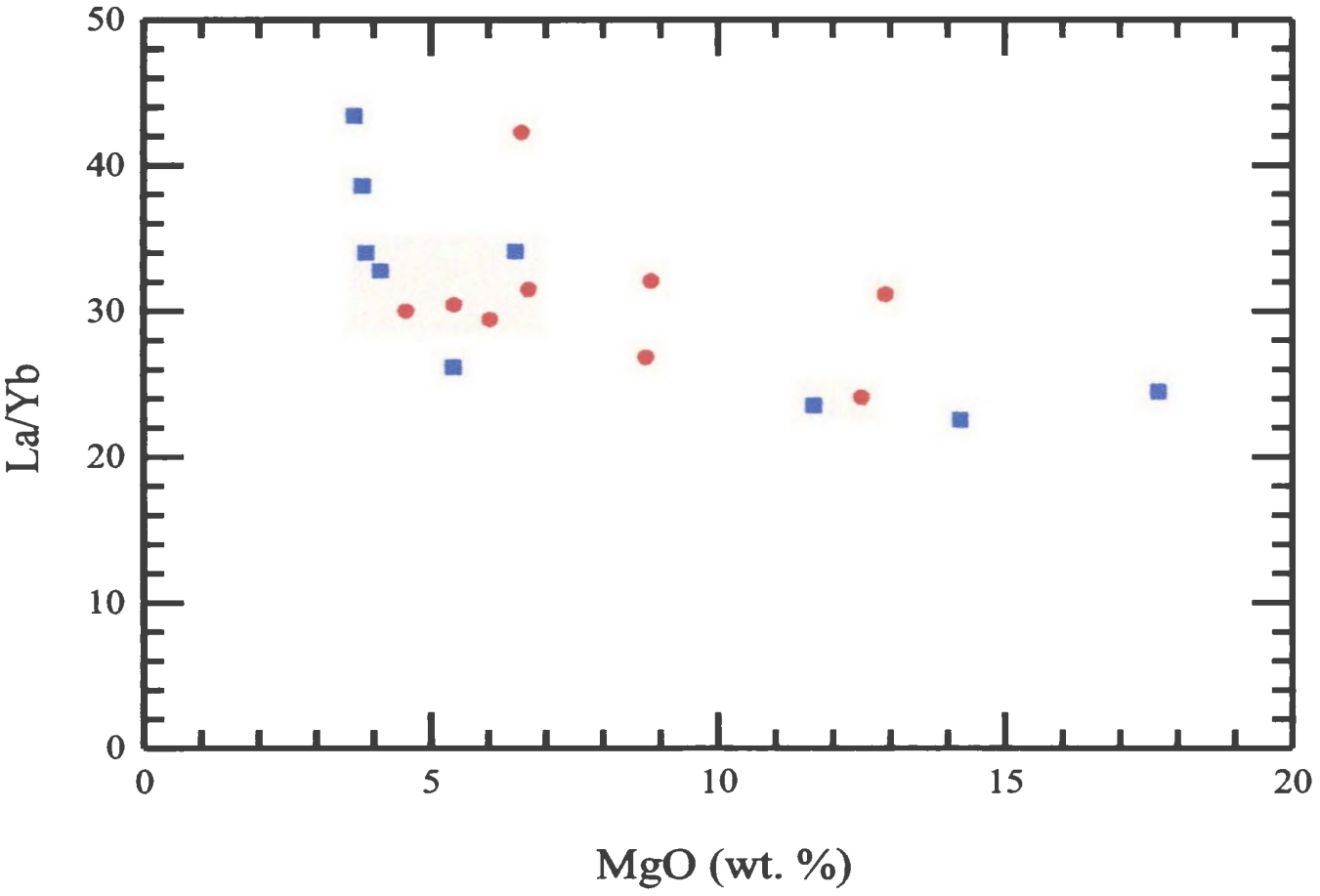

Figure 4.8: La/Yb vs MgO (wt. %) for the mafic rocks. Symbols are the same as Figure 4.1

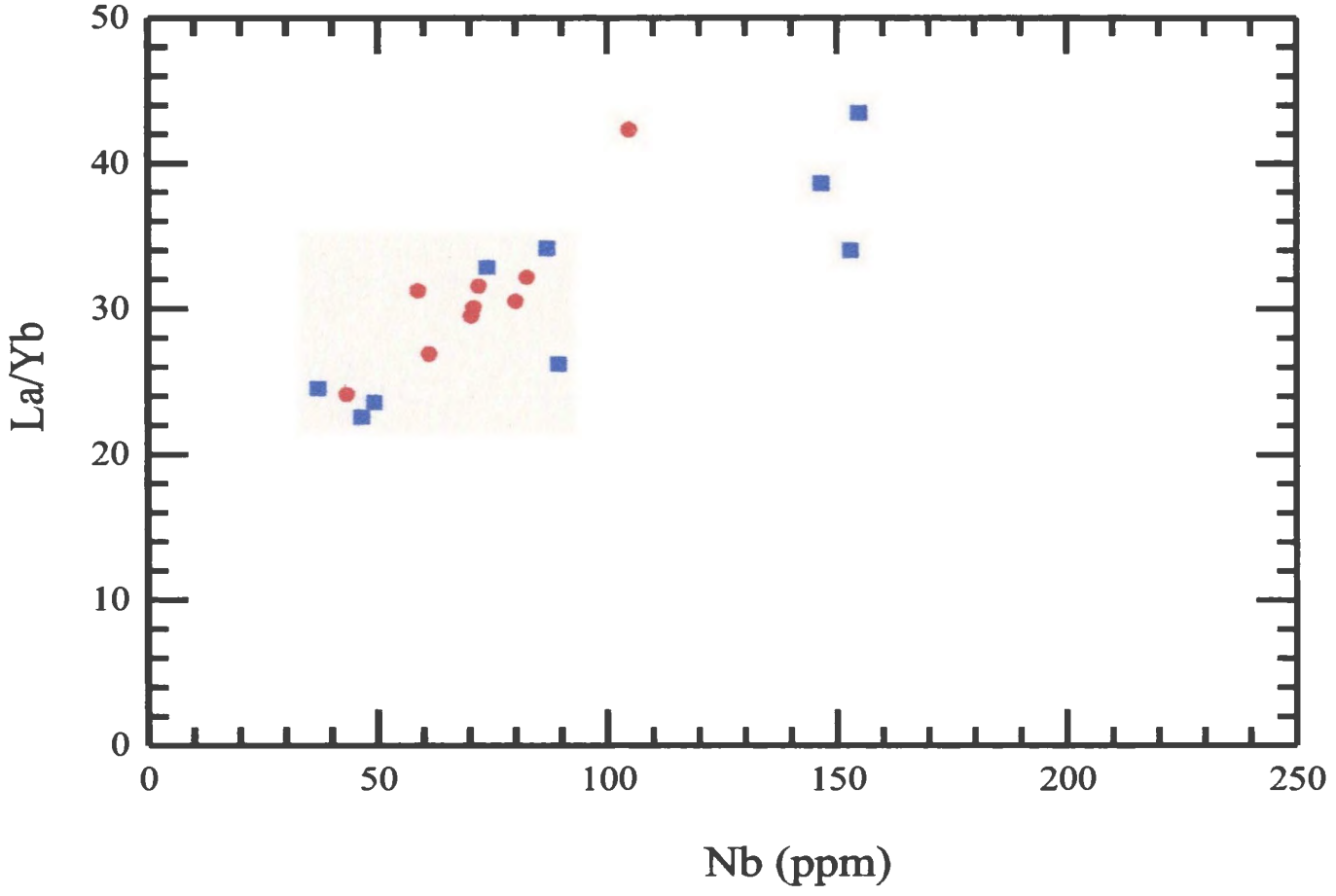

Figure 4.9: La/Yb vs Nb (ppm) for the mafic rocks. Symbols are the same as Figure 4.1

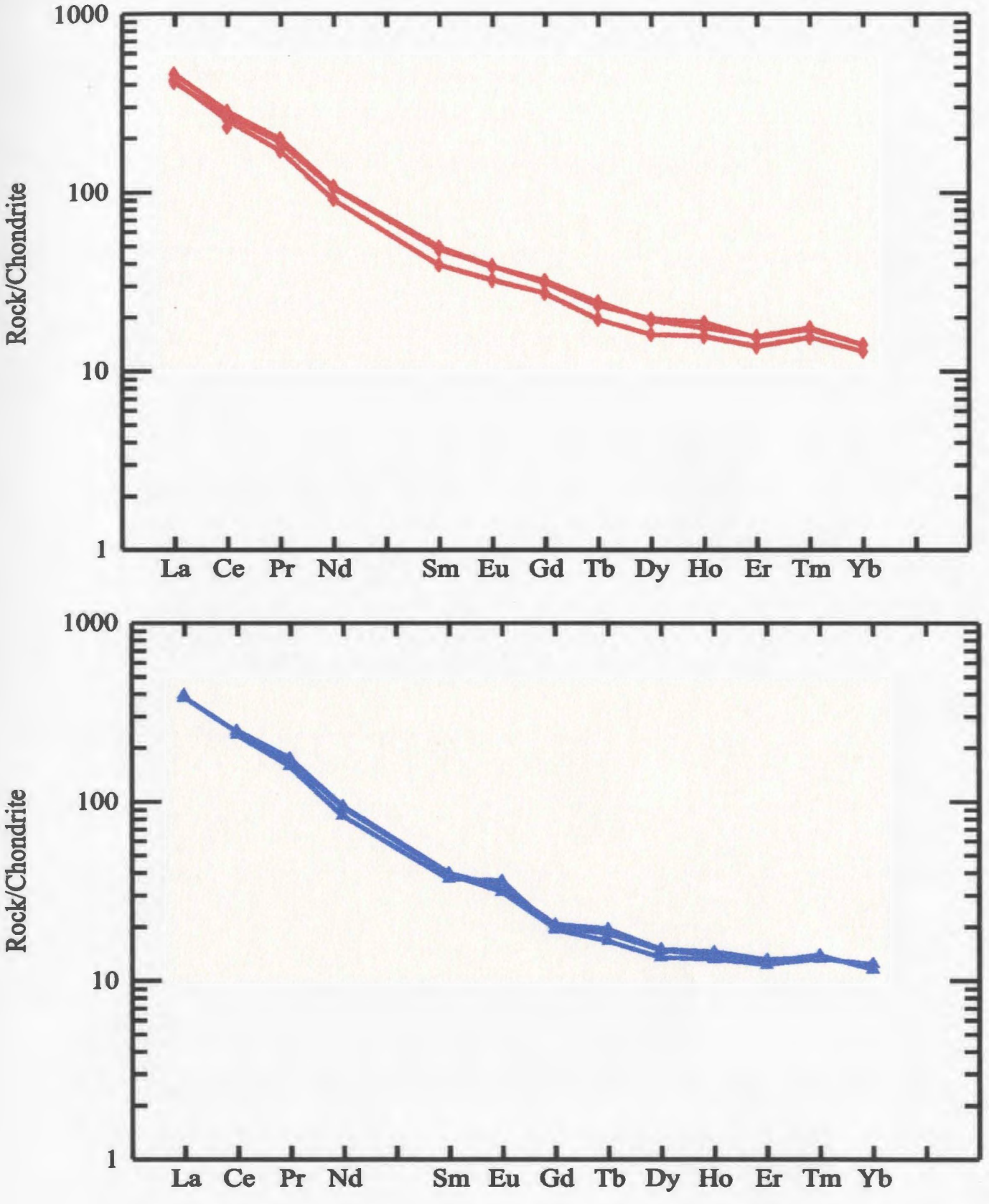

Figure 4.10: Chondrite normalised (Nakamura, 1974) REE plots of selected felsic rocks. Symbols are the same as Figure 4.1

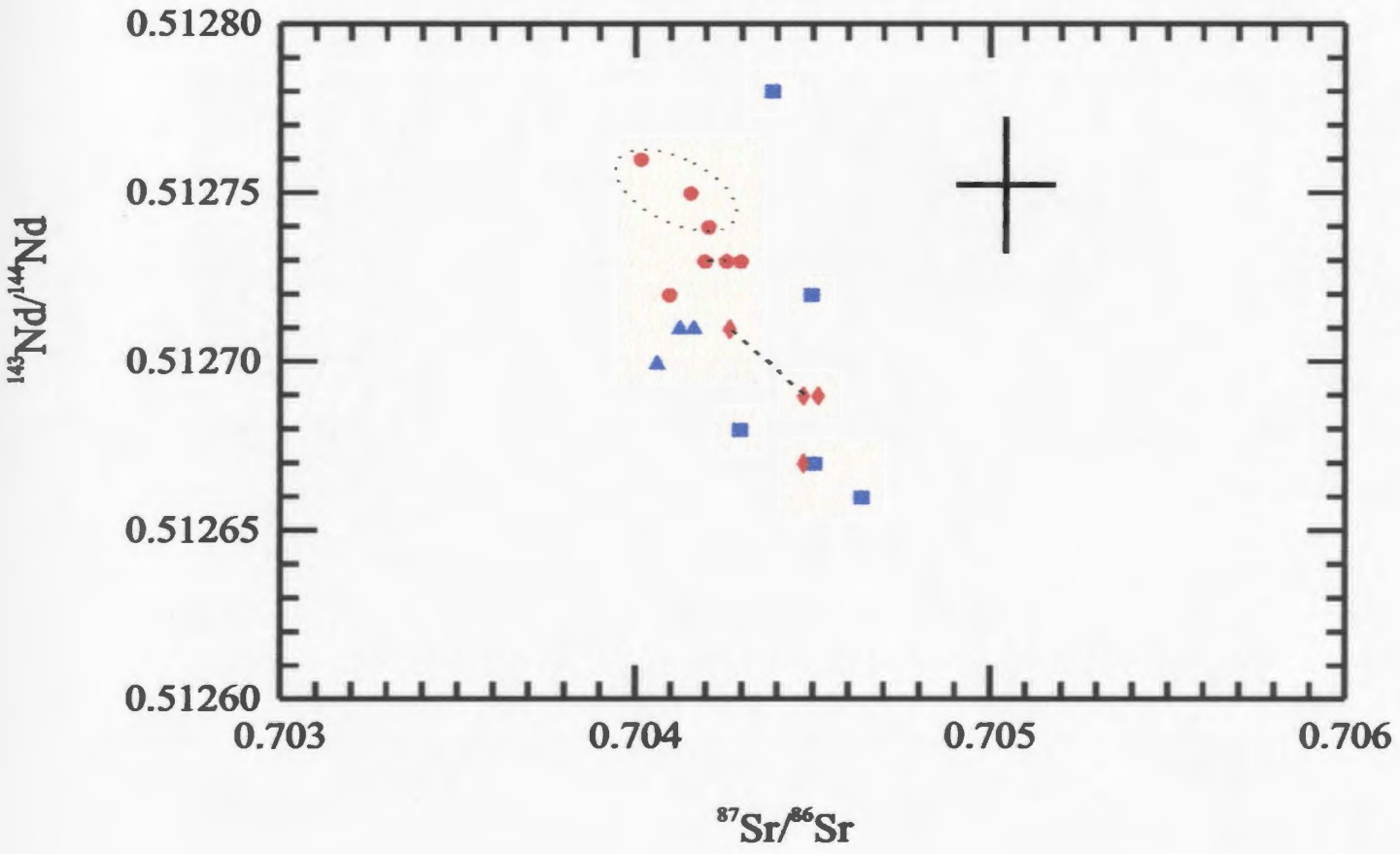

Figure 4.11: $^{143}Nd/^{144}Nd$ vs. $^{87}Sr/^{86}Sr$. The error bar represents the typical error exhibited by reruns of the same sample. Tie lines connect samples which were leached. The dashed field circles mutiple analyses of samples R111. The symbols are the same as Figure 4.1.

while the type II basalts have a higher $^{87}Sr/^{86}Sr$ ratios (~0.7044 - 0.7047) and a wider range of $^{143}Nd/^{144}Nd$ (~0.5126-0.5128).

The phonolites and foidal phonolites plot as two distinct groups each displaying a restricted range of isotopic ratios. The phonolites have a similar isotopic composition to the type I basalts, whereas the foidal phonolites have higher $^{87}Sr/^{86}Sr$ ratios (~0.7045) and slightly lower $^{144}Nd/^{143}Nd$ ratios (~0.5127) than both the type I basalts and the phonolites.

One sample from the type I and II mafic rocks, a foidal phonolite and a phonolite were leached in 6N HCl for 24 hours to determine if isotope ratios had been compromised through alteration by sea-water. The changes observed in isotope ratios after leaching are all insignificant when compared with the analytical error.

4.2.5 Discussion

Alteration

Any study that will ultimately examine the processes involved in the petrogenesis of a suite of igneous rocks will first have to determine what effect alteration (*e.g.*, hydrothermal alteration) has had on the chemistry of the rocks.

Petrographic evidence shows that the mafic rocks as a whole do not exhibit features typical of high level hydrothermal alteration. However, some samples, show replacement of olivine by iddingsite. The type I rocks to a minor extent exhibit replacement of olivine by iddingsite with, at the most, only partial replacement of rare

olivine phenocrysts within a single sample. In the type II rocks this replacement can be extensive with some samples having all of their olivine replaced by iddingsite. This break down of olivine to iddingsite releases Mg, Fe^{2+} and Si from lattice sites which are replaced by Fe^{3+}, Al and Ca ions (Deer et al., 1992).

Although it is easy to discount the above samples from further examination, it may still be possible that in other samples alteration is not visibly manifested. Alteration processes might change some of the more mobile major and trace element concentrations, thus removing any systematic relationship these elements would have with fractionation indices.

There have been numerous studies of the effects of trace element mobility during alteration. The LREE are generally considered to be mobile during alteration (Frey et al., 1974; Ludden and Thompson, 1978; 1979; Juteau et al., 1979; Humphris, 1984; Bienvenu et al., 1990) while non-REE incompatible elements (Y, Zr, Nb, Hf, Ta, and Th) are generally insensitive to low temperature alteration (Cann 1970; Frey et al., 1974; Hart et al., 1974; Floyd and Tarney 1979; Humphris and Thompson, 1978a;1978b; Wood et al., 1979; Bienvenu et al., 1990). If a rock had been affected by alteration it is unlikely that there would be any systematic relationship between the mobile REE and the non mobile incompatible elements. From Figure 4.12 it can be shown that there is a positive relation between the two groups of elements implying that the REE concentrations have not been modified by secondary alteration processes.

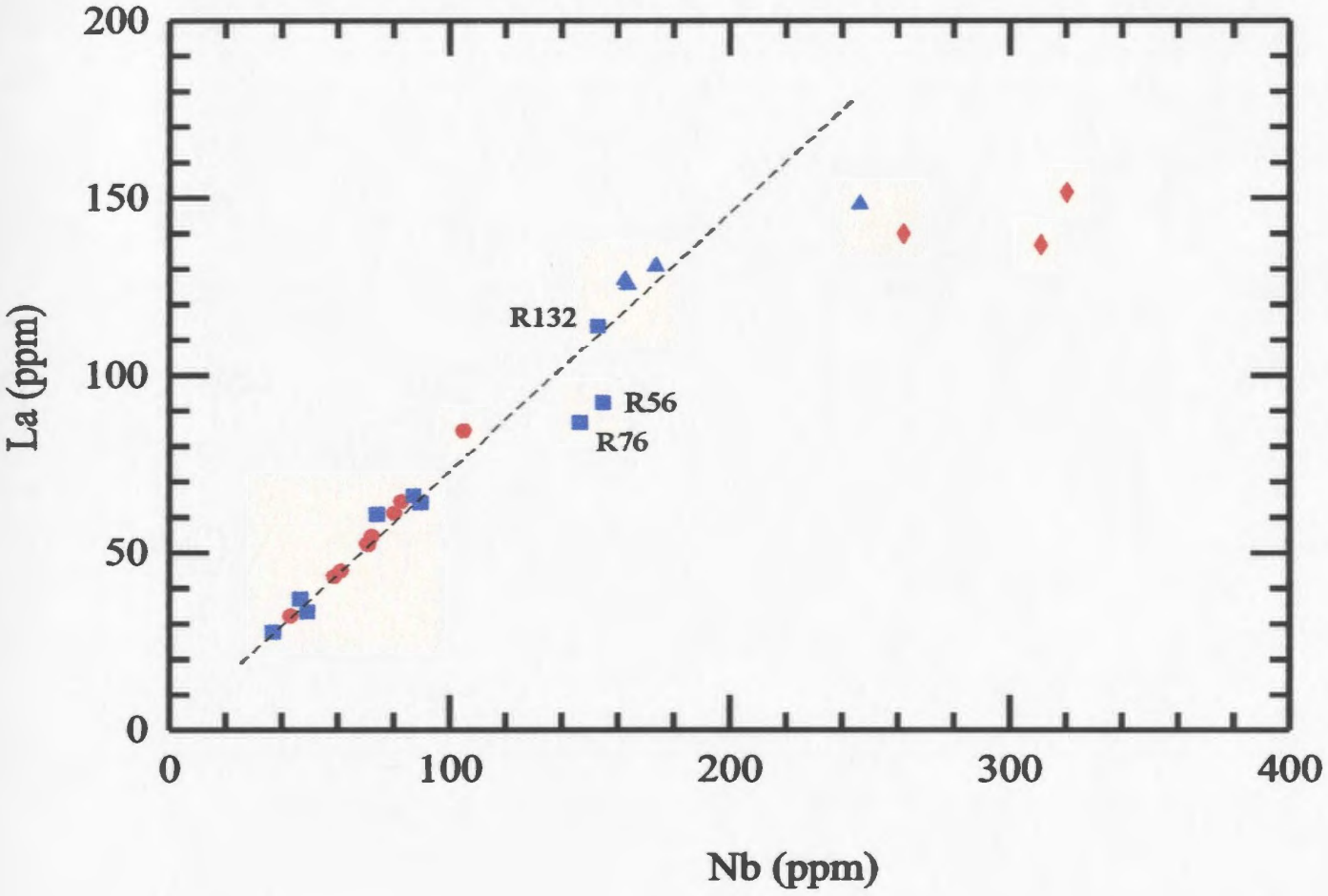

Figure 4.12: La (ppm) vs. Nb (ppm) for Rarotonga samples. The dashed line represents a linear regression analysis for the mafic samples. Symbols are the same as Figure 4.1

Primary Magmas

A primary magma is a magma that is considered unmodified since production from the source; its chemistry should therefore reflect the melting processes and chemistry of the source. Although this concept is simple, it is relatively difficult to identify, unequivocally, a primary magma composition. A simple and widely used criterion for identifying potential mantle primary magmas from mantle sources is the FeO^t/MgO weight ratio or Mg# of a magma. The composition of a melt formed in equilibrium with mantle peridotite is constrained by the behaviour of Fe-Mg partitioning between olivine (the main constituent of mantle peridotite) and silicate melt. This relationship is now well understood (Roeder and Emslie, 1970; Takahashi and Kushiro, 1983) and is summarised in the following equation.

$$Kd_{ol-lq}^{Fe-Mg} = \frac{\left[\frac{Fe}{Mg}\right]_{ol}}{\left[\frac{Fe}{Mg}\right]_{lq}} = 0.3 \qquad \text{.....3.1}$$

Using this value and accepting that the Mg# of mantle olivine is ~90, a mantle -derived primary magma is required to have a FeO^t/MgO ratio less than unity or Mg# greater than 70.

A more qualitative guide to primary magma identification is also provided by the abundance of Ni and Cr in a magma, since these elements are rapidly depleted during the early stage of fractional crystallisation. Magmas with Ni content greater than 200ppm and

Cr content greater than 400ppm are considered possible primary magmas (Sato, 1977; Hart and Davis, 1978).

Using the above considerations only four type I rocks (R35, R54, R82, R77) and two type II rocks (R131, R128) could be possible candidates for primary magma compositions. Although some rocks do have the required chemical characteristics to qualify as potential primary magmas, petrographic evidence (high proportion of phenocrysts) suggests that the low FeO/MgO ratio and high Ni and Cr concentrations are the result of crystal accumulation. These samples are not therefore considered as representative primary magmas.

Since most, if not all, samples do not represent primary magma compositions, it may be possible to estimate the primary magma by accounting for the effects of fractional crystallisation. This necessitates the back addition of fractionated phases until a melt composition is obtained which it is capable of being in equilibrium with mantle olivine. In order to do such a calculation it is necessary to know the chemistry of the phases crystallising, which will be examined in the following sections. In addition, to calculate trace element concentrations in a primary magma from a fractionated magma it is important to have reliable distribution coefficients. The distribution coefficients used in this study will be discussed in Chapter five.

4.3 Major Element Mineral Chemistry

The aim of this section is to characterise the mineral phases found in the mafic rocks *i.e.*, clinopyroxene; olivine; Fe-Ti oxides; kaersutite; feldspar; and nepheline. The major element chemistry of these minerals will be used to elucidate the attributes of the magma chambers from which they crystallised. The following oxide concentrations: SiO_2, TiO_2, Al_2O_3, FeO, MgO, MnO, CaO, Na_2O, K_2O, Cr_2O_3, and NiO were determined using a Cameca Camebax electron microprobe using standard operating conditions. A summary of these conditions and the accuracy and precision of the analyses are given in Appendix 3.

4.3.1 Pyroxene.

The nomenclature used in this section will follow the recommendations of Morimoto et al. (1988). Pyroxene end-members are calculated using the procedure of Cawthorn and Collerson (1974). Their calculation of pyroxene end-members minimises the significance of Fe_2O_3 content. This is important as the electron microprobe cannot distinguish between ferric and ferrous iron, with the total iron reported as FeO. The significance of Fe_2O_3 in the pyroxene structure will be discussed in Section 4.3.9.

The pyroxenes are divided into two broad groups (Figure 4.13), with the majority of pyroxenes being quad, while a small number of pyroxenes fall on the

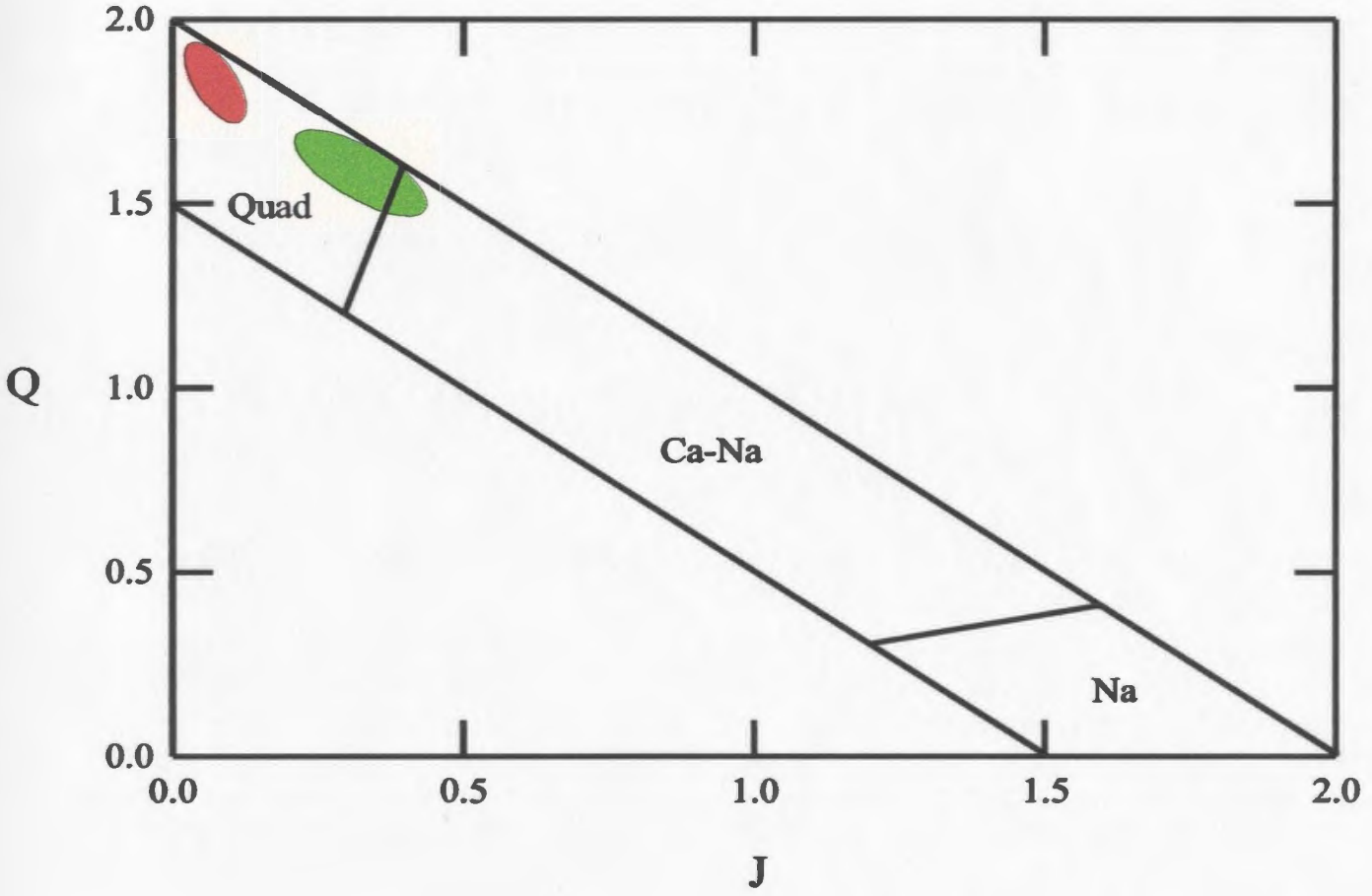

Figure 4.13: Pyroxenes plotted on Q-J diagram from Morimoto et al. (1988). Q= Ca+Mg+Fe, J= 2Na. Pyroxenes from the mafic rocks shown in red, pyroxenes from foidal phonolites and phonolites shown by the green field.

boundary between quad pyroxenes and Ca-Na pyroxenes as defined by Morimoto et al. (1988). The quad pyroxenes, described petrographically as diopside-augites and titanaugites, occupy the compositional range of. *ca.*, En=40-50, Fs=5-20, Wo=50-55 (Figure 4.14). The Ca-Na pyroxenes, identified as aegirine-augites in Chapter three, occur in foidal phonolites and phonolites. Pyroxene compositions from xenoliths are also plotted.

Quad Pyroxenes

Representative clinopyroxene compositions are shown in Table 4.1. The Mg# values of the quad pyroxenes, calculated from the structural formula data, range from *ca* 90 to 70. The diopside-augites tend to have lower Al and Ti contents than titanaugites with similar Mg#. A petrographical division of augites into titanaugites and diopside-augites is reflected in their chemistry by the amount of En end-member calculated from mineral compositions. The diopside-augites generally have less than 10% Fs while the titanaugites have greater than 10% Fs. This chemical difference between the two pyroxene types is also shown by their Si, Al and Ti cation concentrations (Figure 4.15). Titanium contents in the titanaugites range from ~0.08-0.23 atoms per structural formula (apsf), while the Al^{iv} apsf (Al^{iv}= 2-Si apsf) are greater than 0.18, with the majority of the titanaugites having more than 0.2 Al^{iv} apsf. In the diopside-augites there are~0.01-0.08 Ti apsf and 0.16-0.19 Al^{iv} apsf. Where a diopside-augite and titanaugite have the same Al^{iv} apsf, the titanaugites invariably have higher concentrations of titanium. A negative correlation exists between the Mg#, Al and Ti concentrations, while silica content of the

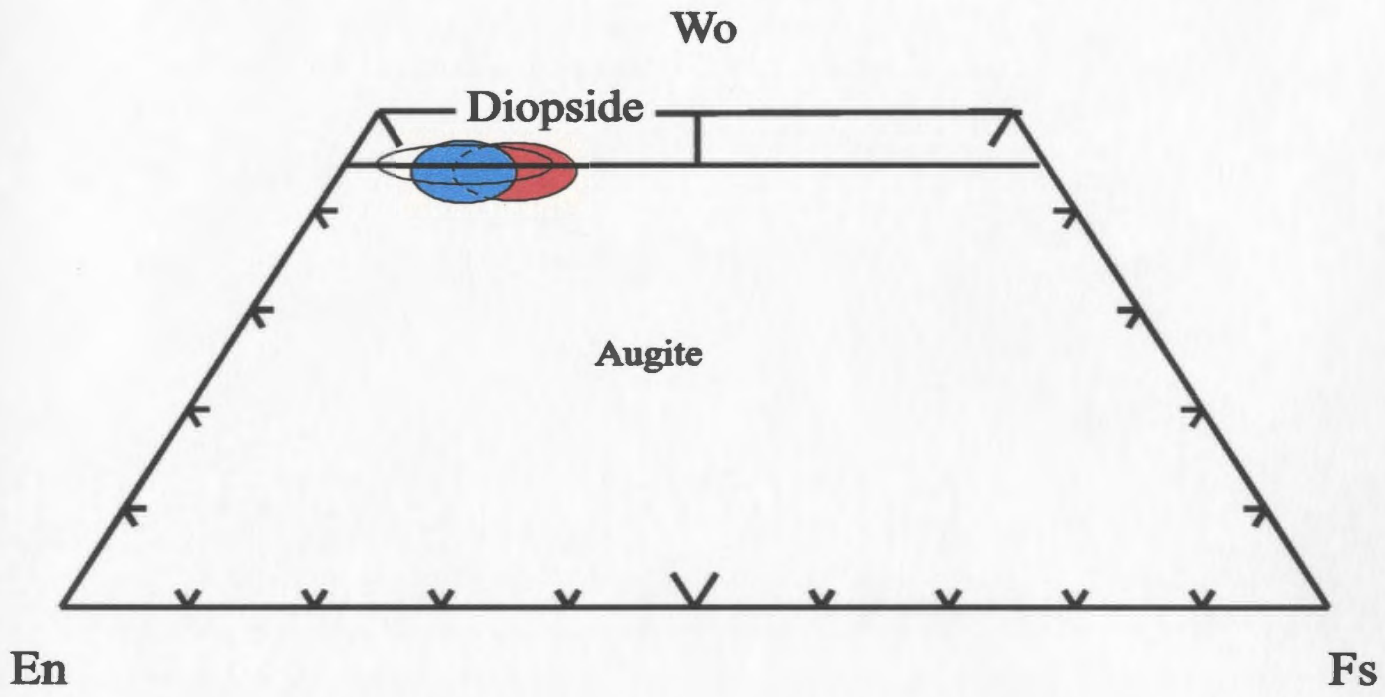

Figure 4.14: Pyroxene compositions. Titanaugite field shown by red; diopside-augites blue; pyroxenes occurring in xenoliths, the clear field.

Table 4.1

Major element chemistry of representative clinopyroxenes

	Titanaugite				Diopside-Augite			
	R94		R36		R42		R102	
	core-	rim-	core	core	core	rim	core	rim
SiO_2	45.60	46.79	46.98	45.08	49.20	49.00	49.80	49.30
TiO_2	3.60	2.85	3.09	4.45	2.32	2.12	1.91	1.99
Al_2O_2	7.90	6.87	7.28	7.50	5.70	5.50	5.00	5.30
FeO^t	6.90	6.90	6.81	8.03	5.50	6.00	6.00	5.90
MgO	12.50	13.00	12.97	11.44	13.60	13.80	14.20	13.80
MnO	0.10	0.07	0.19	0.16	0.10	0.09	0.10	
CaO	23.50	23.50	22.53	22.63	23.40	23.40	22.90	23.40
Na_2O	0.44	0.40	0.60	0.49	0.41	0.38	0.40	0.41
Cr_2O_3	-	0.08			0.32	0.34	0.39	0.63
total	100.54	100.46	99.85	99.78	100.55	100.63	100.70	100.73
Si	1.72	1.76	1.74	1.70	1.81	1.81	1.83	1.82
Ti	0.099	0.078	.086	0.12	0.064	0.059	0.053	0.055
Al^{IV}	0.28	0.24	0.253	0.30	0.19	0.19	0.17	0.18
$Al^{V}I$	0.06	0.06	.07	.04	0.06	0.05	0.04	0.05
Fe	0.21	0.21	0.21	0.25	0.17	0.18	0.19	0.18
Mg	0.69	0.71	0.72	0.64	0.75	0.76	0.78	0.76
Mn	0.003	0.002	.006	.005	0.003	0.003	0.003	0.001
Ca	0.93	0.93	0.90	0.92	0.92	0.93	0.9	0.93
Na	0.032	0.029	.04	.04	0.029	0.027	0.029	0.029
Cr		0.002			0.009	0.01	0.011	0.018
total	4.03	4.02	4.03	4.02	4.01	4.02	4.01	4.02

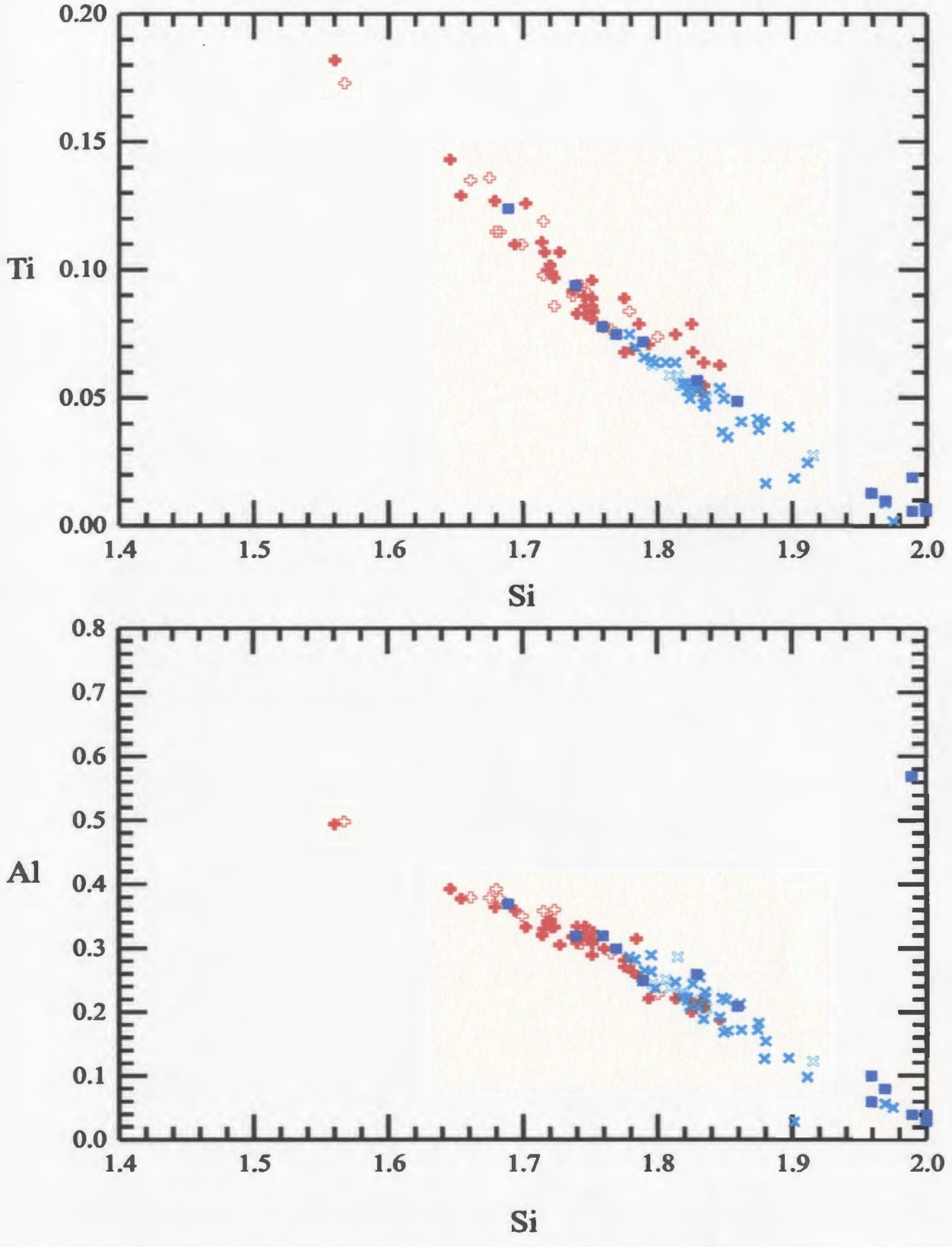

Figure 4.15. Variation of Ti (apsf) and Al (apsf) with Si (apsf) for pyroxenes. Titanaugites red plus symbols, diopside augites blue crosses. An analysis taken from the core is indicated by a filled symbol while an analysis from the rim is shown by an open symbol. Blue squares are pyroxenes from xenoliths.

pyroxenes increases with increasing Mg# (Figure 4.16). The diopside-augites have the highest magnesium numbers and silica concentrations.

Diopside-augites are generally unzoned, but the titanaugites exhibit chemical zoning from core to rim; *i.e.*, increasing Al_2O_3 and TiO_2 concentrations. The remaining major elements do not exhibit a significant change in concentration across the phenocryst.

The pyroxenes in the xenoliths generally have higher Si and lower Ti apsf than the pyroxene phenocrysts (Figures 4.13 to 4.16).

Poly-Phase Pyroxene Phenocrysts

Besides the zoning described in the titanaugites above, where there is a gradual systematic change in chemistry from core to rim, rare phenocrysts occur which exhibit an abrupt chemical change from core to rim (Table 4.2). These pyroxene phenocrysts have a distinctive bimodal composition and will be referred to as poly-phase pyroxene phenocrysts, or POPPs.

The cores of POPPs are pale green, sub-rounded and have irregular margins, while their rims are pink and in places exhibit optical zoning (ref. Figure 3.16, section 3.3.1). In all cases the cores of the these pyroxenes have significantly higher Si and lower Al, Ti and Fe^{2+} apsf compared to their rims. This chemical zonation, an increase in Al, Ti and Fe (from core to rim), is similar to the normal zoning exhibited by the titanaugite phenocrysts described above, but the change in chemistry from core to rim is more substantial and there also appears to be an abrupt compositional change between

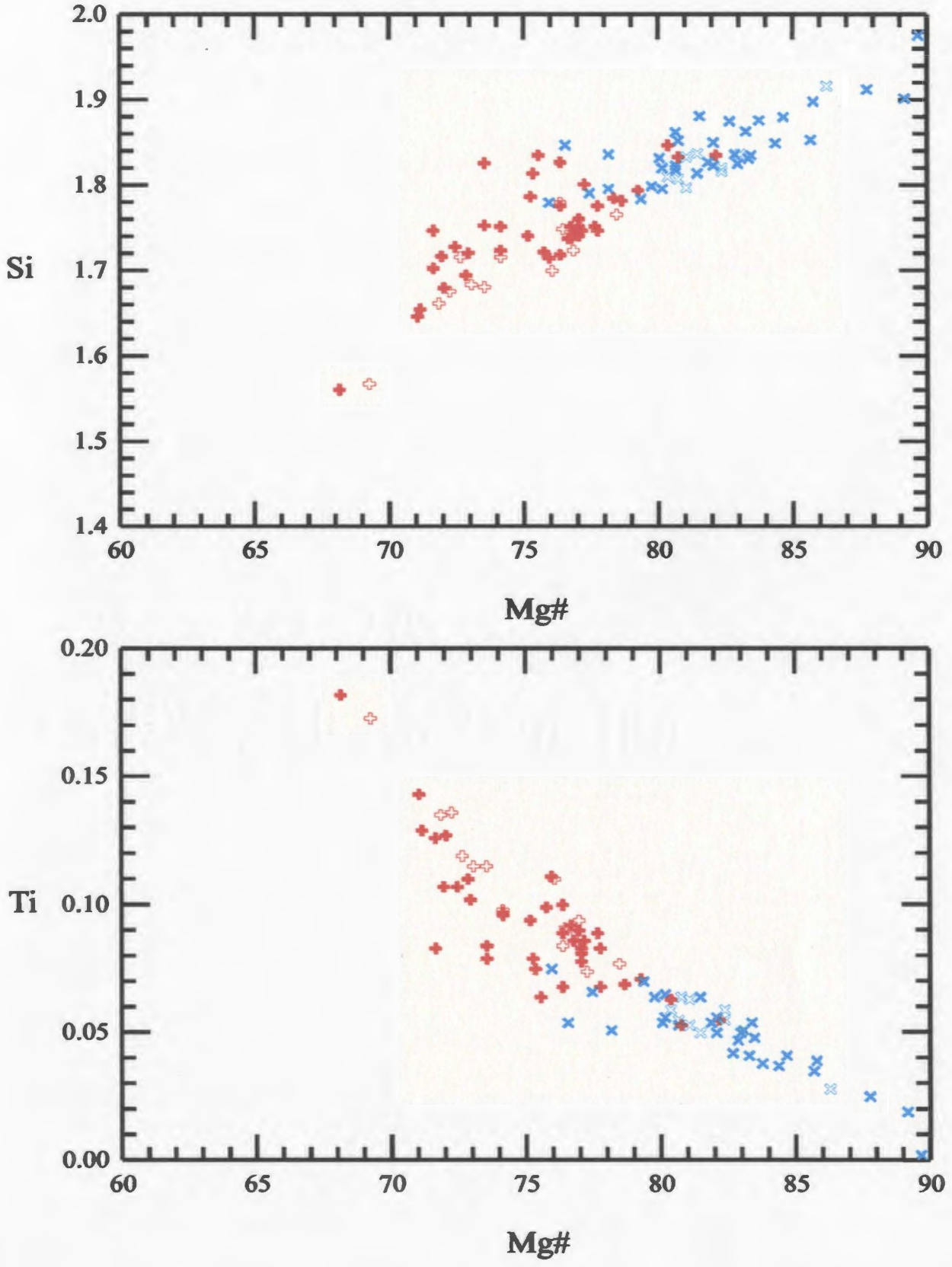

Figure 4.16: Variation of Si (apsf) and Ti (apsf) with Mg# for pyroxenes. Symbols are the same as Figure 4.15.

Table 4.2

Major element chemistry of representative POPPS

	R-74		R-102		R-94 core	
	core	rim	Core	rim	core	rim
SiO_2	47.7	44.1	49.9	48.3	49.35	45.91
TiO_2	3	4.78	1.98	2.37	2	3.94
Al_2O_3	6.3	8.57	4.8	6.07	5.02	7.29
FeO	5.96	5.12	4.52	4.65	4.28	3.86
Fe_2O_3	1.27	3.27	1.09	2.46	1.38	3.56
MgO	12.9	11.55	14.2	13.25	14.19	12.61
MnO	0.1	0.07	0	0.07	0.07	0.13
CaO	22.5	22.62	23.3	23	23.05	22.95
Na_2O	0.4	0.5	0.38	0.45	0.35	0.55
Cr_2O_3			0.66	0.2	0.81	0
total	100.13	100.58	100.83	100.82	100.5	100.8
Si	1.8	1.64	1.81	1.8	1.817	1.71
Al(T)	0.2	0.4	0.2	0.219	0.2	0.3
Al(M1)	0.05	0.03	0.04	0.045	0.04	0.02
Ti	0.08	0.1	0.06	0.066	0.06	0.1
Fe^{2+}	0.2	0.2	0.11	0.144	0.04	0.11
Fe^{3+}	0.04	0.09	0.03	0.068	0.1	0.11
Mg	0.7	0.6	0.8	0.728	0.8	0.71
Mn	0.003	0.002	0	0.002	0.002	0.004
Ca	0.9	0.9	0.9	0.909	0.9	0.9
Na	0.03	0.0 4	0.03	0.032	0.03	0.04
Cr	0	0	0.02	0.006	0.02	0
total	4.00	4.00	4.00	4.02	4.01	4.00

core and margin of the phenocrysts. The cores of these pyroxenes, except for phenocrysts R66-PX1 and R74-PX1, have Mg# above 80. In all cases, except for R66-PX1 the rim of any individual POPP has a lower Mg# (less than 80) and silica concentration than its respective core.

The phenocryst R66-PX1 is also anomalous with respect to other POPPs in having a large variation in Mg# while its core and rim have similar silica concentrations. The core in sample R66-PX1 is enriched in sodium relative to the cores and rims in other POPPs and to the quad pyroxenes described above. The cores and rims of the remaining POPPs have a similar chemistry to the more abundant quad pyroxenes, the cores being similar to the diopside-augites and the rims to the titanaugites.

Ca-Na pyroxenes

Due to the absence of Fe^{3+} data for the Ca-Na pyroxenes it is impossible to further divide them using the classification scheme outlined by Morimoto et al. (1988). The high iron content of these minerals and their petrographic characteristics, however, suggest that they have a significant Fe^{3+} content which would place them in the aegirine-augite field. For this study the classification of the Ca-Na pyroxenes as aegirine-augites is adequate. The Ca-Na pyroxenes have lower Mg# than the quad pyroxenes, generally less than 70. Representative Ca-Na pyroxenes are listed in Table 4.3.

Table 4.3
Major element chemistry of representative Ca-Na pyroxenes

	R25			R38	R107
	core	int	rim	rim	core
SiO_2	48.59	48.54	45.68	49.02	49.61
TiO_2	1.54	1.74	2.70	1.83	1.12
Al_2O_3	5.02	5.43	6.96	4.51	2.20
FeO^t	10.34	10.76	13.62	13.84	19.33
MgO	10.74	10.46	7.97		1.32
MnO	.35	0.32	0.44	7.82	3.94
CaO	22.09	21.73	20.98	19.71	19.83
Na_2O	0.92	0.96	1.42	2.10	2.01
total	99.59	99.94	99.76	98.83	99.36
Si	1.65	1.75	1.75	1.90	1.97
Ti	0.14	0.09	0.09	0.05	0.03
Al	0.39	0.31	0.32	0.21	0.10
Fe^{2+}	0.26	0.22	0.21	0.45	0.64
Mg	0.64	0.71	0.72	0.00	0.04
Mn	0.01	0.00	0.01	0.45	0.23
Ca	0.903	0.901	0.90	0.82	0.84
Na	0.04	0.05	0.04	0.16	0.15
total	4.03	4.03	4.03	3.99	4.00

4.3.2 Olivine

Typical olivine compositions are listed in Table 4.4. The olivines have forsterite (Fo) contents between 77 to 85, but can be as high as 90 (Figure 4.17). The silica concentration in the olivines correlates negatively with their Fo content. Olivines that occur in xenolith-bearing type II mafic rocks have some of the highest Fo contents (85-90). Type I mafic rocks contain the only olivines that have detectable Al_2O_3 and generally these have higher TiO_2 concentrations, between 0.1 and 0.4%, than the olivines in the type II rocks (< 0.1 wt. % TiO_2). The Ni content of the olivine phenocrysts range between 500 and 3500 ppm and is positively correlated with Fo content. Ni contents in xenolith olivines are generally higher, having a range between 2000 ppm and 5000 ppm. Titanium and calcium concentrations do not appear to display any systematic relationship with Fo in olivine. The olivines analysed do not exhibit any chemical zoning, having a uniform composition from core to rim.

4.3.3 Titanomagnetite

A summary of the titanomagnetite chemistry is shown in Table 4.5. In the mafic rocks Fe-Ti oxides have TiO_2 concentrations of 14-20 wt %, FeO concentrations of 58-66 wt. % and Mg# ranging from 29-12. Cr concentrations are < 1wt. %.

Table 4.4
Major element chemistry of representative olivine phenocrysts

	R36c	R40	R74	R129
SiO2	38.92	39.8	39.4	39.1
FeO	19.89	16.6	20.1	19
MgO	41.3	42.6	39.4	41.8
MnO	0.33	0.22	0.26	0.28
CaO	0.26	0	0.3	0.3
NiO	0.1	0.2	0.18	0.17
total	100.8	99.42	99.64	100.65
Si	0.99	1.01	1.01	0.99
Fe^{2+}	0.42	0.35	0.43	0.40
Mg	1.57	1.61	1.51	1.58
Mn	0.01	0.00	0.01	0.01
Ca	0.01	0.00	0.02	0.02
Ni	0.002	0.004	0.004	0.003
total	3.01	2.99	2.99	3.01
Fo	79	82	78	80

Table 4.5
Major element chemistry of representative titanomagnetites

	R36 oxl	R74 oxl	R40 oxl	R94 oxl	R56 oxl	R25 oxl	R107 oxl
SiO_2	0.3	0.5	0.4		0.4	0.2	
TiO_2	19.4	17.9	5	17.7	21.8	7.7	12.4
Al_2O_3	5.9	6.6	9.2	6.9	5.6	0.4	0.6
FeO	62.1	62.4	42.1	62.3	61.5	83.5	78.1
MgO	7.2	6.4	4.7	6.2	6.2	0.2	
MnO	0.34	0.35		0.37	0.5	1.51	2.6
Cr_2O_3	0.42	0.9	34.7	2.6	0.27	0.04	
NiO		0.16	0.07	0.11			
total	95.66	95.21	96.17	96.18	96.27	93.55	93.70

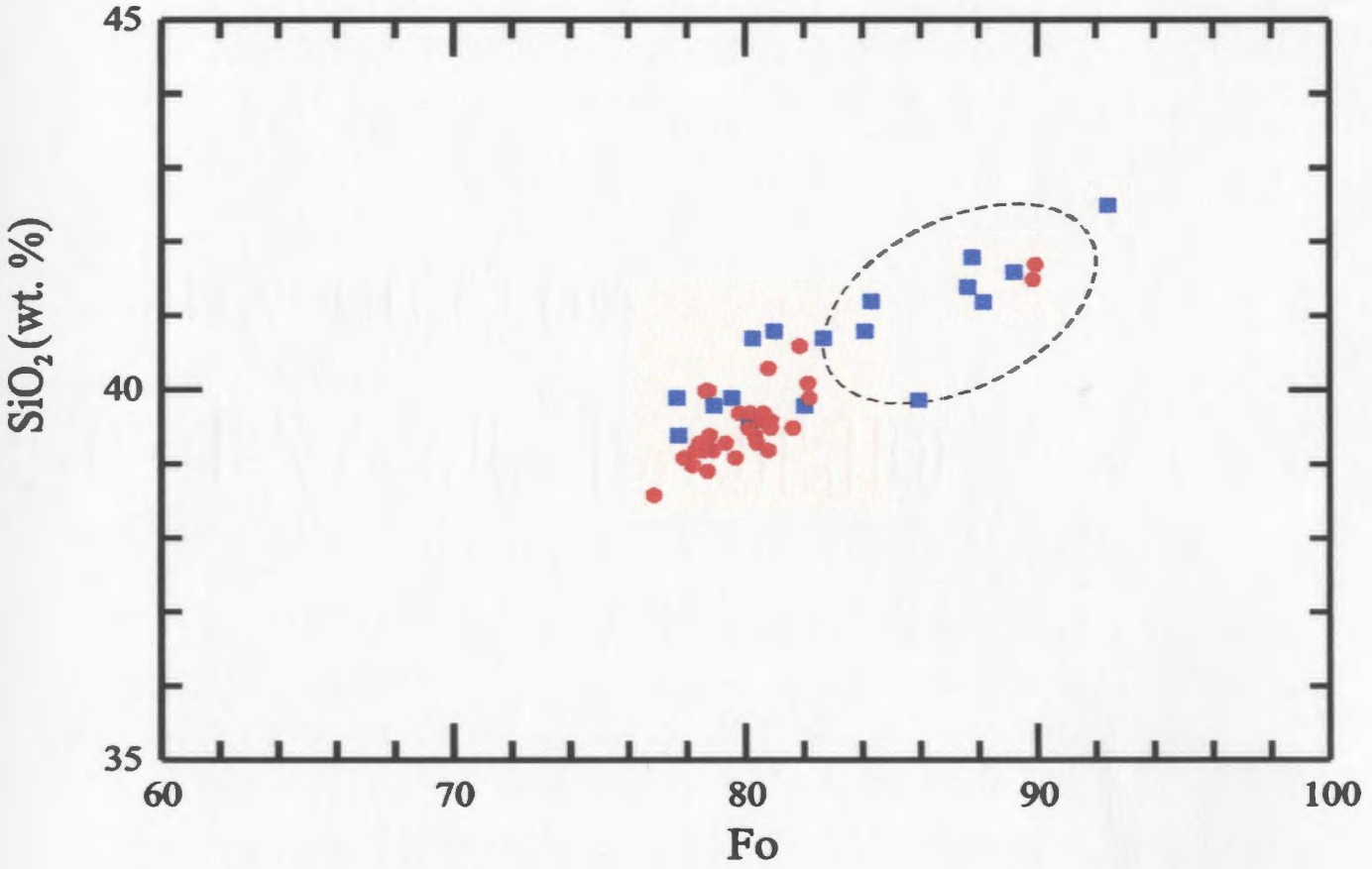

Figure 4.17: Covariation of SiO (wt. %) and Fo in olivine phenocrysts. Olivines from type I mafic rocks- red dots, type II - blue squares. Range of compositions of olivines in xenoliths is shown by dashed line

4.3.4 Kaersutite

A summary of kaersutite compositions is given in Table 4.6. The analysed kaersutite phenocrysts display a relatively uniform composition and do not display any chemical zonation from core to rim. The larger kaersutite phenocrysts have the same chemistry as the small groundmass kaersutite crystals.

4.3.7 Feldspar

Plagioclase compositions do not differ greatly between different mafic samples showing a range of compositions from An 65-75, Ab 20-32, Or 1-3 (Table 4.7 and Figure 4.18). In the phonolites, anorthoclase dominates the mineral assemblage with phenocrysts displaying a wide range of compositons, An 2-20, Ab 52-71, Or 14-37 (Table 4.7 and Figure 4.18). Within individual anorthoclase phenocrysts there is a general increase in Or content from core to rim. However, this is not a simple progression, as shown in Figure 4.19, where oscillatory zoning can be clearly observed.

4.3.8 Nepheline

A summary of nepheline compositions is presented in Table 4.8. The nephelines show a uniform chemistry having similar SiO_2 (46-47 wt. %), Al_2O_3 (~33 wt. %) and Na_2O (14-16 wt. %) in all of the samples.

Table 4.6

Major element compositions of kaesutite phenocrysts

	R56 hrn1	R56 hrn2	R56 hrn3	R56 hrn4	R56 hrn5
SiO_2	38.8	38.7	38.8	39.1	38.2
TiO_2	7.9	7.9	7.9	7.5	7.7
Al_2O_3	13.7	13.5	13.6	13.5	13
FeO	11.3	11.8	10.7	10.6	14.8
MgO	10.8	11.3	11.6	11.5	8.9
MnO	0.15	0.18	0.13	0.09	0.18
CaO	12.4	12.2	12.2	12.4	12
Na_2O	2.19	2.21	2.24	2.13	2.18
K_2O	1.45	1.49	1.37	1.44	1.62
total	98.69	99.28	98.54	98.26	98.58
Si	5.98	5.95	5.97	6.03	6.00
Ti	0.92	0.91	0.91	0.87	0.91
Al	2.49	2.44	2.47	2.45	2.41
Fe2+	1.46	1.52	1.38	1.37	1.94
Mg	2.48	2.59	2.66	2.64	2.08
Mn	0.02	0.02	0.02	0.01	0.02
Ca	2.05	2.01	2.01	2.05	2.02
Na	0.65	0.66	0.67	0.64	0.66
K	0.29	0.29	0.27	0.28	0.32
total	16.33	16.39	16.35	16.34	16.38

Table 4.7

Major element chemistry of representative feldspar phenocrysts

	R56 plag1 core	r129 plag1 core	R107 plag1 core	R107 plag2 core	R107 plag2 rim	R107 plag3 rim
SiO_2	50.8	51.4	65.1	64.8	65.1	64.3
TiO_2	0.08	0	0	0	0	0
Al_2O_3	31.4	30.8	21.2	21.1	21	21.5
FeO^t	0.4	0.49	0.2	0.27	0.56	0.23
MgO	0	0.06	0.02	0	0.02	0
CaO	14.7	13.3	1.3	1.1	1.2	1.2
Na_2O	3.1	3.5	7.4	7.2	8	7.8
K_2O	0.35	0.5	5.25	6.05	4.22	5.33
total	100.83	100.06	100.47	100.52	100.10	100.36
Si	9.21	9.44	11.59	11.58	11.60	11.49
Ti	0.01	0.00	0.00	0.00	0.00	0.00
Al	6.71	6.54	4.45	4.44	4.41	4.53
Fe^{2+}	0.06	0.07	0.03	0.04	0.08	0.03
Mg	0.00	0.02	0.01	0.00	0.01	0.00
Mn	0.00	0.00	0.00	0.00	0.00	0.00
Ca	2.85	2.57	0.25	0.21	0.23	0.23
Na	1.09	1.22	2.55	2.44	2.76	2.7
K	.08	.11	1.19	1.37	.76	1.22
total	20.01	19.96	20.06	20.1	20.05	20.11

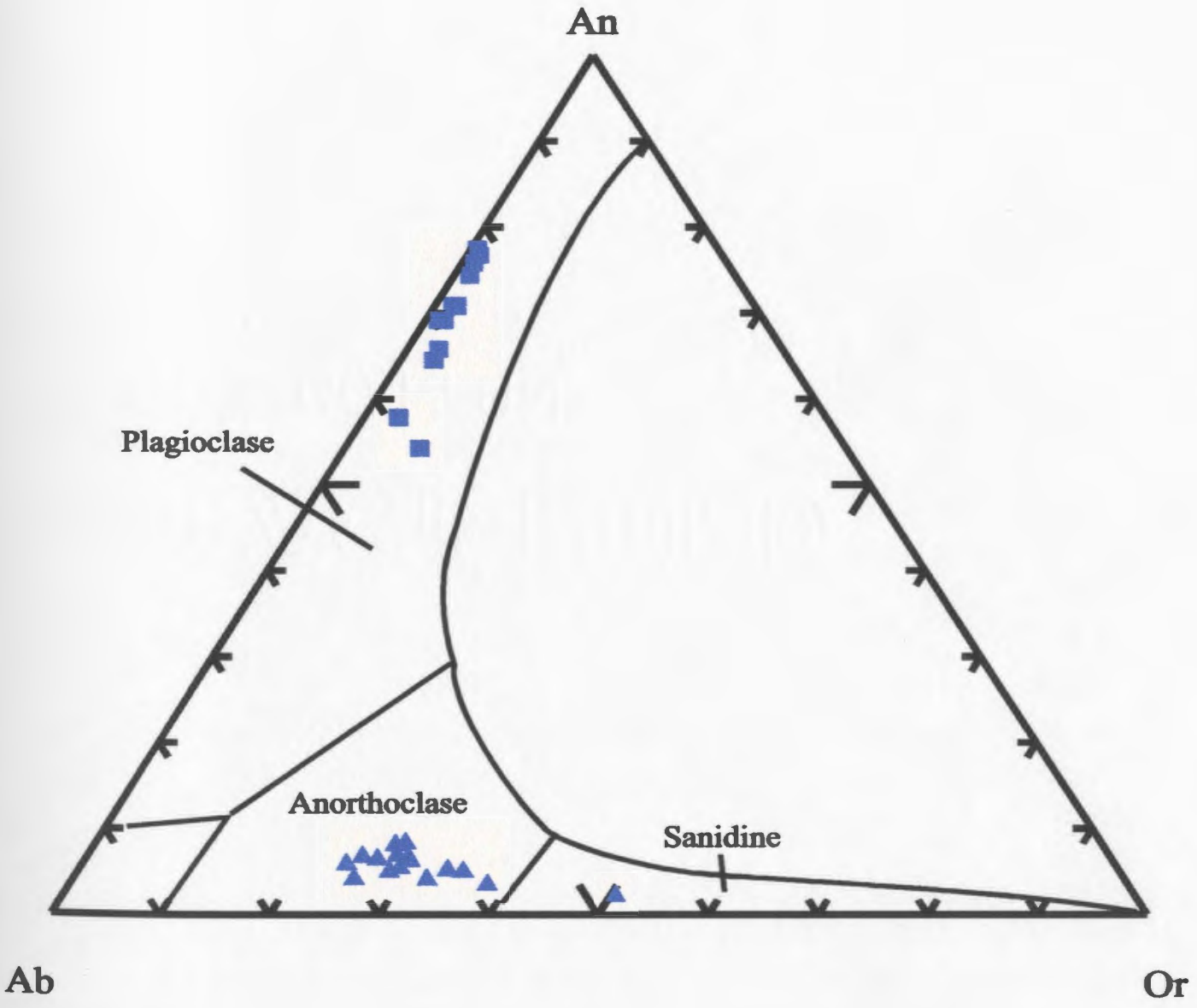

Figure 4.18: Feldspar compositions plotted on feldspar ternary diagram. Mafic type II rocks - blues squares, phonolites - blue triangles.

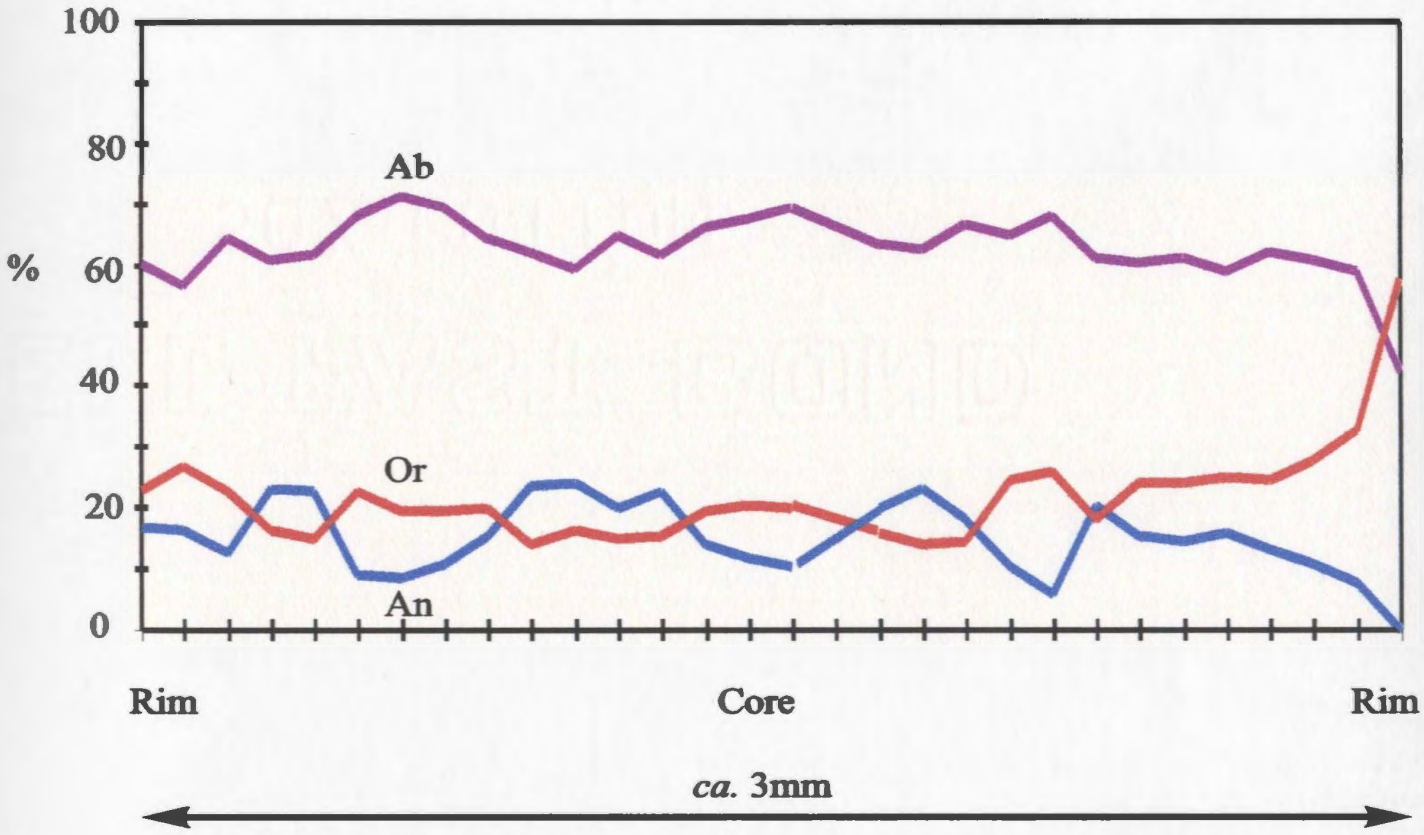

Figure 4.19. Compositional variation of feldspar phenocryst in a phonolite. The phenocryst is the same as the one shown in Figure 3.35.

Table 4.8

Major element chemistry of representative nepheline phenocrysts

	R38 neph		R25 neph	
	core	rim	core	rim
SiO_2	48.6	50.9	45.3	43.65
TiO_2				33.95
Al_2O_3	33.2	31.6	34.14	31.10.58
FeO^t	0.8	2.4	0.58	2.2
CaO	0.5	0.3		
Na_2O	12.8	11.0	14.55	17.65
K_2O	4.9	3.7	4.95	5.04
total	100.8	99.92	99.52	100.88
Si	9.01	9.41	8.51	9.38
Ti	0.00	0.00	0.00	0.00
Al	7.25	6.89	7.62	6.86
Fe^{2+}	0.12	0.37	0.00	0.34
Ca	0.10	0.06	0.00	0.00
Na	1.15	0.99	1.48	1.00
K	0.29	0.22	0.29	0.30
total	17.92	17.94	17.90	17.89

4.3.9 Discussion

It has long been recognised (Kushiro, 1960 and Le Bas, 1962) that the Al content of Ca-rich pyroxenes is inversely related to the silica content of the magmas from which they crystallise. Carmichael et al. (1970) demonstrated that a decrease in silica activity leads to an increase in the $CaAl_2SiO_6$ (Ca-Tschermak's molecule) content of pyroxenes. This suggests that the type I mafic rocks were formed from magmas with a lower silica activity than the type II magmas. Kushiro (1960) also showed that the substitution of Si by Al in clinopyroxene is less in the pyroxenes of tholeiitic magmas than in those of alkali magmas. Thus the number of tetrahedral sites occupied by Al decreases with fractionation in the tholeiites and related magmas and increases in the clinopyroxenes of alkaline rocks (Deer et al., 1978). From the relationship between Si and Al in the Rarotonga rocks it is clear that both titanaugites and diopside-augites crystallised from undersaturated alkali magmas.

Numerous studies of pyroxene compositions in fractionating alkali magmas (Yagi, 1953; Aoki, 1964; Kushiro 1964) have shown that the first pyroxenes to crystallise are diopside-augite in composition, followed by titanaugites and finally aegirine-augites, with the diopside- augites having low concentrations of TiO_2, which increases in the titanaugites and finally decreases in the aegirine-augites. The Rarotonga rocks show this trend to a limited extent. However, there is no final decrease in TiO_2 concentration in the aegirine-augites, which are still relatively enriched in this oxide. If the Rarotonga pyroxenes do in fact follow this common trend observed in other alkali magmas it is

feasible to suggest that the type II mafic rocks contain phenocrysts from the entire fractionation series while the type I mafic rocks have only phenocrysts from the latter stages of fractionation.

FeO and Fe_2O_3 in Pyroxenes

Cameron and Papike (1981) assessed the quality of an individual pyroxene analysis by subjecting each analysis to three crystal-chemical consistency tests: that the octahedral cations (Mn, Fe^{2+}, Fe^{3+}, Mg, Ti, Cr and Al^{vi}) sum to greater than 0.98 apsf; that M2 site occupancy is equal to 1.00±0.02, and that the charge balance equation is balanced ±0.03 of a charge. Using these guidelines it can be shown that a proportion of the total iron content analysed by the electron microprobe in the titanaugites as Fe^{2-} must be present in the Fe^{+3} valence state.

The inability for the electron microprobe to distinguish between Fe^{2-} and Fe^{3+} in an analysis has led to the development of methods where theoretical values of the two valance states of iron are calculated from the structural formula. The method used in this thesis is that of Robinson (1980) whereby the structural formula is recalculated so that the sum of the octahedral cations is equal to four on the basis of six oxygen atoms, by substituting Fe^{3+} for Fe^{2+}. A review of the reliability of calculating hypothetical Fe_2O_3 concentrations from microprobe data is provided by Vieten and Hamm (1971); Cawthorn and Collerson (1974) and Edwards (1976).

In applying these calculations to the Rarotongan samples it can be seen that the majority of titanaugites have Fe^{3+}/Fe^{2+} values greater than 0.5 while the diopside- augites

have lower theoretical Fe^{3+} concentrations, with Fe^{3+}/Fe^{2+} values generally less than 0.5 (Figure 4.20). In both titanaugites and diopside-augites there is a negative correlation between Fe^{2+} and Fe^{3+}, with the titanaugites invariably having higher Fe^{3+} concentrations at a given Fe^{2+} content.

Olivine

In Chapter three it was suggested that some of the phenocryst-bearing rocks may be partially cumulate in origin. It is difficult to prove this hypothesis on chemical or petrographic grounds. However, it is possible to test if a rock might represent a liquid by comparing the most forsteritic olivine phenocrysts in the rock to the composition of the calculated liquidus (BVSP, 1981). In comparing the Mg# in olivines and in the whole rock with theoretical partitioning values of Fe-Mg between olivine and a silicate liquid, an Fe^{3+}/Fe^{2+} value of 0.1 was assumed, a value consistent with Hawaiian magmas (Garcia., 1996). Most of the samples have approximately equilibrium Fe-Mg Kd values (e.g., 0.30±0.03), while the more porphyritic samples have slightly higher Fe-Mg Kd values (*i.e.*, R42- Kd~0.42 and R35= 0.48). This suggests that the more porphyritic rocks are enriched in olivine, probably due to accumulation effects, while the remaining samples may be equilibrium assemblages.

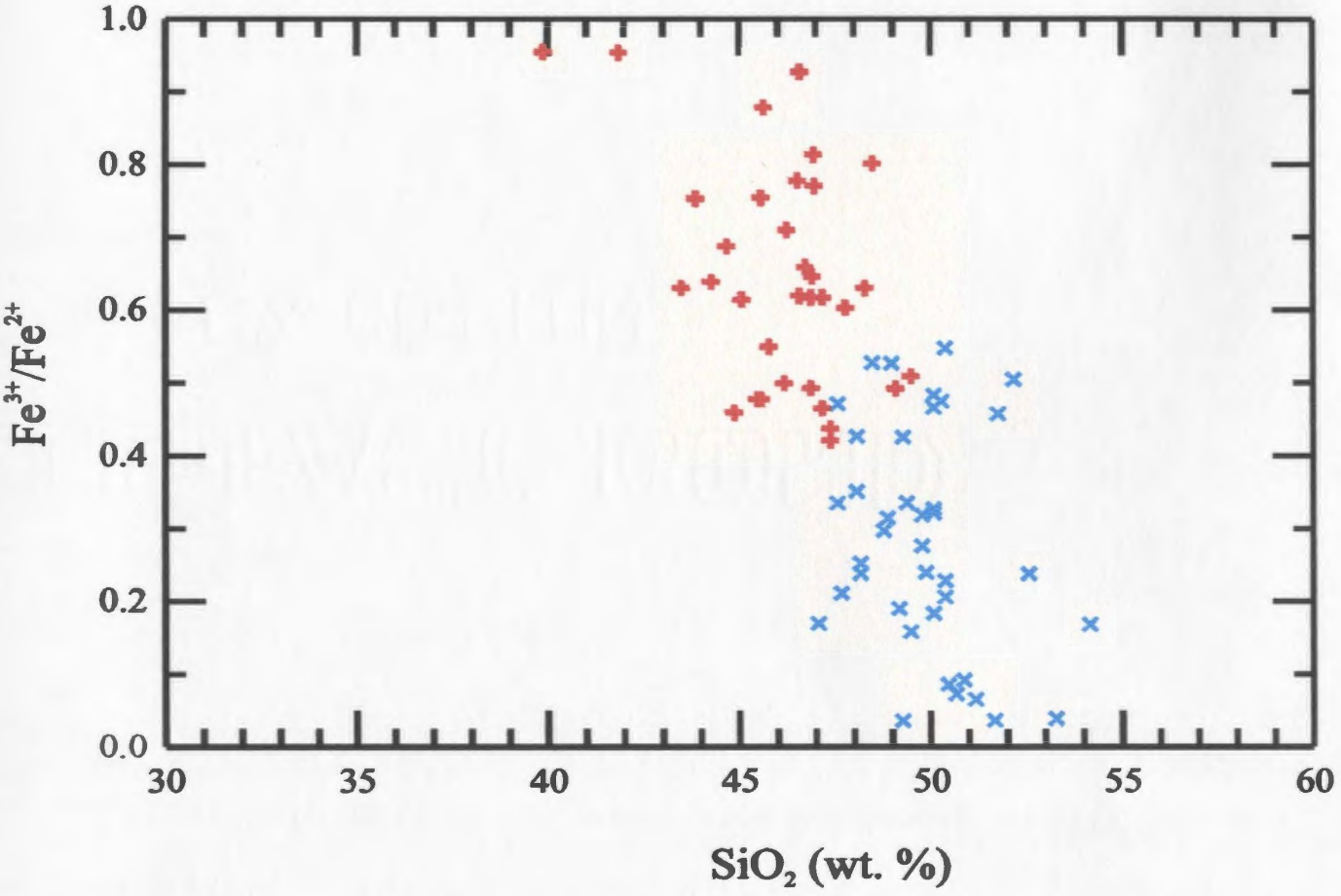

Figure 4.20: Calculated Fe^{3+}/Fe^{2+} vs. SiO (wt. %) pyroxene compositions. Titanaugites shown in red +, diopside-augites blue X.

4.4 Trace Element Mineral Chemistry

Selected trace element concentrations in phenocrysts were measured using a laser ablation microprobe attached to an ICP-MS (LAM-ICP-MS). This technique enables trace element concentrations in individual minerals to be measured *in situ*, *i.e.*, there is no need to physically separate mineral phases before an analysis is performed. A brief description of this technique and its limitations is given in Appendix 4.

4.4.1 Groundmass

In rocks from Rarotonga, instead of a true glassy groundmass that would represent a quenched magmatic liquid, the samples have a microcrystalline groundmass. It is assumed that the crystals within the groundmass are the result of final quenching of the liquid from which the larger phenocrysts crystallised. Therefore, if a sufficiently large area of this microcrystalline groundmass is analysed it should represent the composition of the original magmatic liquid. To analyse an area of sufficient size, the laser beam was defocused to form pits of approximately 100 microns diameter (Figure 4.21). The liquid composition was then taken to be the average of several analyses. A similar approach was taken to determine the major element composition of the groundmass, where instead of using a single spot analysis of (1-2 microns in size) the electron beam was rastered over an area of approximately 100 microns.

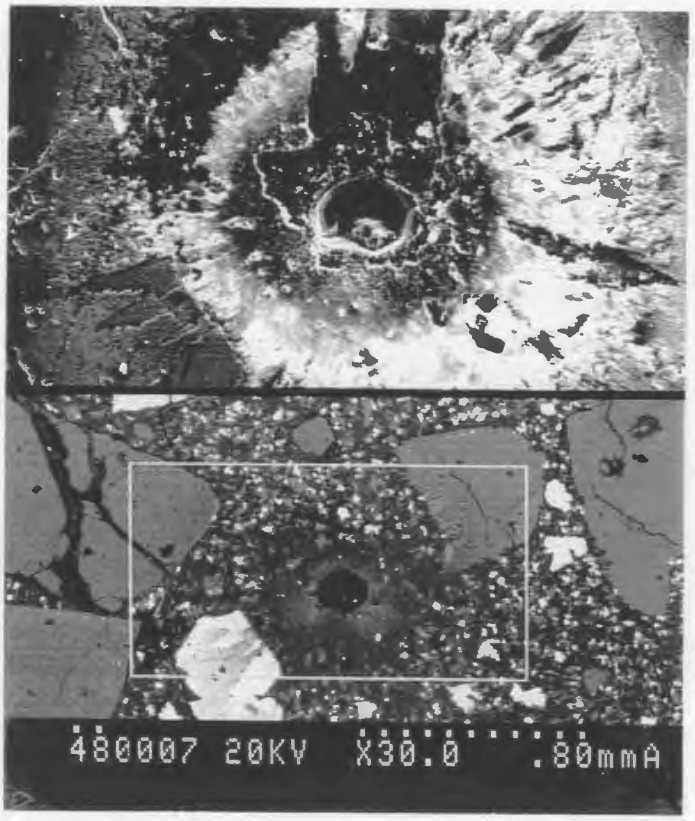

Figure 4.21: Back scattered electron image of a laser ablation pit in the groundmass of sample R36. The size of the pit is approximately 100 microns in diameter. The upper image is an enlarged view of the rectangle shown in the lower section.

The trace element concentrations in the groundmass are summarised in Table 4.9 where averages and the standard deviations (s.d.) of multiple analyses are listed. Generally the s.d is less than 10%, which is well within the precision error of 20% (10% for most elements in a homogeneous sample) given by Gunther (1995) for this technique. The trace element groundmass pattern is LREE-enriched relative to the HREE. LREE concentrations are 100 times greater than chondrite concentrations (Figure 4.22) while HREE 10-20 times greater than chondrite values. Similarly the high field strength and large ion lithophile elements are relatively enriched compared to chondrite values (Figure 4.22).

4.4.2 Pyroxenes

Phenocrysts chosen to be analysed for trace element concentrations were those that lacked obvious optical or major element zoning. These phenocrysts are heterogeneous, within the limitations of precision for this technique (15%; Gunther, 1995) but do not show a systematic variation in trace element concentrations from core to rim (Figure 4.23). Two possible reasons for these trace element distributions within a single phenocryst are crystallographic defects or mineralogical variations in the crystal.

The nature and the origin of these minor variations in trace element concentrations lie beyond the scope of this thesis. However, it should be noted that the

Table 4.9

Average trace element compositions (ppm) of the groundmass

	R36		R81	
	average (n=6)	s.d.	average (n=4)	s.d
Rb	94	5	35	11
Sr	452	81	938	93
Y	22	2	24	3
Zr	320	36	265	31
Nb	86	9	54	10
Cs	0.79	0.6	0.9	.6
Ba	236	191	455	51
La	42	3	44	6
Ce	100	10	92	15
Pr	11	0.6	12	2
Nd	44	2	53	7
Sm	9	0.9	11	2
Eu	3	0.1	4	.3
Gd	7	0.4	9	0.2
Dy	5	0.4	6	0.4
Er	2	0.2	3	0.3
Yb	1	0.3	1	0.3
Hf	7	0.5	6	1
Ta	5	0.5	3	0.5
Th	5	0.3	5	0.8

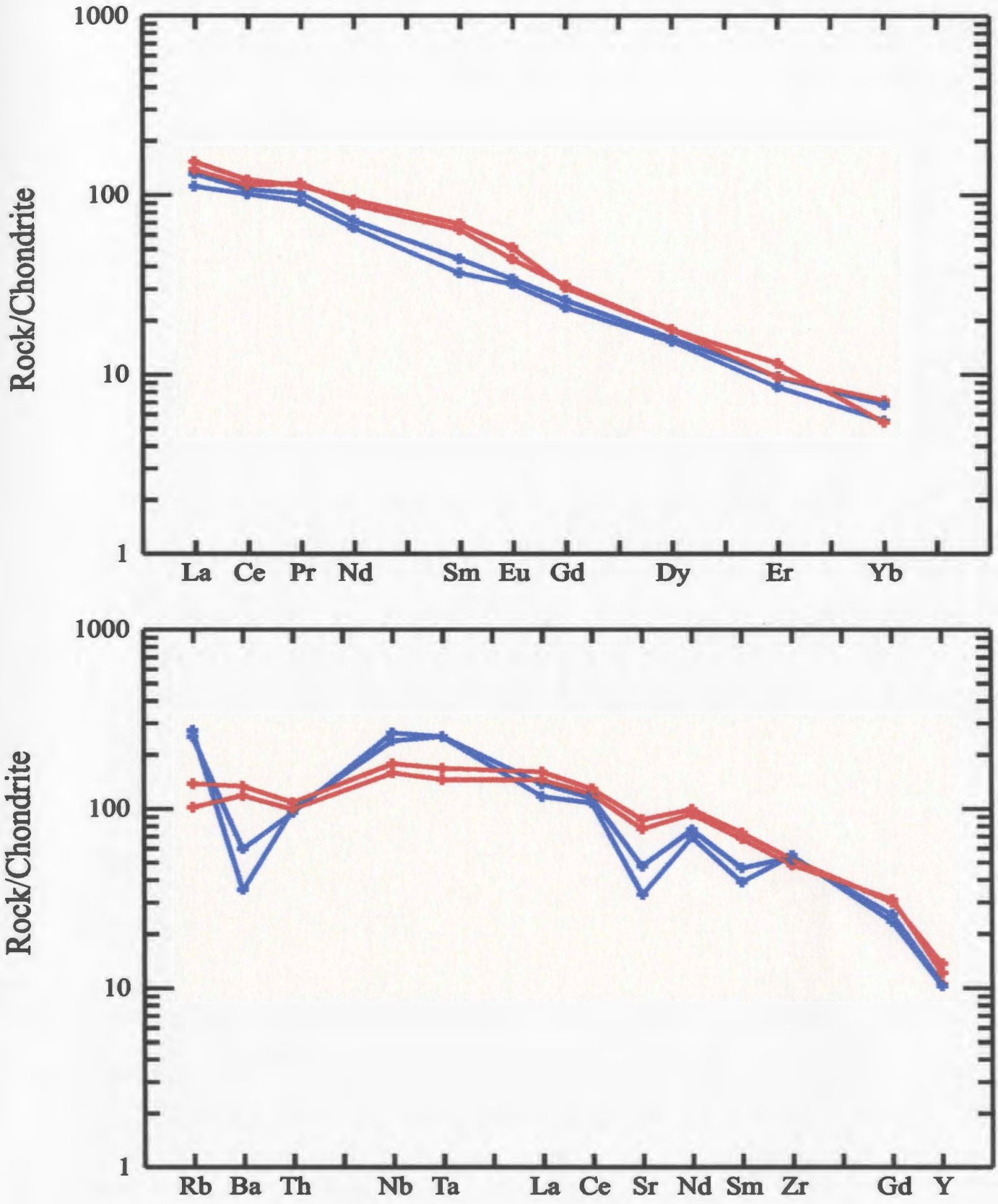

Figure 4.22: Chondrite normalised diagrams showing concentrations of selected groundmass analyses. Chondrite REE values from Nakamura 1974 and the remaining elements (Rb, Ba, Th, Nb, Zr, Gd and Y) from Sun 1980. Sample R36 (blue), Sample R81 (red).

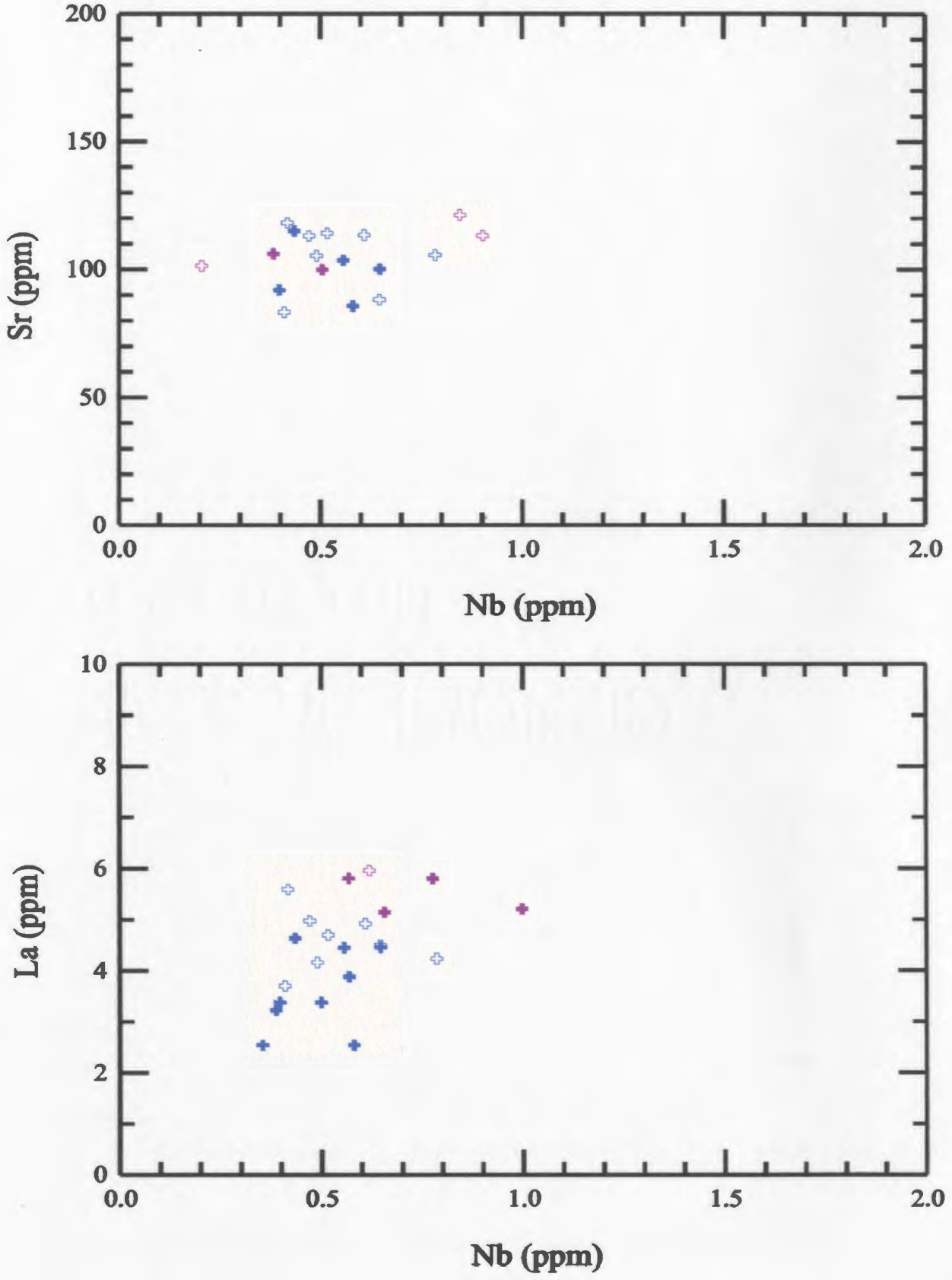

Figure 4.23: the co-variation of La, Sr (ppm) and Nb (ppm) of pyroxenes from sample R36 (blue) and R81 (pink). Analysis of a core is indicated by a filled cross, rims are shown as open crosses.

trace element variation within an individual crystal is of the same order as differences between phenocrysts within the same rock and between samples (Figure 4.23).

Titanaugites

Trace element data for selected clinopyroxenes are given in Table 4.10. The trace element concentrations in the titanaugites are typically higher than chondrite concentrations. REE concentrations in the titanaugites are between 2 and 30 times higher than REE concentrations in chondrites (Figure 4.24). The REE display a concave pattern, with enrichment of the middle REE (Pr-Eu) over the light and the heavy elements. LREE elements in the titanaugites are slightly enriched relative to the HREE.

Diopside-augites

Trace element concentrations in the diopside-augites are given in Table 4.11. The trace element pattern for these phenocrysts is similar to that of the titanaugites (Fig 4.25). However, absolute concentrations of trace elements are typically lower than in most of the titanaugites (*c.f.*, Table 4.10 and 4.11).

POPPs

POPPs from three rocks (R42, R74, and R-94) were analysed. As shown in Figure 4.26 and Table 4.12, there is a clear difference in trace element concentrations between the cores and rims of these phenocrysts which was not apparent in the titanaugite phenocrysts discussed above. The rims all have REE concentrations and

Table 4.10

Average trace element compositions (ppm) of the titanaugites

	R36px3		R36px		81px1		R81px2	
	rim	core	average (n=14)	s.d.	rim	core	average (n=5)	s.d
Rb	1.1	1.09	2	2				
Sr	106	104	102	10	101	110	106	6
Y	13	12	13	1	11	13	13	1
Zr	79	83	85	9	70	90	86	11
Nb	0.8	0.6	0.5	0.2	0.2	.4	0.5	0.2
Ba			2	2	.6	.8	.6	.7
La	4	4	4	0.5	4	5	4	0.9
Ce	22	21	20	3	17	18	18	3
Pr	3	4	3	0.4	3	4	3.4	0.4
Nd	18	19	17	3	17	22	19	4
Sm	5	5	5	1	5	5	5	2
Eu	3	2	2	0.3	2	1	2	0.4
Gd	6	4	5	1	5	4	4	2
Dy	4	3	4	0.7	3	2	3	0.6
Er	1	2	1	0.3	0.9	2	1	0.5
Yb	0.3	0.8	0.9	0.5	1	1	1	1.
Hf	3	3	3	0.7	3	5	4	1
Ta	0.02	0.07	0.1	0.07	0.1	0.2	0.1	0.05
Th			0.2	0.2			0.1	

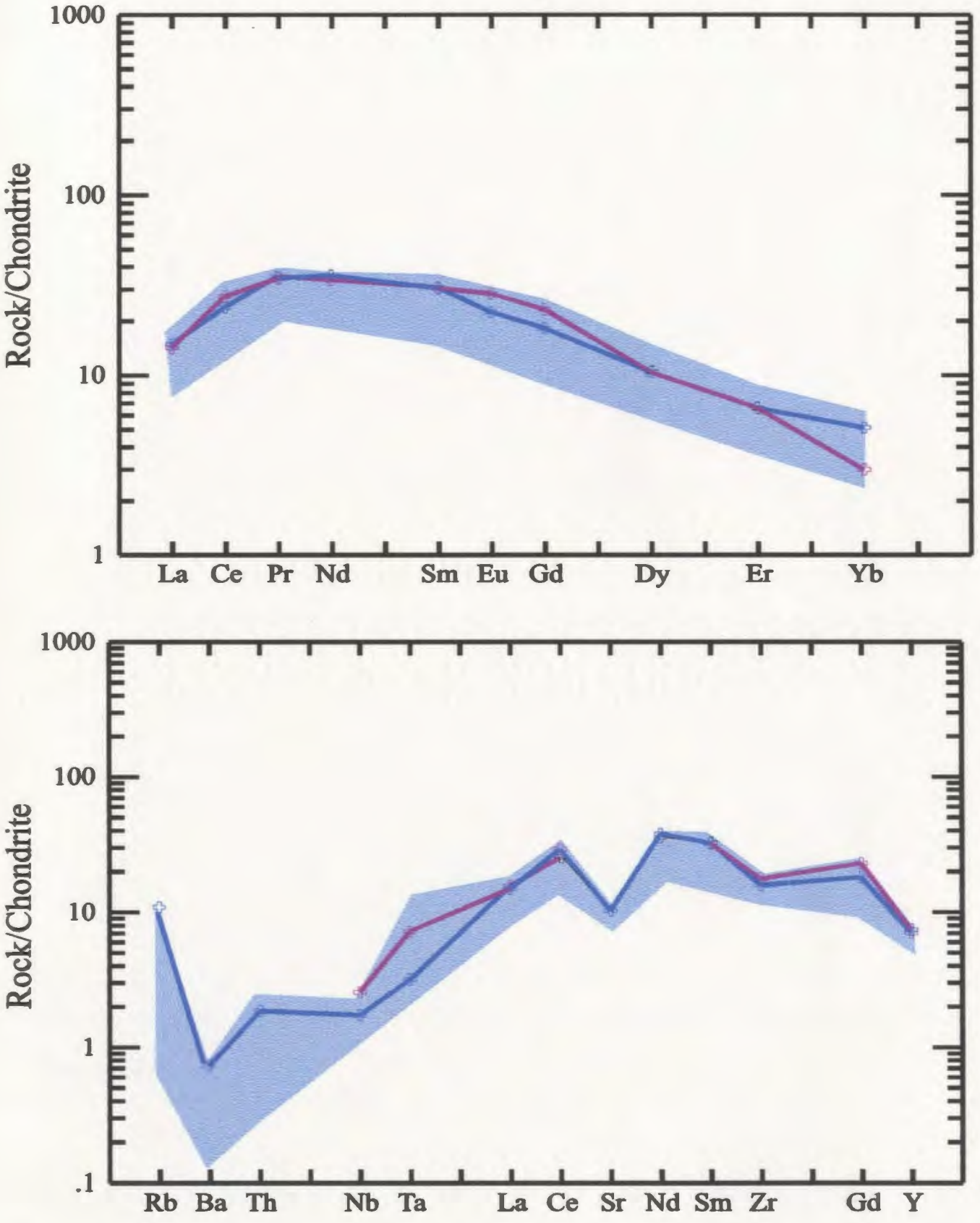

Figure 4.24: Chondrite normalised diagrams showing selected titanaugite samples; R81-px1 rim (pink) and R36-px2 core (blue). The range of values exhibited by all the titanaugites is shown by the shaded region.

Table 4.11

Trace element compositions (ppm) of selected diopside-augites

	94px1			42px1	
V	175.86	183.69	171.69	151.89	184.61
Rb			0.37		
Sr	95.23	92.05	87.96	77.29	98.7
Y	8.99	9.44	8.22	5.63	6.94
Zr	50.06	49.66	44.28	24.83	30.88
Nb	0.44	0.32	0.30	nd	nd
La	3.38	3.05	2.97	2.34	2.81
Ce	11.61	11.94	11.28	6.98	9.89
Pr	2.24	2.69	2.06	1.42	1.7
Nd	11.03	11.50	10.10	6.12	9.67
Sm	3.35	3.55	3.08	2.21	
Eu	1.16	1.43	1.06	nd	nd
Tb	0.49	0.42	0.42	nd	nd
Gd	3.18	3.07	3.22	nd	nd
Dy	2.02	2.19	2.04	nd	nd
Ho	0.33	0.43	0.31	nd	nd
Er	0.81	0.71	0.90	0.54	0.5
Tm	0.08	0.09	0.07	nd	nd
Yb	0.54	0.61	0.38	nd	nd
Lu	0.07	0.07	0.10	nd	nd
Hf	2.77	2.63	2.02		
Ta	0.07	0.08	0.07		
Th		0.03	0.02		

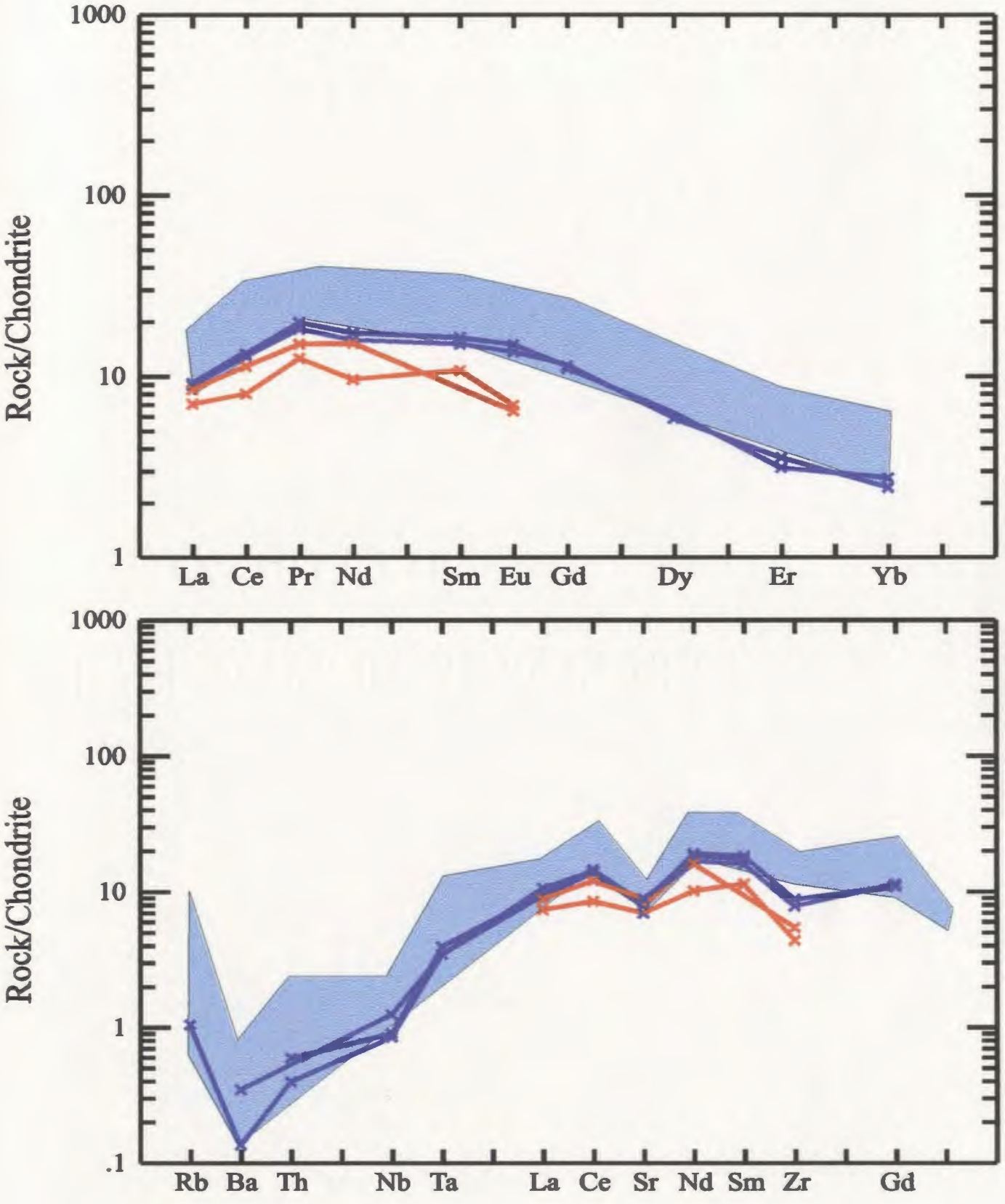

Figure 4.25: Chondrite normalised diagrams showing selected diopside-augite samples; R94-px1core (purple) and R45-px1 core (orange). The range of values exhibited by all of the titanaugites is shown by the shaded region.

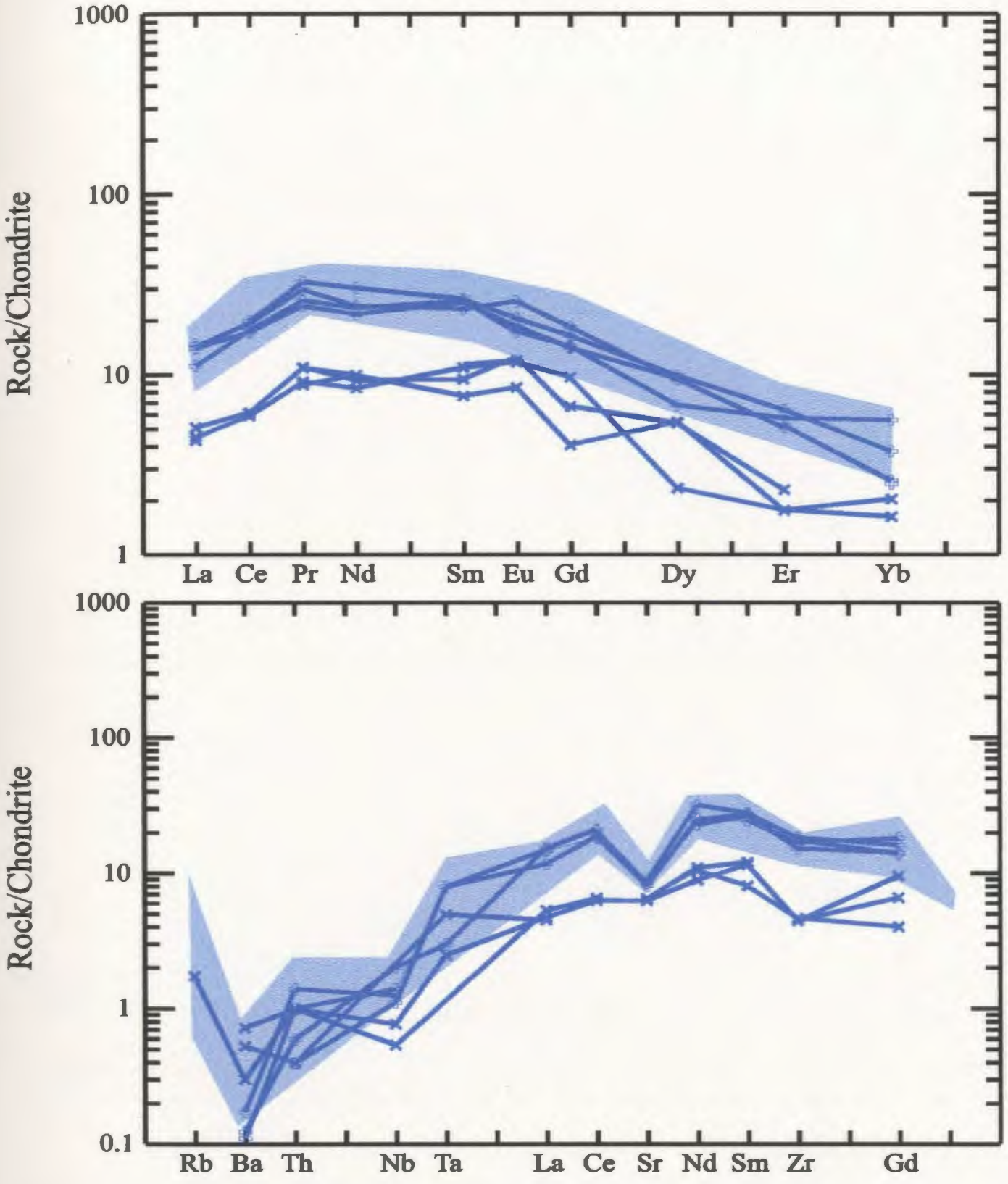

Figure 4.26: Chondrite normalised elemental concentrations of a POPP sample (R74-px1). The analyses from the core are plotted as filled crosses while the rim analyses are plotted as open crosses. The range of concentrations in the titanaugites is shown by the shaded region.

Table 4.12

Average trace element compositions (ppm) of the POPPs

	94px				74px				R66px			
	core		rim		core		rim		core		rim	
	average (n=6)	s.d	average (n=3)	s.d	average (n=3)	s.d	average (n=4)		average (n=5)	s.d	averag e (n=2)	s.d
V	194	20.31	347	28.78	167	9.30	305.05	28.35	165	13.70	162.81	23.14
Rb	3.45	3.68	5.82	6.73	0.33	0.30			0.66	0.48	0.04	0.00
Sr	81	4.58	127	21.17	70	1.18	93.73	3.34	323	7.58	95.46	8.65
Y	9.34	1.15	21	3.82	6.98	0.70	14.64	1.20	21	1.38	8.02	0.86
Zr	41	11.38	143	37.13	25.43	0.65	95.63	7.57	310	18.14	47.37	6.84
Nb	0.62	0.23	1.36	0.53	0.15	0.15	0.51	0.14	2.76	0.54	0.46	0.15
La	2.32	0.37	7.84	2.58	1.54	0.13	4.50	0.53	18	2.31	4.32	0.66
Ce	8.48	0.94	28	9.89	5.28	0.12	16.05	1.07	55	7.08	15.57	1.72
Pr	1.69	0.26	5.67	1.93	1.08	0.13	3.15	0.44	9.47	0.90	2.51	0.40
Nd	8.68	0.64	27	7.01	6.09	0.67	15.77	2.36	36	3.88	10.97	1.49
Sm	2.67	0.69	7.85	2.98	2.04	0.42	5.12	0.27	8.92	0.79	3.46	0.57
Eu	0.91	0.19	2.70	0.38	0.83	0.15	1.59	0.28	2.78	0.62	1.12	0.08
Gd	2.95	0.68	6.70	1.63	1.89	0.78	4.40	0.55	6.61	0.90	2.56	0.07
Dy	2.36	0.31	5.28	1.16	1.52	0.61	3.08	0.50	4.91	0.33	1.65	0.23
Er	0.84	0.13	2.21	0.31	0.44	0.07	1.27	0.13	1.75	0.53	0.67	0.02
Yb	0.62	0.17	1.10	0.21	0.33	0.13	0.80	0.32	1.50	0.59	0.48	0.02
Hf	2.03	0.55	6.96	1.29	0.64	0.44	3.94	0.66	12.05	2.60	2.32	0.41
Ta	0.07	0.04	0.28	0.04	0.08	0.04	0.14	0.05	0.53	0.09	0.08	0.05
Th	0.08	0.04	0.19	0.13	0.04	0.02	0.04	0.02	0.25	0.10	0.07	0.08

patterns similar to that of the large titanaugite phenocrysts. In both R94 and R74 the rims are enriched in REE compared to their respective cores.

4.4.3 Olivine

The trace element concentrations in olivines are below detection limits using the LAM-ICP-MS technique.

4.3.4 Titanomagnetite

The only trace elements that are significantly above detection limits in the oxides analysed are Y, Zr, Nb, (Yb), Hf and Ta. These values are summarised in Table 4.13.

4.4.5 Discussion

As shown by Gunther (1995), the LAM-ICP-MS technique is precise (*i.e.*, analyses of a homogeneous glass sample show little deviation in results between this method and any more conventional method of trace element analysis). In using a relatively new technique, determining the accuracy of the data and providing a suitable test of accuracy are much more difficult tasks than testing precision.

One method to test for this would be to physically separate minerals and then analyse them using conventional solution ICP-MS techniques (*i.e.*, analyse the

Table 4.13

Average trace element compositions (ppm) of titanomagnetites

	R36		R81	
	average (n-7)	std	average (n=3)	std
Y	0.21	0.12	0.43	0.22
Zr	35	12.56	29.16	0.94
Nb	7.07	0.79	7.47	0.56
Yb	0.25	0.03		
Hf	1.10	0.31	1.86	0.18
Ta	0.66	0.19		

mineral as a "whole rock" chemical analysis, see Appendix 2). While other studies have compared LAM-ICP-MS results with minerals analysed by ICP-MS solution (Jackson et al., 1992), these tests lie outside the scope of this thesis.

In the absence of a reliable test of accuracy, the average trace element concentrations for the groundmass, clinopyroxene, olivine and spinels, together with an estimate of modal abundance of these phases, were used to calculate a mass-balanced whole-rock trace element analysis. This calculated whole rock composition can then be compared with concentrations determined by ICP-MS whole rock analysis.

Although the errors involved in such a calculation far exceed the sensitivity of the technique, it does show whether the results are in general correct and if trace element trends are preserved. As can be seen from Figure 4.27 a close correlation exists between the calculated and measured whole rock, with only a few notable exceptions. The calculated element concentrations that are anomalous are for Ba, Sr, and Rb, which tend to exhibit the greatest amount of variation in the glass and pyroxene analyses.

The error in measuring these elements is probably due to their volatile nature (especially Ba) which can lead to errors in determining thier concentrations by LAM-ICP-MS. This is due to material ejected during ablation and depositing near the ablation area. From this material volatile elements are slowly released into the ICP-MS (Simon Jackson, pers. com.).

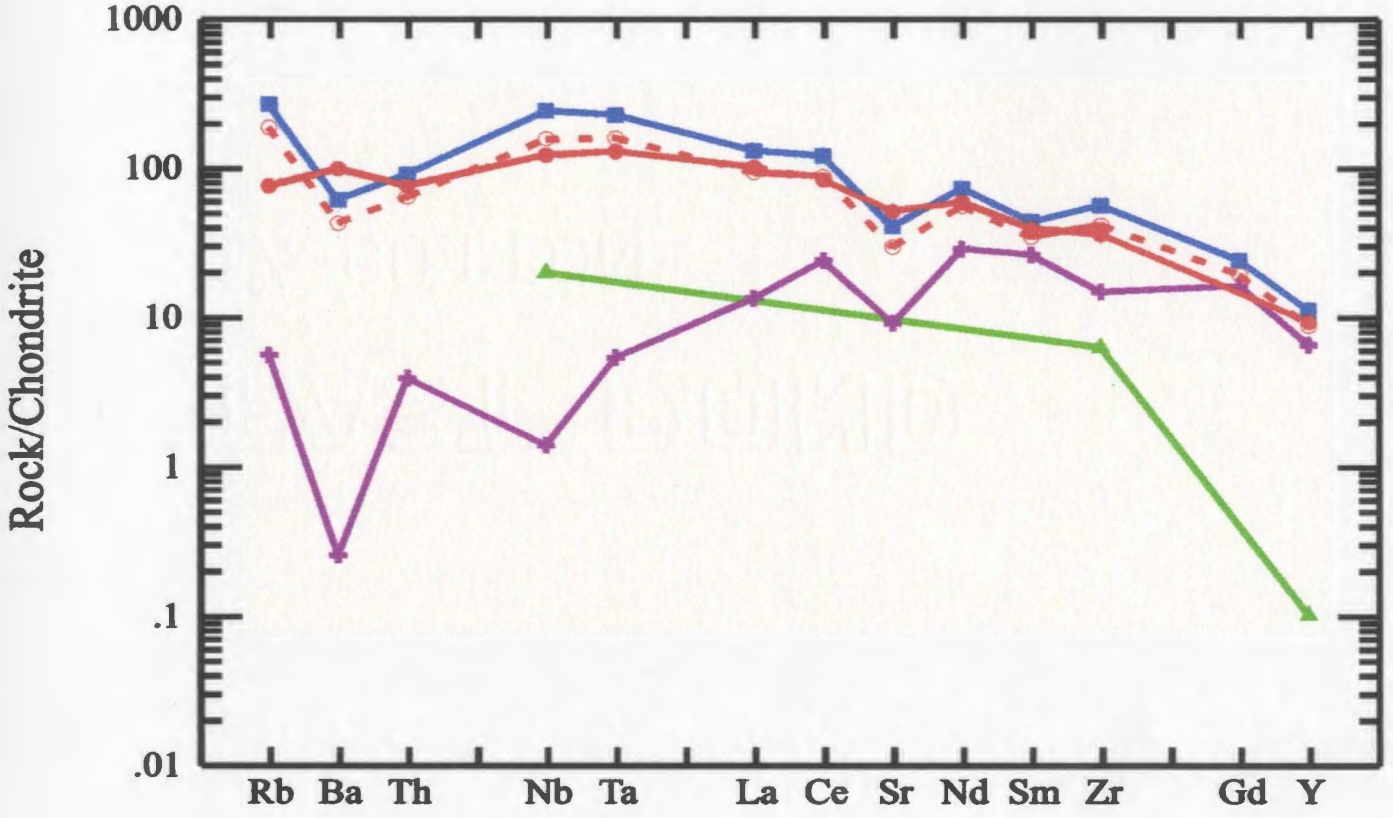

Figure 4.27: Chrondrite normalised plot of sample R36 (filled red circles) and a calculated composition (open red circles) using average trace element concentrations of mineral phases (titanaugite -purple crosses; titanomagnetites green triangles) and groundmass (blue squares) in R36.

POPPs

Polyphase pyroxene phenocrysts have been recorded in a number of studies of alkali basalts. A review of these occurrences is given by Brooks and Printzlau (1978). In their study they suggested that the phenocrysts could be either:

i. cognate but formed under different pressure/temperature regimes;
ii. xenocrysts derived from a different magma (magma mixing); or
iii. xenocrysts derived from the wall rocks traversed by the host magma (assimilation).

Of these, they favoured the second option. The third was negated on the grounds that polymineralic xenocrysts might be expected to occur, rather than just single phenocrysts. The first option was rejected because of the difficulty in defining a mechanism for producing differences in major elements within a single magma chamber. It is clear that the reasoning was based on conjecture rather than solid evidence. However, with the advent of microprobe techniques with enough spatial resolution to be able to determine the trace element concentrations in both the cores and rims of these phases, it should be possible to discount or support the above ideas.

As shown in section 4.2.2 there is a marked difference in the trace element concentrations between the cores and rims of the POPPs in Rarotonga. This difference could be accounted for solely by the major element composition of the phase crystallising. The incorporation of trace elements into the pyroxene structure is generally considered to be controlled by the Ca-Ti -Tschermak's molecule ($CaTiAl_2O_6$; Forsythe et

al., 1994, Gaetani and Grove, 1995). The cores have less than 10 mol% $CaTiAl_2O_6$, while the rims have approximately 15 mol% $CaTiAl_2O_6$. The stoichiometry of the phase crystallising is controlled by many factors other than the chemistry of the magma, *i.e.*, pressure/temperature and other phases crystallising. The examination of ratios of selected trace elements with the same Kd values or where the Kd values are known in the cores and rims, would provide a more accurate picture of the similarities or differences in liquids from which the cores and rims crystallised.

The partition coefficient for a particular element in a mineral phase is highly dependent on the physical properties of a magma, *i.e.*, it is obvious that ratio Kd_a/Kd_b (where *a* and *b* are elements with different ionic radius and possibly different valences) will be effected by variations in pressure and/or temperature in a magma chamber. Therefore in this study, adjacent REE elements were chosen with the caveat that the changes in physical conditions should affect their Kd values equally due to similarities in ionic radii and valence. In Table 4.13 Sm/Nd ratios of cores and rims of polyphase pyroxenes and single phase pyroxenes from different rocks, are listed. Also shown for comparison is the Nd/Sm ratio from pyroxene phenocrysts in a sample from Hawaii and a sample from Tahiti (unpublished data). The similarity of the ratios in the Rarontonga samples suggests that the POPPs, diopside-augite and titanaugite phenocrysts are cognate.

Table 4.14

Summary of Sm/Nd ratios from pyroxene phenocrysts.

(In all cases the values are averages of all analysis.)

	R36	R81	R94		R74		R42		Hawaii	Tahiti
			core	rim	core	rim	core	rim		
Sm/Nd	3.3	3.8	3.3	3.5	3.09	3.07	3.5	3.6	2.5	4.12

Summary

It has already been shown that the shield building mafic rocks can be divided into types I and II which have distinct pyroxene characteristics. Type I is characterised by a single population of pyroxenes, titanaugites. The second group has two populations of pyroxenes, titanaugites and diopside-augites. The titanaugites have low silica concentrations and high trace element concentrations, whereas the diopside-augites have high silica concentrations and low trace element concentrations. The similarity of trace element ratios of the titanaugites and diopside-augites suggests that the two phases are cognate.

4.5 Conclusions

In Chapter three, four problems were identified (p. 66):

i. the relationship between the diopside augites and titanaugites in the type II ankaramites;
ii. The chemical characteristics of the type I and type II mafic rocks;
iii. The relationship between the felsic rocks and the mafic rocks; and
iv. The nature of the underlying mantle;

The following conclusions arise from examination of the geochemistry of the Rarotonga rocks which answer some of the above questions:

i. The diopside-augites and the titanaugites in the type II rocks are cognate, with the diopside-augites crystalising before the titanaugites.

ii. There are two types of mafic rocks; a low silica type and a high silica type. The low silica type comprises the type I ankaramites and basalts, while the high silica group comprises the type II ankaramites and basalts described in Chapter three. The two groups can be only be distinguished chemically by their silica composition with the remaining elements (both major and trace) having similar concentrations in both groups.

iii. Both types are enriched in incompatible trace elements compared to the primitive mantle.

iv. Although some of the mafic rocks have primitive compositions they probably do not represent primary compositions due to the presence of cumulus minerals (*e.g.*, olivine).

It is clear that two of the questions are still unanswered; firstly the relationship beween the felsic and mafic rocks and secondly the nature of the underlying mantle. In the following chapters these two problems will be addressed by examining the petrogenesis of the mafic rocks (Chapter six) and the felsic rocks (Chapter seven) separately.

In trying to understand the petrogenesis of the mafic rocks we should be able to make some assumptions about the mantle from which their primary magmas were produced. However, to develop petrogenetic models we need to understand the

partitioning of trace elements between solid and liquid phases in a magma. This problem will be addressed in Chapter five.

Chapter Five

Distribution Coefficients

5.1 Introduction

A fundamental goal of igneous petrology is to develop petrogenetic models capable of describing the processes that produce an observed range of igneous rocks. In any such modelling, understanding the partitioning behaviour of trace elements between solid and liquid phases in magmas is vital. The measure of the affinity of a particular element towards either the liquid or solid phase(s) is referred to as a distribution coefficient(s) (Kd); which can be summarised by the following equation:

$$Kd^i = \frac{[i]_{mineral}}{[i]_{liquid}} \quad \text{.....5.1}$$

where i designates the element considered, and $[i]$ specifies its concentration.

Implicit in this definition is that a state of equilibrium exists between the mineral and liquid; that trace element behaviour obeys Henry's law; and that the distribution coefficient is dependent only on the temperature, pressure and the composition of all phases (McIntire, 1963). These governing conditions make it difficult to use true thermodynamic Kd values in studies of natural magmatic processes, as the relationships

between physical and chemical parameters are generally poorly known and it is uncertain whether equilibrium has been attained.

True thermodynamic Kd values can be obtained from experimental studies where physical and chemical parameters are controlled and known. A review of these various experimental procedures is given by Irving (1978). In theory, thermodynamic Kd values obtained from experimental studies can be used to model natural magmatic processes, provided that the physical and chemical parameters in the natural and experimental systems are similar. However, in natural rocks these parameters are still poorly understood, thereby making the correct choice of Kd values equivocal.

Even if the above parameters could be successfully determined, there is a general paucity of reliable Kd values for mafic magmas, especially mafic alkali magmas. A review of the literature (Dunn and McCulloch., 1982; Hack et al., 1994; Green and Pearson., 1985; Le Marchende et al., 1987) shows that reported Kd values for individual elements in basaltic magmas have a range covering more than an order of magnitude. Therefore, in modelling the magmatic evolution of igneous rocks, one of the potentially most important constraints is not known within an order of magnitude.

To avoid the uncertainties of using data from experimental or natural systems that are not known to be directly comparable to the compositions represented in the Rarotongan rocks, it was decided to obtain specific distribution coefficients by examination of samples from the island. Instead of using traditional techniques to determine trace element concentrations (*i.e.*, mineral/matrix separations; for examples of such studies see Villemant et al., 1981), use was made of the recent advance in solid

sample introduction, *i.e.*, by laser ablation, coupled to an ICP-MS, pioneered at Memorial University (Gunter et al., 1996 and references therein). *In situ* trace element analysis of minerals by laser ablation microprobe - inductively coupled plasma - mass spectrometry (LAM-ICP-MS) has a number of advantages compared to physical separation and/or other microbeam techniques (Jenner et al., 1994). The major advantages are as follows:

i. Elimination of the possibility of impure mineral separation that can lead to inaccurate phenocryst/matrix determinations (as discussed by McKay, 1986);

ii. LAM-ICP-MS system has the capability to determine trace elements at ppm levels in a very small area, *e.g.*, 10's to 100's of microns; and

iii. With the use of time integrated data acquisition techniques, it is possible to identify and exclude analyses or portions of analyses that are biased by inclusions of accessory phases, a problem that is addressed in detail by Mahood and Hidreth (1983) and Micheal (1988). When analysing mafic phases (Ti-Fe oxides, pyroxenes etc.), analyses that have anomalous trace element concentrations (*e.g.*, extremely high concentrations of Sr, Rb, Ba, *etc.*) are rejected on the assumption that these analyses are biased by inclusions within the mineral, either glass or mineral impurities.

5.2 Sample Selection

Implicit in the determination of a distribution coefficient is that equilibrium has been attained between the solid and liquid (crystal and glass/groundmass). In natural

rocks this assumption is somewhat difficult to prove. It is, however, possible to identify and exclude those phenocrysts that are definitely not in equilibrium. The criteria used to show a phenocryst is out of equilibrium with the groundmass are summarised below:

i. Petrographic information - those exhibiting hour glass zoning (*cf.*, Deer et al. 1978); irregular boundaries/margins on phenocrysts; phenocrysts with a sponge-like texture.

ii. Chemical constraints - whereby the major element chemistry of the crystal and the groundmass that surrounds it are used to evaluate equilibrium. The average proposed exchange coefficient for FeO/MgO between clinopyroxene and its host liquid from different authors (Thompson, 1974; Stolper, 1980; Irving and Frey, 1984) is 0.29. It can therefore be assumed that rocks which have a $FeO/MgO]_{cpx}/[FeO/MgO]_{lava}$ value between 0.2 and 0.4 have minerals that are likely in equilibrium with the once liquid phase. It therefore can be quickly ascertained if a phenocryst is in chemical equilibrium with its groundmass.

Two samples were chosen from Rarotonga that met the above conditions, R36 and R81. In addition, both of these samples are considered to represent relatively primitive magmas having Mg# between 65 and 75, Cr> 200 and Ni>100. The major and trace element chemistry of these rocks and their mineral phases has been previously described in Chapter four.

5.3 Results

5.3.1 Olivine

As discussed in Chapter four trace element concentrations in the olivine phenocrysts from Rarotonga are generally below detection limits. It is therefore not possible to determine the absolute Kd value for elements with respect to olivine, however, it is possible to determine maximum Kd values. This is done by using the limit of detection value as the maximum concentration of that element in a particular olivine crystal (Table 5.1).

5.3.2 Pyroxene

The titanaugite Kd values are summarised in Table 5.2 and graphically depicted in Figure 5.1, where they are compared to the range of reported values from natural mafic rocks (the shaded region). Also included in this diagram are data from a single experiment using an alkali basalt at 30kbar and 1380°C from Hart and Dunn (1993) and data from a natural alkali lamprophyre using LAM-ICP-MS produced by Foley et al. (1996).

The Kd values derived from R36 and R81 are generally in the middle part of the range of values reported from the literature, and below this range for Nb and Ba. The

Table 5.1

Minimum detectable Kd values for Olivine

	Kd
Rb	0.001
Sr	0.0003
Ba	0.0003
Cs	0.02
Y	0.004
Zr	.0007
Nb	0.0005
Hf	0.03
Ta	0.02
Pb	0.002
Th	0.02
U	0.03
La	0.002
Ce	0.0001
Pr	0.001
Nd	0.0007
Sm	0.006
Eu	0.07
Gd	0.009
Dy	0.04
Er	0.04
Yb	0.04

Table 5.2

Partition coefficients for clinopyroxene/groundmass pairs

	R36 Px average	R81 Px average	average Kd	Cpx from Hart and Dunn 1993	Cpx from Foley et. al 1996
Rb	0.02	0.06	0.01	not reported	0.0047
Sr	0.2	0.1	0.15	0.1283	0.0963
Ba	0.007	0.001	.004	not reported	0.00061
Y	0.6	0.5	0.6	0.467	0.438
Zr	0.3	0.3	0.3	0.1234	0.121
Nb	0.006	0.009	0.008	0.0077	0.0027
Hf	0.5	0.6	0.6	0.256	not reported
Ta	0.02	0.05	0.04	not reported	not reported
Th	0.04	0.03	0.03	not reported	0.0056
La	0.1	0.1	0.1	0.0536	0.0435
Ce	0.2	0.2	0.2	0.0858	0.0843
Pr	0.3	0.3	0.3	not reported	0.124
Nd	0.4	0.4	0.4	0.1873	0.173
Sm	0.6	0.5	0.5	0.291	0.283
Eu	0.8	0.5	0.6	not reported	0.312
Gd	0.7	0.5	0.6	not reported	0.336
Dy	0.7	0.5	0.6	0.442	0.363
Er	0.7	0.6	0.6	0.387	0.351
Yb	0.7	0.9	0.8	0.430	0.313

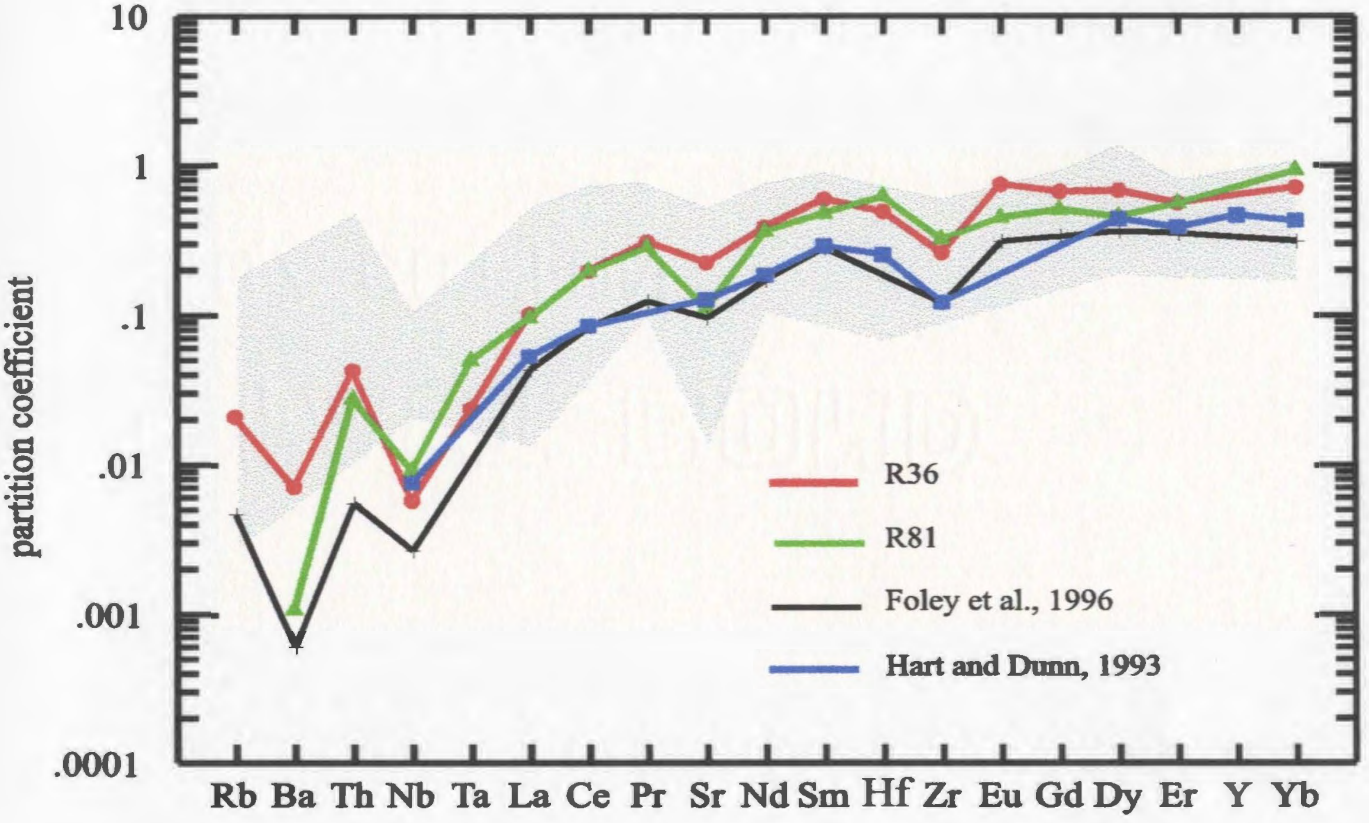

Figure 5.1: Partition coefficients for pyroxenes from Rarotonga. Also shown for reference are data from Foley et al., 1996 and Hart and Dunn, 1993. The shaded region is the range of partition coefficients from the literature (Schock, 1979; McKay et al., 1986; Villemant, 1988; Neilsen et al., 1992, Worner et al., 1993; Horn et al., 1995).

REE (Nd, Sm, Eu) are close to the upper limit of reported values. Compared to the Kd values from Hart and Dunn (1993) and Foley et al. (1996), both R36 and R81 have higher values, although, the general pattern of Kd values shown in Figure 5.1 is similar.

5.3.3 Titanomagnetite

For most trace elements in magnetites the concentrations are too low to accurately determine distribution coefficients. Those that can be determined are summarised in Table 5.3. Magnetites, and oxides in general, have the least number of published partition coefficients, and Kd values reported display a range of 2-3 orders of magnitude (Schock, 1979; Worner et al., 1983; McKay et al., 1986; Le Marchande et al., 1987; Villemant, 1988; Neilsen et al., 1992; Horn et al., 1995). The Kd values (including maximum possible Kd values; Table 5.1) for magnetites in this study generally fall at the lower end of the spectrum of published values. The high Kd values reported in the literature are those analyses obtained by mineral separation techniques while the lower values were obtained using *in situ* trace element techniques similar to the procedure used in this study. This leads to the argument that the high values are biased by inclusions or impure mineral separates.

Table 5.3

Partition coefficients for titanomagnetite/groundmass pairs

	R36	R81
Y	0.009	0.019
Zr	0.1	0.091
Nb	0.08	0.087
Hf	0.16	0.27
Ta	0.14	n.d
Yb	0.2	n.d

5.4 Discussion

5.4.1 Reliability of data

The accuracy of the LAM-ICP-MS technique has already been discussed in Chapter four. In addition it is possible at this stage to show that the data obtained by LAM-ICP-MS on mineral/groundmass pairs is consistent with whole rock data. This can be done by comparing the relative distribution coefficients of trace elements determined from whole rock trace element chemistry with measured distribution coefficients. $Element_a$ vs. $Element_b$ plots and $Element_a/Element_b$ vs $Element_a$ serve to illustrate the relative degree of incompatibility between elements such as Zr and Nb (*e.g.*, Le Roex, et al., 1990). Elements with a similar degree of incompatibility will have trends that when, extrapolated, will intersect the origin. For elements with dissimilar degrees of incompatibility extrapolation of the trend will cut the axis of the least incompatible element. As can be seen from Figure 5.2 the relative order of incompatibility of trace elements determined from the whole rock data is the same as the order of distribution coefficients for the pyroxenes.

5.4.2 Petrogenetic Implications

The specific knowledge of distribution coefficients for the main mineral phases in the basalts from Rarotonga allows for comments to be made on the effects that the

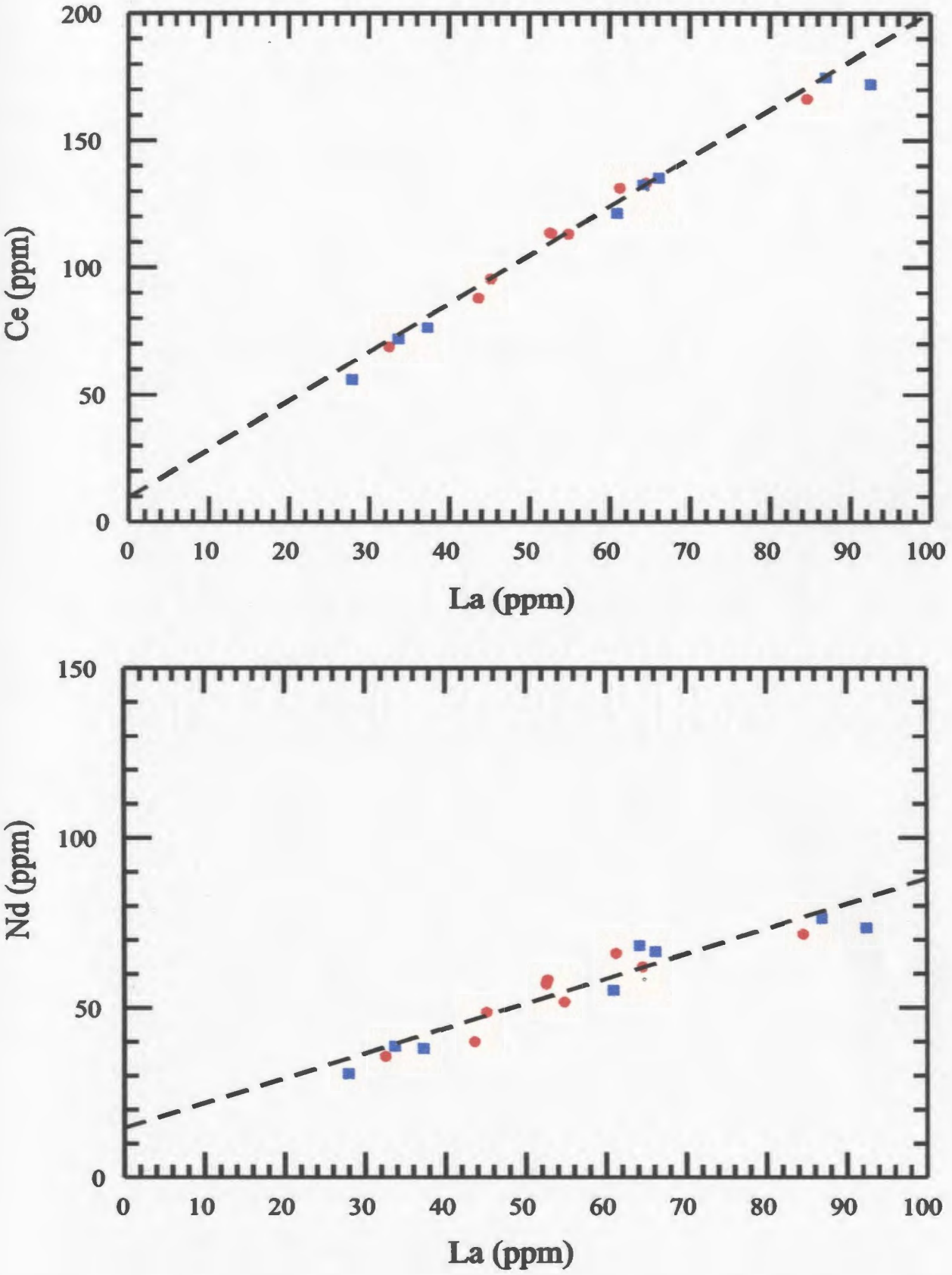

Figure 5.2. Covariation between LREE, Y and Th in Rarotonga mafic rocks. Symbols are the same as Figure 4.1.

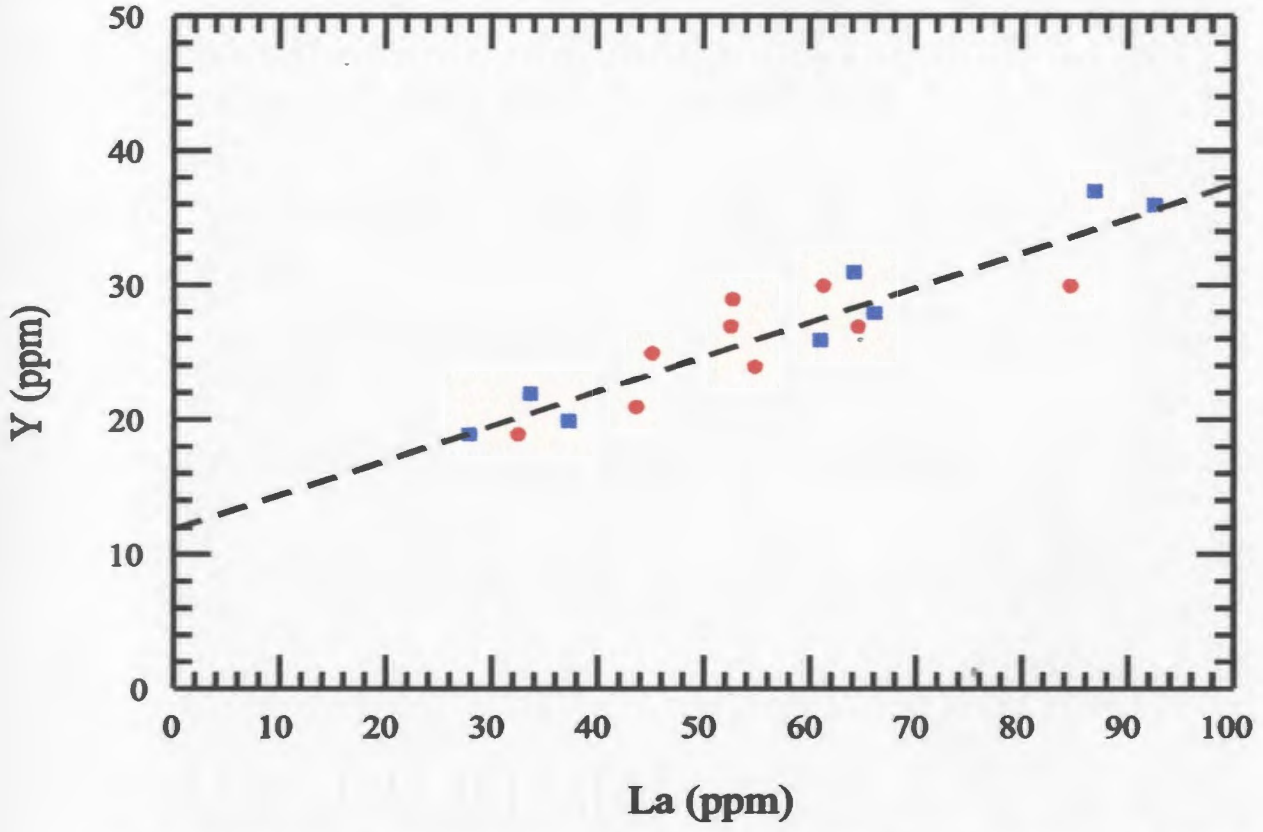

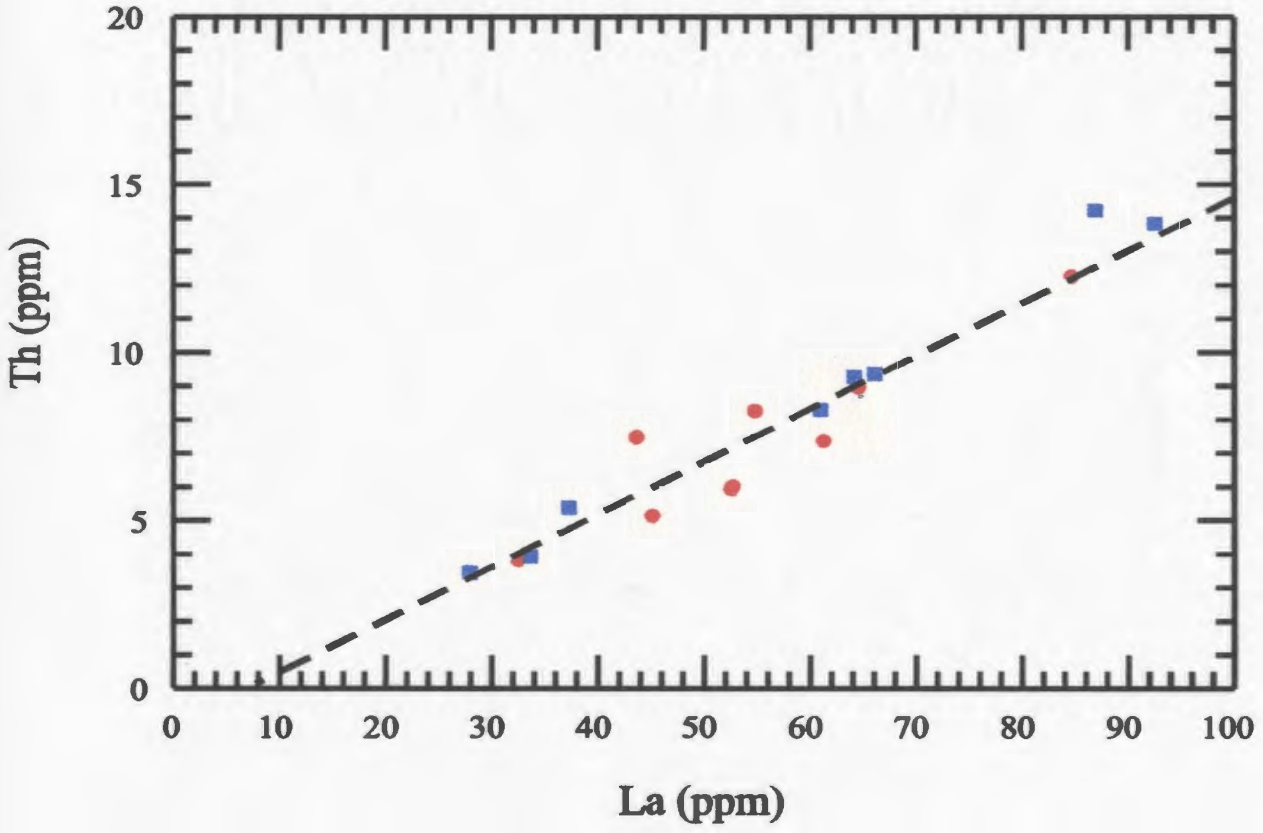

Figure 5.2. Continued

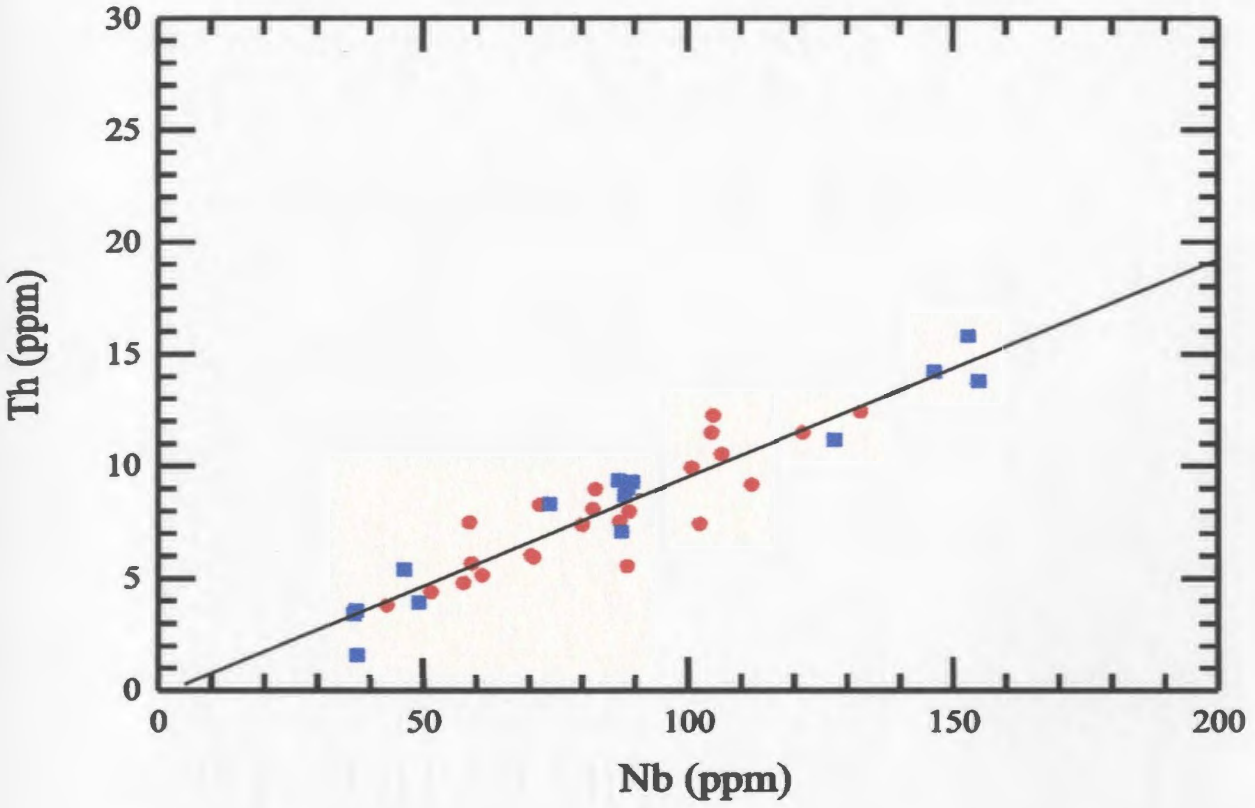

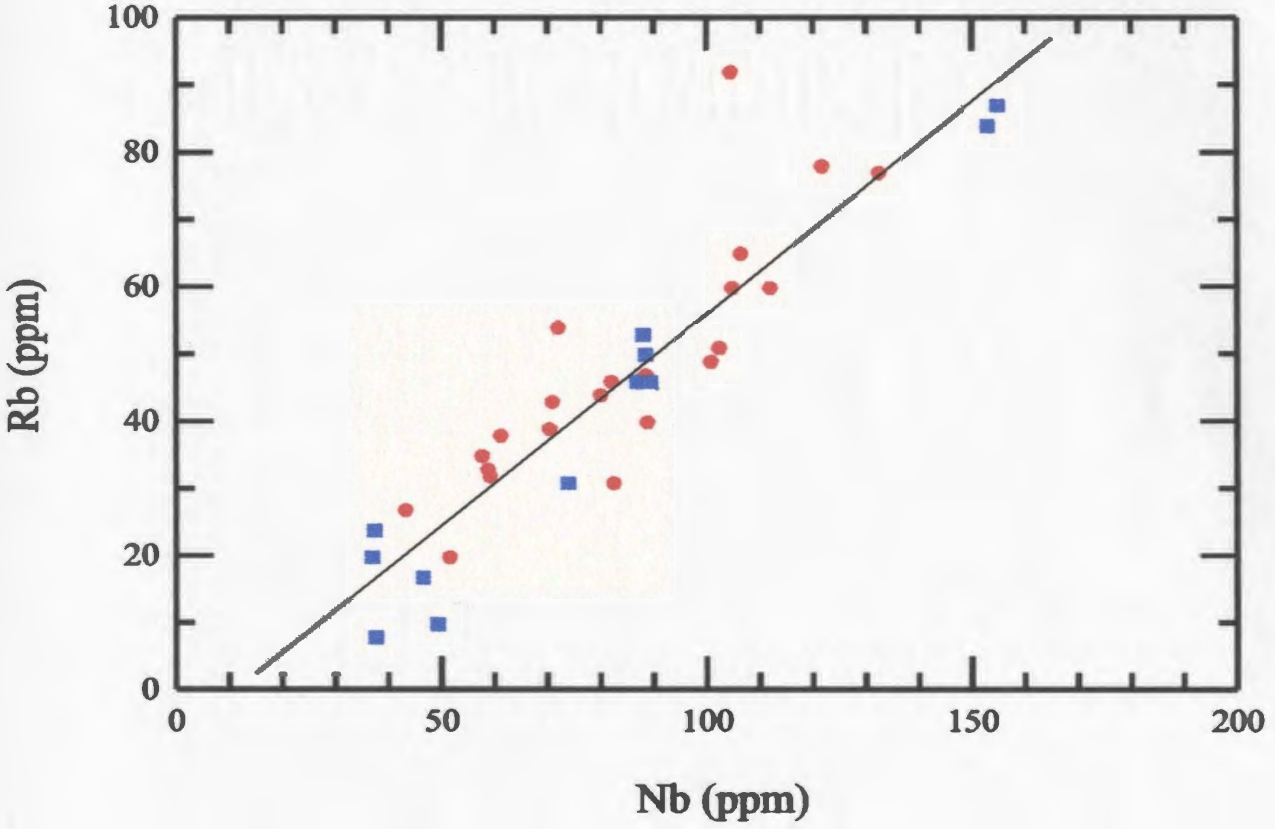

Figure 5.2: Continued

separation of these phases generates in the trace element distributions during low pressure fractionation. These are summarised below:

i) The high concentrations of most of the incompatible trace elements (*e.g.*, Sr, Th, Y, REE etc.) in the pyroxenes relative to the other phases suggest that fractionation of pyroxenes will dominate trace element distributions.

ii) If pyroxenes dominate crystal fractionation, the highly incompatible elements (Kd < 0.001) are the LFSE Ba and Cs, and the HFSE. Elements that could also be classified as strongly incompatible are Nb and Ta (Kd < 0.1). The remaining trace elements have Kd values that range from ~0.1 (La) up to ~0.8 (Yb).

iii) Magnetites incorporate higher amounts of Nb and Ta compared to the titanaugites, and any significant fractionation of magnetite will effect the bulk distribution of Nb and Ta.

iv) The LREE have lower Kd values than MREE and HREE with the HREE having Kd values close to unity. Consequently, the separation of titanaugite produces an overall enrichment of REE in the residual liquid with an increase in the La/Yb ratio.

Chapter Six

Petrogenesis of the Mafic Rocks

"... the concept of differentiation has come to be regarded as a fact as well established as the observed rock associations themselves. Only the processes which bring about differentiation are ordinarily regarded as of hypothetical character"

(Bowen, 1928)

6.1 Introduction

The mafic rocks on Earth's surface originated by partial melting of a solid source to produce a primary magma and a residuum. By examining the composition, particularly trace element concentrations, of these primary magmas, it is possible to determine the nature of the source region and the processes taking place during partial melting.

It appears to be one of the implicit assumptions in the study of ocean islands, especially in those studies which use incompatible trace elements to characterise the composition of the mantle, that near surface post magma production processes have had minimal influence on the chemistry, particularly trace element ratios, of the erupted

basaltic rocks (*e.g.*, Haase, 1996). This is despite the profusion of evidence which indicates that most erupted basalts have been modified since production in the mantle (*e.g.*, Le Roex, 1990). There is also abundant evidence on Rarotonga, both chemical and petrographic, that crystal fractionation was a significant factor in the development of the chemical trends, *e.g.*:

- zoned minerals, phenocryst-rich rocks, *etc.*;
- large range in Mg# and a systematic variation of major and trace elements with respect to Mg#.

Additional qualitative evidence for the influence of low-pressure fractional crystallisation is found by considering the compositional variations of the Rarotonga rocks with respect to the ternary Ol-Di-Ne (+Pl) phase diagram. The 1-atm Ol-Cpx-Pl cotectic in this system is well defined by natural and synthetic experimental studies (Sack et al., 1987). If the Rarotonga samples are plotted on this diagram (Figure 6.1) it is evident that the more evolved (MgO wt. % < 6) type I basalts lie along the 1-atm cotectic, suggesting shallow fractionation within the upper lithosphere, while some of the less evolved basalts (MgO wt. % > 6) plot between the 8-30 kbar cotectic and the 1-bar cotectic, pointing towards fractionation at less than 30 kbars but greater than 1 bar. While there is some scatter in the data, the most primitive type I basalts (high Mg#'s) plot closest to the Di-Ol join, while the more evolved basalts plot closest to the Di-Ol-Ne ternary eutectic. Some of the scatter observed is probably due to minor amounts of crystal accumulation, which will cause rock compositions to plot off the liquidus.

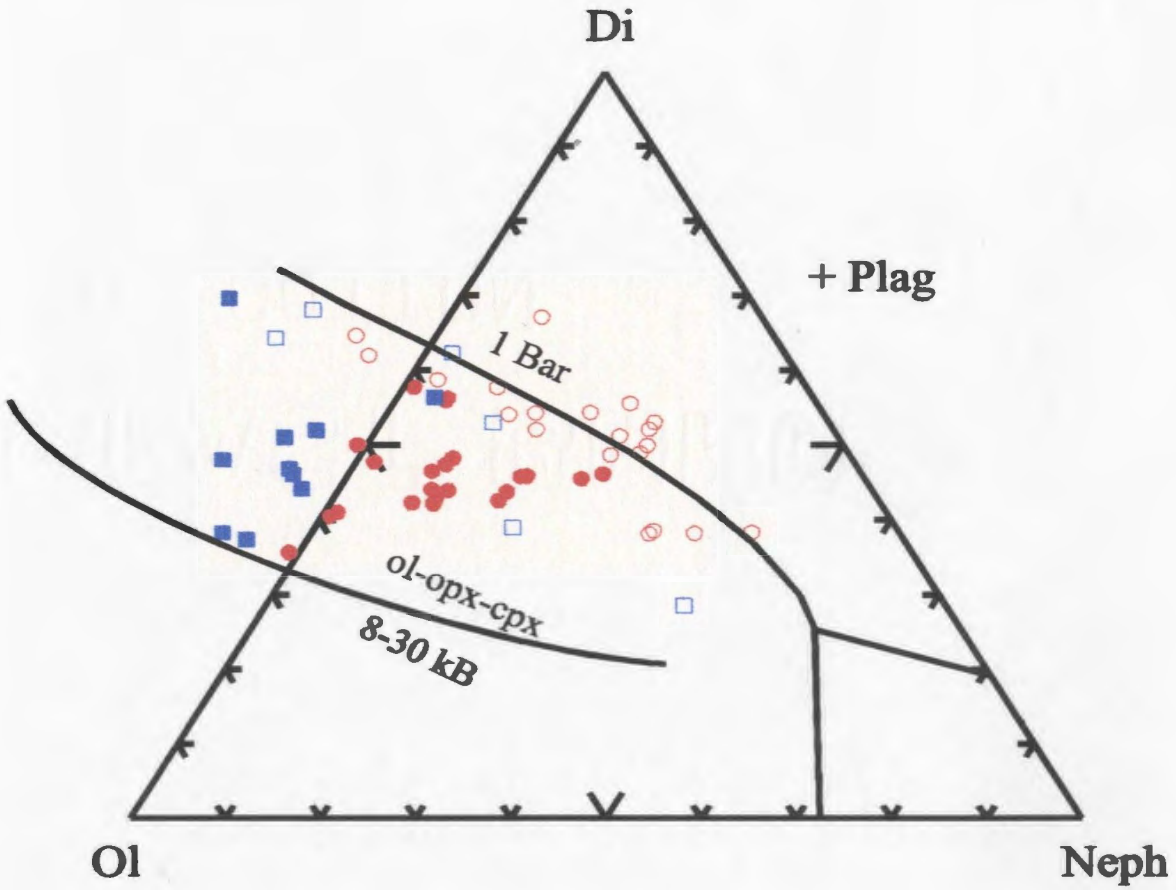

Figure 6.1: Mafic compositions from Rarotonga plotted on the olivine-diopside-nepheline system and the 1atm cotectic. The "curve" labeled "ol-opx-cpx 88-30 kB" defines the maximum Di/Ol ratios exhibited by liquids at these pressures (Sack et al., 1987). Type I rocks with MgO wt. % > 6 filled red circles, rocks with MgO wt. % < 6 open red circles; Type II rocks with MgO wt. % > 6 filled blue squares, with MgO wt. % < 6 open blue squares.

In this chapter, the lack of any lavas that represent primary magma compositions on Rarotonga necessitates that primary magma compositions are calculated from the chemical composition of rocks found at the surface and which have undergone differing degrees of fractionation. Once the composition of primary magmas are known, constraints can be placed on their source region and the partial melting processes. To do this, the chapter has been divided into the following sections:

- A discussion and identification of possible fractionation processes;
- The identification of fractionating phases from petrographic and chemical data;
- Major element modelling using least squares methods to determine the degree of fractionation and proportions of mineral phases fractionating;
- Calculation of primary magma compositions using information from major element modelling and trace element distribution coefficients determined in Chapter four;
- Semi-quantitative conclusions about the source composition *e.g.*, presence or absence of garnet, enrichment of trace elements prior to partial melting, *etc.*;
- Constraints on partial melting processes. *e.g.*, presence of volatiles, depth of melting, *etc.*

6.2 Magmatic Differentiation

This section will use the data and conclusions presented in Chapters three, four and five to evaluate and model the processes operating during the differentiation of the mafic lavas on Rarotonga and to determine the amount of variation in both major and trace element chemistry resulting from these processes. A comprehensive review of ideas on magmatic differentiation over the last 150 years is provided by Wilson (1993). From this review it becomes clear, as most petrologists agree, that some form of crystal fractionation is a dominant mechanism in the variation observed within suites of igneous rocks. However, many other differentiation mechanisms, including thermogravitational diffusion, liquid immiscibility, magma mixing and recharge, are also capable of producing significant compositional variations. Although it is possible that all these processes may have modified mafic rock compositions to some degree at some stage during the evolution of Rarotonga, the dominant process as with most other ocean island basalts (*e.g.*, Hofmann and Fiegenson, 1983; Caroff et al., 1993; Reynolds and Geist, 1995), was probably crystal fractionation.

Although modelling of major elements in a suite of rocks is a relatively simple task, trace element concentrations may be strongly dependent on the specific type of crystal fractionation occurring within the magma, *e.g.*, closed system fractionational crystallisation or equilibrium crystallisation. The effects that these two types of crystallisation have on trace element concentrations are summarised below:

i. Closed system fractionational crystallisation (CSF) following Rayleigh's law, was first proposed by Bowen (1928). During CSF, the melt does not react with early-formed crystals to bring them into equilibrium as its composition changes:

$$\frac{C_L^i}{C_O^i} = F^{(D-1)} \quad \text{.....5.1}$$

C_L^i = concentration of trace element *i* in the liquid

C_O^i = concentration of trace element *i* in the parental magma

F = weight proportion of residual liquid

D = bulk distribution coefficient for element *i*

ii. Equilibrium crystallisation (EC) is described by Shaw (1970). During EC as the melt changes in composition the phenocrysts that have already crystallised re-equilibrate with the melt:

$$\frac{C_L^i}{C_L^i} = F + D^{(1-F)} \quad \text{.....5.2}$$

Using these two models it can be shown for the Rarotonga rocks that for low to moderate degrees of crystallisation (where F < 0.5), the difference in predicted trace element concentrations between the two models is negligible (Figure 6.2). Because only moderate amounts of crystallisation (F < 0.5) are needed to produce the range of compositions on Rarotonga, the simple CSF model will be used to calculate changes in trace element concentrations. The choice of this simplified model for Rarotonga is supported by the study of Caroff et al. (1993) on the trace element behaviour in alkali

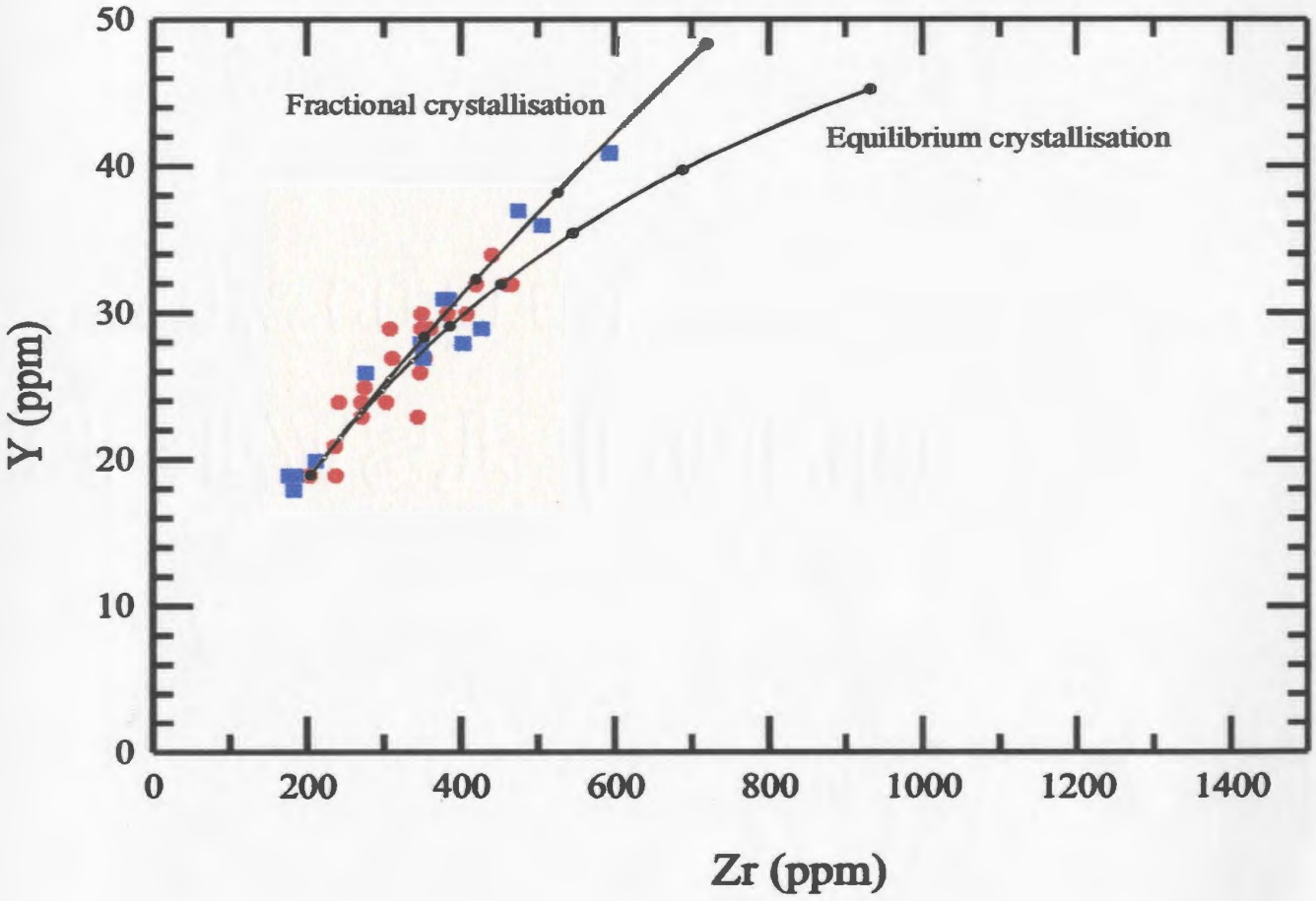

Figure 6.2: Y (ppm) vs. Zr (ppm) and fractional crystallisation and equilibrium crystallisation trends if a primitive magma (R36) underwent crystal fractionation by one of these processes . Mineral proportions are 70:25:5 (px:ol:mt) and Kds from chapter four. Symbols are the same as Figure 4.1.

basalts from Mururoa Atoll, French Polynesia. Using both open and closed system models, these workers showed that trace element variations can be accounted for using CSF.

6.3 Identification of Mineral Phases

The petrographic identification of mineral phases involved during crystal fractionation has been previously discussed in Chapter three. In summary, the petrography of the mafic rocks indicates that the phases involved in crystal fractionation were olivine + pyroxene ± magnetite. To support this, Bowen diagrams (section 4.2.1) are used in conjunction with average mineral chemistry. MgO is chosen as the abscissa due to the large range (3-18 wt. %) exhibited by the mafic rocks and because at low pressures olivine is a liquidus phase in many ocean island lavas. Therefore, a wide range in MgO content should reflect the accumulation and segregation dominantly of olivine. In addition, the MgO vs. major oxide trends exhibit the extent of segregation of some other major crystal phases, *e.g.*, pyroxene. Decreasing MgO content therefore reflects the extent of early fractionation, with the most fractionated rocks having the least amount of MgO. These diagrams (Figure 6.3) show that removal of olivine and pyroxene can account for the major element variation in the mafic rocks until approximately 5-8 MgO wt. % is reached, at which point magnetite begins to crystallise. The fractionation of clinopyroxene is supported by a consistent decrease in CaO/Al_2O_3 with decreasing MgO. The fractionation of olivine is shown by the relationship between Ni and Mg#, illustrated

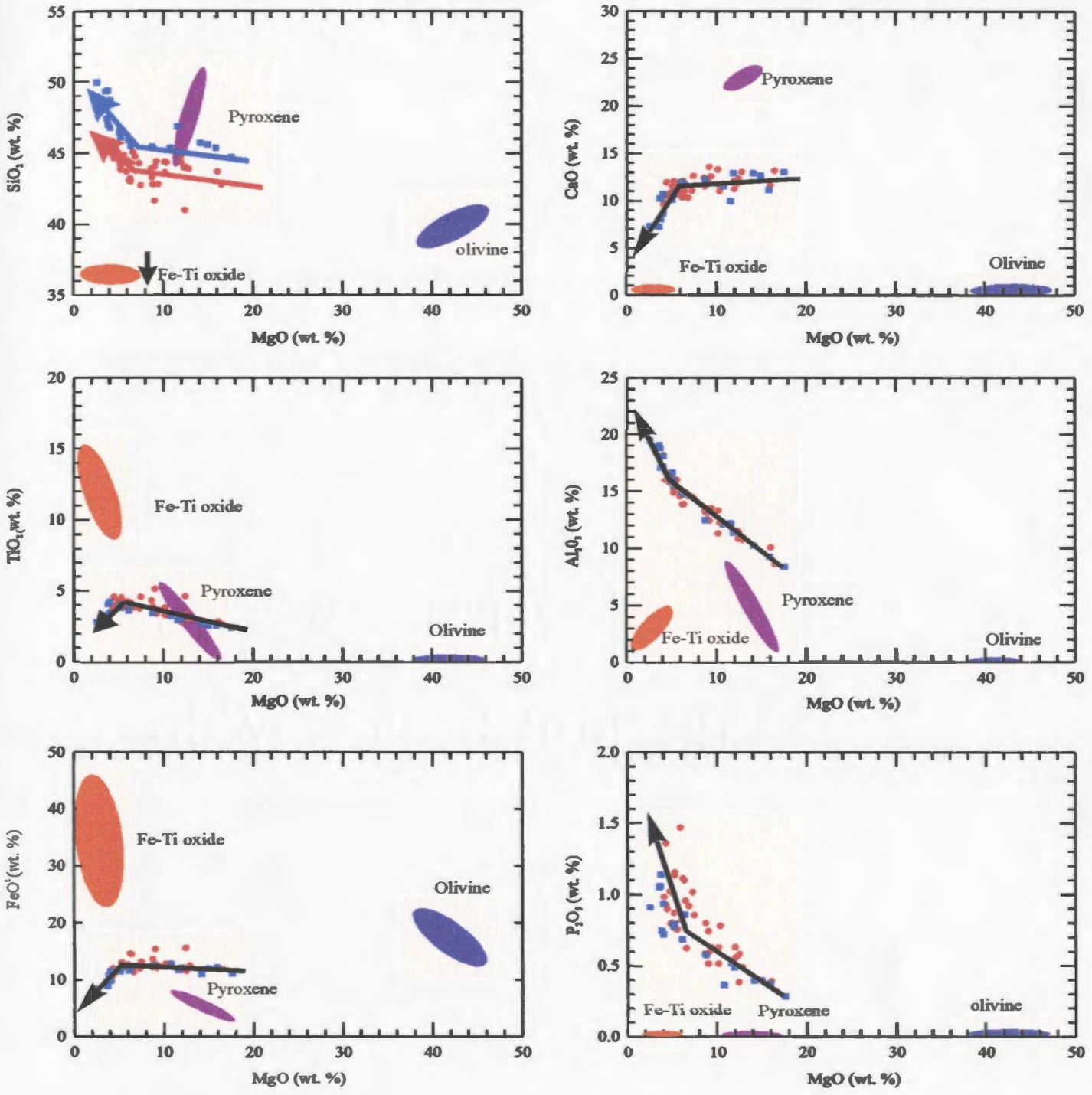

Figure 6.3: Rarotonga mafic rock compositions plotted on Bowen diagrams. Compositional fields for the phenocryst phases found in the rocks and hypothetical fractionation trends are plotted. Symbols are the same as Figure 4.1.

in Figure 6.4, where the fractional crystallisation of olivine + clinopyroxene trends are plotted.

Plagioclase can be a common fractionating phase in oceanic island basalts (*e.g.*, Le Roex, 1985), however, chemical evidence (*i.e.*, no decrease in Sr or the development of an Eu anomaly with fractionation) suggests that plagioclase fractionation was not a significant factor during the differentiation of the Rarotonga magmas.

6.4 Major Element Modelling

The major element oxide variations can be modelled using least-square calculations of Bryan et al. (1969), which involve the addition of the observed phenocryst phases to fractionated magmas to generate compositions similar to the one of parent magmas. The advantage of this method is that the sum of the squares of residuals (SSR) can be used to indicate spurious models.

Previous workers have arbitrarily accepted models as being satisfactory if the SSR value is less than 1.5 (Luhr and Carmichael, 1980), or less than 0.1 (Le Roex and Erlank, 1982). Fisk et al. (1982) applied a number of criteria, including the absolute and/or relative difference between the calculated daughter oxide content and the proposed daughter oxide content, to make the choice of reasonable SSR values more quantitative. In the present study a solution with SSR values less than 1 was accepted because the solutions in this range are within the analytical uncertainty for the techniques used to measure major elements and well within the variations in major element concentrations.

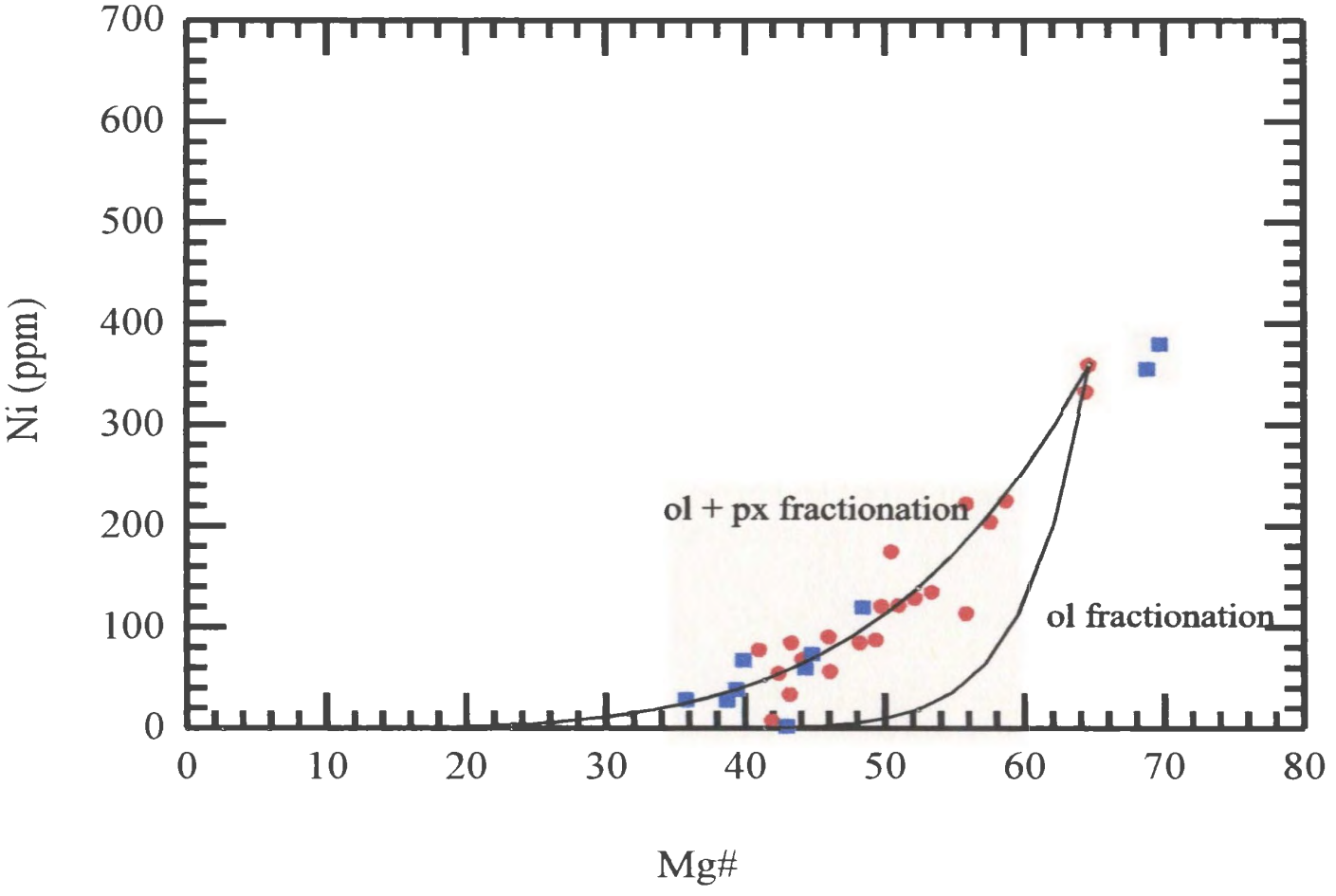

Figure 6.4: Plot of Ni (ppm) vs Mg# for Rarotonga rocks. For the fractionation trends the variation in Mg# was calculated according to Pearce (1978), assuming K Fe-Mg = 0.3 for both cpx and ol (Roeder and Emslie, 1970). Ni abundances during crystal fractionation were calculated using D for px +ox = 10 and D for Ol = 29, Kd for Ni from Rollinson (1993). Symbols are the same as Figure 4.1.

Mineral compositions used in the least square models were those determined from the core compositions of minerals in phenocryst-rich ankaramites assuming that cores were in equilibrium with the bulk composition of the magma. In all cases relatively primitive phases were chosen, using Mg# as the major criterion for their recognition.

The choice of mineral analyses that show variations in the chemistry of the phases used, *i.e.*, slightly higher FeO and SiO_2 and lower TiO_2 and MgO wt. %, can slightly improve the SSR for some models. However, these manipulations of the data are deemed unnecessary as they provide no further insight into the processes operating during crystallisation or significantly change the relative proportions of phases involved, or their degree of fractionation.

6.4.1 Type I mafic rocks

In the type I mafic rocks, R82 was identified as one of the most primitive magmas (see 4.2.5) and is , therefore, used to represent a parental magma from which the amount of olivine + titanaugite ± magnetite fractionation needed to produce the likely daughter magmas can be calculated. A summary of results of the type I least square models is listed in Table 6.1 and graphically depicted in Figure 6.5. As can be seen, there is some scatter of the major element rock compositions around the possible fractionation trend. Some of this scatter could be due to the presence of cumulate crystals, in which case these rocks do not represent pure liquids.

Table 6.1

Selected Least square models from the type I rocks

Parent #	R82			R16			R19		
daughter #	R16			R19			R50		
F	0.69			0.78			0.77		
	%			%			%		
magnetite	0.024			0.095			0.18		
olivine	0.305			0.212			0.105		
pyroxene	0.672			0.693			0.716		
SSR	0.8			0.84			0.99		
	OBS-R82	CALC-R82	DIF	OBS-R16	CALC-R16	DIF	OBS-R19	Calc-R-19	DIF
SiO_2	43.93	43.96	-0.03	44.07	43.85	0.22	44.32	44.12	0.2
TiO_2	3.07	3.25	-0.18	3.57	3.68	-0.11	3.85	3.98	-0.13
Al_2O_3	10.8	10.62	0.18	13.13	13.04	0.09	14.93	15.01	-0.08
FeO	12.58	12.53	0.05	12.82	12.73	0.09	12.04	11.96	0.08
MnO	0.23	0.23	0.0	0.24	0.25	-0.01	0.25	0.24	0.01
MgO	12.93	12.94	-0.01	9.12	9.21	-0.09	6.6	6.69	-0.1
CaO	13.12	13.09	0.03	12.15	12.19	-0.04	11.17	11.2	-0.04
Na_2O	1.36	1.49	-0.13	2.42	2.56	-0.14	3.54	3.31	0.23
K_2O	1.5	1.29	0.21	1.73	1.84	-0.11	2.36	2.48	-0.12
P_2O_5	0.5	0.52	-0.02	0.75	0.75	0	0.96	0.94	0.02

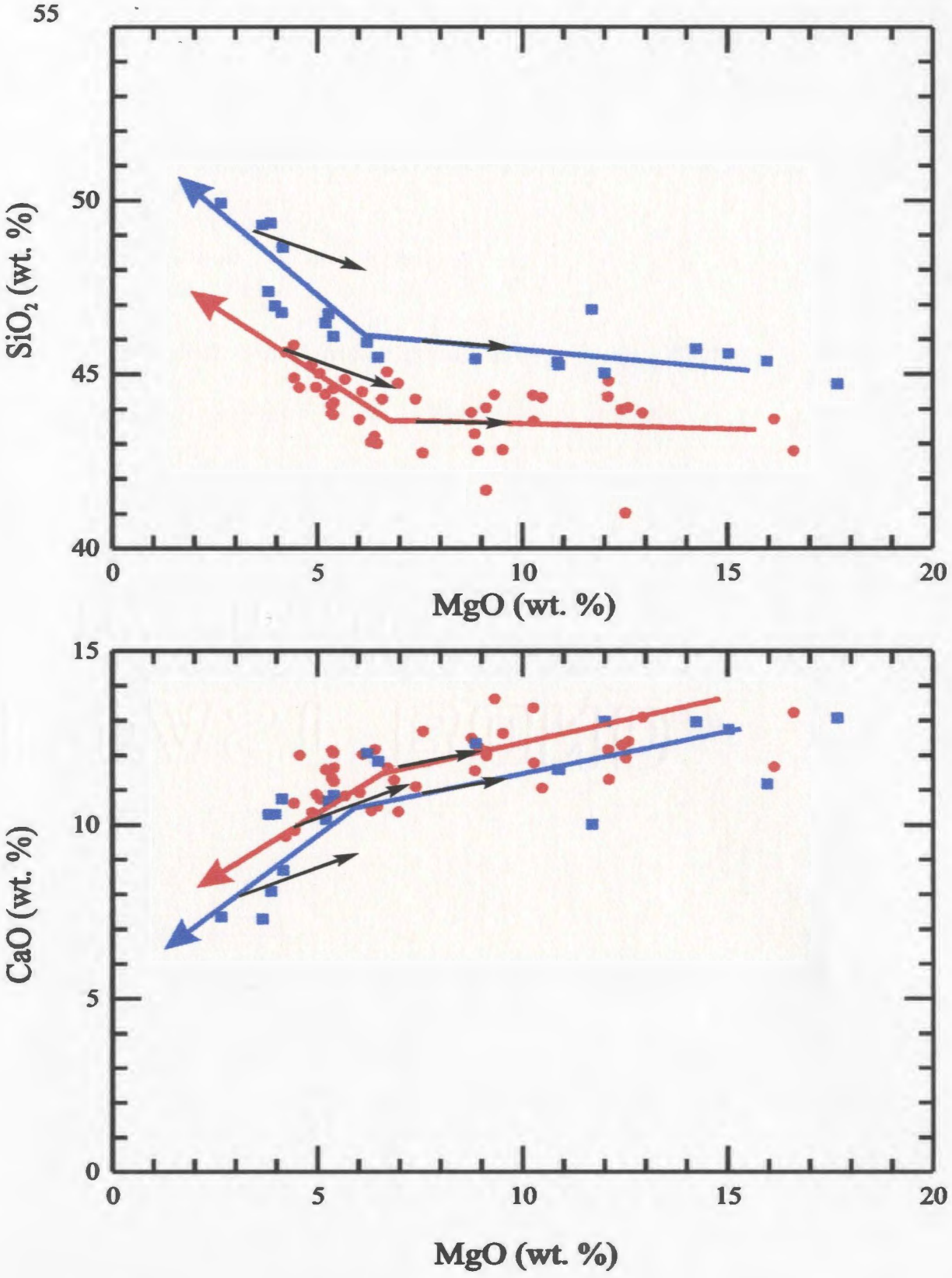

Figure 6.5: CaO (wt. %) and SiO (wt. %) vs. MgO (wt. %) for the mafic rocks. Fractionation trends predicted from least square modelling shown by solid blue and red lines. The effect that primary magma recharge will have on daughter magma chemistry at different stages of fractionation is shown by solid black lines and arrows.

There is also the possibility that magma recharge, *i.e.*, an influx of more primitive magma into the magma chamber, affected the chemical composition. It is clear from Figure 6.5, where hypothetical mixing lines are plotted, that rocks which have MgO greater than *ca.* 6 wt. % would still lie on the fractionation trend if magma recharge occurred. For rocks with less than *ca.* 6 wt. % MgO magma recharge will drive compositions away from the fractionation trend. Several lavas have compositions which could represent such a recharge process (Figure 6.5).

6.4.2 Type II mafic rocks

As discussed in Chapter two, the type II rocks have a more complex petrography than the type I rocks particularly with the presence of diopside augite, which leads to the question: "Is it possible to produce a fractionation trend using the same phases as for the type I rocks, or does the modelling of a suitable fractionation trend require the additional removal of diopside-augite?"

Least square modelling shows that fractionation of olivine + titanaugite ± magnetite, followed by fractionation of titanaugite + magnetite, can produce the major element variation observed within the type II rocks (Table 6.2 and Figure 6.5). When diopside-augite is substituted for titanaugite in the least square models, only major element variations for samples with greater than *ca.* 6 Mg wt. % can be produced by fractionating slightly less diopside-augite and more magnetite than that required when titanaugite compositions are used. In rocks with less than *ca.* 6 MgO wt. %

Table 6.2

Selected Least square models from the type II rocks

parent #	R128			R119			R119		
daughter#	R119			R56			R56		
F	0.441			0.262			0.351		
	%			%			%		
magnetite	0.016			0.159			0.16		
olivine	0.351								
pyroxene	0.633			0.841			0.84		
SSR	0.95			0.79			0.96		
	OBS-R128	CALC-R128	DIF	OBS-R119	CALC-R119	DIF	OBS-R56	CALC-R56	DIF
SiO_2	45.6	45.48	0.12	46.78	46.8	-0.02	49.33	49.29	0.04
TiO_2	2.6	2.75	-0.15	3.85	3.79	0.06	3.13	3.21	-0.08
Al_2O_3	9.5	9.56	-0.06	16.02	16	0.02	19.09	19.1	0
FeO	12.18	12.08	0.10	11.57	11.53	0.04	9.82	9.87	-0.05
MnO	0.17	0.22	-0.05	0.21	0.18	0.03	0.16	0.2	-0.04
MgO	15.02	15.14	-0.12	5.29	5.36	-0.07	3.67	3.92	0.25
CaO	12.76	12.86	-0.10	10.71	10.83	0.12	7.32	7.41	-0.09
Na_2O	1.18	1.26	-0.08	2.37	2.19	0.19	2.78	3.03	-0.25
K_2O	0.66	0.77	-0.11	2.43	2.68	-0.18	3.63	3.48	0.15
P_2O_5	0.4	0.34	0.06	0.78	0.78	0	1.05	1.05	0

unsatisfactory SSR values are obtained (*i.e.*, SSR > 1) when diopside augite compositions are substituted for titanaugite.

Comparing the results of least square modelling between the type I and type II rocks it is evident that there are subtle differences in the amounts of the crystallising phases required to provide satisfactory SSR values. In magmas with less than 6 wt. % MgO, the type I rocks require significant amounts of magnetite fractionation (up to 10 %) to obtain low SSR , while the type II mafic rocks require only 2-5 % magnetite fractionation. For these magmas (i.e., MgO < 6 wt. %) the type II trend can only be modelled using titanaugite and magnetite fractionation, while in the type I rocks minor amounts of olivine can be included in models to produce the observed fractionation trend (although it is not necessary to produce satisfactory SSR). The diopside augite phenocrysts in the type II magmas could only have crystallised in magmas with greater than 6 wt. % MgO.

6.5 Constraints on Primary Magmas

Once an adequate model for crystal fractionation has been developed it is then possible to calculate potential primary magma compositions. Primary magma compositions are obtained by adding mineral phases, which are presumed to have fractionated during the ascent of the magma, back into to the observed lava composition. To do this however, several principal assumptions need to be made.

i. The approximate composition of the primary magma, or more specifically the MgO wt. %. of the primary magma must be known. In the absence of lavas which represent primary compositions on Rarotonga (see Chapter four) primary magmas were calculated with a range of MgO content between 13 and 15 wt. %. This range is similar to identified primary magma compositions on a number of ocean islands which have ca. 13 MgO wt. % (*e.g.*, Feigenson et al., 1996). Differences in the calculated primary magmas compositions of the high SiO_2 and low SiO_2 types may be due to the incorrect choice of the initial MgO content. Calculating theoretical primary magma compositions with a range of MgO concentrations will enable the identification of differences which are insensitive to errors in the choice of MgO content.

ii. The compositions of the different suites from the two parent types are controlled firstly by different degrees of partial melting and subsequently by crystal fractionation.

iii. Partial fusion in the mantle should generate magmas of approximately identical compositions, therefore suggesting that melting of invariant, perhaps eutectic-like compositions, occurs. This concept is discussed in detail by Yoder (1976).

A complete table of the calculated primary magma compositions along with amounts of mineral phases added to produce them are given in Appendix 5 and graphically depicted in Figure 6.6. As shown, the major element compositions of calculated primary magmas of the two types are very similar. It is readily apparent that

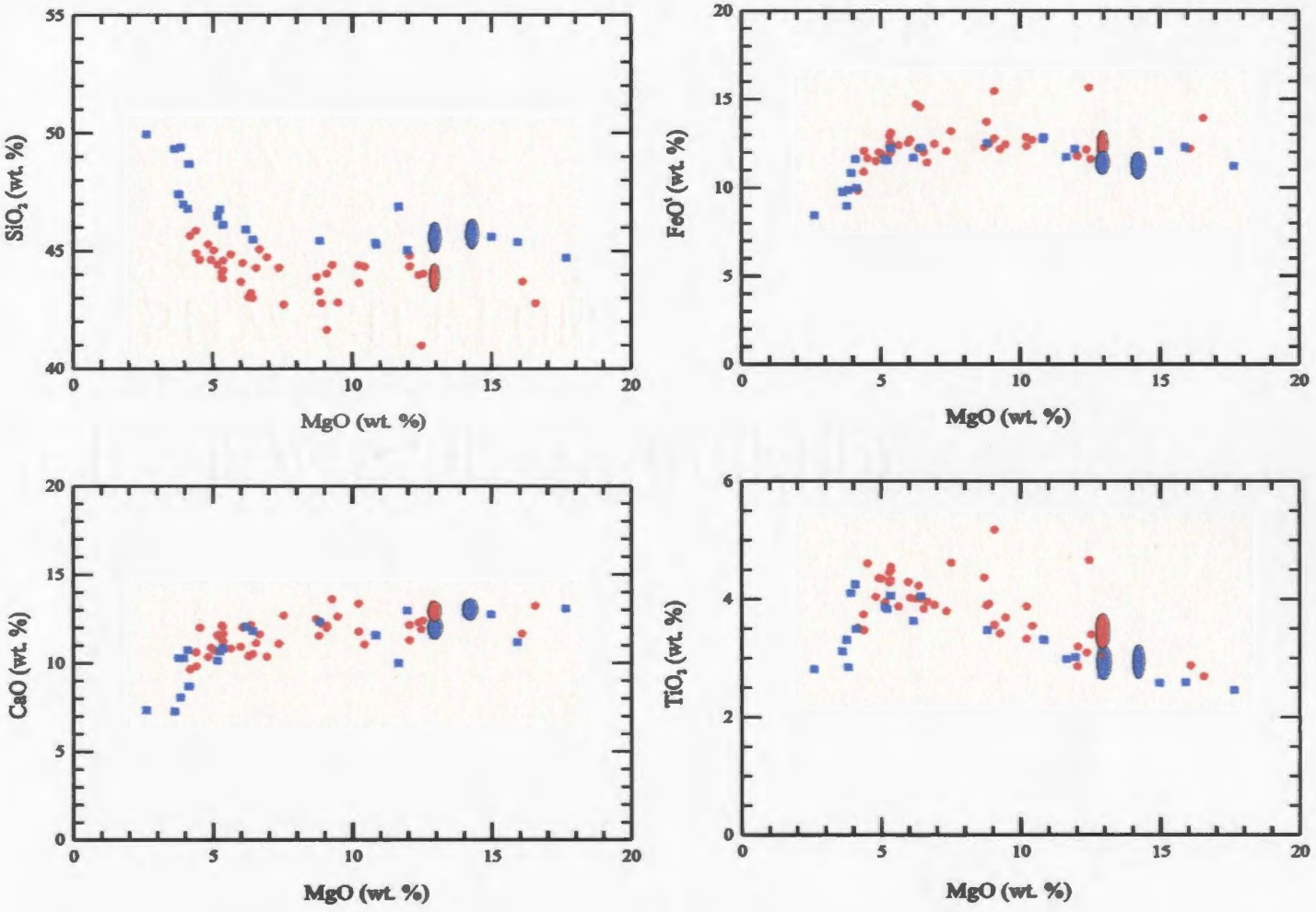

Figure 6.6: Mafic rock compositions and ranges of calculated primary magma compositions plotted on Bowen diagrams . Type I shown by the red field (MgO=13 wt %), type II by the blue fields (MgO= 13 wt. % and 14 wt. %). Symbols are the same as Figure 4.1.

the choice of MgO concentration for primary magmas can significantly effect some of the calculated major element compositions (*e.g.*, CaO, Al_2O_3). Thus, any assumptions about differences between the type I and type II primary magmas using these elements will be equivocal. In addition to those errors caused by the choice of MgO concentration, errors may also arise from any number of uncertainties inherent in this simple approach: changes in melt composition with degree of source melting; changes in mineral composition during fractionation (*i.e.*, zoned minerals); or use of incorrect mineral compositions. For these reasons the major element concentrations obtained from the calculation of primary melt compositions should only be used as a first order estimation and may not be strictly correct in detail.

Taking the above provisos into consideration there are some differences between the two types, which may be real and not artefacts of incorrect assumptions. The difference in silica composition is still apparent in their respective calculated primary magma compositions, while the FeO^t and TiO_2 concentration of the type II primary magmas, for both MgO = 15 wt. % and MgO=13 wt. % in the primary magmas, are in general lower than the type I primary magmas. Sodium concentrations in the type II primary magmas also appear to be lower than in the type I magmas. For the remaining elements the differences between the two types are minor (*e.g.*, P_2O_5) or ambiguous (CaO, Al_2O_3).

Although the information obtained from major element concentrations in calculated primary magma compositions is limited, trace elements can offer much more quantitative information. Major element concentrations are buffered by the mineral

assemblage while trace element concentrations in magmas are controlled by partitioning laws (see Chapter five) and therefore are not buffered in the same way. When calculating primary magma trace element compositions the choice of MgO = 15 or 13 wt. % in the primary magma has little effect. It is apparent that the calculated trace element concentrations for the primary magmas of both type I and type II are very similar. The fractionation-corrected REE patterns for both groups (Figure 6.7) show a much more restricted range than the uncorrected data. There is however, still more than a threefold increase in La concentration and an approximately 70% variation in Yb for these hypothetical primary melts.

6.6 The Composition of the Mantle Source.

Hofmann and Feigenson demonstrated in a series of papers (Hofmann and Feigenson, 1983; Feigenson et al, 1983; Feigenson et. al., 1996) that once primary magma compositions have been determined, restrictions can be placed on the source characteristics. Their approach uses element ratios in conjunction with formulas originally described by Minster and Allègre (1978), which follow the equation for batch melting first described by Gast (1968) and Shaw (1970).

$$C_l^i = \frac{C_o^i}{\left[D_o^i + F\left(1 + P^i\right)\right]} \qquad \text{6.2}$$

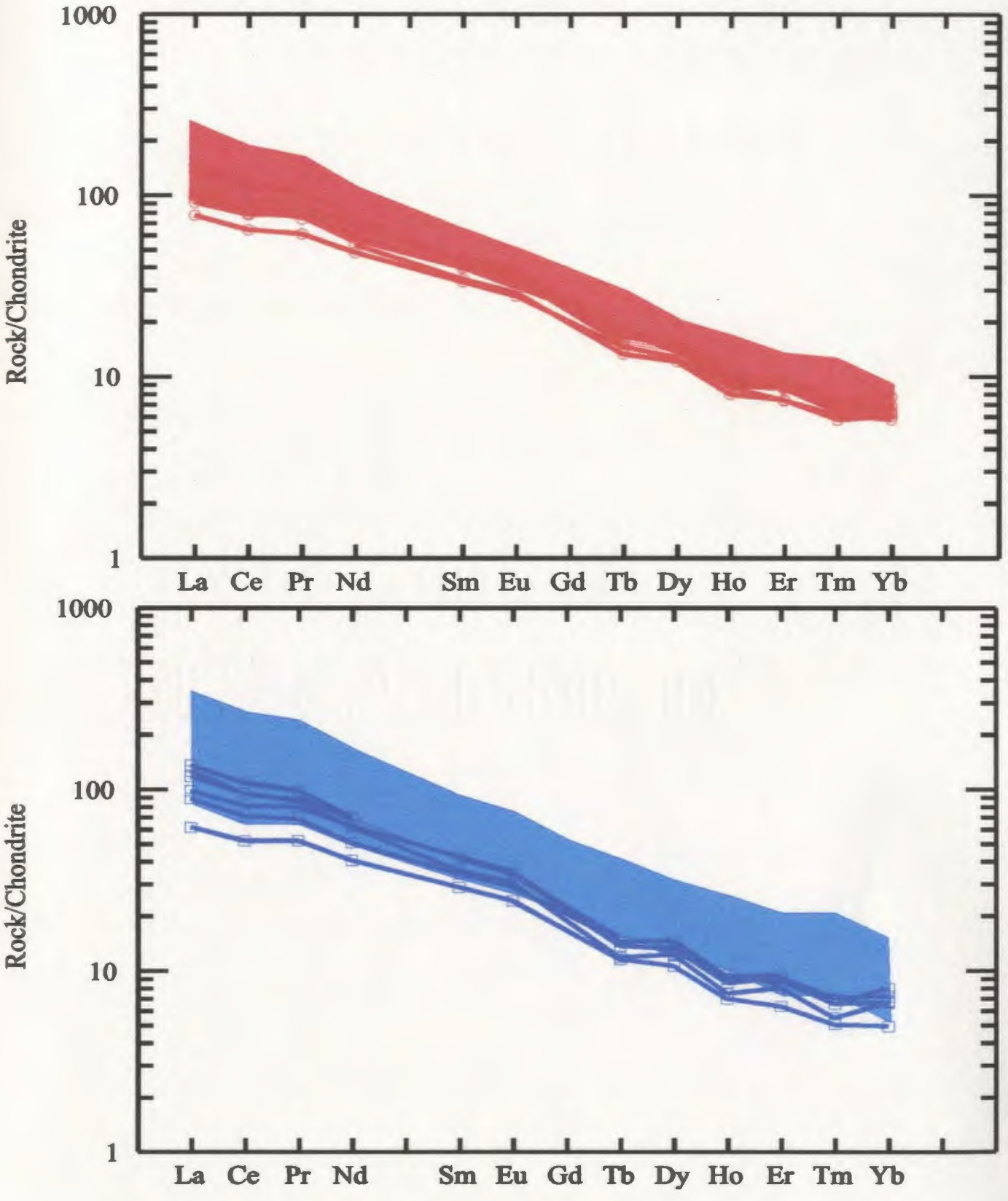

Figure 6.7: Calculated primary magma compositions and the range of mafic rock compositions from each type (shaded region: type I - red; type II - blue). The symbols for the calculated compositions are open circles for the type I mafic rocks and open sqaures for the type II mafic rocks.

C_l^i concentration of element i in the melt

C_o^i concentration of that element in the initial source

D_o^i bulk distribution coefficient of i in the source

P^i sum of partition coefficients of phases in proportions that they enter the melt

F degree of melting.

Hofmann and Fiegenson (1983) used the assumption that for a highly incompatible element, x, which is characterised by $D^{(x)} = P^{(x)} = 0$ and a slightly less incompatible element y, a series of relations can be formulated;

$$C^x = \frac{C_x^o}{F} \quad \text{.....6.3}$$

$$\frac{C^x}{C^y} = S^y C^x + I^y \quad \text{.....6.4}$$

$$S^y = \frac{D_o^y}{C_o^y} \quad \text{.....6.5}$$

$$I^y = \frac{C_o^x}{C_o^y\left(1 - P^y\right)} \quad \text{.....6.6}$$

where S^y and I^y are the slope and intercept of straight line described by 6.2

The partition coefficient P^y is the sum of the mineral/melt coefficients of element y weighted in the proportions in which the minerals are consumed by the melt. P^y is evaluated directly from the major element composition of the primary melt assuming that the solid phases consumed by the formation of the melt are ol-opx-cpx-gnt or ol-opx-cpx-sp. For simplicity, only the five major components, SiO_2, Al_2O_3, CaO, FeO and MgO are

used to describe the composition of the melt and mineral phases. Although this model relies on invariant melting, an assumption which is not valid for FeO and MgO, this problem can be ignored as trace elements in general (except Cr, Ni, *etc.*) are not fractionated by olivine, but provide information about other minerals in the source, such as clinopyroxene and garnet.

Once the above variables have been determined it is relatively easy to eliminate inappropriate source compositions and to obtain the relative trace element concentrations in the source (*e.g.*, a REE pattern normalised to an incompatible element concentration).

Applying the above method to the two types of mafic rocks on Rarotonga, (Figure 6.8 and Figure 6.9; a summary of the calculations is given in Appendix 5) it becomes readily apparent that a model which requires residual garnet in the source (*e.g.*, a garnet lherzolite) yields the unacceptable result of a negative Yb concentration in the source (Figure 6.8), while a model with residual clinopyroxene and without garnet in the source (*e.g.*, a spinel lherzolite) is qualitatively compatible with the relations shown in Figure 6.9. A simple inspection of Figure 6.10 shows significant fractionation of the LREE (Ce-Eu), but little or no fractionation of the HREE (Dy-Yb). This is contrary to the pattern that would result from pure garnet control, whereby a strong relative fractionation of both the light and heavy REE would occur.

Another important constraint on the mantle source for the Rarotonga rocks is that it must have been enriched in light REE over heavy REE elements. This enrichment of LREE would have to have occurred after the establishment of the positive ε_{Nd} signature. The trace element patterns of primary magmas (Figure 6.11) also show a relative

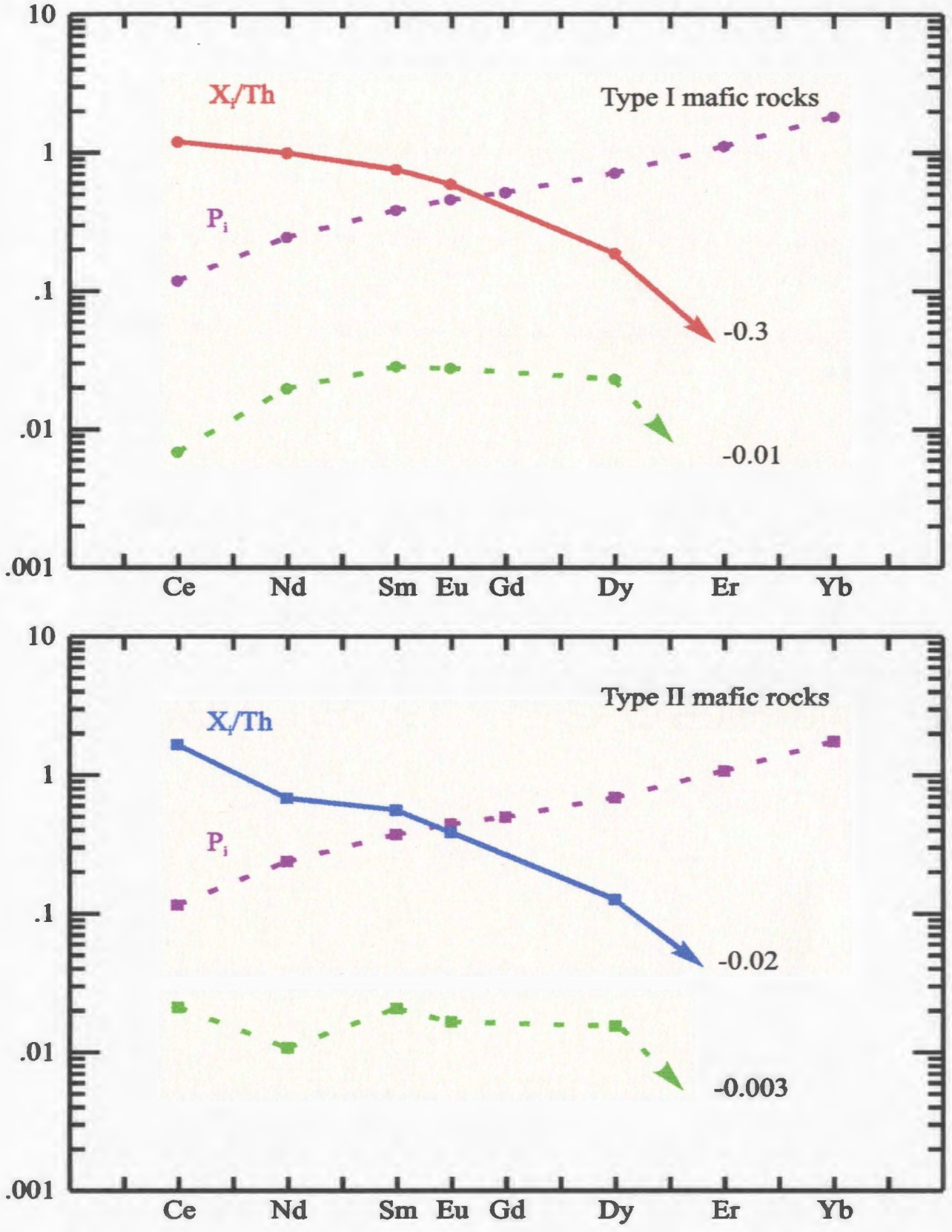

Figure 6.8: Garnet lherzolite model: Relative source concentrations (X/Th) and bulk partition coefficients for calculated primary magmas for a source containing garnet (P = sum of partition coefficients of phases in proportions that they enter the melt; D = bulk distribution coefficient of element i in the source). The method and parameters used are outlined in the text and Appendix 5.

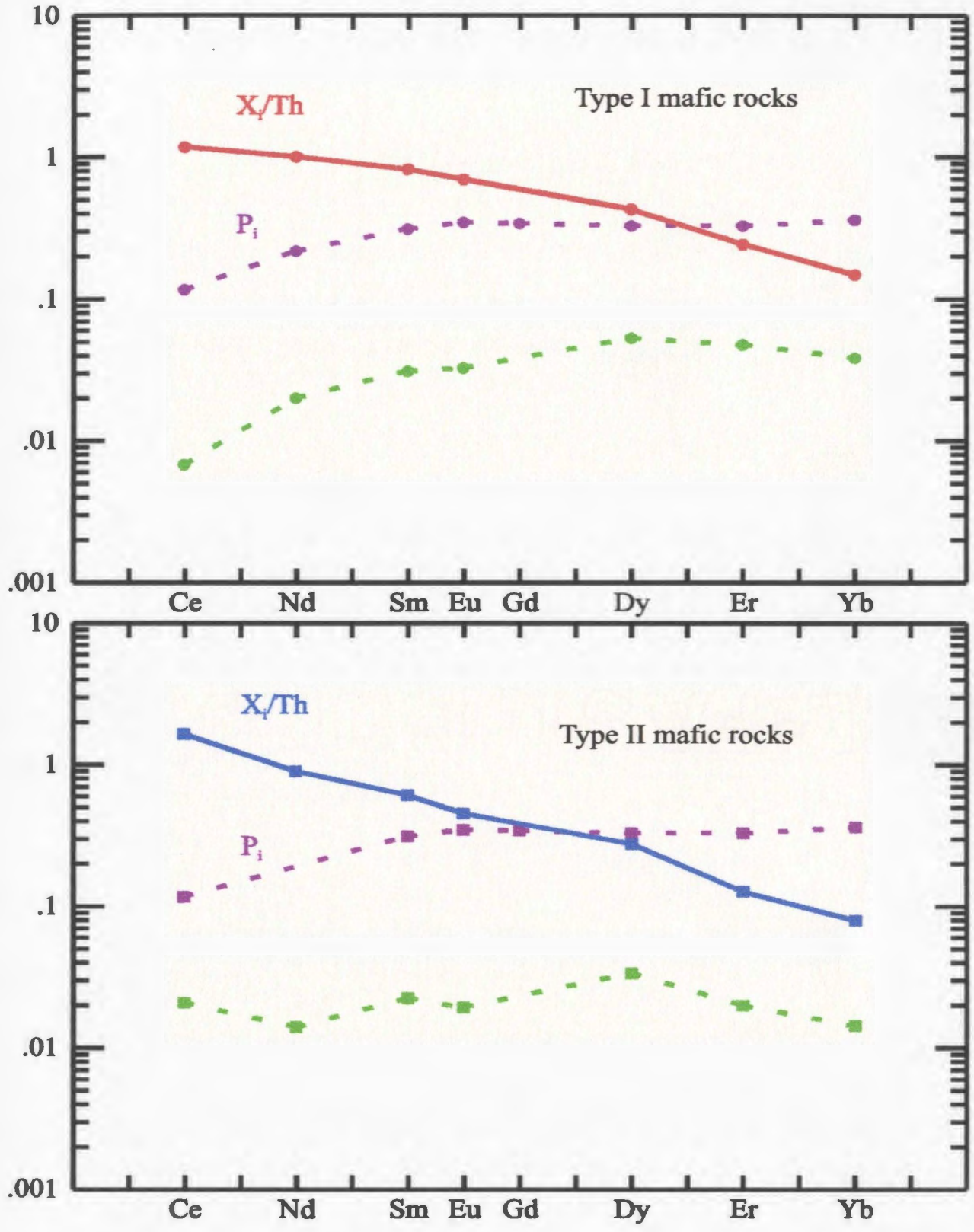

Figure 6.9: Spinel lherzolite model: Relative source concentrations (X/Th) and bulk partition coefficients for calculated primary magmas for a garnet free source (P = sum of partition coefficients of phases in proportions that they enter the melt; D = bulk distribution coefficient of element i in the source). The method and parameters used are outlined in the text and Appendix 5.

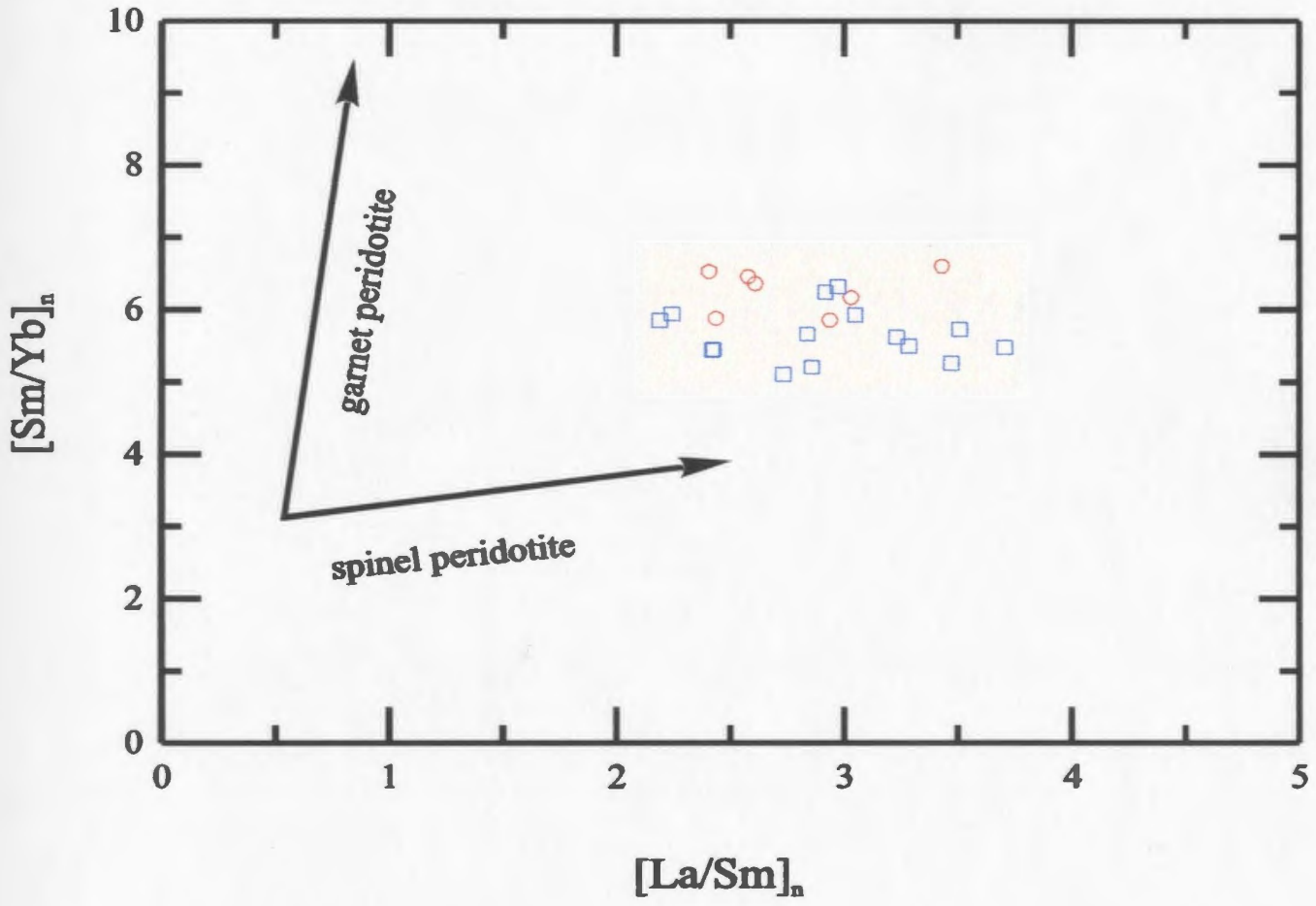

Figure 6.10: $(Sm/Yb)_n$ vs. $(La/Sm)_n$ of the fractionation corrected mafic rocks on Rarotonga. The arrows show the change in ratios that would be expected by melting in a spinel or garnet lherzolite. Type I rocks open red circles, type II rocks open blue squares.

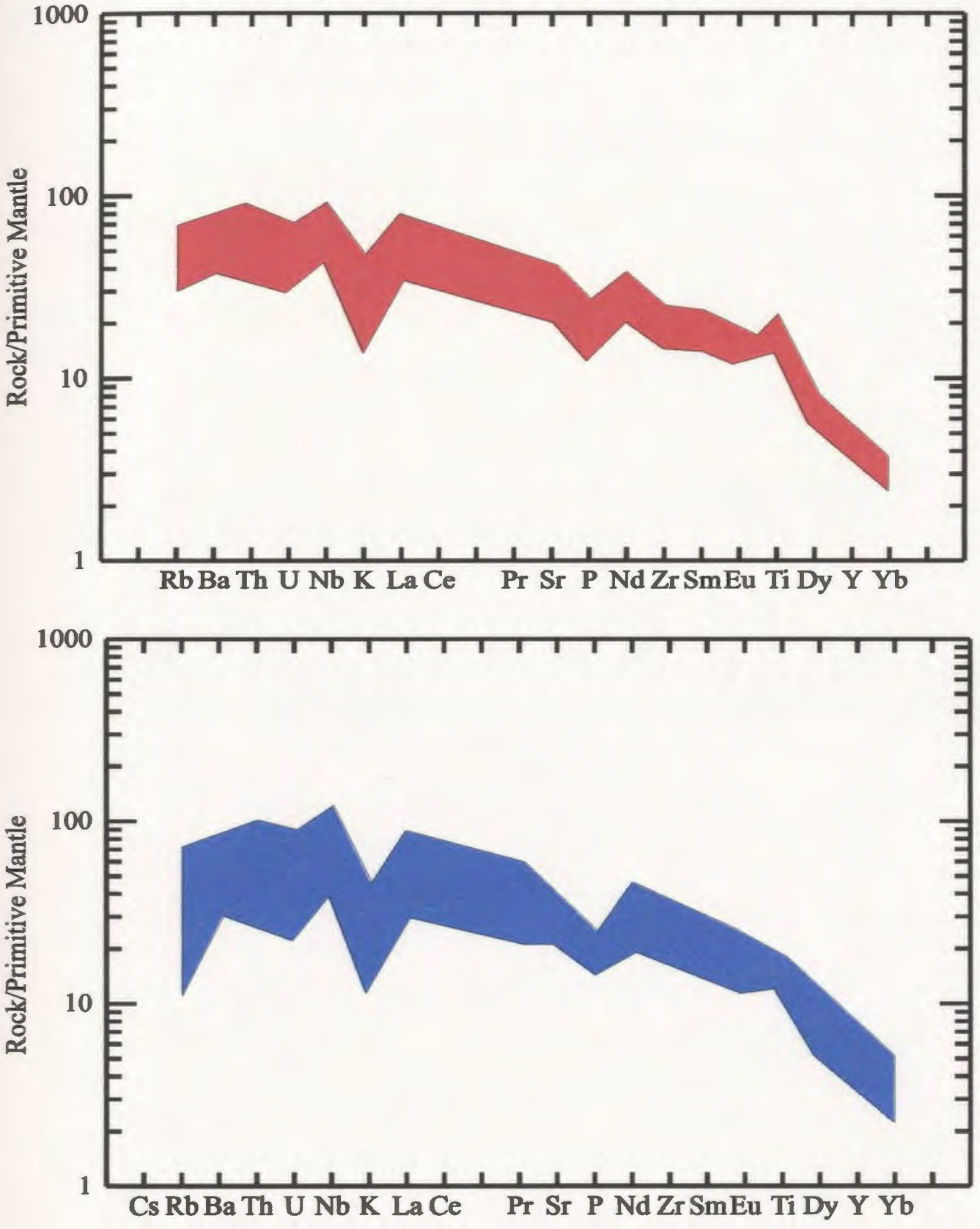

Figure 6.11: The range of calculated primary magma compositions normalised to primitive mantle (Sun and McDonough, 1989). The type I rocks are shown in red, type II in blue.

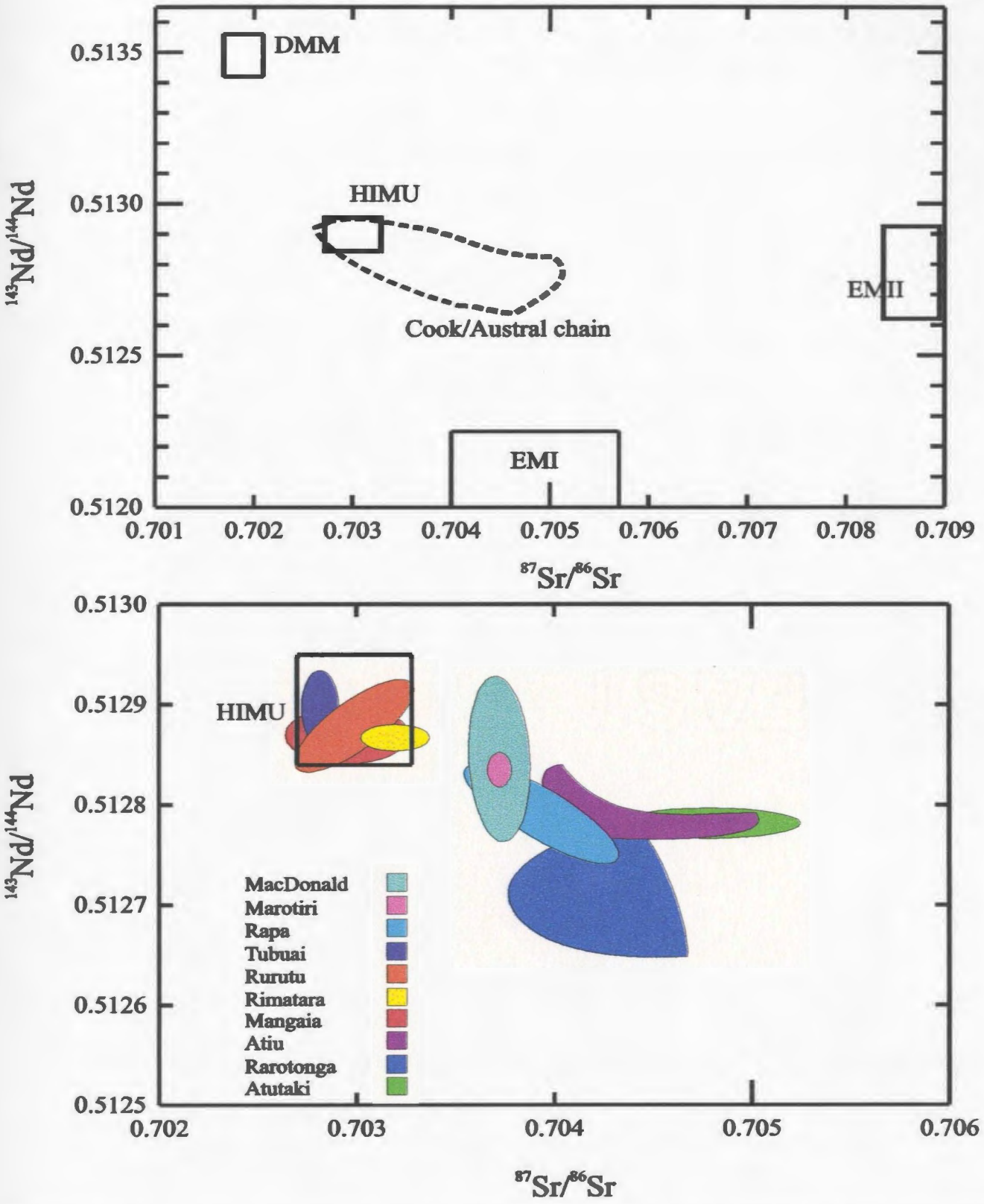

Figure 6.12: Isotopic signature of the islands from the Cook/Austral chain compared with the hypothetical mantle end members discussed in Chapter two. The upper diagram shows the complete range of the Cook/Austral chain while the lower diagrams show the ranges of individual islands within the chain. The data are a compilation from this study; Palacz and Saunders, 1986; Nakamura, 1988; Chauvel et al., 1992; Hemond et al. 1994.

depletion of K and Rb. This may partially reflect the presence of a K-rich phase, e.g., phlogopite or an amphibole, in the mantle source region during melting which would affect the incompatibility of K and Rb, *i.e.*, the D_K and D_{Rb} are higher in a mantle source which has a K-rich phase than the respective values in a mantle which does not include a K-rich phase.

From the above it is possible to conclude that the mantle from which the primary magmas were generated was a spinel lherzolite containing a K-rich phase which had been previously enriched in incompatible elements before partial melting occurred.

The Nd and Sr isotopic signatures of the Rarotonga and other islands in the Cook/Austral chain are shown in Figure 6.12. The chain can be divided into two groups of islands based on the isotope data. One group consists of Tubuai, Rurutu, Rimatara and Mangaia that have a restricted range of $^{143}Nd/^{144}Nd$ and $^{87}Sr/^{86}Sr$ values and plot with in the HIMU field. The second group, MacDonald, Marotiri, Rapa, Atiu, Rarotonga and Atutaki show a larger range of isotopic values and have higher $^{87}Sr/^{86}Sr$ values. From this data it possible to suggest that at least two mantle sources were involved in the formation of the Cook/Austral chain. One of these sources with a pure HIMU signature produced the first group of islands. The composition of the second source is more ambiguous, with the respective group of islands showing variable mixing between this source and the HIMU mantle source.

6.7 Origin of the Type I and Type II Magmas.

Several processes may be responsible for the variations in trace- and major-element concentrations of primary magmas. In this section the origin of the two mafic types is examined. It has been shown in previous sections that type I and type II rocks appear to have fractionated from slightly different primary magmas; the low silica type fractionating from a low silica primary magma and the high silica type fractionating from a more silica-rich primary magma. This difference in major element compositions is not reflected in the trace elements. Variations in primary magma compositions can be ascribed to mineralogical control, *i.e.*, changes in the mineralogy of the mantle due to the stability of mineral phases at different pressures (Greenough, 1988), partial melting processes (Richter, 1986; McKenzie and Bickle, 1988), and to the chemical composition of the source, *i.e.*, a chemically heterogeneous mantle (Dixon and Batiza, 1979; Hickey and Frey, 1982). Therefore primary magma differences could be due to the:

i. Different extents of recent mantle metasomatism or other recently established heterogeneity; and
ii. Extraction of magmas from different depths in the mantle.

These are not mutually exclusive and in all probability each may have some effect on the compositional variation observed within the two Rarotonga suites.

The evidence for or against the above scenarios will be examined below in the following order:

i. different source compositions due to variable degrees or types of metasomatism
ii. differences in degree of partial melting of the same source to produce two different primary magmas; and
iii. differences in pressure/temperature conditions of melting of the same mantle source.

6.7.1 Different Source Compositions.

The presence of potassium will increase the degree of silica undersaturation in a magma. Low degrees of partial melting of a mantle source, in which most of the K is contained within a K-rich phase (*e.g.*, amphibole and/or phlogopite), will produce a liquid depleted in K relative to mantle without a potassium bearing phase, providing that the K-rich phase is not consumed during melting (Späth et al., 1996). Thus melting of a mantle source with a K-rich phase will produce high silica, low K primary magmas compared to those from a mantle source of the same chemical composition but without the K-rich phase.

Alternatively, it has also been shown that the presence of CO_2 and H_2O can affect the silica composition of mantle melts. The presence of CO_2 will decrease the amount of silica while H_2O has the opposite effect of increasing silica in melts. The presence of CO_2 will also increase the CaO concentration in partial melts (Eggler, 1978). Therefore,

silica-poor melts produced by melting mantle rich in CO_2 should also be relatively richer in CaO than those from CO_2-free mantle melts.

The depletion of K and Rb in the relatively primitive compositions (Figure 6.11) in both types compared to primitive mantle rocks and the possible presence of a mica or amphibole phase in the source region has been discussed above. Since the source area for both types is assumed to have phlogopite and/or amphibole present, the difference in silica content could not be due to partial melting of a modally metasomatised source (which would produce a low SiO_2 primary magmas depleted in K and Rb) or a cryptically metasomatised source (which would produce a high SiO_2 primary magmas, and no K, Rb anomaly).

The possibility that the difference in silica content between the two groups is due to differences in CO_2 or H_2O concentrations in the source cannot be tested with the available data. Using a comparison of the LOI contents to identify differences in initial volatile compositions is of limited value due to the effects of fractional crystallisation which will mask any original variations between the two types. The primitive rocks from both groups also have similar concentrations of CaO, suggesting that the concentration of CO_2 in the mantle was the same for both.

6.7.2 Degree of Partial Melting

It can be seen that the primary magmas of both suites have similar absolute trace element concentrations. If the partial melts from a compositionally similar mantle were

produced by differing degrees of partial melting this difference should be reflected in the trace element concentrations. For example, if the type I primary magmas were produced by lower degrees of partial melting of the same mantle source as the type II primary magmas, this should be reflected in higher ratios of highly incompatible trace element concentrations with respect to somewhat more compatible trace elements. Both types from Rarotonga have similar incompatible trace element ratios suggesting similar degrees of partial melting if produced from identical sources.

However, although highly unlikely because this would be a unique case, it is still possible that the two sources had slightly different initial trace element concentrations, and thus different degrees of partial melting of the two sources could result in two primary magmas with similar trace element concentrations. Therefore, it would be useful to know the degree of partial melting required to produce the primary magmas. Determining the degree of partial melting is problematic due to uncertainties in the composition of the source and the primary magmas. However, several models have been developed (*e.g.*, Treuil and Joron, 1975; Maaløe, 1994; Cebria and Lopez-Ruiz, 1996) that use a minimum of assumption. *i.e.*: the distribution coefficients (Kd) and bulk distribution coefficients (D) for the trace elements are known; the samples used for the calculations represent primary magmas; and variation observed in trace element concentrations are due to differences in partial melting of a homogeneous source.

Applying Maaløe's (1994) models to the Rarotonga rocks it appears that very low degrees of partial melting (1-3%; Appendix 5) are required to produce the primary magmas for both the type I and type II rocks. This is consistent with many studies (*e.g.*,

Gast, 1968) which suggest that alkali magmas are produced by low degrees of partial melting. Richter and McKenzie (1984) has also shown that as little as 1% partial melting of the mantle is all that is required for melts to separate from their respective sources.

6.7.3 Physical parameters of partial melting.

The mineralogy of the two suites precludes the use of some of the well constrained mineral geothermeters and geobarometers. However, the fact that trace element modelling suggests that the source for the Rarotonga rocks was a spinel lherzolite indicates that melting occurred approximately between 25 and 10 Kbars.

From extensive experimental studies it is now possible to constrain the behaviour of mantle peridotite during partial melting processes. For example, for low degrees of partial melting there is a general increase in FeO and decrease of SiO_2 with increasing pressure of melting (Jacques and Green, 1980; Takahashi and Kushiro, 1983; Fujii and Scarfe, 1985; Takahashi, 1986; Klein and Langmuir, 1987; Falloon et. al, 1988; Hirose and Kushiro, 1983). Herzberg (1992) showed that although melts become silica-poor and iron-rich with increasing pressure, the decrease of SiO_2 with increasing pressure may not continue in low degree partial melts when garnet becomes a residual phase (at pressures > 30kbar), in which case SiO_2 appears to become effectively constant at ~45 wt. %. Adam (1988) suggested that at pressures above 20kbars, liquids continue to increase in normative olivine content with increasing pressure, but there is a decrease in the effect of

pressure on SiO_2 content. If the primary magmas of the high and low silica types were produced at different pressures they should have corresponding silica and iron differences. This appears to be the case for the calculated primary magma compositions for the two mafic types of rocks on Rarotonga (Figure 6.6), *i.e.*, type II primary magma has higher SiO_2 and lower FeO concentrations than type I primary magma.

6.7 Conclusions

Nearly all of the mafic rocks on Rarotonga have been modified by shallow level fractionation prior to eruption. This involved the fractionation of ol+cpx+mt, in varying amounts. The first clinopyroxenes to crystallise were diopside-augites (in type II) which probably started to crystallise at depth, and as the magma ascended, titanaugites crystallised. The preservation of the diopside-augites is probably constrained by ascent rates and magma storage times resulting in the preservation of only minor amounts of these phenocrysts in some of the type II rocks.

Trace element modelling shows that simple closed system fractionation or equilibrium crystal fractionation can account for the variation observed in the trace elements. However, these models probably represent an over simplification and fractional crystallisation probably involved a model more similar to that of O'Hara (1977) in which fractional crystallisation occurs in a chamber together with cyclic replenishment and only partial extraction of the differentiated liquid during each cycle. Due to the uncertainties in the composition and amount of the fraction of liquid erupted it

is thought unnecessary to test this model when concentrations could already be adequately modelled using less complicated equations and fewer assumptions.

Both type I and type II rocks were produced by similar amounts of partial melting (1-3%) of an enriched spinel lherzolite mantle containing amphibole and/or phlogopite. The type I rocks were formed at slightly higher pressures (greater depth) than the type II rocks from the same source, leading to lower SiO_2 and higher FeO^t.

Chapter Seven

Petrogenesis of the Felsic rocks

7.1 Introduction

There is considerable debate on the petrogenesis of felsic alkali rocks, as to whether they represent primary or relatively primitive melts of anomalous mantle (Bailey, 1987), or the final products of crystal fractionation of mafic alkali magmas (*e.g.*, Garcia et al., 1986). This uncertainty to a large extent is due to the existence of a chemical discontinuity between rocks of mafic composition and the felsic rocks in alkali provinces (Chayes, 1963). This geochemical gap has become known as the "Daly gap" after Daly (1910), who was one of the first to discuss the absence of intermediate rocks in oceanic alkali igneous provinces. The term "intermediate" is used here to describe samples with chemical compositions between basalt (~ 40-44 wt. % SiO_2) and phonolite (~51-60 wt. % SiO_2), and not in the usual sense indicating a SiO_2 content of 54 to 65 wt. % SiO_2. Although it is debated whether this gap is real or an artefact of inadequate sampling (Baker, 1968; Chayes 1977), the evidence for it is: the absence of intermediate rocks in the field; the lack of intrusive bodies of intermediate composition; and that the only cognate xenoliths found in lavas are simply the plutonic equivalent of the observed

extrusive rocks.

If, in fact, there are no intermediate rocks, it leads to the suggestion that simple crystal fractionation may not be the process involved in the genesis of felsic alkali rocks. Bailey (1987) suggested that phonolites are formed by partial melting of an upper mantle composition resulting from recent metasomatism. An alternative to partial melting of the upper mantle is the formation of phonolites by equilibrium partial melting of alkali basalts in the lower lithosphere (Hay and Wendlant, 1995; Hay et al, 1995).

Rarotonga displays all the features typical of alkali igneous provinces discussed above, having a bimodal distribution of rocks types: mafic rocks, type I and type II; and felsic rocks, the phonolites and foidal phonolites. The absence of rocks with an intermediate composition obscures the petrologic relationship which may exist between the mafic and felsic rocks.

However, the close spatial and temporal relationships between the felsic and mafic rocks on Rarotonga suggest that a genetic relationship exists between them. The presence of two suites of mafic rocks lends weight to the argument that fractionation of parental mafic magmas was the principle process operating to form the two types of felsic rocks. If crystal fractionation was the process that formed the felsic alkali rocks, the question has to be answered: why are the intermediates not there?

7.2 Partial Melting

If the foidal phonolites and/or the phonolites were to have formed by partial melting there are at least two obvious scenarios; partial melting of anomalous upper mantle material; or partial melting of the lower oceanic crust.

In arguing that phonolitic magmas are produced by partial melting of anomalous upper mantle material, Bailey (1987) relies principally on experimental work which shows that the stability fields for felsic minerals can persist at pressures and temperatures typical of the upper mantle. Without knowledge of the composition and physical parameters of the upper mantle under Rarotonga it is not possible to prove or disprove whether the foidal phonolites and/or the phonolites were derived from phonolitic magmas that were formed directly by partial melting in the upper mantle.

A model involving the melting of the oceanic crust is easier to test, as relatively good approximations of the composition of the source region can be made, to which partial melting models can then be applied. It is possible to identify at least two geochemically different sources within the oceanic crust under Rarotonga: the old oceanic crust formed at the East Pacific Rise and the younger mafic rocks produced during the initial stage of the formation of Rarotonga.

Comparing the trace element chemistry and Nd and Sr isotope pairs of the phonolites and the ocean lithosphere shows that the ocean lithosphere could not be the source region. Normal mid ocean ridge basalts have a distinctive REE signature (LREE depleted) while the phonolites and foidal phonolites are LREE enriched. To produce a

LREE enriched pattern from a LREE depleted or even a flat REE pattern requires the presence of garnet as a residuum in the source, a mineral phase which is not typically found in rocks produced at the mid-ocean ridges. The isotopic signature of the felsic rocks also show that they are not related to a MORB type rock. The phonolites and foidal phonolite have a broadly similar isotopic signature to the mafic rocks on Rarotonga, which have higher $^{87}Sr/^{86}Sr$ and lower $^{143}Nd/^{144}Nd$ values than MORB. Although the isotopic signature and REE patterns are similar for the felsic and mafic rocks on Rarotonga, equilibrium batch melting models of the mafic rocks will produce trace element concentrations different from what is observed in the felsic rocks, even for moderately large degrees of melting (Figure 7.1)

The above suggests that the foidal phonolites and phonolite magmas are not produced directly by partial melting and that one must look for an origin by fractionation of a mafic alkali magma.

7.3 Fractionation

When the rocks from Rarotonga are plotted on the pseudo-ternary, pseudo-liquidus diagram for experimental melts saturated with olivine, leucite, spinel and one or more of the minerals nepheline, high-calcium pyroxene, plagioclase and alkali feldspar (Sack et al., 1987), it becomes readily apparent how the two felsic suites could be produced from the two mafic groups with similar chemistry. The type I basalts fall within the clinopyroxene field and as they fractionate, compositions move towards the

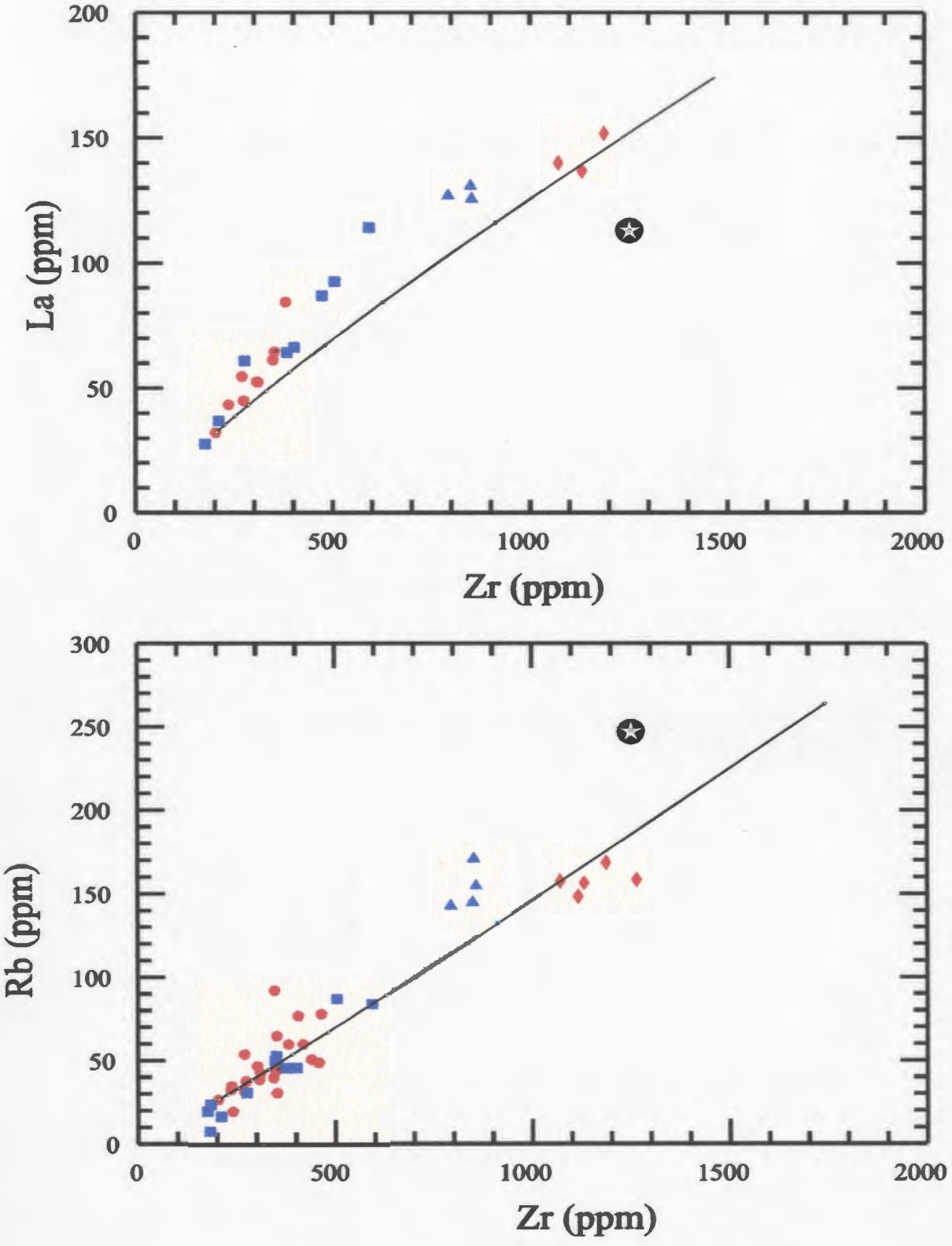

Figure 7.1: Predicted trace element concentrations resulting from fractional crystallization of a parent magma represented by sample R36 and partial melting of a basaltic source composition represented by sample R36 . The fractional crystallisation path is shown by the line, while the star represents a 10% partial melt of a basaltic source. Symbols are the same as Figure 4.1.

Di-Neph cotectic (Figure 7.2). As the type II basalts fractionate, successive compositions will plot on the trend towards the alkali-feldspar cotectic and the plagioclase reaction point. These trends suggest that the foidal phonolites could be produced by fractionation of type I magmas and the phonolites from type II magmas.

The limited range of major element abundances in the phonolites compared to the foidal phonolites (see section 4.2.2) can be explained by plotting these rocks on the $NaAlSiO_4$-$KAlSiO_4$-SiO_2 phase diagram at 1atm (Figure 7.3). The phonolites plot close to the leucite - feldspar - nepheline eutectic therefore with further fractionation their composition should not change.

Quantitative modelling of the evolved Rarotonga lavas is made difficult by the presence of mineral phases (*e.g.*, apatite, sphene etc.), involved in late stage crystal fractionation, which have high concentrations of otherwise incompatible elements (*e.g.*, Nb, Zr, REE etc.). In addition, the absence of reliable distribution coefficients for these elements in felsic rocks makes it difficult to independently evaluate the results of major element models with any confidence. However, an attempt will be made to evaluate the evolution of the lavas as accurately as possible.

7.3.1 Foidal phonolites

Sample R49 can be identified as the least fractionated of the foidal phonolites using the following criteria; highest Mg#, TiO_2, CaO, P_2O_5 wt % and lowest D.I and SiO_2 wt. %. Conversely R25 is one of the most fractionated of the foidal phonolites.

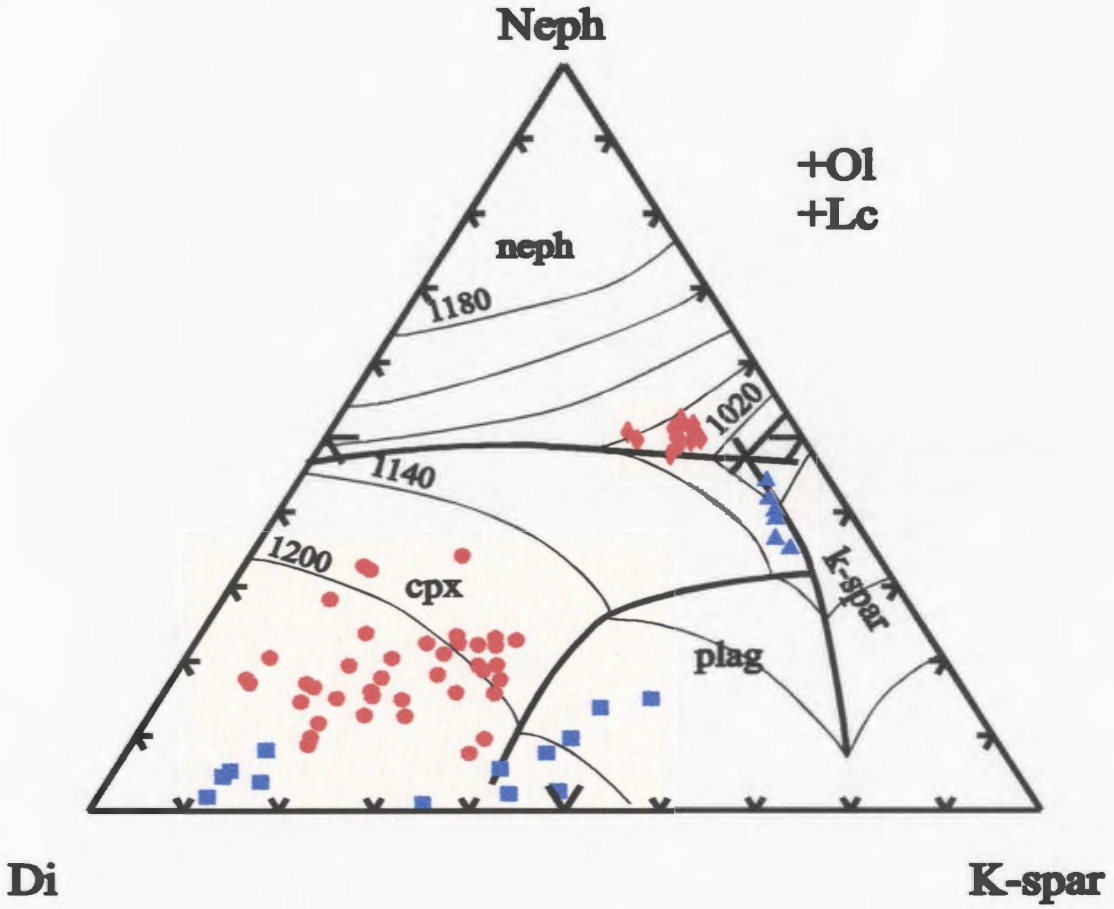

Figure 7.2: Samples from Rarotonga plotted on a pseudo-ternary, pseudo-liquidus diagram for experimental melts saturated with olivine, leucite, spinel, and one or more of the minerals nepheline, high calcium pyroxene, plagioclase, and alkali feldspar (Sack et al., 1987). Symbols are the same as Figure 4.1.

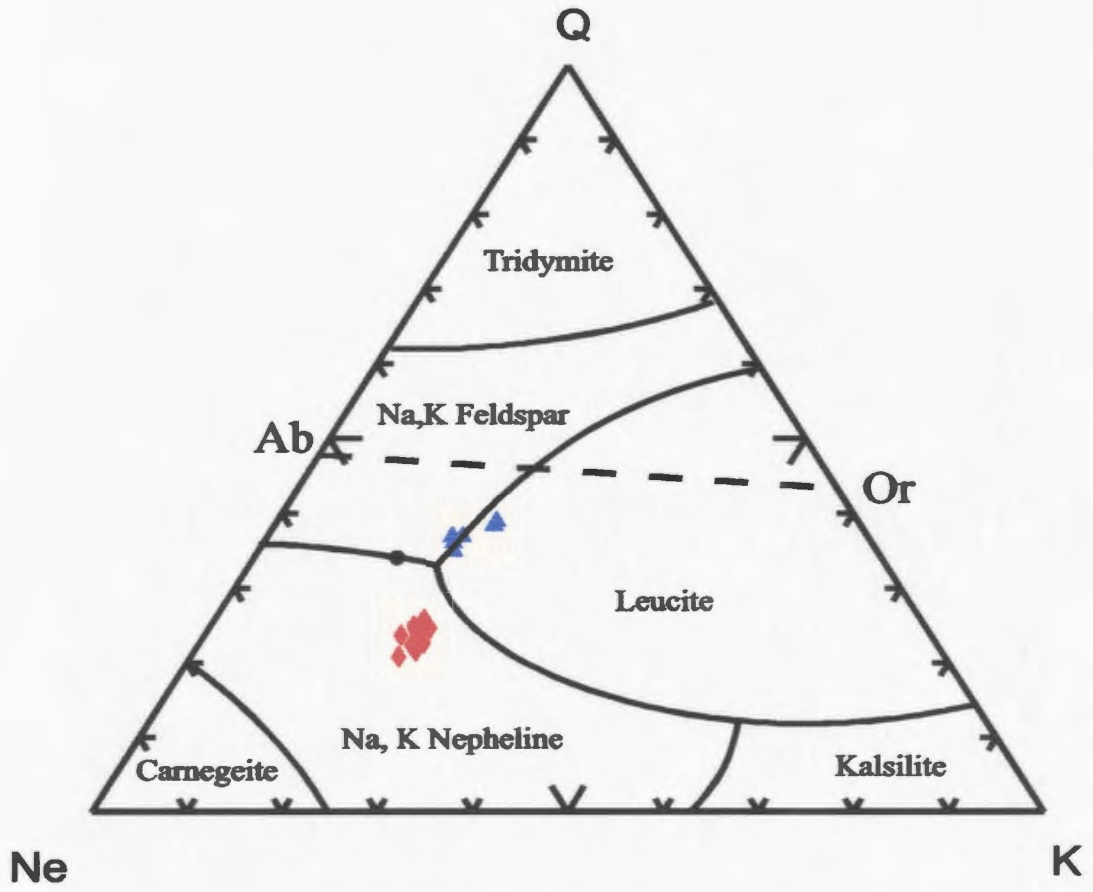

Figure 7.3: The phonolites and foidal phonolites plotted in the $NaAlSiO_4$ - $KAlSiO_4$ - SiO_2 system at 1 atm (Schairer, 1950). The filled circle denotes the minimum along the feldspar-nepheline boundary curve. The symbols are the same as Figure 4.1.

Least square modelling of the type I mafic rock-foidal phonolite series was performed using the following mineral phases: clinopyroxene, kaersutite, spinel and apatite (Table 7.1). All of these mineral phases are observed in the most fractionated mafic rocks and their mineral compositions have been determined in these rocks. It is clear from such modelling that although the concentrations of most major elements could be assessed with some degree of confidence, calculated Na_2O wt. % in the phonolites are significantly lower, resulting in unsatisfactory models (*i.e.*, SSR values >1). When SSR values are calculated without considering Na_2O, values of less than 1 can be obtained. Least square models suggests that the range of major element abundances in the foidal phonolites is due to low degrees of fractionation of aegirine-augites + spinel + apatite + nepheline (Table 7.1).

As previously mentioned, trace element modelling is equivocal due to the mineral phases involved and the lack of control on when these phases first started to crystallise in the "intermediate magmas". For example, yttrium is generally considered an incompatible element during basaltic fractionation (D<1; see section 6.1.5), but if apatite starts to crystallise it will behave as a compatible element ($Kd^{Y}_{apatite} \approx 40$; Pearce and Norry, 1979). In trace element diagrams (Figures 7.4) the effect on trace elements of different crystallising phases is shown. From these diagrams it is apparent that most of the trace element concentrations observed in the phonolites could be obtained from mafic magmas by fractionation of the mineral phases used in least square modelling. The elements which are hygromagmatophile (*e.g.*, Th and U) have higher concentrations in

Table 7.1

Type I mafic rocks to foidal phonolite series

The parent is R50 the daughter is R49				
	mineral proportion	mineral phase		
	0.14	mt		
	0.08	apt		
	0.54	kaersutite		
	0.24	px		
F=.23				
	R-49	R50obs	Calc-R50	DIF
SiO_2	49.99	45.68	45.88	-0.2
TiO_2	1.56	3.53	3.82	-0.29
Al_2O_3	20.22	18.21	18.15	0.06
Fe_2O_3	0	0	0	0
FeO	6.23	9.88	9.82	0.06
MnO	0.33	0.24	0.27	-0.03
MgO	1.7	4.23	4.22	0.01
CaO	5.96	9.7	9.44	0.26
Na_2O	8.95	4.05	6.84	-2.79
K_2O	4.6	3.49	3.58	-0.09
P_2O_5	0.46	0.99	1.23	-0.24

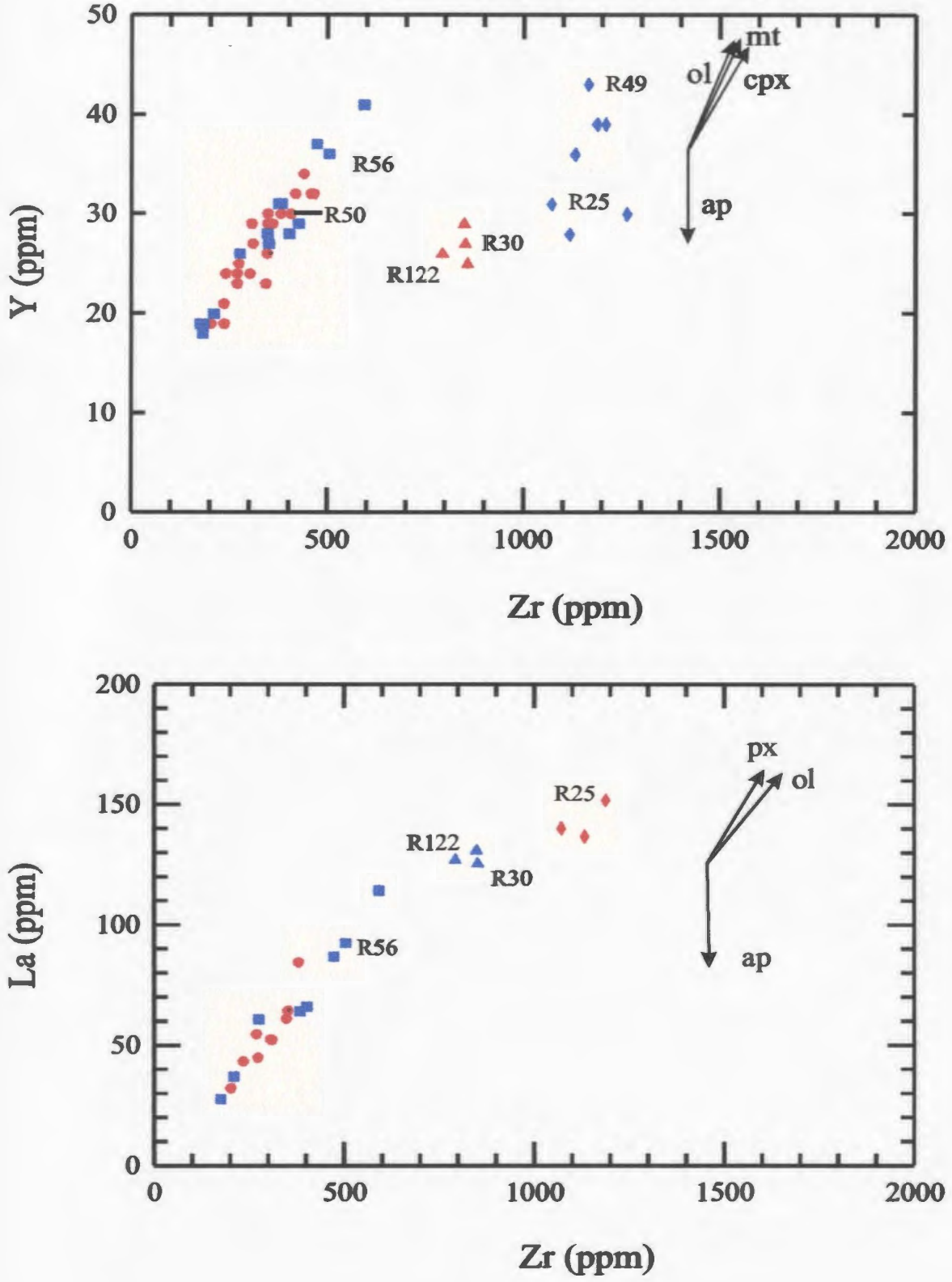

Figure 7.4: Trace element plots with vectors showing effects the crystallisation of different phases will have on trace element concentrations. Samples discussed in the text are also shown. R50 and R56 are the samples used in least square modelling to represent parental magma compositions to model foidal phonolite and phonolite compositions. Symbols the same as Figure 4.1.

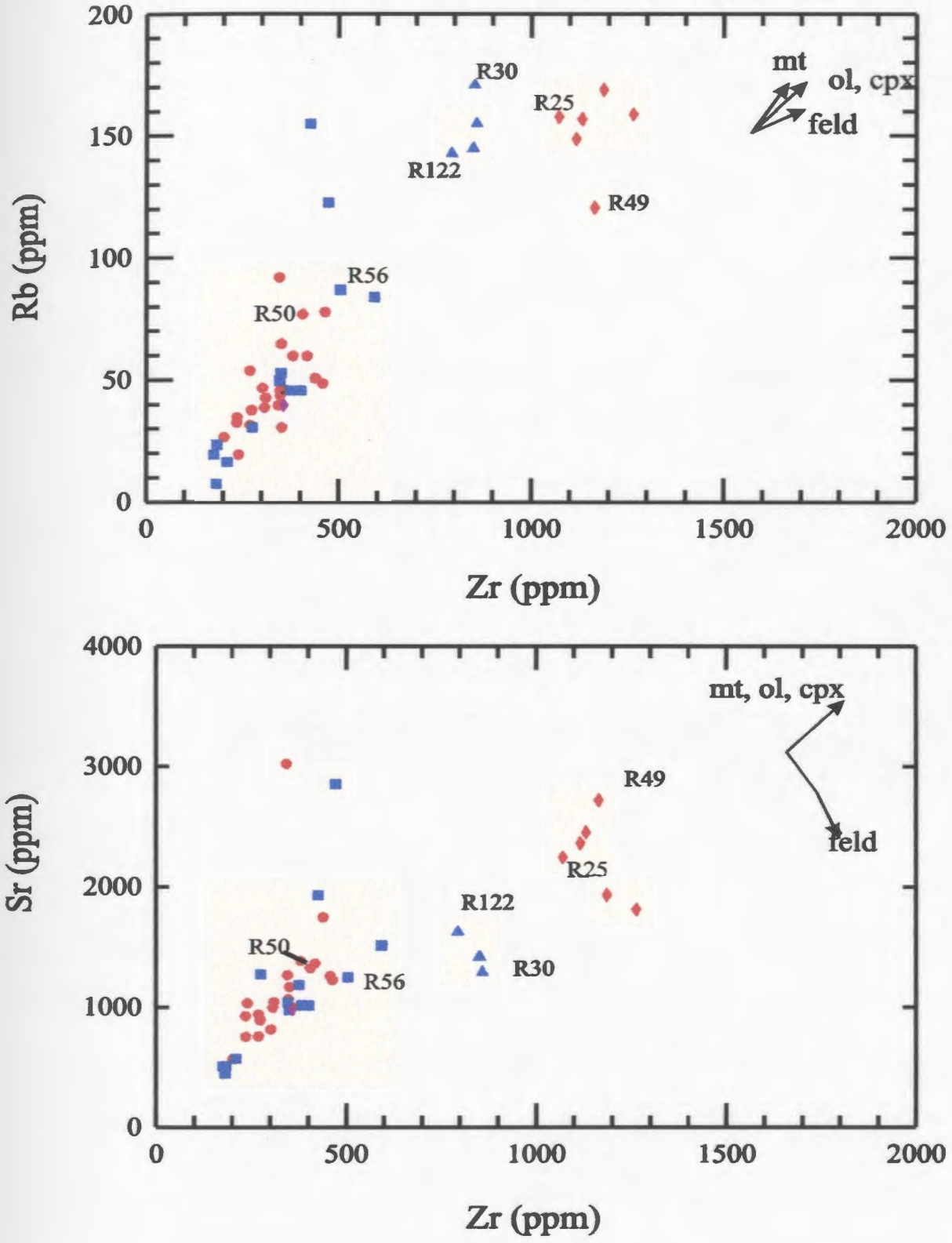

Figure 7.4: Continued.

the foidal phonolites than what would be expected if crystal fractionation was the only process operating.

7.3.2 Phonolites

The phonolites have a much more limited range of major element abundances when compared with the foidal phonolites, making the selection of the least and most fractionated samples more equivocal. Sample R30 was identified as being the most fractionated on the basis of high SiO_2 wt. %, CaO wt. %, and K_2O wt. %, and low Na_2O wt. %., TiO_2 wt. % and Mg#, while R122 is less fractionated having lower SiO_2, CaO and K_2O, and higher Na_2O and TiO_2 concentrations and a higher Mg#. Using a similar approach as with the type I-foidal phonolite series, the phonolitic compositions can be modelled from one of the most fractionated of the type II rocks (R56) by approximately 40% crystal fractionation of potassium feldspar + kaersutite + clinopyroxene + spinel + apatite (Table 7.2).

Least square modelling suggests that low degrees of fractionation (<20%) of potassium feldspar and spinel (± aegirine-augite, ± nepheline) is required to produce a composition similar to R30 from R122 (Table 7.2). The dominance of potassium feldspar fractionation in the least square model concurs with the modal abundance of feldspar in the phonolites. The relatively constant concentration of P_2O_5 in the phonolites precludes any significant crystallisation of apatite.

Table 7.2

Type II mafic rocks to phonolite series

The parent is R56 the daughter is R107				
	mineral proportion	mineral phase		
	0.17	mt.		
	0.05	apt		
	0.49	kaersutite		
	0.29	feld.		
F=.4				
	R107	R56 OBS	R56 CALC	DIF
SiO_2	58.57	49.33	49.42	-0.09
TiO_2	0.69	3.13	3.35	-0.22
Al_2O^3	19.69	19.09	18.91	0.18
FeO	4.01	9.82	9.64	0.18
MnO	0.21	0.16	0.16	0.01
MgO	0.73	3.67	3.52	0.15
CaO	3.02	7.32	7.4	-0.08
Na_2O	8.01	2.78	5.63	-2.85
K_2O	4.92	3.63	3.42	0.21
P_2O_5	0.15	1.05	0.96	0.09

7.4 Pneumatolysis

In the foidal phonolites, observed high concentrations of Na_2O and some trace elements cannot be accounted for by simple crystal fractionation. However, these high concentrations might be explained by pneumatolysis occurring during the latter stages of fractionation. Kennedy (1955) suggested that during fractionation a significant amount of water could concentrate in the upper portions of a magma chamber. Hughes (1982) argued that zoned ash flows on Iceland, with continuous subtle compositional variations upward, were evidence for pneumatolytic processes. Alkalis and incompatible elements (*e.g.*, Th and U) would tend to be concentrated in this water-rich portion of the magma chamber. These higher concentrations of dissolved water would reduce magmatic crystallisation temperatures and accentuate the temperature gradient during crystallisation (Hughes, 1982). This could enhance convection cells within the magma chamber, mixing and homogenising the magma, thus lowering the overall viscosity.

7.5 Intermediate Rocks

As Bailey (1987) pointed out, any study on the origin of phonolites which invokes crystal fractionation must explain the absence of the intermediate rocks. At least three explanations can be offered:

i. Magmas with an intermediate composition were not produced;

ii. The intermediate rocks were erupted on Rarotonga but were are not available for collection; or

iii. Rocks of intermediate composition did not erupt on the surface.

An obvious example of the first scenario is for a phonolite liquid to form by some sort of immiscibility process. However, without available evidence for or against liquid immiscibility it is not possible at this stage to determine if the felsic rocks were produced in this way.

The second case, implies that they were not available for collection for various reasons. There are several possible reasons why intermediate rocks were not collected. The first is that rocks of intermediate composition were originally erupted but subsequent erosion has totally removed them. The island is relatively young so any significant volume of intermediate rocks should not have been completely removed by erosional processes. Another possibility is that the intermediate rocks form an offshore volcanic-clastic apron surrounding the island. This case was argued for the absence of intermediate rocks on the Canary islands. However, recent work on the volcaniclastic apron has failed to find any intermediate rocks (Schmincke et al., 1994).

The third explanation is that the lack of intermediate rocks on the surface is due to the physical properties of the fractionating magma. Generally the more felsic a magma is, the higher its viscosity. Thus, as a mafic magma fractionates it becomes more viscous. At some stage the viscosity may be high enough to inhibit movement of the magma and, therefore, eruption. On Rarotonga, as the magmas became more fractionated the

viscosity reached a stage where eruption ceased. However, the magma chamber continued to fractionate. When the magmas were relatively fractionated a decrease in viscosity occurred which enabled the felsic magmas to erupt. For this to be feasible an explanation is required as to why magma viscosity should decrease rather than increase with extensive fractionation.

A typical viscosity vs. time profile for a fractionating magma chamber, where viscosity increases with increasing differentiation, is compared with the profile required for such a model to work on Rarotonga in Figure 7.5. Using whole rock major element compositions it may be possible to estimate the viscosity of a magma (Bottinga and Weill, 1972). However, due to uncertainties in many of the variables which effect viscosity *e.g.*, pressure, temperature, volatile content and the crystallinity of the magmas, *etc.*, these estimates would not help constrain the viscosity differences between intermediate and felsic magmas. The eruption of magma is also dependent on many other factors *e.g.*, the density contrast between the magma and the country rock, and the amount of magma. Taking all of this into consideration, it is still thought possible to make some qualitative remarks about possible changes in viscosity occurring during fractionation of the magma chambers under Rarotonga.

The primary controls on viscosity are composition, temperature and pressure. Elements in a silicate liquid can either form networks as central cations of TO_4 tetrahedra capable of forming strong T-O-T bridging bonds (increasing viscosity), or occupy space interstitial to the network and act as modifiers (decreasing viscosity). It is generally considered that in silicate liquids, with approximately 35-85 mol. % SiO_2, silica is

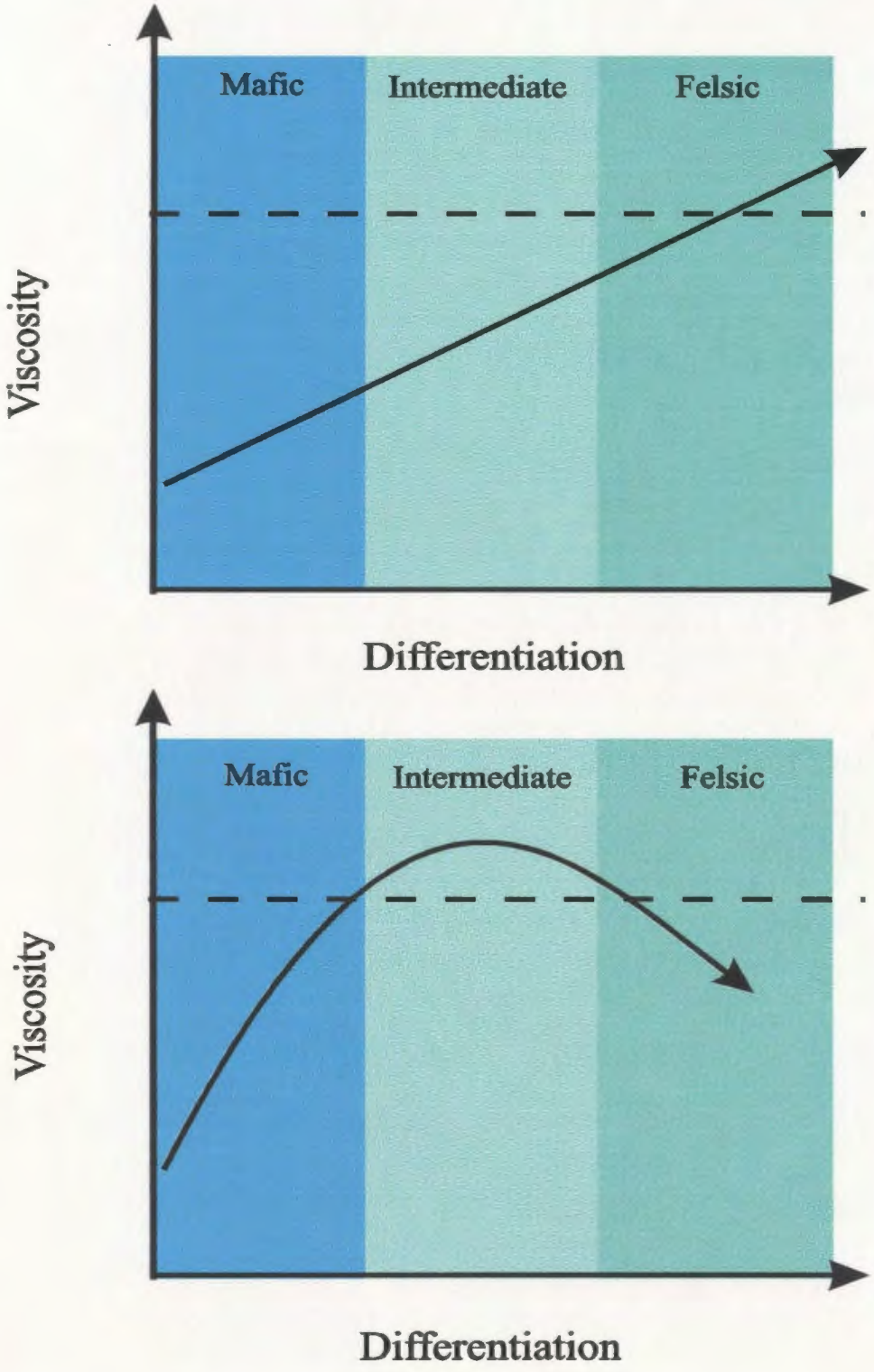

Figure 7.5 Possible viscosity changes with increasing differentiation of a magma. The top diagram shows a possible tholeiitic trend with increasing viscosity with increasing differentiation. The bottom diagram shows the viscosity model for Rarotonga (alkali trend) where viscosity increases and then decreases with increasing differentiation. The dashed line represents the point at which the viscosity of the magma inhibits eruption of lavas.

a network former and Na, K, Ca, and Mg are network modifiers (Bottinga et al, 1982). The influence of Al in the structure of silicate melts is generally less clear due to the common occurrence of aluminium in two oxidation states, Al^{iv} in tetrahedral co-ordination which acts as a network former, and Al^{vi} which acts as a network modifier. Although the ratio of Al^{iv} to Al^{vi} is pressure dependant (Kushiro, 1980) there also appears to be some chemical control (Bottinga et al, 1982). When $Al_2O_3/Na_2O >> 1$, Al is present almost entirely as Al^{iv} cation and acts as a network former, but as Al_2O_3/Na_2O approach unity there is an increase in the amount of Al^{vi}, with Al^{vi} becoming the dominant Al cation in peraluminous silicate liquids (Bottinga et al., 1982). The presence of volatiles dissolved in the magmas also lowers viscosity, *e.g.*, a granitic magma containing 1 wt. % H_2O has a viscosity of 10^8 Pa, whereas with 10 wt. % H_2O the viscosity is only 10^4 Pa (Shaw, 1965).

An examination of the relationship between Al_2O_3 and Na_2O in the rocks on Rarotonga (Figure 7.6) shows there is a significant decrease in Al_2O_3/Na_2O between the mafic rocks and the felsic rocks. Working on the principle that low Al_2O_3/Na_2O will lead to more Al^{vi} cations, the addition of a Na_2O rich fluid phase will have a two fold effect on the viscosity, firstly by introducing Na as a network modifier and secondly by breaking down Al^{iv} networks and releasing more Al^{vi} network modifiers. In addition, a fluid phase rich in H_2O will also decrease the viscosity.

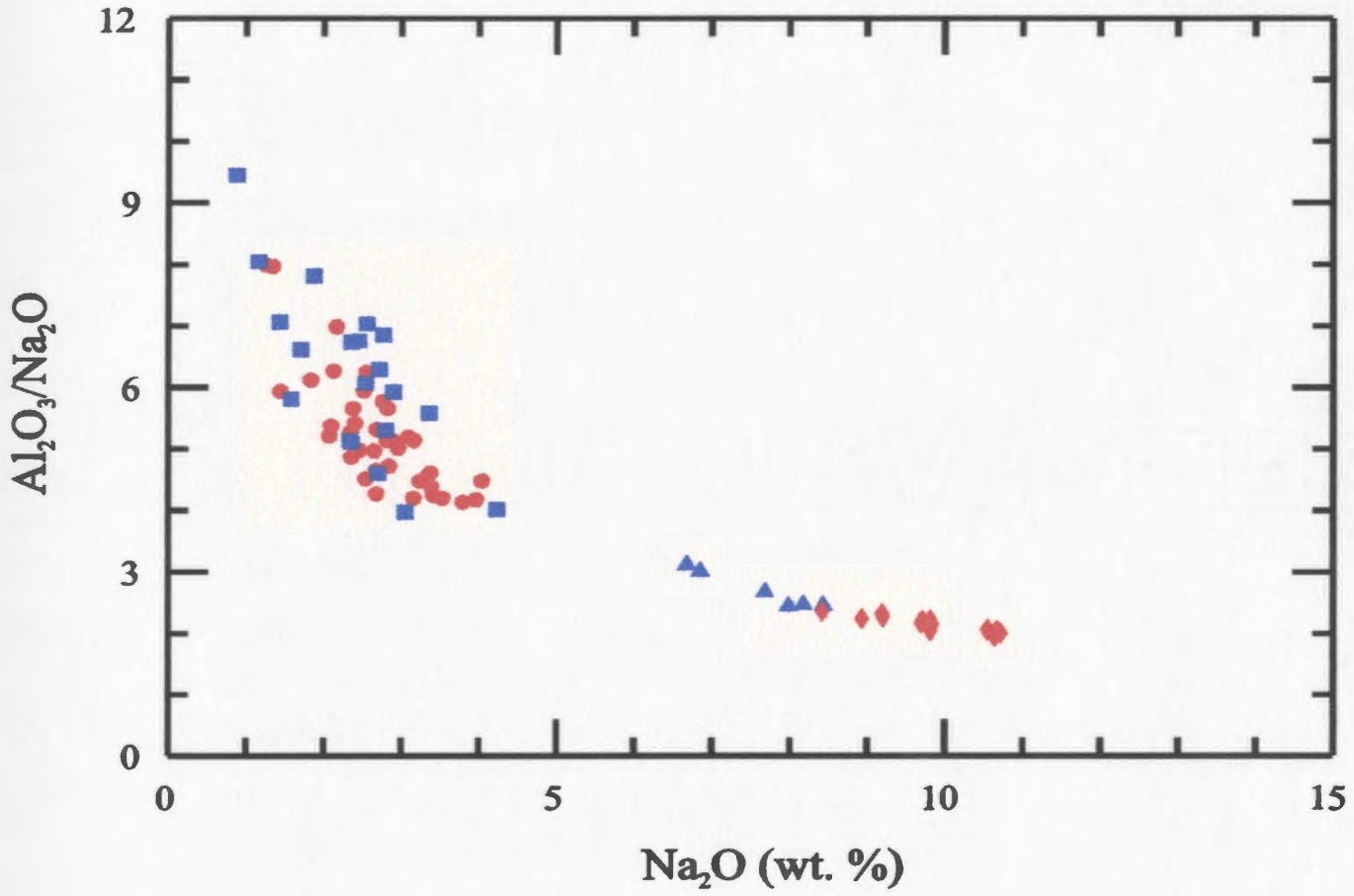

Figure 7.6: Al_2O_3/Na_2O vs. Na_2O for Rarotonga samples. Symbols are the same as Figure 4.1

7.6 Conclusions

The foidal phonolites and phonolites were formed by crystal fractionation of the type I and type II mafic magmas, producing respectively a basanite-foidal phonolite series and an alkali-basalt-phonolite series. The foidal phonolite compositions evolved from the most fractionated type I mafic magmas by approximately 30% fractionation of titanaugite + kaersutite + apatite + nepheline + Fe-Ti oxide. In the foidal phonolite magmas, fractionation continued with the crystallisation of aegirine-augites + nepheline + apatite + Fe-Ti oxides (Figure 7.7). The phonolites formed by approximately 20% fractionation of titanaugite + anorthoclase + kaersutite + apatite + Fe-Ti oxide (± nepheline). The phonolite magmas continued to evolve by fractionation of anorthoclase + aegerine-augites + nepheline + Fe-Ti oxides (Figure 7.8).

As the magmas fractionated in both series, the overall viscosity of the magmas increased. The increase in viscosity inhibited the eruption of magmas with compositions intermediate between the mafic rocks and the felsic rocks. A late fluid was introduced into the magma chambers, possibly a hydrous fluid concentrated in the upper portions of the magma chamber by pneumatolysis, which was enriched in Na_2O and some trace elements (*e.g.*, Th, U). Due to this concentration of Na_2O and H_2O the viscosity of the magma decreased, resulting in eruption of the fractionated magma. The different styles of eruption can be explained by differences in viscosity, with the phonolite magma being slightly more viscous due to a high crystallinity index and/or slightly lower Na_2O concentrations.

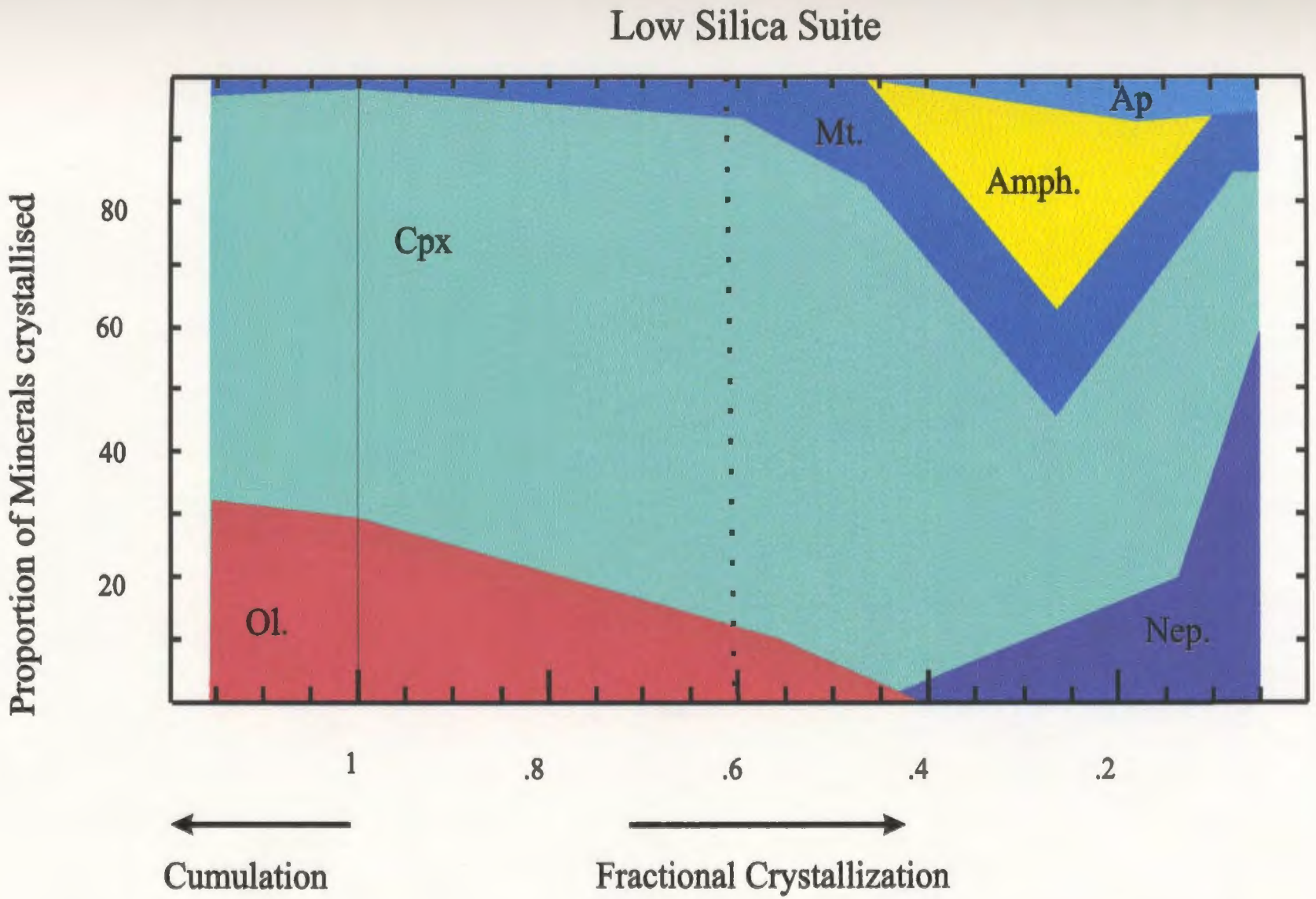

Figure 7.7: Schematic representation of the change in relative proportions of fractionating minerals with differentiation of the type I-foidal phonolite rocks (low silica suite). Mineral proportions were calculated using major element least-squares modelling techniques. The dashed line represents the inflection of major element trends at *ca.* 6 MgO wt. %

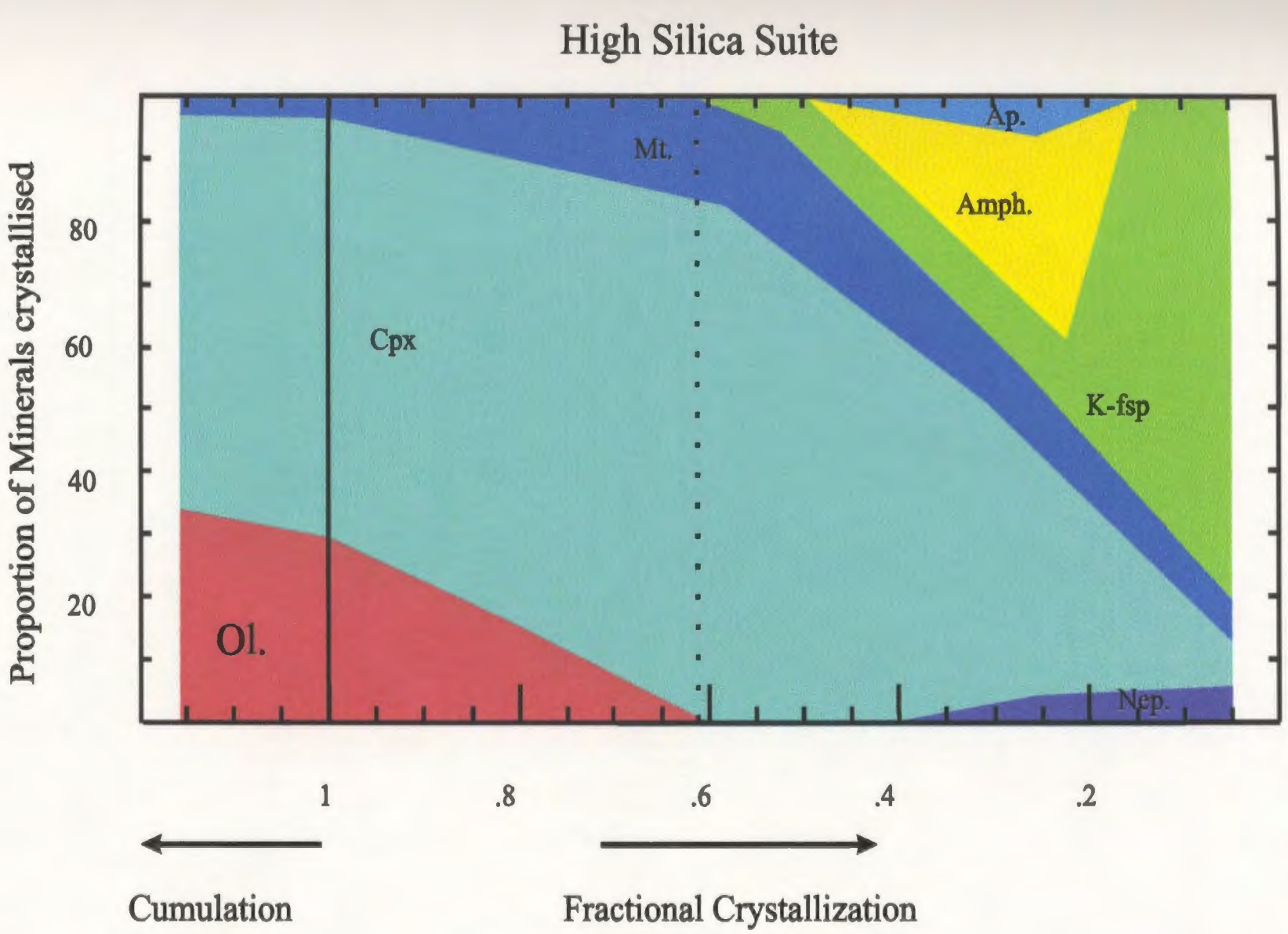

Figure 7.8: Schematic representation of the change in relative proportions of fractionating minerals with differentiation of the type II - phonolite rocks (high silica suite). Mineral proportions were calculated using major element least-squares modelling techniques. The dashed line represents the inflection of major element trends at *ca.* 6 MgO wt. %

Chapter Eight

Petrogenesis of Rarotonga and underlying mantle

"No man is an island, entire of itself"

John Donne (1571-1631)

8.1 Introduction

In this chapter a model for the formation of Rarotonga will be constructed using the information presented in this thesis and what we know about the formation of other ocean islands. The genesis of Rarotonga will be compared to other such island volcanoes. The model for the formation of Rarotonga will be examined with respect to the underlying mantle to provide insight to mantle chemistry and processes occurring within the mantle.

In chapters three, four and five the following conclusions were made which were then used to model the formation of the mafic and felsic rocks in Chapters six and seven

Chapter three

i. The morphology of Rarotonga is controlled by two processes, the initial formation of the island by volcanic activity and subsequent modifications to the volcanic edifice by

erosion;

ii. There are four major igneous rock types found on Rarotonga: two types of mafic lavas (including both ankaramites and basalts), felsic lavas (fodial phonolites) and felsic breccias (phonolites);

iii. The two mafic types are distinguished by the presence of diopside-augite phenocrysts, POPPs and a greater degree of alteration of olivine phenocrysts in the type II mafic rocks;

iv. No temporal or spatial difference exists between the two types of mafic rocks with both types being ubiquitous over the entire island;

v. The felsic rocks appear to be the youngest rocks, with the foidal phonolite lavas occurring on the flanks of the island, while the phonolite breccia is concentrated in the centre.

Chapter four

vi. The diopside-augites and the titanaugites in the type II rocks are cognate, with the diopside-augites crystallising before the titanaugites;

vii. There are two types of mafic rocks; a low silica type and a high silica type. The low silica type is comprised of the type I ankaramites and basalts, while the high silica type is comprised of the type II ankaramites and basalts described in Chapter three. The two types can be only be distinguished chemically by their silica composition

with the remaining elements (both major and trace) having similar concentrations in both types;

viii. Both types are enriched in incompatible trace elements compared to the primitive mantle;

ix. Although some of the mafic rocks have primitive compositions they probably do not represent primary compositions due to the presence of accumulated minerals (*e.g.*, olivine).

Chapter five

x. The high concentrations of most of the incompatible trace elements (*e.g.*, Sr, Th, Y, REE etc.) in the pyroxenes relative to the other phases suggest that fractionation of pyroxenes will dominate trace element distributions;

xi. If pyroxenes dominate crystal fractionation, the highly incompatible elements (Kd < 0.001) are the LFSE Ba and Cs, and the HFSE. Elements that could also be classified as strongly incompatible are Nb and Ta (Kd < 0.1). The remaining trace elements have Kd values that range from ~0.1 (La) up to ~0.8 (Yb);

xii. Magnetites incorporate higher amounts of Nb and Ta compared to the titanaugites, and any significant fractionation of magnetite will effect the bulk distribution of Nb and Ta.

xiii. The LREE have lower Kd values than MREE and HREE with the HREE having Kd values close to unity. Consequently, the separation of titanaugite produces an overall enrichment of REE in the residual liquid with an increase in the La/Yb ratio;

8.2 Partial melting

Whereas much of the compositional variability observed amongst Rarotonga rocks can be attributed to fractional crystallization, important differences in incompatible element ratios and bulk composition of primitive Rarotonga lavas must have been inherited from processes occurring in their mantle source regions. Evidence suggests that mafic alkaline magmas result from relatively small degrees of partial melting of enriched mantle (*e.g.*, Frey et al., 1978; Clauge and Frey, 1982). In addition, numerous experimental and trace element studies have suggested that progressively more silica under-saturated magma may be produced at progressively greater depths by decreasing degrees of partial melting of a hydrous lherzolite mantle source (*e.g.*, Green, 1971; Sun and Hanson, 1975; Frey et al, 1978). A model showing the petrogenesis of the primary magmas for Rarotonga is given in Figure 8.1. Quantitative modeling shows that the Rarotonga lavas were produced by low degrees of partial melting (<5%) of a (garnet-free) spinel lherzolite source. The mantle source also contained an amphibole and/or mica phase and was enriched relative to primitive mantle in the highly incompatible elements. This suggests that modal metasomatism occurred prior to formation of the

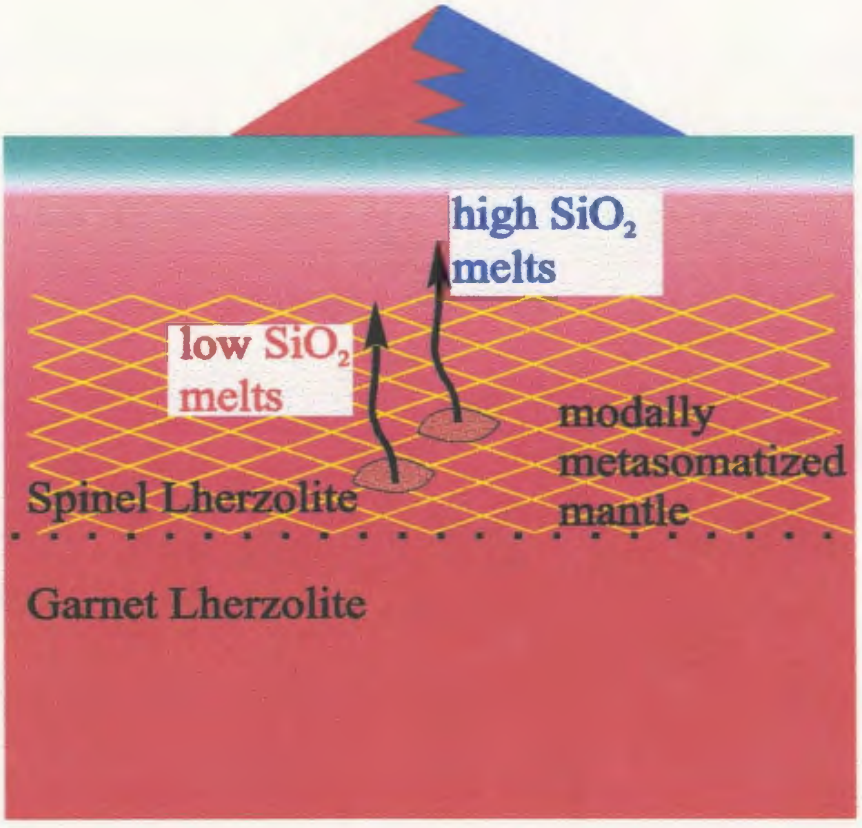

Figure 8.1: Model for the formation of Rarotonga. The primary magmas are formed by low degrees of partial melting of a spinel lherzolite mantle which has previously undergone modal metasomatism. The type I primary magmas (low silica magmas) were produced at slightly greater pressures than the type II primary magmas (high silica magmas).

primary magmas. In accord with the above, the low silica magmas were probably produced slightly deeper in the mantle than the high silica magmas

8.3 Fractional crystallization

Most of the bulk compositional variation observed in the Rarotonga lavas is due to crystal fractionation processes. Rayleigh fractionation is preferred to equilibrium crystallization on account of the abundance of zoned phenocrysts in many of the Rarotonga rocks. Olivine and clinopyroxene were the two phases controlling crystal fractionation of the mafic rocks. In the type II magmas, the first clinopyroxenes to crystallize had diopside-augite compositions while later clinopyoxenes had titanaugite compositions. However, only rare magmas from the high silica type II rocks rose rapidly enough to preserve these early fractionating phases (diopside-augites) and xenoliths. An inflection of the chemical trends at about 6 MgO wt. % is caused by an increase in Fe-Ti oxide and a sympathetic decrease in olivine fractionation. As the magma fractionated towards more intermediate compositions kaersutite began to crystallize. Due to slight differences in silica saturation the type I magmas fractionated toward a foidal phonolite end-member forming a low silica suite. The type II magmas fractionated towards phonolite forming a high silica suite. The low silica mafic magmas were modified by crystallization of clinopyroxene + oxides + kaesutite + apatite + nepheline, while the

high silica mafic magmas were fractionated by crystalization of clinopyroxene + oxides + kaesutite + apatite + feldspar.

Viscosity increased during fractionation of the magma chambers inhibiting eruption of the intermediate compositions. A late stage fluid (probably formed during pneumatolysis) was concentrated in to the fractionating magma chambers (Na_2O and Th, Y *etc.*). This fluid along with continued increase of alkalis decreased the overall viscosity of the magma to a point where eruptions could start again. The phonolite magmas, which only formed pyroclastic eruptions, were slightly more viscous than the foidal phonolites which erupted as flows.

8.4 Physical evolution of Rarotonga

Rarotonga was formed by the initial eruption of alkali basaltic rocks during the Pliocene on ocean lithosphere of Palaeocene age. Two types of basalts were involved in this initial formation of Rarotonga, a low silica type and a high silica type. After this initial period of mafic volcanic growth, felsic rocks erupted; phonolite breccia which blanketed the central region of the island and foidal phonolite flows which erupted on the flanks of the island.

Wood and Hay (1970) proposed that the geologic evolution of Rarotonga was similar to that of Hawaii, *i.e.*, an initial shield building stage followed by caldera collapse, accompanied by extensive faulting and dyke emplacement. Their proposal was

based on the presence of multiple dykes and faulting within the proposed caldera, and the large central valleys of the Avatiu and Takuvaine Rivers. However, detailed mapping has shown that the density of dyke intrusion is no greater within the proposed caldera than outside it and there is no evidence for ring faults, ring dykes, collapse structures or caldera-fill breccia. The ridges on the northern side of the island are semicircular, but this is an erosional feature rather than a relic feature of caldera collapse. On the Hawaiian islands, the post-caldera stage is characterised by a new period of mafic volcanism, which is chemically and temporally distinct from the rocks of the shield building stage. Although there are two petrographically distinct types of mafic rocks on Rarotonga, there is no evidence that they are separated by a significant hiatus, or that spatial distribution of one of the types is restricted to a region of caldera collapse. The presence of high and low silica types is not unique to Rarotonga, many well studied islands have similar suites (*e.g.*, Samoa, Wright 1986; Tristan de Cuhan, Le Roez et al., 1990). On Samoa the two suites are contemporaneous and even though appearing to erupt from the same center there is no evidence of mixing between them (Wright, 1986). In the absence of positive evidence, it is suggested there was no stage of caldera collapse in the evolution of Rarotonga and that the present topography is solely the result of erosion. A stratigraphic nomenclature is proposed here that is based on new and detailed field observations, together with the petrography and geochemistry. The differences between previously published and proposed stratigraphic groupings are summarised in Table 8.1.

Table 8.1
Nomenclature of the volcanic stratigraphic units of Rarotonga

Wood & Hay (1970)		This Study	
Unit	Description	Unit	Description
Intra-Caldera Manureva Flows	Dark green phonolite containing sodalite, aegirine, nepheline; zeolite-filled vesicles.	Raemaru Flows	Dark green-grey dense foidal phonolite forming thick lava flows. Locally flow banded. Modal assemblage sodalite, nepheline, aegirine, analcime.
Tuakata flows	Dark green flow banded nepheline phonolite containing sodalite, nepheline.		
Extra-Caldera Raemaru Flows	Light olive green to grey dense phonolite.		
Muri Flows	Dark green to grey, dense phonolite containing sodalite, aegirine, analcime; zeolite-filled vesicles.		
Intra-Caldera Maungatea Breccia	Roughly stratified breccia of angular basaltic and phonolitic rocks with beds of pale-grey phonolitic primary tuff and ash.	Maungatea Breccia	Roughly stratified breccia of angular basaltic and phonolitic rocks with beds of pale-grey phonolitic primary tuff and ash
Extra-Cal..ra Maungatapu Breccia	Light brown to light grey phonolitic-basaltic breccia; sub-horizontal bedding, with thin beds of fine vitric tuff.		
Te Kou Complex	Weathered phonolitic and trachytic flows and pyroclastic, yellow brown cinders and tuff forming residual cinder cone.		
	Erosional episode	Te Manga Group	Type I and type II mafic rocks. Grey to black basalt, . ankaramite, in flows, dykes, and pyroclastic dipping generally seaward with parasitic cones, comprising the bulk of the primitive volcano.
Avatiu Caldera Complex	Grey to black basalt, oceanite, ankaramite, in flows, dykes, breccia, scoria, and ash.		
	Caldera formation		
Te Manga Group	Grey to black basalt, ankaramite, limburgite in flows, dykes and pyroclastic deposits dipping generally seaward comprising the bulk of the primitive volcano.		
Pue Ash	Yellow-brown plagiogranitic ash, approximately 50 ft thick, passing up to about 500 ft of sub-aerial cross-bedded grey cinder, ash and fine breccia. Deposits of an early littoral eruption on the flank of primitive volcano.		

8.5 Mantle Plumes

The structure and nature of mantle plumes are still pooly understood *i.e.*, shape, physical properties. It has been suggested that two types of plume exist (Zindler et al., 1984) thermal plumes and chemical plumes in which in addition to a thermal anomaly there is also a transfer of material. Zindler et al. (1984) suggested that the plume under Hawaii is a chemical plume (diapirically ascending masses of relatively enriched source material) while the plume under Iceland is a thermal plume. Although a detailed discussion and review of plume structure is beyond the scope of this thesis, theoretical modeling suggests that plumes are mushroom in shape (*e.g.*, Courtney and White, 1986) and have a higher heat flow in the core than the head of the plume. White and McKenzie (1995) suggest that melting occurs in a relatively restricted area in the plume core. In the following discussion the assumption is made that all plumes are similar in structure as it is the nature of the melts that are produced within a plume that is most important here.

The growth of Hawaiian islands has been previously discussed (Chapter one) and a simplified model to account for the growth of such islands above a rising chemical plume is presented in Figure 8.2. This model does not take into account plume structure or dynamics. The first melts are produced by low degrees of partial melting deep within the mantle, resulting in alkali magmas. As the plume (or the region of melting within a plume) rises, somewhat larger degrees of partial melting occur at shallower depths producing tholeiitic magmas. This stage is manifested by the rapid effusion of tholeiitic shield lavas at the surface. There is some shallow level storage of the magmas during

Direction of plate motion

Stage 1

The initial period of ocean island growth appears to consist of alkali volcanism (*e.g.*, Loihi seamount)

Stage 2

The eruption of massive basalt shield volcanoes ranging from 3000 (Kauai) to 40 000 km (Mauna Loa) covers the earlier alkali rocks. The bulk of the lava that erupted during the shield building stage is tholeiitic basalt. The magmas are generally modified by shallow level fractionation.

Figure 8.2: Simplified model of formation of a Hawaiian islands.

Stage 3&4

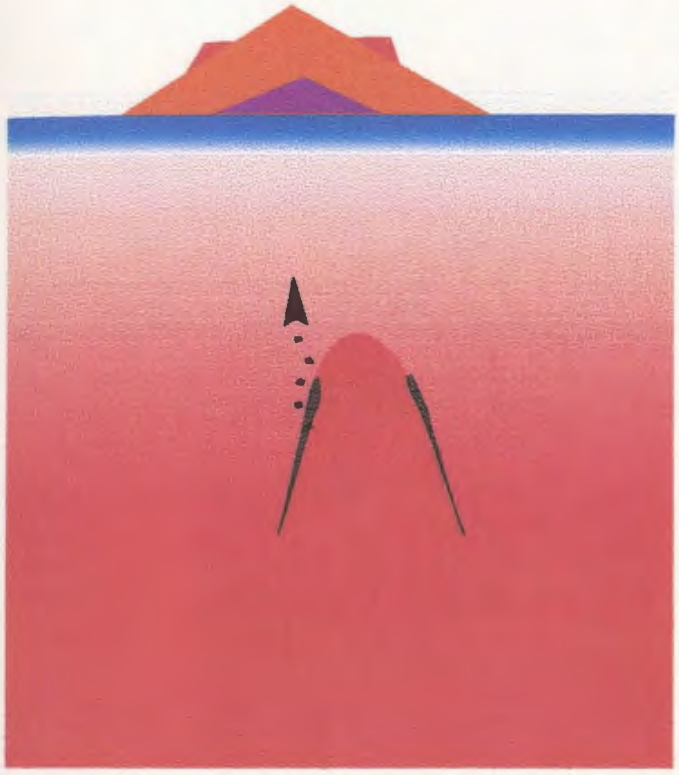

The stage following the building of the shield is highly variable. Collapse of the summit occurs on some volcanoes, with continuing eruption of lava from these volcanoes filling and overflowing the result caldera. The change in eruptive pattern is always accompanied by a change in magma composition, with the late lavas being more alkali than the shield building lavas

Stage 5

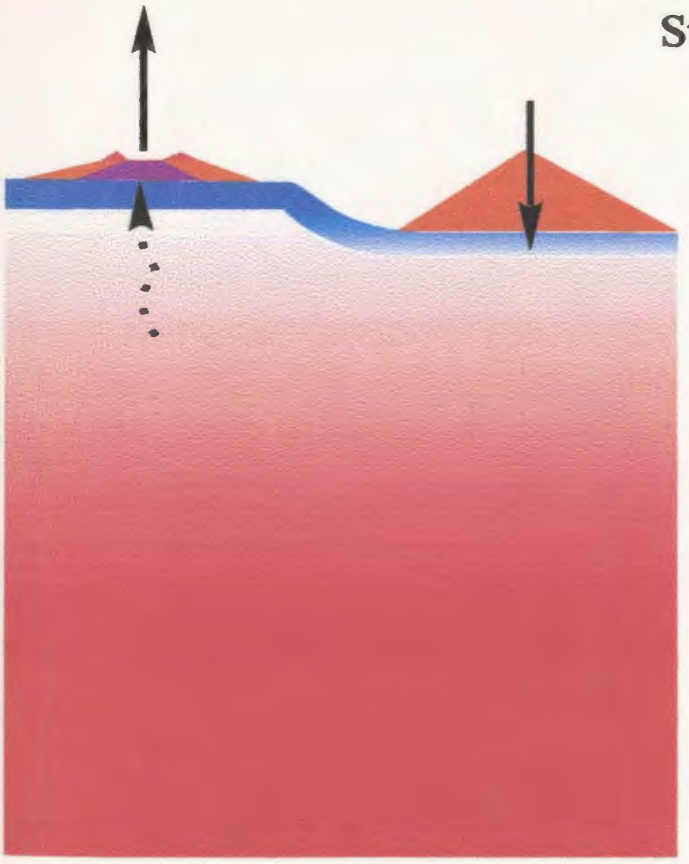

Following a period of extensive erosion highly alkali mafic lavas erupt. The eruption of these lavas may be due to adiabatic melting during the passage of an island over the flexural bulge associated with coeval edifice construction.

Figure 8.2: Continued

which crystal fractionation occurs together with mixing of subordinate volumes of alkali magmas produced at depth. After this period of shield building, the shallow level melting wanes for a number of reasons *e.g.*, the plume cools to below the solidus or only refractory mantle is left, inhibiting melting. Melting still takes place deeper in the mantle producing alkali magmas which are manifested by the stage 4 alkali lavas found on Hawaiian islands. This simplified model can account for most of the features observed on Hawaiian islands. The important aspect of the model is that there is a progression from magmas with relatively low silica saturation, to magmas with a higher degree of silica saturation and finally back to low silica magmas.

As shown in this thesis, there are two suites of rocks on Rarotonga, a low silica suite and a high silica suite. It can be suggested that these two suites represent a similar progression in magmatism to that observed on Hawaii, *i.e.*, a tholeiitic suite (high silica) and an alkali suite (low silica). The principle differences between Rarotonga and Hawaii are:

i. The degree of chemical difference between the two suites of rocks. As discussed above, while the difference in silica abundance between the two suites on Hawaii is large, resulting in alkali and a tholeiite rocks, on Rarotonga the difference is more subtle producing two alkali suites with one being more undersaturated than the other;
ii. Temporal relationships. On Hawaii there is a clear temporal separation of the two suites while on Rarotonga the two suites appear to be of similar age; and
iii. The volume of lavas extruded. Hawaii is much larger than Rarotonga by at least two orders of magnitude.

Assuming that plumes all have the same general mechanics, these differences could be a direct result of differences in the size of mantle plumes under Hawaii and Rarotonga, the plume under Hawaii being much larger than Rarotonga. This is reflected in the relative sizes of the two islands. In a large plume, melting can occur over a broader melting profile resulting in vastly different magmas (*i.e.*, the tholeiitic and alkali magmas found on Hawaii). A smaller plume will result in a narrower melting profile and while magmas of slightly different composition are formed the difference is more subtle (*i.e.*, the low and high silica suites found on Rarotonga). As discussed above, the structure of plumes is not considered in this model and it is therefore important to stress that no specific location of melting within the plume is implied *i.e.*, the two suites of rocks (high and low silica) could result from melting in different portions of the region of melt generation *e.g.*, the core vs. head of the plume.

In the Cook/Australs, Turner and Jarrard (1982) proposed that three plumes would be required for the formation of the island chain. In accepting this model, slight refinements can be made. Principally these would be:

i. The existence of a long lived primary plume which tapped a HIMU source and produced most of the islands on the chain (*e.g.*, Mangaia, Tubui and Rapa); and
ii. Secondary plumes which were generally short lived and tapped an EM source. These secondary plumes account for the formation of Rarotonga and the long lived volcanism on Rimatara and Rurutu.

Chauvel et al, (1992) showed that in the Austral chain the lavas with HIMU signature formed from magmas produced from a hotter and deeper source in the mantle compared to EMI and EMII lavas. The concept of chemical and thermal plumes could explain the formation of the Cook/Austral chain. In such a model, a long lived chemical plume is situated at the south eastern extent of the chain and taps a deep HIMU mantle source (Figure 8.3). This explains the uniformity of isotopic signatures observed in islands within the chain *i.e.*, Mangaia and Tubuai. Small secondary thermal plumes resulting from temperature instabilities within the mantle result in localized melting of metasomatised mantle producing young islands within a pre-existing chain (Rarotonga) or resurgent volcanism on old Islands (Raivavae).

The high number of small thermal plumes within this region may be explained by the fact that the mantle in this region already displays a higher than normal heat flow (see Chapter one, p. 21). Any small rise in temperature, *e.g.*, by a rising chemical plume or a region hotter than normal due to radioactive decay (*i.e.*, HIMU), may be enough to form multiple small thermal plumes. Compared to a single large plume in a region of normal mantle heat flow (*e.g.*, Hawaii).

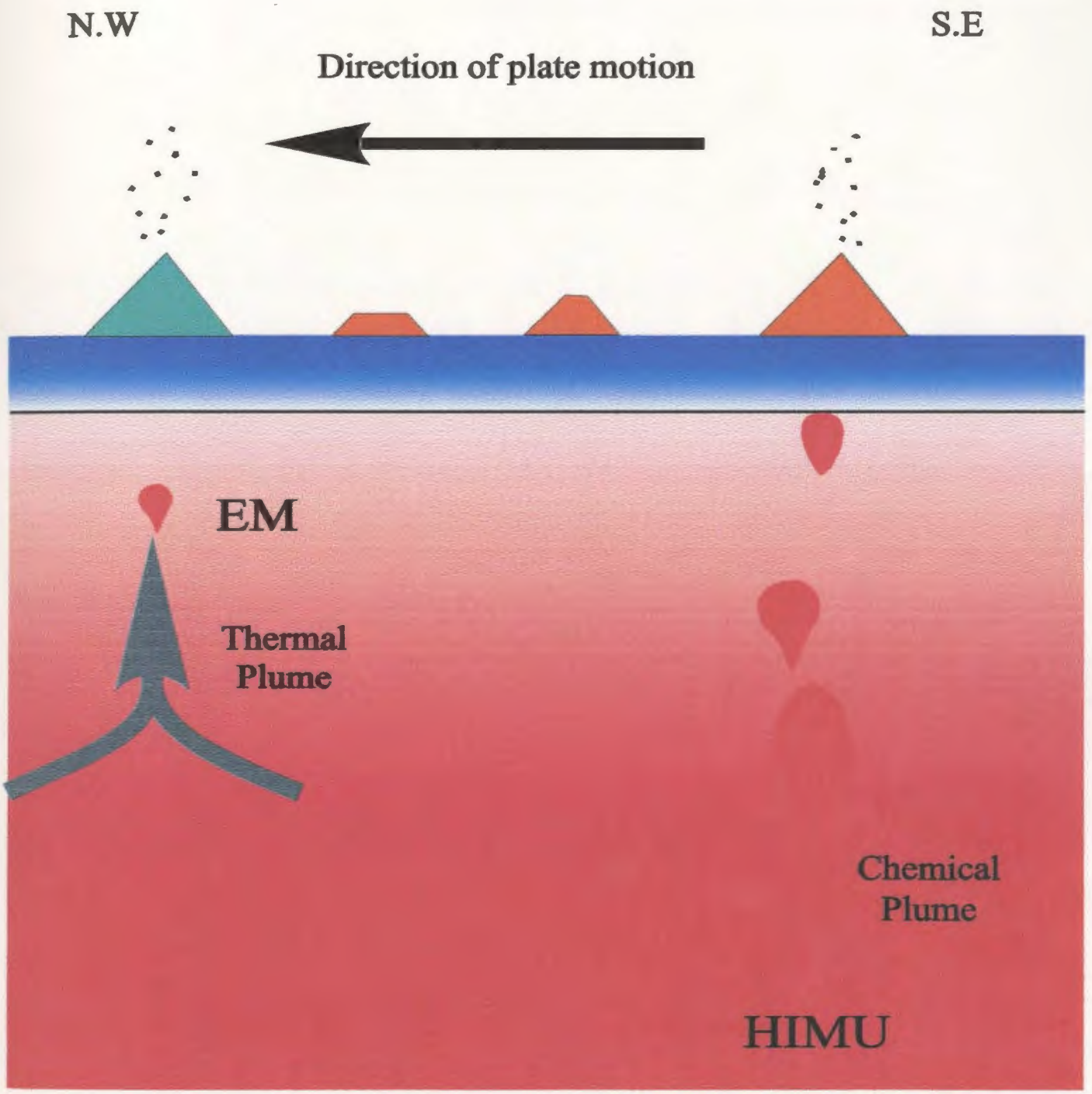

Figure 8.3: Model for the formation of the Cook/Austral chain. A long lived chemical plume is located at the southern-most end of the chain. This taps a deep mantle source with a HIMU signature. Volcanism resulting from this plume results in a linear chain of islands (shown in orange) which get progressively older to the north west. Short lived thermal plumes result in localised melts which form young islands (shown in blue, *e.g.*, Rarotonga) or cap older volcanoes within the chain. The mantle from which these melts are produced has an EM mantle signature.

References

Adam J., 1988. Dry, hydrous, and CO_2 bearing liquidus phase relationships in the CMAS system at 28kb, and their bearing on the origin of alkali basalts. Journal of Petrology, v. 96, p.709-719.

Allègre C.J. and Turcotte, 1986. Implications of a two component marble cake mantle. Nature, v. 323, p. 123-127.

Aoki K.I., 1964. Clinopyroxenes from alkaline rocks of Japan. American Mineralogist, v.49, p. 119-1223.

Bailey D.K., 1987. Mantle metasomatism - perspective and prospect. *In* Fitton J.G. and Upton B.G.J. (eds). Alkaline Igneous Rocks. Geological Society Special Publication No 30, p. 1-14

Baker I., 1968. Intermediate oceanic volcanic rocks and the "Daly gap". Earth and Planetary Science Letters, v. 4; p. 103-106.

Barling J. and Goldstien S, 1990, Extreme isotopic variations in Heard Island lavas and the nature of mantle reservoirs. Nature, v. 348, p. 59-62.

Basaltic Volcanism Study Project (BSVP), 1981. Basaltic volcanism on the terrestrial planets. Pergamon Press, Inc., Elmsford, NY, 1280p.

Bienvenu P., Bougault H., Joren J.L., Treuil M. and Dmitriev L., 1990. MORB alteration; rare earth element/ non rare-earth hygromagmaphile element fractionation. Chemical Geology, v. 82, p. 1-14.

Bottinga Y. and Weill D.F., 1972. The viscosity of magmatic silicate liquids; a model calculation. American Journal of Science, v. 272, p 438-475.

Bottinga Y., Weill D. and Richet P., 1982. Density calculations for silicate liquids; I, Revised method for aluminosilicate compositions. Geochimica et Cosmochimica Acta., v. 46; p. 909-919.

Bowen N.L., 1928. The evolution of igneous rocks. Princeton University Press (reprinted by Dover publications, New York, 1956), 334p.

Brooks C.K. and Printzlau I., 1978. Magma mixing in mafic alkaline volcanic rocks: the evidence from relic phenocryst phases and other inclusions. Journal of Volcanology and Geothermal Research. v. 4, p.315-331.

Bryan W.B., Finger L.W. and Chayes F.A., 1969. Least-squares approximation for estimating the composition of a mixture. Year Book Carnegie Institution of Washington. p. 243-244.

Cameron M. and Papike J.J., 1981. Structural and chemical variations in pyroxenes. American Mineralogist, v. 66, p.1-50.

Cann J.R., 1970. Rb, Sr, Y, Zr and Nb in some ocean floor basaltic rocks. Earth and Planetary Science Letters, v. 10, p. 7-11.

Carlson R.W., 1988, Mantle structure; layer cake or plum pudding? Nature, v. 34 p.380-381.

Carmichael I.S.E., Nicholls J. and Smith A.L., 1970. Silica activity in igneous rocks. American Mineralogist, v. 55, p. 246-263.

Caroff M., Maury R.C., Leterrier J., Joron J.L., Cotton J. and Guille G., 1993. Trace element behaviour in the alkali basalt-comenditic trachyte series from Murruroa. Atoll, French Polynesia. Lithos, v. 30, p. 1-22.

Cawthorne R.G. and Collerson K.D., 1974. The recalculation of pyroxene End-Member parameters and the estimation of ferrous and ferric iron content from electron microprobe analyses. American Mineralogist, v. 59 p. 1203-1208.

Cazenave A. and Thoraval C., 1994. Mantle dynamics constrained by degree 6 surface. topography, seismic tomography and geoid: Inference on the origin of the South Pacific Superswell. Earth and Planetary Science Letters, v. 122, p. 207-219.

Cebria J.M. and Lopez-Ruiz J., 1996. A refined method for trace element modeling of nonmodal batch partial melting processes; the Cenozoic continental volcanism of Calatrava, central Spain. Geochimica et Cosmochimica Acta, v. 60, p.1355-1366.

Chauvel C., Hofmann A.W. and Vidal P., 1992. HIMU-EM; the French Polynesian connection. Earth and Planetary Science Letters, v.110, p.99-119.

Chayes F., 1963. Relative abundance of intermediate members of the oceanic basalt-trachyte association. Journal of Geophysical Research. v. 68, p. 1519-1534.

Chayes F., 1977. The oceanic basalt-trachyte relation in general and in the Canary Islands. American Mineralogist, v. 62, p 666-671.

Christofferson E., 1968. The relationship of sea-floor spreading in the Pacific to the origin of the Emperor Seamounts and the Hawaiian Islands chain (abstract). American Geophysical Union, v. 49, p. 214.

Clague D.A. and Dalrymple G.B., 1987. The Hawaiian-Emperor volcanic chain: Geologic evolution. US Geol. Survey Prof Paper, v. 1350, p. 5-54.

Clauge D.A. and Frey F.A., 1982. The petrology and trace element geochemistry of the Honolulu volcanics, Oahu; Implications for oceanic mantle below Hawaii. Journal of Petrology, v.23, p.447-504.

Coffin M.F.and Eldholm O., 1993, Large igneous provinces. Scientific American, v. 269, p 42-49.

Courtney R.C. and White R.S., 1986. Anomalous heat flow and geod across the Cape Verde Rise; evidence for dynamic support from a thermal in the mantle. Geophysical Journal of the Royal Astronomical Society, v.87, p.815-867.

Dalrymple G.B., Jarrard R.D. and Clague D.A., 1975. K/Ar ages of some volcanic rocks from the Cook and Austral Islands. Geological Society of. America. Bulletin., v. 86, p. 1463-1467.

Daly R.A., 1910. The origin of alkaline rocks. Science, v. 32, p.220

Deer W.A, Howie R.A., Zussman J., 1978. Single chain silicates (2nd edition). Longman Group Limited. 668p.

Deer W.A, Howie R.A., Zussman J., 1992. The rock forming minerals (2nd edition). Longman Group Limited. 696p.

DePaolo D.J.,1979. Implications of correlated Nd and Sr isotopic variations for the chemical evolution of crust and mantle. Earth and Planetary Science Letters, v. 43, p.201-211.

Duncan R.A. and McDougall I., 1976. Linear volcanism in French Polynesia. Journal of. Volcanology and Geothermal Research, v. 1, p. 197-227.

Dixon T.H. and Batiza R., 1979. Petrology and chemistry of Recent lavas in the northern Marianas; implications for the origin of island arc basalts. Contributions to Mineralogy and Petrology, v. 70, p. 167-181.

Duncan R.A., McCulloch M.T., Barsczus H.G. and Nelson D.R., 1986. Plume versus lithospheric sources for melts at Ua Pou, Marquesas Islands. Nature, v. 322, p. 534-538.

Dunn T. and McCallum I.S., 1982. The partitioning of Zr and Nb between diopside and melts in the system diopside-albite-anorthite. Geochimica et Cosmochimica Acta, v. 46, p. 623-629.

Dupre B. and Allègre C.J., 1983. Pb-Sr isotope variation in Indian Ocean basalts and mixing phenomena. Nature, v. 303, p. 142-146.

Dupuy C., Barsczus H.G., Liotard J.M. and Dostal J., 1988. Trace element evidence for the origin of ocean island basalts: An example from the Austral Islands (French Polynesia). Contributions to. Mineralogy and. Petrology., v. 98, p. 293-302.

Dupre B., Lambret B. and Allègre C.J., 1982. Isotopic variations within a single oceanic island: The Terceira case. Nature, v. 299, p. 620-622.

Edwards A.C., 1976. A comparison of the methods for calculating Fe3+ contents of clinopyroxenes from microprobe analysis. N. ahrbah et Mineralogie, p. 508-512.

Eggler D.H., 1978. The effect of CO_2 upon partial melting of peridotite in the system Na_2O-CaO-Al_2O_3-MgO-SiO_2-CO_2 to 35kb with and analysis of melting in a peridotite H_2O-CO_2 system. American Journal of Science, v. 278, p.305-343

Falloon T.J., Green D.H., Hatton C.J. and Harris K.L., 1988. Anhydrous partial melting of a fertile and depleted peridotite from 2 to 30 kb and application to basalt pretrogenesis. Journal of Petrology, v. 29, p. 1257-1282.

Feigenson M.D., Hofmann A.W. and Spera F.J., 1983. Case studies on the origin of basalt II. The transition from tholeiitic to alkali volcanism on Kohala volcano, Hawaii. Contributions to Mineralogy and Petrology, v. 84, p. 390-404.

Feigenson M.D., Patino L.C. and Carr M.J., 1996. Constraints on partial melting imposed by rare earth element variations in Mauna Kea basalts. Journal of Geophysical Research, v. B101, p.11815-11829.

Fisk M.R., Bence A.E. and Schilling J.G., 1982. Major element chemistry of Galapagos rift zone magmas and their phenocrysts. Earth and Planetary Science Letters, v. 61, p. 171-189

Fitton J.G. and James D., 1986. Basic volcanism associated with intraplate linear features Philosophical Translators of the Royal Society of London, series A. Mathematical and Physical Sciences, v. 317, p. 253-266.

Floyd P.A. and Tarney J., 1979. First order alteration chemistry of leg 49 basement rocks. *In:* Luyendylz B.P., Cann J.R., Duffield W.A, Faller A.M., Kobayashi K., Vennun W., Wood D.A. and Zolotarev B.P., (eds). Initial reports of the Deep Sea

Drilling Project leg 49 of the cruises of the drilling vessel Glomar Challenger Aberdeen, Scotland to Funchel Madeira, July-September 1976, Texas A and M university (pub) p. 693-708.

Foley S., Jackson S., Fryer B., Greenough J. and Jenner G., 1996. Trace element partition for clinopyroxene and phlogopite in an alkaline lamprophyre from Newfoundland by LAM-ICP-MS. Geochimica et Cosmochimica Acta, v. 60, p. 629-638.

Forsythe L.M., Nielsen R.L. and Fisk M.R., 1994. High-field strength element partitioning between pyroxene and basaltic to dacitic magmas. Chemical Geology, v. 117, p.107-125.

Frey F.A., Bryan W.B. and Thomson G., 1974. Atlantic ocean floor geochemistry and petrology of basalts from legs 2 and 3 of the deep sea drilling project. Journal of Geophysical Research, v. 79, p. 5507-5527.

Frey F.A., Green D.H. and Roy S.D., 1978. Integrated models of basalt petrogenesis; a study of quartz tholeiites to olivine melilitites from South eastern Australia utilizing geochemical and experimental petrological data. Journal of Petrology, v. 19, p463-513.

Frey F.A. and Rhoden M.F., 1987. The mantle source for the Hawaiian Islands: constraints from lavas and ultramafic inclusions. *In:* Menzies M. and Hawkesworth C. (eds). Mantle metasomatism. p 423-463.

Fujii T. and Scarfe C.M., 1985. Composition of liquids coexisting with spinel lherzolite at 10 kbar and the genesis of MORBs. Contributions to Mineralogy and Petrology, v. 90; p. 18-28.

Fukao Y., 1992. Seismic tomogram of the earth's mantle; geodynamic implications. Science, v. 258 p. 517-520.

Gaetani G.A. and Grove T.L., 1995. Partitioning of rare earth elements between clinopyroxene and silicate melt, crystal-chemical controls. Geochimica et Cosmochimica Acta, v. 59, p.1951-1962.

Garcia M.O., Frey F. and Grooms D.G., 1986. Petrology of volcanic rocks from Kaula Island, Hawaii: Implications for the origin of Hawaiian phonolites. Contributions to Mineralogy and Petrology, v. 94, p. 461-471.

Garcia M.O., 1996. Petrography and olivine and glass chemistry of lavas from the Hawaii Scientific Drilling project. Journal of Geophysical Research, v. 101, p 11701-11713.

Gast P.W., 1968. Trace element fractionation and the origin of tholeiitic and alkaline magma types. Geochimica et. Cosmochimica Acta, v.32, p. 1057-1086

Green D.H., 1971. Composition of basaltic magmas as indicators of conditions of origin; application to oceanic volcanism. Philosophical Transactions of the Royal Society of London, Series A, v. 268, p. 707-725.

Green T.H. and Pearson N.J., 1985. Rare earth element partitioning between clinopyroxene and silicate liquid at moderate to high pressure. Contributions to Mineralogy and Petrology, v. 91, p. 24-36.

Greenough J.D., 1988. Minor phases in the Earth's mantle; evidence from trace- and minor-element patterns in primitive alkaline magmas. Chemical Geology, v. 69; p177-192.

Gunther D., Longerich H.P., Forsythe L. and Jackson S.E., 1995. Laser ablation microprobe- inductively coupled plasma spectrometry (LAM-ICP-MS. American laboratory v. 27, p. 24-29.

Haase K.M., 1996. The relationship between the age of the lithosphere and the composition of oceanic magmas: Constraints on partial melting, mantle sources and the thermal structure of plates. Earth and Planetary Science Letters, v. 144, p. 75-92.

Hack P.J., Nielsen R.L. and Johnston A.D., 1994. Experimentally determined rare-earth element and Y partitioning behavior between clinopyroxene and basaltic liquids at pressures up to 20 kbar. *In*: Foley S.F.; Vander Laan S.R., (eds). Trace-element partitioning with application to magmatic processes. Chemical Geology, v. 117, p. 89-105.

Hart S.R., 1984. A large-scale isotope anomaly in the Southern Hemisphere mantle. Nature, v. 309, p. 753-757.

Hart S.R. and Davis K.E. 1978. Nickel partitioning between olivine and silicate melt. Earth and Planetary Science Letters, v. 40, p.203-219.

Hart S.R. and Dunn T., 1993. Experimental cpx/melt partitioning of 24 trace elements. Contributions to Mineralogy and Petrology, v. 113, p. 1-8.

Hart S.R., Erlauk A.J. and Kable E.J.D., 1974. Sea floor basalt alteration: Some chemical and Sr isotopic effects. Contributions to Mineralogy and Petrology, v. 44, p. 219-230.

Hart S.R., Hauri E.H., Oschmann L.A. and Whitehead J.A., 1992. Mantle plumes and entrainment: Isotopic evidence. Science, v. 256, p. 517-520.

Hay D.E. and Wendlantt R.F., 1995. The origin of Kenya rift plateau-type flood phonolites: Results of high-pressure/high-temperature experiments in the systems phonolite- H_2O-CO_2. Journal of Geophysical Research, v. 100, p. 401-410.

Hay D.E., Wendlantt R.F. and Wendlantt E.D., 1995. The origin of Kenya rift plateau-type flood phonolites: Evidence from geochemical studies for fusion of lower crust modified by alkali basaltic magmatism. Journal of Geophysical Research, v. 100, p. 411-422.

Hemmond C., Devey C.W. and Chauvel C., 1994. Source compositions and Austral plumes (South Pacific Ocean): Element and isotope (Sr, Nd, Pb, Th) geochemistry. Chemical Geology, v. 115, p. 7-45.

Herzberg C., 1992. Depth and degree of melting of komatiites. Journal of Geophysical Research, B, Solid Earth and Planets. v. 97, p. 4521-4540

Hickey R.L. and Frey F.A., 1982. Geochemical characteristics of boninite series volcanics; implications for their source. Geochimica et Cosmochimica Acta., v. 46, p. 2099-2116.

Hirose K. and Kushiro I., 1983. Partial melting of dry peridotites at high pressures; determination of compositions of melts segregated from peridotite using aggregates of diamond. Earth and Planetary Science Letters, v. 114, p. 477-489;

Hofman A.W. and Fiegenson M.D., 1983. Case studies on the origin of basalt. I theory and reassessment of Grenada basalts. Contributions to Mineralogy and Petrology, v. 84, p. 382-389.

Horn I., Foley S.F., Jackson S. and Jenner G., 1994. A Experimentally determined partitioning of high field strength- and selected transition elements between spinel and basaltic melt. *In*: Foley-S.F; Van-der-Laan-S.R., (eds.). Trace-element partitioning with application to magmatic processes. Chemical Geology, v. 117, p. 193-218.

Hughes C.J., 1982. Igneous Petrology, Developments in Petrolgy 7. Elsevier Sci. Publ. Co., Amsterdam Netherlands, 568p.

Humphris S.E., 1984. The mobility of the rare earth elements in the crust. *In*: Henderson P. (ed). Rare Earth Element Geochemistry, p. 317-342.

Humphris S.E. and Thompson G., 1978a. Hydrothermal alteration of oceanic basalts by seawater. Geochimica et Cosmochimica Acta., v. 42, p. 107-125.

Humphris S.E. and Thompson G., 1978b. Trace element mobility during hydrothermal alteration of oceanic basalts. Geochimica et Cosmochimica Acta, v. 42, p. 127-136.

Irving A.J., 1978. A review of experimental studies of crystal/liquid trace element IUGS Sub-commission on the Systematics of Igneous Rocks (1989).

Irving A.J. and Frey F.A., 1984. Trace element abundances in megacrysts and their host basalts: Constraints on partition coefficients and megacryst genesis. Geochimica et Cosmochimica Acta, v. 48, p. 1201-1221.

Jackson E.D., 1968. Xenoliths in Hawaiian basalts. Special Paper - Geological Society of America. p. 101-102. 1968.

Jackson E.D. and Wright T.L., 1970. Xenoliths in the Honolulu volcanic series. Hawaii. J. Petrol., v. 11, p. 405-430.

Jackson S.E., Longerich H.P., Dunning G.R. and Freyer B.J., 1992. The application of laser-ablation microprobe, inductively coupled plasma-mass spectrometry (LAM-ICP-MS) to insitu trace-element determination in minerals. Canadian Mineralogist, v. 30, p. 1049-1064.

Jacques A.L. and Green D.H., 1980. Anhydrous melting of Peridotite at 0-15kb pressure and the genisis of theolitic basalts. Contributions to Mineralogy and Petrology, v. 73, p. 287-310.

Jarrard R.D. and Clague D.A., 1977. Implications of Pacific island and seamount ages for the origin of volcanic chains. Revs. Geophys. Space Phys., v. 15, p. 57-76.

Jenner G.A., Foley S.F., Jackson S.E., Green T.H., Fryer B.J. and Longerich H.P., 1994. Determination of partition coefficients for trace elements in high pressure-temperature experimental run products by laser ablation microprobe-inductively coupled plasma-mass spectrometry (LAM-ICP-MS). Geochimica et Cosmochimica Acta, v. 58, p. 5099-5103.

Jenner G.A., Longerich H.P., Jackson S.E., and Fryer B.J., 1990. ICP-MS A powerful tool for high-precision trace element analysis in Earth sciences: Evidence from analysis of selected U.S.G.S reference samples. Chemical Geology, v.83, p. 133-148.

Juteau T., Bingol F., Noack Y., Whitechurch H., Hoffet M., Wirrman D. and Courtois C., 1979. Preliminary results; mineralogy and geochemistry of alteration products in leg 45 basement samples. In initial reports of the deep sea drilling leg 45, p. 613-645.

Kear D., 1957. Erosional stages of volcanic cones as indicators of age. New Zealand Journal of Science Technology, v. 38, p.671-682.

Kellogg L.H. and Turcotte D.L., 1990. Mixing and the distribution of heterogeneties in a chaotically convecting mantle. Journal of Geophysical Research, v. 95, p. 421-432.

Kennedy G.C., 1955. Some aspects of the role of water in rock melts. *In:* Poldervaart, A., (ed.) Crust of he earth--a symposium. Special Paper - Geological Society of America. p. 489-503

Klein E.M. and Langmuir C.H., 1987. Global correlation of ocean ridge basalt chemistry with axial depth and crustal thickness. Journal of Geophysical Research, B, Solid Earth and Planets, v. 92; p. 8089-8115.

Kushiro I., 1960. Si-Al relations in clinopyroxenes from igneous rocks. American Journal of Science, v.258, p. 548-554

Kushiro I., 1964. The system diopside-forsterite-enstatite at 20 kbars. Carnegie Inst Washington Ann. Rept. Dir Geophys Lab. 1963, v64, p. 101-108.

Kushiro I., 1980. Viscosity, density, and structure of silicate melts at high pressures, and their petrological applications. *In*: Hargraves R.B., (ed). Physics of magmatic processes. p. 93-120

Le Bas M.J., 1962. The role of aluminum in igneous clinopyroxenes with relation to their parentage. American Journal of Science, v 260, p. 267-288.

Le Bas M.J., Le Maitre R.W., Strecheisen A. and Zanettin B., 1986. A chemical classification of volcanic rocks based on the total alkali-silica diagram. Journal of Petrology, v. 27, p. 745-750.

Le Maitre R.W., 1989. A classification of igneous rocks and glossary of terms, the international; union of geological Sciences Subcommission on systematics of igneous rocks. Blackwall Scientific Pub. 193p.

Le Marchande F., Villemant B. and Calas G., 1987. Trace element distribution coefficients in alkaline series. Geochimica et Cosmochimica Acta, v. 51, p. 1071-1081.

Le Roex A.P., 1985. Geochemistry, Mineralogy and magmatic evolution of the basaltic and trachytic lavas from Gough Island, South Atlantic. Journal of Petrology, v. 26, p. 149-186.

Le Roex A.P., Cliff R.A. and Adir B.J.I., 1990. Tristan da Cunha, South Atlantic: Geochemistry and petrogenesis of a Basanite-phonolite lava series. Journal of Petrology, v. 31, p. 779-812.

Le-Roex A.P. and Erlank A.J., 1982. Quantitative evaluation of fractional crystallization in Bouvet Island lavas. Journal of Volcanology and Geothermal Research, v.13, p. 309-337.

Longerich H.P., Jenner G.A., Fryer B.J. and Jackson S.E., 1990. Inductively coupled plasma-mass spectrometric analysis of geological samples: A critical evaluation based on case studies. Chemical Geology, v. 83, p.105-118.

Ludden J.N. and Thompson G., 1978. The modification of the rare earth elements during submarine weathering of tholeiitic basalt. Nature, v. 274, p. 147-149.

Ludden J.N. and Thompson G., 1979. An evaluation of the behavior of the rare earth elements during the weathering of sea floor basalt. Earth and Planetary Science Letters, v. 43, p. 85-92.

Luhr J.F, and Carmichael I.S.E., 1980. The Colima volcanic complex, Mexico; I, Post-caldera andesites from Volcan Colima. Contributions to Mineralogy and Petrology, v. 71, p. 343-372.

Maaløe S., 1994. Estimation of the degree of partial melting using concentration ratios. Geochimica et Cosmochimica Acta, v. 58, p. 2519-2525.

Maaløe S. and Aoki K., 1977. The major element composition of the upper mantle estimated from compositions of lherzolites. Contributions to Mineralogy and Petrolgy, v. 63, p.161-173.

MacDonald G. A. and Katsura T., 1964. Chemical composition of Hawaiian lavas. Journal of Petrology, v. 5, p. 82-133.

Mahood G.A. and Hidreth W., 1983. Large partition coefficients for trace elements in high-silica rhyolites. Geochimica et Cosmochimica Acta, v. 47, p. 11-30.

Marshall P., 1930. Geology of Rarotonga and Atiu. Bulletin Bernice P. Bishop Museum, 72p.

McDougall I., 1964. Potassium-argon ages from lavas of the Hawaiian Islands. Geological Society of America Bulletin., v. 75; p. 107-128.

McDougall I. and Swanson D.A., 1972. Potassium-Argon Ages of Lavas from the Hawaii and Pololu Volcanic Series, Kohala Volcano, Hawaii. Geological Society of America Bulletin., v. 83, p. 3731-3737.

McIntire W.L., 1963. Trace element partition coefficients - A review of theory and applications to geology. Geochimica et Cosmochimica Acta, v. 27, p. 1209-1264.

McKay G. and Wagstaff J., Yang S.-R., 1986. Clinopyroxene REE distribution coefficients for shergottites. The REE content of the Shergotty melt. Geochimica et Cosmochimica Acta, v. 50, p. 927-937.

McKay G.A., 1986. Crystal/liquid partitioning of REE in basaltic systems: Extreme fractionation of REE in Olivine. Geochimica et Cosmochimica Acta, v. 50, p. 60-79.

McKenzie D. and Bickle M.J., 1988. The volume and composition of melt generated by extension of the lithosphere. Journal of Petrology, v. 29, p. 625-679.

Mckenzie D., and O'Nions R.K, 1995. The source region of Ocean Island Basalts. Journal of Petrology, v.96, p. 133-159.

McNutt M. K. and Fischer K.M., 1987. The South Pacific superswell. *In*: B.H. Keating, P. Fryer, R. Batiza and G.W. Boehlert (eds.). Seamounts, Islands and Atolls. Am. Geophys. Union, Washington D.C., p. 25-34.

McNutt M. K. and Judge A.V., 1990. The superswell and mantle dynamics beneath the South Pacific. Science, v. 248, p. 969-975.

McNutt M. K., Winterer E. L., Sager William W., Natland J. H. and Ho G., 1990. The Darwin Rise; a Cretaceous superswell? Geophysical Research Letters, v. 17, p. 1101-1104.

Middlemost E.A.K., 1989. Oxidation ratios, norms and the classification of volcanic rocks. Chemical Geology, v. 77, p. 19-26.

Micheal P.J., 1988. Partition coefficients for rare earth elements in mafic minerals of high silica rhyolites: The importance of accessory mineral inclusions. Geochimica et Cosmochimica Acta, v. 52, p. 275-282.

Minster J., and Allegre C.J., 1978. Systematic use of trace elements in igneous processes; Part III, Inverse problem of batch partial melting in volcanic suites. Contributions to Mineralogy and Petrology, v. 68, p. 37-52

Minister J. and Jordan T.H., 1978. Present-day plate motions. Journal of Geophysical Research, v. 83, p. 5331-5354.

Moore J.G.; Clague D.A. and Normark W.R., 1982. Diverse basalt types from Loihi Seamount, Hawaii. Geology, v. 10; p. 88-92.

Morgan W.J., 1971. Convection plumes in the lower mantle. Nature, v. 230, p. 42-43.

Morgan W.J., 1972. Plate motions and deep mantle convection. Geological. Society of. Ameria. Memoirs, v. 132, p. 7-22.

Morimoto N., Fabries J., Ferguson A.K., Ginzburg I.V., Ross M., Seifert F.A., Zussman J., Aotcik and Gottardi G., 1988. Nomenclature of pyroxenes. Mineralogy and Petrology, v. 39, p. 55-76.

Morton R.L., 1996. Music of the earth: volcanoes, earthquakes and other geological wonders. New York Plenum Press. 298p.

Murata K.J, and Richter D.H., 1966. Chemistry of the lavas of the 1959-60 eruption of Kilauea Volcano, Hawaii. p. A1-A26. 1966.

Nakamura N., 1974. Determination of REE, Ba, Fe, Mg, Na and K in carbonaceous and ordinary chrondrites. Geochimica et. Cosmochima Acta, v.38, p. 757-775.

Nakamura Y. and Tatsumoto M., 1988. Pb, Nd, and Sr isotopic evidence for a multicomponent source of rocks of Cook-Austral Islands and heterogeneities of mantle plumes. Geochimica et Cosmochimica Acta, v. 52, p. 2909-2924.

Neilsen R.L., Forsythe L.M., Gallahan W.E. and Fisk M., 1994. Major and trace element magnetitie-melt equilibria. Chemical Geology, v.117, p167-191.

Norris R. A. and Johnson R. H. 1969. Submarine volcanic eruptions recently located in the Pacific by SOFAR hydophones. Journal of Geological Research. V. 64, p.650-654.

O'Hara M.J., 1977. Geochemical evolution during fractional crystallization of a periodically refilled magma chamber. Nature, v. 266, p.503-507

Okal E.A. and Batiza R., 1987. Hotspots: The first 25 years. *In:* Keating B.H., Fryer-P., BatizaR., Boehlert G.W., (eds). Seamounts, islands, and atolls. Geophysical Monograph. 43, p. 1-11

Palacz Z. and Saunders A.D., 1986. Coupled trace element and isotope enrichment in the Cook-Austral-Samoa islands, Southwest Pacific. Earth and Planetary Science Letters, v. 79, p. 270-280.

Pearce J.A., and Norry M.J., 1979. Petrogenetic implications of Ti, Zr, Y and Nb variations in volcanic rocks. Contributions to Mineralogy and Petrology, v. 69, p. 33-47.

Pearce T.H:, 1978. Olivine fractionation equations for basaltic and ultrabasic liquids. Nature, v. 276 p.771-774.

Peltier, 1989. Mantle convection; plate tectonics and global dynamics. Publisher Gordon and Breach Science Publishers, NY USA. 881p.

Phillotts, A.R., 1990. Principles of igneous and metamorphic petrology. Prentice Hall International. 498 p.

Pitman W.C., Larson R.L. and Herron E.M., 1974. The age of the ocean basins. Geological Society of America Map Series Mc 6.

Reynolds R.W. and Geist D.J., 1995. Petrology of Lavas from Sierra Negra volcano Isabela Island, Galapagos archpelago. Journal of Geophysical Research, v. 100, p. 24537-24553.

Richter F.M., 1986. Simple models for trace element fractionation during melt segregation. Earth and Planetary Science Letters, v. 77, p. 333-344.

Richter F.M. and Mckenzie D., 1984. Dynamical models for melt segregation from a deformable matrix. Journal of Geology, v.92, p. 729-740.

Ringwood A.E., 1985. Mantle dynamics and basalt petrogenesis. *In*: Kobayashi K., Sacks I.S., (eds). Structures and processes in subduction zones. Tectonophysics, v. 112 p. 17-34.

Robinson P., 1980. The composition space of terrestrial pyroxenes; internal and external limits In Prewitt C. (ed) Reviews in Mineralogy, Minerogical Society of America (pub).

Robinson P., Higgins N., and Jenner G.A., 1986. Determination of rare-earth-elements, yttrium and scandium in rocks by ion exchange X-ray florescence technique. Chemical Geology, v. 55, p. 121-137.

Roeder P.L. and Emslie R.F., 1970. Olivine liquid equilibrium: Contributions to Minerology and Petrology, v. 29, p. 275-289.

Rollinson H., 1993. Using geochemical data: Evaluation, presentation, interpretation. Longman Group Limited. 352p

Sack R.O., Walker D. and Carmichael I.S.E., 1987. Experimental petrology of alkalic lavas: constraints on cotectics of multiple saturation in natural basic liquids. Contributions to Mineralogy and Petrology, v. 96, p. 1-23.

Sato H., 1977. Nickel content of basaltic magmas; identification of primary magmas and a measure of the degree of olivine fractionation. Lithos, v. 10, p.113-120.

Saunders A.D., Norry M.J. and Tarney J., 1988. Origin of MORB and chemically-depleted mantle reservoirs; trace element constraints: *In*: Menzies M.A., Cox K. (eds). Oceanic and continental lithosphere; similarities and differences. Journal of Petrology. p. 415-445.

Schairer J.F., 1950. The alkali feldspar join in the system $NaAlSiO_4$-$KAlSiO_4$-SiO_2. Journal of Geology, v. 58, p. 512-517.

Schilling J.G., 1971. Sea floor evolution: rare earth evidence. Philosophical Translators of the Royal Society of London, series A. Mathematical and Physical Sciences, v. 268A p. 663-706.

Schilling J.G., 1973. Iceland mantle plume: Geochemical evidence along the Reykjanes Ridge. Nature, v. 242, p.565-569

Schilling J.G. and Winchester J.W., 1967. Rare earth fractionation and magmatic processes. *In*: Runcorn K. (ed), Mantle of the earth and terrestrial planets,. p. 267-283. Interscience Publishers, London.

Schilling J.G., Zajac M., Evans R., Johnston T., White W., Devine J.D. and Kingsley R., 1983. Petrologic and geochemical variations along the Mid-Atlantic Ridge from 29°N to 73°N. American. Journal of Science, v. 283, p. 510-586.

Schmincke H.U., Weaver P.P.E., Firth J., Baraza J., Bristow J.F., Brunner C., Carey S., Coakely B., Fuller M., Funck T., Gerand M., Goldstand P., Herr B., Hood J., Howe R., Jarvis I., Lebreiro S., Lindlom S., Lykke-Anderson h., Maniscalco R., Rothwell G., Sblendorio-Levy J., Schneider J., Sumila M., Tangiguchi H., Tu P.,

and Wallace P., 1994. Leg 157 Initial reports Gran Caranria and Madeira abyssal Plan leg 157 sites 950-956. Texas A&M University, Ocean Drilling program Scientific Results, v.159.

Schock H.H., 1979. Distribution of rare earth and other trace elements in magnetites. Chemical Geology, v. 26, p. 119-133.

Shaw D.M, 1970. Trace element fractionation during anatexis. Geochimica et Cosmochimica Acta, v. 34, p. 237-243.

Shaw H.R., 1965. Comments on viscosity, crystal settling, and convection in granitic magmas. American Journal of Science, v. 263, p. 120-152.

Smith W.H.F., Staudigel H., Watts A.B. and Pringle M., 1989. The Magellan Seamounts; Early Cretaceous record of the South Pacific isotopic and thermal anomaly. Journal of Geophysical Research, B,. 94, p. 10501-10523.

Späth A., Le Roex A.P. and Duncan R.A., 1996. The geochemistry of lavas from the Comores Archipelago, Western Indian Ocean: Petrogenesis and mantle source region characteristics. Journal of Petrology, v. 37, p. 961-991.

Staudigel H., Park K.H, Pringle M.S. Rubenstone J.L., Smith W.H.F. and Zindler A., 1991 The longevity of the South Pacific isotopic and thermal anomaly. Earth and Planetary Science Letters, v.102 p. 24-44.

Staudigel H., Zindler A., Hart S.R., Leslie T., Chen C.Y. and Clague D.,1984. The isotope systematics of a juvenile intraplate volcano: Pb, Nd and Sr isotope ratios of basalts from Loihi Seamount, Hawaii. Earth and Planetary Science Letters, v. 69, p. 13-29.

Stolper E., 1980. Predictions of mineral assemblages in planetary interiors. *In*: Criswell P.R. and Merrill R.B., (eds). Igneous processes and remote sensing. Proceedings of the Lunar and Planetary Science Conference. 11, v.. 1, p. 235-250.

Stolz A. J. and Davis G. A., 1988. Chemical and isotopic evidence from spinal therzolite xenoliths for episodic metasomatism of the upper mantle beneath southeastern Australia. *In*: Menzies Martin A. and Cox K. (eds). Oceanic and Continental Lithospere; Similarities and Differences, p. 303-330.

Sun S.S., 1980. Lead isotopic study of young volcanic rocks from mid ocean ridges, ocean islands and island arcs. Philosophical Translators of the Royal Society of London, series A. Mathematical and Physical Sciences, v.A297, p. 409-445.

Sun S.S., 1982. Chemical composition and Origin of the Earths primitive mantle. Geochimica et Cosmochimica Acta, v. 46, p.179-192.

Sun S.S and Hanson G.N., 1975. Origin of Ross Island basanitoids and limitations upon the heterogeneity of mantle sources for alkali basalts and nephelinites. Contributions to Mineralogy and Petrology, v. 52, p. 77-106.

Sun S.S. and McDooaugh W.F, 1989. Chemical and isotopic systematics of oceanic basalts: implications for mantle composition and processes. *In:* Saunders A.D and Norry M.J. (eds), Magmatism in ocean basins. Geological Society Special Publication, v42, p. 313-345.

Takahashi E., and Kushiro I., 1983. Melting of a dry peridotite at high pressures and basaltic magma genesis. American Mineralogist, v. 68, p. 859-879.

Takahashi E., 1986. Melting of a dry peridotite KLB-1 up to 14 GPa; implications on the origin of peridotitic upper mantle. Journal of Geophysical Research. B. v. 91, p. 9367-9382.

Tarney J., Wood D.A., Saunders A.D., Cann J.R. and Varet, 1980. The nature of mantle heterogeneity in the North Atlantic: Evidence from deep sea drilling. Philosophical Transactions of the Royal Society of London, A, v. 297 ,p. 179-202.

Tatsumoto M., Hedge C.E. and Engel A.E.J., 1965. Potassium, rubidium, strontium, thorium, uranium and the ratio $^{87}Sr/^{86}Sr$ in oceanic tholeiitic basalt. Science, v. 150, p. 886-888.

Thompson R.N., 1974. Some high-pressure pyroxenes. Mineralogical Magazine and Journal of the Mineralogical Society. v.39; p. 768-787.

Thorton C.P. and Tuttle O.F., 1960. Chemistry of igneous rocks: Diferentation Index. American Journal of Science, v. 258, p. 664.

Treuil M. and Joron J.L., 1975. Utilisation des elements hydromagmatophiles pour la simplification de la modelisation quantitative des processus magmatiques; exemples de l'Afar et la Dorsale Medioatlantique. Translated Title: Utilization of hydromagmatic elements for the simplification of quantitative modelling of magmatic processes; examples from Afar and the Mid-Atlantic Ridge. Rendiconti della Societa Italiana di Mineralogia e Petrologia. v. 31, p. 125-174.

Turner D.L. and Jarrard R.D., 1982. K/Ar dating of the Cook-Austral Island chain: A test of the hot spot hypothesis. Journal of Volcanology and Geothermal Research, v. 12, p. 187-220.

Verne J. 1872. A Journey to the center of the Earth. (reprinted by Penguin Group, 1986) 288p.

Vieten K. and Hamm H.M., 1971. Additional note "On the calculation of crystal chemical formula of clinopyroxene and their contents of Fe3+ from microprobe analysis". Neues Jahrbuch. Fuer Mineralogie, v. 7, p310-314

Villemant B., 1988. Trace element evolution in the Phlegrian Fields (Central Italy): fractional crystallization and selective enrichment. Contributions to Mineralogy and Petrology, v. 98, p. 169-183.

Villemant B., Jaffrezic H., Joron J.L. and Treuil M., 1981. Distribution coefficients of major and trace elements; fractional crystallization in the alkali basalt series of Chaine des Pays (Massif Central France). Geochimica et Cosmochimica Acta V. 45, p. 1997-2016.

Vogt P.R., 1988. Is post-erosional volcanism on mid-plate edifices triggered by passage over the flexural bulge, by thermal contraction of the deep magma conduit's root, or by episodic reduction of mid-plate compression? In: AGU 1988 fall meeting. Eos, Transactions, American Geophysical Union. v. 69, p.1476.

Weaver B.L., 1991. The origin of ocean island basalt end-member compositions: trace element and isotopic constraints. Earth and Planetary Science Letters, v. 104, p. 381-397.

White R.S. and McKenzie D., 1995. Mantle plumes and flood basalts. Journal of Geophysical Research, v. 100, p.17543-17585

White W.M. and Hofmann A.W., 1982. Sr and Nd isotope geochemistry of oceanic basalts and mantle evolution. Nature, v. 296, p. 821-825.

White W.M., 1985. Sources of oceanic basalts: Radiogenic isotopic evidence. Geology, v. 13, p. 115-118.

White R.W., 1966. Ultramafic inclusions in basaltic rocks from Hawaii. Contributions to Mineralogy and Petrology, v. 12; p. 245-314.

Wilson M., 1993. Magmatic differentiation. Journal of the Geological Society London, v. 150, p. 611-624.

Wilson J.T., 1963. Continental Drift. Scientific American, v. 208, p. 86-100.

Wood B.L. and Hay R.F. 1970. Geology of the Cook Islands. New Zealand Geological Survey Bulletin, v. 82, 103p.

Wood D.A., Joron J.L., Treuil M., Noraz M. and Tarney J., 1979. Elemental and Sr isotope variations in basic lavas from Iceland and the surrounding ocean floor. The nature of mantle source inhomogeneties. Contributions to Mineralogy and petrology, v. 70, p.319-339.

Worner G., Beusen J.M., Duchateau N., Gijbels R. and Schmincke H.U., 1983. Trace element abundances and mineral melt distribution coefficients in phonolites from See volcano (Germany), Contributions to Mineralogy and Petrology, v. 84, p. 152-173.

Wright-E., 1986 Petrology and geochemistry of shield-building and post-erosional lava series of Samoa; implications for mantle heterogeneity and magma genesis. Unpublish PhD. Thesis University of San Diego.

Yagi K., 1953. Petrochemical studies of alklai rocks of the Morotu district Sakhali. Bulliten of the Geological society of America, v. 64, p. 769-809

Yoder H.S., 1976. Generation of basaltic Magma. National Academy of Sciences. 265 p.

Zindler A. and Hart S., 1986. Chemical Geodynamics. Annual. Reviews of Earth and Planetary Sciences, v. 14, p. 493-571.

Zindler A., Staudigel H.and Batiza R., 1984. Isotope and trace element geochemistry of young Pacific seamounts: Implications for the scale of upper mantle heterogeneity. Earth and Planetary Science Letters, v. 70, p. 175-195.

Appendix 1

Sample Description and Location

Table A1.1- Sample list

Figure A1.1- Location map of samples (in map pocket)

Table A1.1
Brief description of samples analyzed

sample #	Sample description	Petrography: approximate modal abundances and size of phenocrysts are given first followed by the composition of the groundmass minerals given in order of decreasing abundance.
		Type I Mafic Rocks
R4	basalt	px ~20% 1mm, ol ~8% .5mm, mt ~5% 0.1mm, gm. px+plag+mt
R7	basalt	px ~ 25%, 0.5mm, mt ~5%, 0.1mm. gm. px+plag+mt
R16	dyke 060/90	px ~20%, 0.5 mm; mt .~1-2%, <.5mm;gm. px +plag+mt
R19	dyke 080/90	px ~15% 1mm, ol ~3% 0.5mm, gm. plag+px+mt
R20	basalt boulder	px ~8% 5mm, gm px +plag
R22	dyke 092/75N	px ~8% 1mm, ol~ 3% 0.5mm g.m plag+px
R23	basalt	px ~15% 5mm, ol ~3% 1mm, mt~ 1-2% .5mm, gm px +plag+mt
R27	basalt	px ~10% 1-2mm. oxides 0.5mm g.m plag+px
R29	basalt clast in breccia	px ~20%, 1mm; gm px+plag
R35	ankaramite boulder	px ~10%, 0.5mm; ol ~5%, 0.5mm; mt ~1-2%, 0.2mm; gm. px, plag, mt
R36	basalt	px ~10%, 2mm; ol ~5%, 1mm; mt ~1%, .1mm; gm. plag+px+ol
R37	ankaramite	px ~20% 1mm, ol~10% 0.5mm,mt -3%, 0.1mm, gm. px+plag+mt
R43	ankaramite boulder	px ~15%, 0.5mm; gm px+plag+mt
R44	ankaramite boulder	px ~15% 0.55mm, mt ~5% .1mm. gm. plag+px+ol
R45	basalt	px~ 10% 5mm, gm plag+px+ol
R46	basalt	px ~20%, < 1mm; mt ~5%; gm.. px + plag +mt
R50	dyke (cuts R51)	px ~10% 1mm. g.m plag +px +mt
R51	ankaramite	px, ~20%, 0.2mm; mt ~5%, < 0.1mm; gm. px+plag
R52	basalt	px ~20% 2mm, mt. ~8%0.1mm, gm. plag+px
R53	basalt	px ~15-20% <0.5mm; gm. px+plag+mt+glass
R54	basalt	px ~20%, mt ~8% 0.1mm, gm plag+px+mt
R77	basalt	px ~10% 1mm, g.m px+plag+mt
R81	dyke 284/80S	px ~10% 5mm, ol ~2% 3mm, mt ~3%, 0.5mm g.m px+plag
R82	basalt	plag ~5% 1mm, px ~1-2% .5mm
R83	basalt	px ~10% 1mm mt ~3% 0.1mm , g, px+plag
R84	basalt	px 10% 1mm, ol 3% 0.5mm, plag+px+mt
R87	ankaramite	px ~25% 2-3mm, ol ~10% 1-2mm, 3% mt 0.1mm, g.m plag+px
R89	ankaramite (boulder)	px 20%, 2-3mm, ol~8% 1mm mt ~1% .5mm, gm. plag+px+mt
R93	ankaramite	px 25% 1mm, ol 10% 0.5mm, plag+px+mt
R95	basalt	px 20%% 2-3mm, ol 10% 0.5mm, plag+px+mt
R97	boulder	px 20% 1mm, ol 10% 0.5mm, plag+px+mt
R99	basalt	px 15% 1mm, ol 5% 0.5mm, plag+px+t
R101	ankaramite	px ~10%, 10mm, ~20%, 5mm; ol ~10 5mm; gm px +plag+ol+mt
R106	dyke (100/90)	px ~25% 5mm, ol~10% 2mm,mt 3%, .5mm, gm. px+plag+mt
R110	dyke (060/70W)	px ~20% 1mm, ol ~10S 0.5mm, mt .~5% 0.1mm, g.m px+plag
R111	dyke (010/54E)	ol ~7-10% 1mm, ~1%, 1mm; px ~5%, 3mm; mt ~1%, .5mm
R113	basalt	px ~5%, 0.5mm, ~2% 5mm; gm. px+plag+mt
R115	dyke (060/90)	px ~15% 1mm, ol ~8% 0.5mm, mt 5% .5mm gm. px+plag+mt
R116	dyke (060/70E)	px 20% 10mm, ol 5mm 3%, gm plag+px+mt
R120	ankaramite	px~ 30%, 2mm; ol ~20%, 1-2mm; mt ~10%, .5-1mm; gm px+plag+ol+mt

R129	basalt	px ~20% 5mm, ol ~5% 3mm, mt ~3% 0.3mm, gm. plag+px+mt
R130	basalt	px ~ 10% .1mm; ol ~5%, < 1mm;mt ~1-2%, .5mm; gm. px+plag+mt
R134	basalt	px ~20%, 0.5mm; gm px+plag

Type II mafic rocks

R17	basalt clast	px 10% 1mm, ol 1% 0.5mm, gm. plag+px+mt
R30	basalt	px ~15% 1-2mm. g.m plag+px+mt
R33	basalt	px ~15% 1mm. ol 1-2% 0.1mm, gm. plag+px+mt
R40	ankaramite boulder	ol~ 3% .1mm g.m plag+px+ol
R41	ankaramite	px 20% 1mm, ol ~1% 0.5mm, gm., plag+px
R42	ankaramite	px ~20%, 1mm; mt ~5% 0.5mm; gm plag+px+mt
R47	basalt	px ~10%, 5mm, mt~ 3%, .2mm; gm px+ plag+ mt
R55	dyke 110/90	px 25% 1mm, gm. plag+px+mt
R56	dyke 75/90	px ~10% 5mm. g.m plag +px+mt
R70	basalt boulder	px ~5% 1mm ol 35 1mm, gm. px+plag
R76	dyke 312/90	px ~10 .5mm, g.m plag+px+mt
R78	basalt	px ~15% 1.5mm, ol~5% ..5mm, gm. plag+px
R80	dyke 294/50N	hrn ~15% 1mm, gm. hrn.+plag+px+
R94	ankaramite	px ~20% 5mm. ol ~5% 3mm, gm. plag+px+mt
R102	ankaramite	px 20% 5mm, ol 10%, 1mm; mt. 3%, .5mm; gm. px+plag+mt
R119	dyke (330/80NE)	px ~10% 1-2mm. g.m plag+px+mt
R127	dyke (250/70N)	px ~15% 1mm ol 5% < 1mm, gm. px+plag
R128	ankaramite	px ~20% 10mm,, ol ~8% 5mm, mt 3%, .5mm, gm px+plag
R131	basalt	px ~10% 1mm ,ol ~3% 0.5mm, gm. px+plag
R133	basalt	px ~5%, 0.5mm, g.m plag+px

Foidal Phonolites

R11	boulder	neph ~10% 0.5mm,sodalite ~6%, 0.3mm px ~1% 0.5mm,
R14	Muri	neph ~3% 0.5mm,sodalite ~1%, 0.3mm px ~2-3% 0.5mm,
R25	Raemaru	neph ~10% 0.5mm,sodalite ~5%, 0.3mm px ~1% 0.5mm,
R26	Raemaru	neph ~10-15% 0.5mm,sodalite ~3-6%, 0.3mm px ~1% 0.5mm,
R28	Raemaru	neph ~10% 0.5m, px~3% 0.5mm,
R38	Maungatea bluff	neph ~10% 0.5mm,sodalite ~1%, 0.1mm px ~3% 0.5mm,
R49	Muri	neph ~3% 0.5mm,sodalite ~1%, 0.3mm px ~2-3% 0.5mm,
R90	boulder	neph ~10% 0.5mm,sodalite ~6%, 0.3mm px ~1% 0.5mm,
R91	boulder	neph ~8% 0.5mm,sodalite ~3%, 0.3mm px ~1% 0.5mm,
R123	Tuakata	neph ~2-3% 0.5mm,, 0.3mm px ~3% 0.5mm,
R125	Tuakata	neph ~2-3% 0.5mm px ~5% 0.5mm,
R126	boulder	neph ~2% 0.5mm,sodalite ~6%, 0.3mm px ~3% 0.5mm,
R137	Black Rock	neph ~15% 0.5mm,sodalite ~10%, 0.3mm px ~1% 0.5mm,

Phonolites

R30	clast	plag ~15% 1mm, ~20% 0.1mm, neph 3% 0.1mm mt 1%, 0.1mm, px ~1% 0.1mm
R68	boulder	plag ~15% 1mm, ~20% 0.1mm, neph 3% 0.1mm mt 1%, 0.1mm, px ~1% 0.1mm
R107	phonolite (boulder)	plag ~15% 1mm, ~20% 0.1mm, neph 3% 0.1mm mt 1%, 0.1mm, px ~1% 0.1mm
R114	phonolite (boulder)	plag ~15% 1mm, ~20% 0.1mm, neph 3% 0.1mm mt 1%, 0.1mm, px ~1% 0.1mm
R117	boulder	plag ~15% 1mm, ~20% 0.1mm, neph 3% 0.1mm mt 1%, 0.1mm, px ~1% 0.1mm
R122	clast	plag ~30% .5mm, neph ~3%

Appendix 2

Whole rock Geochemical analysis

A2.1 Major and Trace elements Methodology

Before crushing, rock chips were washed in distilled water and dried. They were ground to a fine powder in a tungsten carbide puck mill. Major elements were determined on fused glass beads on a Phillips XRF at the Geology Department, Auckland University, New Zealand. The following elements Ba, Rb, Sr, Pb, Th, U, Zr, Y, Ce, Sc, V, Cr, Ni, Cu, Zn and Ga were determined on a XRF at Memorial University of Newfoundland. The REE, Hf, Ta, Li, Cs and Nb were determined on a ICP-MS at Memorial University of Newfoundland (Longerich et al., 1990; Jenner et al., 1990). A Na_2O_2 sinter dissolution (Robinson et al., 1986) technique was used. The precision and limits of detection of the XRF and ICP-MS are shown in Table A2.3 and A2.4 respectively where analyses done on selected international standards are compared with their reported concentrations.

The oxidation state for iron in norm calculations follows the recommendations of Middlemost (1989).

Table A2.1 Whole Rock Geochemistry
Type I mafic rocks

Sample #	R44	R43	R82	R115	R54	R22	R99	R116	R36	R35	R77	R120	R53	R27
SiO_2	41.96	41.75	40.82	43.62	41.94	42.59	41.96	42.91	42.59	39.76	41.77	40.67	40.65	41.46
TiO_2	2.77	2.76	2.86	3.12	2.72	3.01	3.73	3.44	3.30	4.52	3.14	3.14	3.51	3.80
Al_2O_3	9.72	9.67	10.04	11.25	10.90	11.19	12.83	11.94	11.00	10.56	10.67	11.42	12.87	13.09
$Fe_2O_3^t$	13.04	12.97	12.99	12.74	12.45	13.09	13.21	13.68	12.50	16.86	13.47	12.41	13.15	13.45
MnO	0.22	0.22	0.21	0.20	0.19	0.19	0.21	0.24	0.21	0.20	0.31	0.19	0.21	0.22
MgO	15.47	15.39	12.01	11.77	11.42	12.01	9.87	10.13	12.15	12.12	9.65	8.53	9.03	8.64
CaO	11.22	11.16	12.19	11.02	11.51	11.91	11.34	10.72	12.01	11.57	12.58	12.48	12.00	11.86
Na_2O	1.22	1.21	1.26	2.48	2.54	2.29	3.04	2.39	2.04	2.02	1.74	2.16	2.27	2.76
K_2O	1.25	1.24	1.40	1.72	1.53	1.20	0.56	1.87	1.50	0.57	1.53	1.18	1.86	2.28
P_2O_5	0.38	0.38	0.46	0.62	0.53	0.56	0.61	0.76	0.57	0.38	0.49	0.56	0.60	0.56
LOI	3.64	3.62	5.48	1.58	4.79	2.32	2.57	1.85	2.04	1.07	4.56	2.39	3.44	1.54
total	100.88	100.37	99.72	100.12	100.52	100.36	99.93	99.93	99.91	99.63	99.91	95.13	99.59	99.66
Mg#	83.22	82.47	78.57	78.54	78.43	78.42	74.76	74.58	74.58	74.01	73.95	73.14	73.12	71.81
Cr			776		679				413		996		331	
Ni			359		333				225		402		204	
Sc			26		24				30		28		25	
V			260		219				419		320		294	
Pb			4		7				3		2		6	
Rb			33		35				27		32		47	
Cs			0.22						0.28					
Ba			481		717				383		596		789	
Sr			935		764				576		767		824	
Ga			20		17				20		20		19	
Li			5.76						3.71					
Ta			3.33						2.64					
Nb			59		57.9				43.5		59.4		88.7	
Hf			6.07						5.98					
Zr			238		239				205		272		304	
Y			21		19				19		23		24	
Th			7.52		4.84				3.86		5.7		5.58	
U			1.38		2.57				0.9		0.47		1.02	
La			43.74						32.63					
Ce			88.28		143.33				69.27		106.75		148.76	
Pr			10.19						8.3					
Nd			40.31						36					
Sm			7.63						7.71					
Eu			2.47						2.4					
Gd			0						7.816					
Tb			0.86						0.9					
Dy			4.68						4.94					
Ho			0.79						0.8					
Er			2.04						1.88					
Tm			0.25						0.24					
Yb			1.4						1.35					

Sample #	R16	R93	R113	R134	R37	R129	R7	R83	R19	R52	R81	R130	R29	R95
SiO_2	41.22	42.34	41.98	41.24	39.99	43.68	39.80	42.61	42.87	41.38	43.08	42.22	42.53	43.47
TiO_2	3.34	4.21	3.78	3.54	4.97	3.84	4.30	3.72	3.72	4.05	4.23	3.82	3.68	4.44
Al_2O_3	12.28	12.93	12.86	13.56	12.05	14.49	13.39	13.89	14.44	14.36	14.39	14.29	15.22	15.65
$Fe_2O_3^t$	13.33	13.19	14.80	12.50	16.48	12.33	13.67	13.23	12.94	13.01	13.75	13.43	13.08	13.02
MnO	0.22	0.20	0.22	0.18	0.21	0.19	0.16	0.24	0.24	0.21	0 22	0.22	0.22	0.20
MgO	8.53	8.44	8.57	6.89	8.75	6.50	7.05	6.64	6.38	6.13	5.95	5.79	5.39	5.27
CaO	11.36	12.06	11.22	10.35	11.52	11.30	11.83	9.90	10.80	11.66	10.79	11.42	10.29	10.98
Na_2O	2.26	2.06	2.58	2.63	2.58	2.88	2.51	3.09	3.42	2.79	3.37	2.40	2.63	2.50
K_2O	1.62	1.68	1.59	2.45	0.49	2.25	0.90	2.28	2.28	2.61	2.65	1.77	2.29	2.06
P_2O_5	0.70	0.57	0.78	0.95	0.50	0.61	0.80	0.88	0.93	0.75	1.45	0.78	0.72	1.13
LOI	4.83	2.01	1.74	5.61	2.78	2.02	5.15	3.56	1.56	3.22	1.04	2.30	2.41	0.86
total	99.69	99.69	100.12	99.90	100.32	100.09	99.56	100.04	99.58	100.17	100.92	98.44	98.46	99.58
Mg#	71.71	71.71	69.65	68.59	67.79	67.61	67.15	66.52	66.16	65.12	63.16	63.06	61.99	61.62
Cr	436	286	217	188		105	55	187	144	107	89	85		
Ni	222	114	135	129		122	175	121	88	85	57	91		
Sc	17	29	18	16		21	32	26	13	19	19	22		
V	282	376	298	279		329	564	309	274	337	297	335		
Pb	8	4	6	5		6	5	2	10	6	4	8		
Rb	40	38	31	60		54	20	49	60	65	39	46		
Cs		0.55	0.64			0.59			0.64		0.48			
Ba	943	550	619	1223		719	588	851	840	1102	571	1015		
Sr	3029	901	987	1369		947	1041	1266	1391	1175	1004	1008		
Ga	22	23	25	28		25	24	28	28	24	27	26		
Li		15.22	8.73			6.36			8.83		6.69			
Ta		3.82	5.25			4.51			6.2		4.23			
Nb	89	61.4	82.7	112.1		72.2	51.8	101	105	106.6	70.6	82.2		
Hf		7.18	9.54			7.19			9.21		7.61			
Zr	345	276	354	420		272	243	460	383	353	309	361		
Y	23	25	27	32		24	24	32	30	27	29	29		
Th	8	5.19	8.99	9.21		8.29	4.44	9.97	12.29	10.57	6.06	8.11		
U	3.45	1.16	1.91	2.64		1.76	0.09	0.84	2.52	1.02	1.3	1.92		
La		45.24	64.65			54.91			84.72		52.82			
Ce	176.33	95.74	133.44	215.34		113.5	124.71	185.06	166.66	191.62	113.77	139.16		
Pr		11.87	15.82			13.23			18.88		14.17			
Nd		48.88	62.39			52.08			71.9		58.49			
Sm		10.36	12.13			10.22			13.34		11.82			
Eu		3.12	3.77			3.2			4.05		3.82			
Gd		9.707	10.311			9.115			0		9.839			
Tb		1.16	1.28			1.12			1.43		1.31			
Dy		5.82	6.88			5.98			7.35		6.88			
Ho		0.98	1.09			1			1.21		1.14			
Er		2.43	2.71			2.41			3.02		2.8			
Tm		0.3	0.34			0.31			0.39		0.35			
Yb		1.68	2.01			1.74			2		1.79			

Sample #	R84	R23	R87	R51	R106	R50	R45	R20	R110	R46	R111	R89	R4
SiO_2	41.79	42.32	40.92	40.94	42.06	43.47	43.58	44.56	42.83	42.91	40.00	43.90	42.04
TiO_2	3.90	3.77	4.00	4.04	3.92	3.36	4.21	3.98	4.33	4.19	4.06	3.59	4.34
Al_2O_3	13.52	14.90	14.30	14.34	13.57	17.33	15.61	15.56	14.49	15.74	13.78	15.95	15.15
$Fe_2O_3^t$	15.71	12.43	12.78	13.03	15.98	10.45	12.81	12.62	13.95	12.85	13.20	11.63	12.25
MnO	0.26	0.22	0.21	0.20	0.31	0.23	0.20	0.23	0.21	0.17	0.23	0.23	0.22
MgO	6.28	4.96	5.00	5.04	6.17	4.03	4.91	4.80	5.20	4.79	4.90	4.25	4.31
CaO	10.25	11.05	11.33	11.28	10.19	9.23	10.42	10.21	11.04	10.47	10.55	10.19	11.32
Na_2O	4.85	3.22	3.12	4.16	4.82	3.85	3.00	3.74	3.29	3.05	1.97	3.80	2.67
K_2O	1.02	2.60	2.07	0.87	1.10	3.32	2.48	2.88	2.23	2.42	2.05	2.42	2.22
P_2O_5	1.07	0.96	0.73	0.72	1.09	0.94	0.78	1.01	0.85	0.77	1.03	0.89	0.85
LOI	1.67	3.30	5.33	5.39	1.15	3.54	2.10	0.41	1.53	2.28	7.99	3.13	4.96
total	100.32	99.73	99.79	100.01	100.36	99.75	100.10	100.00	99.95	99.64	99.76	99.98	100.33
Mg#	61.3	61.27	60.78	60.5	60.46	60.42	60.31	60.09	59.65	59.64	59.54	59.16	58.21
Cr	58			96		8				5		7	31
Ni	69			85		34				55		8	78
Sc	18			19		10				16		15	16
V	277			343		215				302		281	305
Pb	12			9		11				6	5	5	4
Rb	78			92		77				46	44	51	43
Cs											0.36		0.62
Ba	980			1196		1201				697	681	830	668
Sr	1233			1273		1331				1076	1019	1753	1050
Ga	27			24		25				25		28	30
Li											7.94		4.75
Ta											4.57		6.74
Nb	121.9			104.7		132.7				87.2	80.2	102.5	71.1
Hf	0			0		0				0	8.6	0	7.79
Zr	466			348		408				350	350	441	312
Y	32			26		30				29	30	34	27
Th	11.53			11.53		12.47				7.55	7.41	7.46	5.98
U	3.09			0.75		1.7				3.2	1.81	1.31	1.61
La											61.37		52.65
Ce	230.08			186.15		216.84				135.7	131.42	187.92	113.95
Pr											16.09		14.15
Nd											66.34		57.33
Sm											12.83		11.99
Eu											3.89		3.7
Gd											11.133		10.318
Tb											1.33		1.25
Dy											7.22		6.73
Ho											1.17		1.12
Er											2.97		2.72
Tm											0.36		0.34
Yb											2.01		1.75

	R97
SiO_2	39.95
TiO_2	3.10
Al_2O_3	14.26
$Fe_2O_3^t$	11.96
MnO	0.25
MgO	3.96
CaO	8.77
Na_2O	4.94
K_2O	1.71
P_2O_5	1.21
LOI	2.85
total	92.96
Mg#	56.75
Cr	
Ni	
Sc	
V	
Rb	
Cs	
Ba	
Sr	
Ga	
Li	
Ta	
Nb	
Hf	
Zr	
Y	
Th	
U	
La	
Ce	
Pr	
Nd	
Sm	
Eu	
Gd	
Tb	
Dy	
Ho	
Er	
Tm	
Yb	

Type II mafic rocks

sample #	R42	R102	R47	R128	R40	R131	R129	R70	R127	R17	R119	R33	R133
SiO_2	43.06	44.37	44.36	42.89	45.47	42.67	43.60	44.78	44.56	41.63	43.19	43.71	42.85
TiO_2	2.38	2.55	2.69	2.44	2.91	2.87	3.34	3.28	3.53	3.71	3.55	3.64	3.78
Al_2O_3	8.14	9.09	9.97	8.93	11.86	10.80	12.01	11.98	14.51	13.52	14.79	15.70	14.41
$Fe_2O_3^t$	12.02	13.36	12.03	12.62	12.69	12.84	13.35	14.16	12.64	12.49	11.87	12.15	12.66
MnO	0.19	0.21	0.17	0.16	0.18	0.20	0.21	0.21	0.21	0.19	0.19	0.16	0.20
MgO	17.02	15.59	13.80	14.12	11.34	11.37	8.50	10.77	6.04	5.94	4.88	4.90	5.02
CaO	12.62	10.94	12.58	11.99	9.74	12.30	11.86	11.47	11.72	10.84	9.89	9.57	10.09
Na_2O	0.86	1.56	1.41	1.11	2.97	1.63	2.60	2.34	2.73	1.73	2.19	2.32	2.37
K_2O	0.87	1.02	0.75	0.62	0.56	0.82	1.18	0.91	1.64	1.86	2.24	2.29	2.04
P_2O_5	0.28	0.37	0.39	0.38	0.51	0.47	0.56	0.37	0.67	0.79	0.72	0.75	0.74
LOI	1.86	1.30	2.03	4.96	2.11	3.66	3.70	0.12	1.79	7.30	4.78	4.82	5.27
total	99.30	100.36	100.18	100.22	100.34	99.63	100.91	100.39	100.04	100.00	98.29	100.01	99.43
Mg	84.88	82.22	81.97	81.59	77.98	77.82	76.15	75.1	65.44	65.32	61.97	61.52	61.1
Cr		901		977						138	17	16	0
Ni		380		356						120	74	60	0
Sc		28		26						24	20	14	0
V		227		183						297	288	247	0
Rb	20	24	17	8	10					46	53	50	46
Cs	0.13	0	0.28	0	2					0.45			0.32
Ba	353	459	714	341	437					737	978	945	761
Sr	517	522	581	457	724					1023	987	1046	1024
Ga		16	0	13						27	24	25	
Li	5.89		5		5.5					3.31			8
Ta	1.96		2.96		2.67					4.82			5.11
Nb	37.3	37.7	46.8	37.8	49.5					87.1	88.2	88.7	89.6
Hf	4.58	0	6.15	0	5.72					9.53			9.5
Zr	179	187	213	185	724					404	352	349	385
Y	19	19	20	18	22					28	27	28	31
Th	3.47	3.63	5.43	1.65	3.97					9.38	8.71	9.03	9.3
U	0.62	3.23	1.11	1.93	0.83					2.04	1.08	0.35	2.2
La	28.01		37.35		33.76					66.23			64.29
Ce	56.18	103.1	76.59	98.54	72.2					135.41	193.53	169.2	132.73
Pr	7.14		9.34		9.07					16.07			16.07
Nd	30.92		38.27		38.87					66.76			68.59
Sm	6.53		8.06		8.4					12.24			13.8
Eu	2.05		2.56		2.64					3.75			4.18
Gd	5.84		7.784		8.243					11.906			13.639
Tb	0.76		0.89		0.93					1.27			1.41
Dy	4.11		4.9		5.15					6.66			7.85
Ho	0.72		0.86		0.84					1.12			1.35
Er	1.64		2.19		2.03					2.85			3.35
Tm	0.22		0.27		0.26					0.35			0.41
Yb	1.14		1.65		1.43					1.94			2.45

sample #	R76	R41	R94	R56	R80	R55	R78
SiO_2	43.77	45.01	47.97	45.39	43.16	41.99	47.50
TiO_2	3.07	3.24	2.78	2.88	3.77	3.82	2.69
Al_2O_3	17.40	16.76	16.64	17.57	15.85	15.44	18.51
$Fe_2O_3^t$	9.24	10.28	10.70	10.04	11.11	11.61	8.99
MnO	0.21	0.17	0.24	0.15	0.18	0.23	0.26
MgO	3.53	3.87	3.78	3.38	3.66	3.72	2.54
CaO	9.53	8.07	7.88	6.74	9.49	9.66	7.03
Na_2O	3.11	2.38	4.12	2.56	2.67	2.45	5.93
K_2O	2.39	2.82	2.98	3.34	2.35	1.30	1.67
P_2O_5	0.98	0.87	1.11	0.97	0.69	0.65	0.87
LOI	6.74	6.30	2.07	6.85	6.53	9.59	3.78
total	99.97	99.77	100.27	99.87	99.46	100.46	99.77
Mg#	60.19	59.87	58.33	57.14	56.64	55.93	52.81
Cr	4			10	5	1	10
Ni	3			68	39	28	29
Sc	11			9	16	15	3
V	177			114	277	302	96
Cu	11			18	21	65	8
Pb	10		11	10	5	6	8
Rb	123		84	87	46	31	155
Cs	2.4		0.99	0.77		0.34	
Ba	1181		1105	1217	836	814	1388
Sr	2864		1520	1256	1194	1281	1933
Ga	26			29	26	28	25
Li	7.32		12.1	8.55		7.2	
Ta	6.77		9.6	6.9		4.39	
Nb	146.8		153.2	155.1	87.6	74.1	127.9
Hf	8.38		15.52	8.47		7.26	
Zr	475		595	506	378	278	428
Y	37		41	36	31	26	29
Th	14.26		15.83	13.86	7.1	8.33	11.2
U	2.74		3.48	2.58	0.93	1.46	2.5
La	87.03		114.45	92.64		61.07	
Ce	174.89		234.96	172.21	164.63	121.61	217.92
Pr	19.62		27.28	19.04		14.35	
Nd	76.48		105.51	73.67		55.52	
Sm	13.17		19.11	12.43		11.01	
Eu	4.08		5.92	3.9		3.36	
Gd	10.322		14.793	11.858		9.839	
Tb	1.31		1.97	1.32		1.21	
Dy	7.1		10.85	7.06		6.39	
Ho	1.22		1.83	1.24		1.06	
Er	3.23		4.76	3.04		2.76	
Tm	0.43		0.63	0.39		0.35	
Yb	2.25		3.36	2.13		1.86	

Foidal Phonolites

	R137	R25	R26	R11	R90	R125	R123	R91	R126	R38	R28	R49	R14
SiO_2	51.48	51.74	51.12	50.20	51.03	49.49	50.33	47.95	50.17	49.48	50.03	46.56	47.45
TiO_2	0.71	0.71	0.70	0.83	0.81	0.95	0.98	1.23	0.97	0.94	0.87	1.45	1.34
Al_2O_3	21.04	21.05	21.12	20.38	20.38	20.35	21.15	19.02	20.29	20.44	20.24	18.83	19.21
$Fe_2O_3^t$	4.43	4.58	4.51	4.89	4.87	5.13	5.22	6.11	5.00	5.07	5.15	6.45	6.23
MnO	0.26	0.24	0.25	0.28	0.26	0.23	0.24	0.29	0.24	0.26	0.26	0.31	0.29
MgO	0.50	0.55	0.58	0.63	0.66	0.78	0.89	1.17	1.04	1.15	1.19	1.58	1.53
CaO	2.62	3.01	3.08	4.38	3.70	4.19	3.14	6.09	3.41	3.47	4.44	5.55	4.65
Na_2O	10.31	10.44	10.21	9.29	10.34	8.71	9.47	7.97	9.39	9.24	8.85	8.34	9.27
K_2O	5.51	5.27	5.25	5.05	5.20	5.06	5.19	4.90	5.13	5.24	5.26	4.28	4.57
P_2O_5	0.11	0.14	0.14	0.16	0.16	0.18	0.17	0.29	0.17	0.14	0.17	0.43	0.35
LOI	2.18	1.42	2.19	3.06	1.74	4.08	2.37	4.13	3.34	3.72	2.69	5.37	4.26
total	99.15	99.15	99.15	99.15	99.15	99.15	99.15	99.15	99.15	99.15	99.15	99.15	99.15
	16.63	17.66	18.67	18.8	19.55	21.31	23.27	25.41	27.11	28.8	29.11	30.4	30.49
Cr	2	4	7	4			5			6		8	
Ni	27	31	27	65			30			30		31	
Sc		2	4	15			1			3		0	
V	51	59	55	328			80			69		111	
Pb	33	35	32	5			36			36		36	
Rb	159	158	149	40			169			157		121	
Cs	0	2.62	0	0			2.38			2.15			
Ba	1588	1764	1908	837			1578			1507		1886	
Sr	1820	2251	2367	990			1937			2459		2726	
Ga	43	38	41	25			43			40		40	
Li		38.78					7.26			14.46			
Ta		6.2					8.56			8.26			
Nb	291.1	262.3	263.3	80.2			320.5			311.4		337.7	
Hf	0	17.53	0	0			17.29			17.2		0	
Zr	1267	1075	1120	360			1190			1135		1168	
Y	30	31	28	29			39			36		43	
Th	46.52	50.41	42.67	6.7			57.86			54.25		47.55	
U	9.86	10.41	8.92	2.08			6.06			10.35		9.68	
La		140.37					152.01			137.07			
Ce	240.63	220.75	242.15	201.56			246.42			232.51		409.3	
Pr		19.24					22.37			21.47			
Nd		58.07					68.15			67.2			
Sm		8.06					10.14			9.87			
Eu		2.52					3.02			2.99			
Gd		7.633					8.728			8.95		13.157	
Tb		0.93					1.11			1.16			
Dy		5.57					6.81			6.64			
Ho		1.11					1.33			1.24			
Er		3.13					3.51			3.56			
Tm		0.47					0.52			0.53			
Yb		2.87					3.13			3.13			

Phonolites

sample #	R30	R68	R107	R114	R117	R122
SiO_2	57.03	57.52	56.49	56.73	57.63	56.58
TiO_2	0.35	0.44	0.67	0.38	0.36	0.44
Al_2O_3	20.13	19.99	18.99	20.21	20.56	20.04
Fe_2O_3'	3.68	4.01	4.30	3.82	3.74	4.07
MnO	0.21	0.24	0.20	0.23	0.21	0.21
MgO	0.20	0.30	0.70	0.48	0.31	0.37
CaO	3.40	2.84	2.91	3.10	2.43	3.05
Na_2O	6.66	8.05	7.73	6.47	8.34	7.47
K_2O	5.52	5.06	4.75	5.43	5.33	4.96
P_2O_5	0.06	0.07	0.14	0.06	0.06	0.07
LOI	1.91	0.63	2.27	2.24	0.18	1.89
total	99.15	99.15	99.15	99.15	99.15	99.15
Mg#	8.87	11.68	22.58	18.21	12.95	14.04
Cr			6			0
Ni			30			0
Sc			4			0
V			2			0
Pb	18	20	19			19
Rb	171	145	155			143
Cs	1.93	2.14	0			1.34
Ba	1543	1537	1670			1730
Sr	1428	1427	1301			1633
Ga	0	0	30			0
Li	20.62	20.18	0			18.31
Ta	6.23	7.26	0			7.16
Nb	163.9	173.9	166.5			162.9
Hf	15.25	16.25	0			15.6
Zr	855	852	861			797
Y	27	29	25			26
Th	24.88	25.45	24.8			25.03
U	5.37	5.38	4.18			5.2
La	125.86	131.08				127.18
Ce	205.16	217.18	265.44			213.82
Pr	17.75	19.68				19.04
Nd	52.76	59.84				58.76
Sm	7.55	8.14				8.03
Eu	2.8	2.6				2.43
Gd	5.37	5.74				5.47
Tb	0.79	0.92				0.87
Dy	4.67	5.18				5.11
Ho	0.93	1.02				0.97
Er	2.79	2.97				2.89
Tm	0.4	0.41				0.42
Yb	2.75	2.76				2.57

Table A2.2
CIPW Norms
Type I mafic rocks

sample#	R44	R43	R82	R115	R54	R22	R99	R116	R36	R35	R77	R120	R53
or	2.38	7.58	8.88	10.36	9.47	7.28	3.44	11.44	9.12	3.50	9.69	7.66	11.62
ab	0.00	6.37	5.40	10.38	5.87	8.36	16.34	12.03	7.45	8.56	7.33	9.78	3.42
an	12.92	17.90	18.95	14.78	14.49	17.16	20.47	16.91	16.90	18.78	18.00	19.76	20.55
lc	4.56	0.00	0.00	0.00	0.00	0.00	0.00	0.00	0.00	0.00	0.00	0.00	0.00
ne	7.78	2.92	4.07	7.40	10.82	7.65	7.20	6.11	6.84	6.17	5.65	6.92	10.88
di	40.00	29.48	34.31	29.49	33.38	31.81	27.05	26.41	32.46	30.65	36.39	35.42	30.60
ol	23.40	26.33	18.09	16.91	16.22	17.39	13.11	15.16	16.12	18.43	11.94	9.03	10.90
mt	4.52	4.61	4.99	4.93	4.62	4.84	5.68	5.35	5.16	6.54	5.20	5.33	5.54
il	3.74	3.98	4.28	4.43	3.97	4.31	5.40	4.96	4.73	6.54	4.69	4.81	5.17
ap	0.69	0.82	1.04	1.32	1.16	1.20	1.32	1.64	1.23	0.83	1.10	1.29	1.33

sample#	R27	R16	R93	R113	R134	R37	R129	R7	R83	R19	R52	R81	R130
or	13.93	10.30	10.41	9.77	15.65	3.07	13.82	5.79	14.25	13.98	16.27	16.05	11.22
ab	1.30	10.90	11.98	11.64	11.17	15.26	12.88	15.52	15.41	11.71	4.60	13.04	16.35
an	17.17	19.99	22.10	19.58	19.43	21.03	20.76	24.64	18.30	17.98	20.00	16.72	24.67
lc	0.00	0.00	0.00	0.00	0.00	0.00	0.00	0.00	0.00	0.00	0.00	0.00	0.00
ne	14.60	6.56	4.45	7.48	8.62	5.57	8.40	5.42	8.36	12.10	13.10	10.79	4.06
di	31.94	28.59	29.40	26.43	23.52	28.84	26.71	26.89	22.06	25.07	28.70	22.76	24.52
ol	8.64	11.63	8.01	12.19	8.42	10.64	4.73	6.79	8.43	6.11	3.59	5.35	5.77
mt	5.73	5.44	6.26	5.74	5.70	7.16	5.80	6.61	5.77	5.66	6.12	6.14	5.97
il	5.48	5.01	6.15	5.48	5.33	7.33	5.56	6.53	5.48	5.38	5.95	6.04	5.71
ap	1.21	1.57	1.25	1.70	2.15	1.11	1.33	1.82	1.95	2.02	1.65	3.11	1.75

sample#	R29	R95	R84	R23	R87	R51	R106	R50	R45	R20	R110	R46	R111
or	14.47	12.72	6.22	16.28	13.27	5.54	6.68	20.59	15.35	17.42	13.76	15.07	13.72
ab	15.97	21.33	16.19	10.61	10.62	17.23	16.45	12.75	17.13	15.00	13.82	15.76	18.50
an	24.56	26.56	12.50	19.64	20.52	19.27	12.48	21.21	22.84	17.58	19.00	23.31	25.72
lc	0.00	0.00	0.00	0.00	0.00	0.00	0.00	0.00	0.00	0.00	0.00	0.00	0.00
ne	5.57	1.28	17.24	12.02	11.87	13.80	16.81	14.12	6.65	11.63	10.22	7.86	0.92
di	20.01	18.15	26.21	25.46	28.26	28.76	25.72	16.33	20.78	22.03	25.94	20.92	20.76
ol	6.53	4.60	7.91	2.45	1.51	1.48	8.08	2.70	3.14	2.64	2.74	2.96	4.96
mt	5.79	6.27	5.82	5.84	6.24	6.24	5.82	5.33	6.25	5.87	6.37	6.27	6.58
il	5.48	6.47	5.61	5.57	6.05	6.06	5.61	4.91	6.14	5.68	6.30	6.15	6.41
ap	1.61	2.47	2.31	2.13	1.66	1.62	2.34	2.06	1.71	2.16	1.86	1.70	2.44

sample#	R89	R4	R97
or	15.02	14.18	11.32
ab	17.68	15.77	18.77
an	20.29	24.66	13.09
lc	0.00	0.00	0.00
ne	10.89	6.09	18.55
di	21.36	24.06	21.44
ol	1.96	0.63	3.77
mt	5.59	5.25	5.39
il	5.25	6.54	4.84
ap	1.95	1.92	2.83

Type II mafic rocks

sample#	R42	R102	R47	R128	R40	R131	R129	R70	R127	R17	R119	R33	R133
or	5.26	6.09	4.54	3.88	3.38	5.12	7.32	5.45	10.11	12.26	14.59	14.63	13.21
ab	5.84	13.00	12.97	10.55	26.99	13.77	16.53	17.58	19.23	17.33	21.67	22.53	23.25
an	16.15	14.95	19.12	18.58	17.77	20.87	18.49	19.76	23.47	26.37	26.36	27.76	24.84
lc	0.00	0.00	0.00	0.00	0.00	0.00	0.00	0.00	0.00	0.00	0.00	0.00	0.00
ne	1.23	0.69	0.00	0.00	0.17	1.03	4.78	2.23	3.80	0.00	0.00	0.00	0.04
di	36.83	29.98	33.77	33.40	22.59	32.33	31.54	28.37	26.10	22.30	18.03	14.64	19.79
ol	26.55	26.64	19.02	18.92	19.14	16.79	9.92	16.14	5.22	2.78	2.65	4.00	5.33
mt	4.15	4.28	4.49	4.36	4.71	4.83	5.31	5.06	5.48	6.08	5.82	5.81	6.05
il	3.39	3.59	3.84	3.60	4.15	4.23	4.88	4.63	5.13	5.77	5.45	5.48	5.77
ap	0.60	0.78	0.84	0.84	1.09	1.04	1.23	0.78	1.46	1.84	1.66	1.70	1.70

sample#	R76	R41	R132	R56	R80	R55	R78
or	15.38	18.27	18.15	21.68	15.36	8.74	10.24
ab	24.88	23.44	30.60	25.26	25.22	25.04	38.69
an	28.83	29.31	18.67	29.22	26.92	31.08	19.68
lc	0.00	0.00	0.00	0.00	0.00	0.00	0.00
ne	3.33	0.00	4.52	0.00	0.79	0.00	9.95
di	12.57	6.70	11.33	0.45	16.16	14.92	8.50
ol	3.25	0.00	5.73	0.00	2.33	0.00	2.61
mt	4.19	5.44	4.61	5.03	5.26	6.33	4.55
il	4.66	4.95	3.99	4.41	5.81	6.06	3.89
ap	2.23	2.00	2.39	2.23	1.60	1.55	1.89

Foidal Phonolites

sample#	R137	R25	R26	R11	R90	R125	R123	R91	R126	R38	R28	R49
or	31.66	30.05	30.19	29.56	29.80	30.06	30.11	29.39	30.06	30.82	30.73	25.94
ab	9.60	10.30	9.61	14.08	7.95	16.16	15.87	11.02	13.00	11.38	12.96	12.67
an	0.00	0.00	0.00	0.00	0.00	1.50	0.00	1.68	0.00	0.00	0.00	1.34
lc	0.00	0.00	0.00	0.00	0.00	0.00	0.00	0.00	0.00	0.00	0.00	0.00
ne	42.26	42.33	43.44	39.94	42.09	37.48	40.44	36.98	40.06	41.32	39.34	38.49
di	7.57	8.13	8.15	6.67	9.06	6.47	7.09	9.71	8.88	9.38	9.33	11.59
ol	0.00	0.00	0.00	0.00	0.00	0.00	0.00	0.00	0.00	0.00	0.00	0.00
mt	0.00	0.00	0.07	1.82	0.00	2.58	2.47	2.90	1.41	1.84	2.43	3.16
il	0.96	0.95	0.95	1.15	1.09	1.33	1.34	1.74	1.34	1.30	1.20	2.07
ap	0.22	0.28	0.28	0.33	0.32	0.38	0.35	0.62	0.35	0.29	0.35	0.92

sample#	R14
or	27.14
ab	6.41
an	0.00
lc	0.00
ne	43.12
di	13.34
ol	0.00
mt	1.36
il	1.88
ap	0.74

Phonolites

sample#	R30	R68	R107	R114	R117	R122
or	32.63	29.28	28.03	32.23	30.57	29.17
ab	38.58	40.15	42.18	39.01	37.82	39.80
an	8.74	3.40	3.09	10.12	2.84	6.47
lc	0.00	0.00	0.00	0.00	0.00	0.00
ne	12.75	18.39	16.29	11.61	20.93	16.18
di	3.31	4.16	5.53	3.95	3.90	4.69
ol	0.00	0.00	0.00	0.44	0.00	0.00
mt	1.94	1.99	2.27	1.97	1.89	2.02
il	0.49	0.60	0.93	0.53	0.49	0.61
ap	0.13	0.14	0.29	0.13	0.12	0.15

Table A2.3
XRF analysis at Memorial University compared with International Standards and Limit of Detection for this method.

		Sc	V	Cr	Ni	Ga	Rb	Sr	Y	Zr	Nb	Ba	Ce	Pb	Th	U
run (n=4)	DST-1	4	10	3990	2360	-1	0	0.4	0	0.2	0.1	6	0	7	1	0
Govindaraju (1989)	DST-1	4	11	3990	2360	1	0.1	0.3	0	4	2.2	2	0	12	0	0
standard deviation	DST-1	2	3	24	3	0	0.1	0.3	0.3	0.2	0.2	9	9	1	1	1
run (n=4)	BHVO-1	32	317	320	151	21	8.9	396.4	24.3	180.6	20.7	142	25	4	1	-1
Govindaraju (1989)	BHVO-1	32	317	289	121	21	11	403	27.6	179	19	139	39	3	1	0
standard deviation	BHVO-1	4	9	4	2	1	0.3	1.5	0.2	0.7	0.5	10	9	1	1	0
run (n=4)	SY-2	8	51	17	37	30	220	271	119	296	33.6	450	174	86	347	290
Govindaraju (1989)	SY-2	7	50	10	10	29	217	271	128	280	29	460	175	85	379	284
standard deviation	SY-2	0	1	2	2	0	0.2	0.6	0.5	1.3	0.2	16	16	3	1	2
run (n=4)	SY-3	5	17	10	37	27	209	307	624.9	364.7	253	447	2406	144	953	764
Govindaraju (1989)	SY-3	7	50	11	11	27	206	302	718	320	148	450	2230	133	1003	650
standard deviation	SY-3	2	1	2	2	1	0.4	1.1	1	1.8	0.4	17	35	1	2	4
run (n=4)	SiO2	0	0	29	32	0	0	0	0	0	0	0	0	0	0	0
standard deviation	SiO2	1	2	2	1	1	0	0.4	0.1	0.1	0.2	6	6	1	1	0
run (n=4)	PACS-1	15	149	141	77	16	46.9	270	15.5	132.7	9.5	672	42	339	-3	-2
Govindaraju (1989)	PACS-1	0	127	113	44	0	0	277	0	0	0	0	0	404	0	0
standard deviation	PACS-1	2	4	2	1	1	0.3	0.3	0.1	0.5	0.2	15	22	3	1	1
Limit of detection		6	6	6	4	2	0.7	1.1	0.6	1.1	0.7	20	19	4	3	4

A2.2 Isotopic Technique
Sm-Nd and Rb-Sr Procedure

The Sm-Nd and Rb-Sr isotopic analyses were carried out at the Department of Earth Sciences, Memorial University of Newfoundland. Chemical separations were carried out in clean laboratory conditions using reagents doubly distilled in quartz and/or two bottle Teflon sills. Approximately 0.10000 g of a powdered sample were dissolved in HF-HNO_3, in an open Teflon bomb and then for 1-2 days at 220°C in high pressure Teflon bombs. Fluorides were converted to perchlorates which were dissolved in HCL. Samples were then taken up in 6N HCL. Sr and REE were separated in HCl using 10 ml of Amberlite CG-120 cation exchange resin in 30 cm quartz columns. Nd and the REE were separated in quartz columns using Teflon powder coated with di-2-ethylhexyl orthophosphoric acid. Sample were analyzed in static mode on a Finnigan Mat 262 multi-collector mass spectrometer.

Table A2.5 Isotopic ratios

Sample #	$^{143}Nd/^{144}Nd$	2 sigma	$^{87}Sr/^{86}Sr$	2-sigma
R25-leached	0.512707	0.000009	0.704272	0.000007
R25	0.512687	0.000005	0.704478	0.000038
R30	0.512712	0.000009	0.704171	0.000027
R38	0.512673	0.000006	0.704478	0.000022
R40	.512668	0.000013	0.704506	0.000012
R42-leached	0.512781	0.000010	0.704410	0.000018
R42	0.512777	0.000029	0.704392	0.000015
R49	0.512689	0.000009	0.704523	0.000039
R55	0.512661	0.000019	0.704639	0.000040
R56	0.512721	0.000008	0.704497	0.000023
R68	0.512703	0.000007	0.704072	0.000039
R76	0.512677	0.000008	0.704295	0.000022
R81-leached	0.512731	0.000005	0.704262	0.000029
R81	0.512731	0.000009	0.704202	0.000030
R82	0.512722	0.000011	0.704095	0.000033
R94	0.512760	0.000010	0.700519	0.000069
R107-leached	0.512708	0.000004	0.704128	0.000021
R107	0.512706	0.000004	0.704129	0.000020
R111	0.512753	0.000007	0.704262	0.000029
R111	0.512739	0.000008	0.704207	0.000037
R111	0.512756	0.000009	0.704024	0.000010
R113	0.511865	0.000005	0.704297	0.000030

Appendix 3
Mineral Analyses. Major Elements.

A3.1 Methodology.

Quantitative microprobe mineral analyses were performed at the Department of Earth Sciences, Memorial University of Newfoundland, on a Chamexa SX50, equipped with a Si energy dispersive detector (ED) and four wavelength dispersive spectrometers (WDS), using a beam of 1-2μm diameter, an accelerating voltage of 15 kV and a beam current of 20 nA. Natural standards of olivine, hypersthene, hornblende, diopside and anorthite were systematically measured over the period in which analytical work was carried out to determine analytical precession.

The ED technique was used in most of the mineral analyses where major element variation in MgO, FeO, CaO, Al_2O_3 and/or Na_2O are of primary interest. The WD method was employed together with the ED technique for better minor element analyses. In olivine, the WDS method was utilized for Cr_2O_3, NiO, TiO_2, CaO and MnO. In pyroxene, the WDS method was utilized for Cr_2O_3, NiO, Na_2O and MnO. In feldspars, the WDS method was utilized for FeO, MnO and TiO_2,.

In the following tables, mineral analyses and their formula are grouped for olivine, pyroxene, plagioclase, hornblende, nepheline and magnetite. All mineral formula calculations were based on the assumption that $Fe^{total} = Fe^{2+}$. The method for end member calculations are from Deer et al., 1992 except for pyroxene which is from Cawthorne and Collerson, 1974.

Table A3.1
Olivine Analyses

Sample #	R36-ol1-c	R36-ol2-c	R36-ol2-c	R36-ol2-i	R36-ol2-r	R36-ol2-r	R36-ol3-c	R36-ol3-i	R36-ol3-r	R36-ol4-c	R36-ol4-r	R36-ol5-c	R36-ol5-r	R36-ol6-l
SiO_2	38.10	38.40	38.25	38.20	38.26	38.14	38.35	38.20	38.38	38.19	38.25	38.29	38.19	38.38
TiO_2	0.19	0.17	0.00	0.29	0.11	0.17	0.00	0.19	0.00	0.04	0.17	0.21	0.00	0.13
Al_2O_3	0.10	0.00	0.05	0.00	0.19	0.22	0.30	0.28	0.32	0.03	0.23	0.27	0.26	0.00
FeO	19.59	19.69	20.15	19.58	19.42	19.75	19.66	19.58	19.48	19.52	19.32	19.58	19.78	19.63
MgO	40.43	40.16	39.92	40.34	40.37	39.80	40.11	40.34	40.30	40.53	40.28	40.04	40.14	40.14
MnO	0.23	0.29	0.29	0.27	0.29	0.31	0.29	0.27	0.29	0.32	0.28	0.29	0.27	0.29
CaO	0.25	0.30	0.27	0.28	0.32	0.28	0.01	0.00	0.00	0.26	0.28	0.00	0.01	0.27
Cr_2O_3	0.00	0.00	0.00	0.00	0.00	0.18	0.00	0.00	0.19	0.00	0.12	0.00	0.19	0.00
NiO	0.09	0.00	0.06	0.06	0.06	0.06	0.00	0.06	0.06	0.10	0.10	0.05	0.05	0.05
total	99.03	99.02	99.02	99.03	99.04	99.02	99.02	99.03	99.04	99.02	99.03	99.03	99.03	99.02
Si	0.99	1.00	0.99	0.99	0.99	0.99	1.00	0.99	1.00	0.99	0.99	0.99	0.99	1.00
Ti	0.00	0.00	0.00	0.01	0.00	0.00	0.00	0.00	0.00	0.00	0.00	0.00	0.00	0.00
Al	0.00	0.00	0.00	0.00	0.01	0.01	0.01	0.01	0.01	0.00	0.01	0.01	0.01	0.00
Fe	0.42	0.43	0.44	0.42	0.42	0.43	0.43	0.43	0.42	0.42	0.42	0.43	0.43	0.43
Mg	1.56	1.55	1.55	1.56	1.56	1.54	1.55	1.56	1.56	1.57	1.56	1.55	1.56	1.55
Mn	0.01	0.01	0.01	0.01	0.01	0.01	0.01	0.01	0.01	0.01	0.01	0.01	0.01	0.01
Ca	0.01	0.02	0.02	0.02	0.02	0.02	0.00	0.00	0.00	0.01	0.02	0.00	0.00	0.02
Cr	0.00	0.00	0.00	0.00	0.00	0.00	0.00	0.00	0.00	0.00	0.00	0.00	0.00	0.00
Ni	0.00	0.00	0.00	0.00	0.00	0.00	0.00	0.00	0.00	0.00	0.00	0.00	0.00	0.00
total	3.01	3.00	3.00	3.00	3.00	3.00	3.00	3.00	3.00	3.01	3.00	3.00	3.00	3.00
Fo%	78.6	78.4	77.9	78.6	78.8	78.2	78.4	78.6	78.7	78.7	78.8	78.5	78.3	78.5

Sample #	R36-ol6-r	R40-ol4-c	R40-ol1-c	R40-ol1-r	R40-ol2-c	R40-ol3-c	R42-ol1-c	R42-ol2-c	R42-ol3-c	R42-ol3-r	R64-ol1-c	R64-ol1-c	R65-ol1-c	R67-ol1-c
SiO_2	38.27	39.90	39.80	38.90	41.20	40.70	40.70	39.90	40.80	39.80	42.50	40.80	41.40	41.60
TiO_2	0.00	0.00	0.00	0.00	0.00	0.00	0.05	0.04	0.04	0.00	0.00	0.00	0.00	0.00
Al_2O_3	0.00	0.60	0.00	0.50	0.00	0.00	0.00	0.00	0.00	0.00	0.00	0.00	0.00	0.00
FeO	19.82	20.20	16.60	26.30	14.70	16.30	18.40	18.80	17.80	19.40	7.40	14.70	11.70	10.30
MgO	40.23	39.50	42.60	30.20	44.30	43.70	42.00	41.10	42.60	40.80	50.90	43.60	46.70	48.00
MnO	0.27	0.36	0.22	0.50	0.22	0.30	0.30	0.30	0.28	0.31	0.19	0.37	0.13	0.21
CaO	0.26	0.30	0.00	0.30	0.30	0.30	0.30	0.20	0.40	0.20	0.00	0.00	0.20	0.20
Cr_2O_3	0.00	0.20	0.00	0.00	0.06	0.08	0.00	0.00	0.00	0.00	0.00	0.00	0.11	0.00
NiO	0.05	0.25	0.20	0.12	0.20	0 20	0.15	0.10	0.22	0.11	0.25	0.22	0.34	0.39
total	99.02	101.33	99.44	96.85	100.98	101.58	101.90	100.44	102.14	100.62	101.25	99.69	100.59	100.70
Si	0.99	1.01	1.01	1.06	1.02	1.01	1.01	1.01	1.01	1.01	1.02	1.02	1.02	1.01
Ti	0.00	0.00	0.00	0.00	0.00	0.00	0.00	0.00	0.00	0.00	0.00	0.00	0.00	0.00
Al	0.00	0.02	0.00	0.02	0.00	0.00	0.00	0.00	0.00	0.00	0.00	0.00	0.00	0.00
Fe	0.43	0.43	0.35	0.60	0.30	0.34	0.38	0.40	0.37	0.41	0.15	0.31	0.24	0.21
Mg	1.56	1.49	1.61	1.23	1.63	1.62	1.56	1.55	1.57	1.55	1.81	1.63	1.71	1.74
Mn	0.01	0.01	0.00	0.01	0.00	0.01	0.01	0.01	0.01	0.01	0.00	0.01	0.00	0.00
Ca	0.01	0.02	0.00	0.02	0.02	0.02	0.02	0.01	0.02	0.01	0.00	0.00	0.01	0.01
Cr	0.00	0.00	0.00	0.00	0.00	0.00	0.00	0.00	0.00	0.00	0.00	0.00	0.00	0.00
Ni	0.00	0.01	0.00	0.00	0.00	0.00	0.00	0.00	0.00	0.00	0.00	0.00	0.01	0.01
total	3.01	2.98	2.99	2.93	2.98	2.99	2.98	2.99	2.99	2.99	2.98	2.98	2.98	2.99
Fo%	78.3	77.7	82.1	67.2	84.3	82.7	80.3	79.6	81.0	78.9	92.5	84.1	87.7	89.3

Sample #	R67-ol2-c	R67-ol2-r	R67-ol3-c	R67-ol4-r	R74-ol1-c	R74-ol1-r	R74-ol2-c	R74-ol3-c	R74-ol4-c	R81-ol1-c	R81-ol1-r	R81-ol2-c	R81-ol2-r	R81-ol3-c
SiO_2	39.60	37.60	41.20	41.80	39.40	39.50	39.30	39.70	39.10	38.44	38.54	38.19	38.47	38.70
TiO_2	0.00	0.06	0.00	0.00	0.00	0.00	0.00	0.00	0.00	0.19	0.00	0.00	0.20	0.20
Al_2O_3	0.00	0.80	0.00	0.00	0.00	0.00	0.00	0.00	0.00	0.04	0.03	0.05	0.05	0.04
FeO	18.00	25.80	11.20	11.60	20.30	20.10	20.20	20.40	20.50	17.91	18.14	18.13	17.88	18.50
MgO	40.80	28.90	47.00	47.00	39.40	39.30	39.60	39.20	39.40	41.82	41.78	41.58	41.48	41.20
MnO	0.30	0.56	0.15	0.15	0.26	0.21	0.23	0.25	0.26	0.29	0.26	0.26	0.24	0.30
CaO	0.40	0.60	0.20	0.30	0.30	0.20	0.40	0.30	0.30	0.33	0.32	0.34	0.35	0.34
Cr_2O_3	0.00	0.00	0.00	0.09	0.00	0.00	0.00	0.00	0.00	0.22	0.00	0.29	0.16	0.23
NiO	0.16	0.14	0.32	0.30	0.18	0.18	0.18	0.16	0.18	0.17	0.16	0.19	0.15	0.18
total	99.28	94.51	100.07	101.26	99.84	99.49	99.91	100.01	99.74	99.42	99.31	99.03	99.03	99.69
Si	1.01	1.05	1.01	1.02	1.01	1.02	1.01	1.02	1.01	0.99	0.99	0.99	0.99	0.99
Ti	0.00	0.00	0.00	0.00	0.00	0.00	0.00	0.00	0.00	0.00	0.00	0.00	0.00	0.00
Al	0.00	0.03	0.00	0.00	0.00	0.00	0.00	0.00	0.00	0.00	0.00	0.00	0.00	0.00
Fe	0.39	0.60	0.23	0.24	0.44	0.43	0.43	0.44	0.44	0.38	0.39	0.39	0.38	0.40
Mg	1.56	1.20	1.72	1.70	1.51	1.51	1.52	1.50	1.51	1.60	1.60	1.60	1.59	1.58
Mn	0.01	0.01	0.00	0.00	0.01	0.00	0.01	0.01	0.01	0.01	0.01	0.01	0.01	0.01
Ca	0.02	0.04	0.01	0.02	0.02	0.01	0.02	0.02	0.02	0.02	0.02	0.02	0.02	0.02
Cr	0.00	0.00	0.00	0.00	0.00	0.00	0.00	0.00	0.00	0.00	0.00	0.00	0.00	0.00
Ni	0.00	0.00	0.01	0.01	0.00	0.00	0.00	0.00	0.00	0.00	0.00	0.00	0.00	0.00
total	2.99	2.94	2.99	2.98	2.99	2.98	2.99	2.98	2.99	3.01	3.01	3.01	3.00	3.00
Fo%	80.2	66.6	88.2	87.8	77.6	77.7	77.8	77.4	77.4	80.6	80.4	80.4	80.5	79.9

Sample #	R81-ol4-r	R81-ol5-c	R81-ol6-r	R92-ol1-c	R92-ol1-r	R92-ol2-c	R92-ol2-r	R92-ol3-c	R92-ol4-r	R94-ol1-c	R94-ol1-r	R94-ol2-c	R94-ol2-r	R94-ol13-c
SiO_2	38.30	38.40	38.60	38.62	38.76	38.24	37.70	38.49	38.25	39.89	40.59	39.03	38.73	39.92
TiO_2	0.00	0.00	0.21	0.21	0.00	0.30	0.33	0.00	0.33	0.14	0.00	0.00	0.00	0.00
Al_2O_3	0.03	0.05	0.05	0.04	0.02	0.03	0.03	0.03	0.04	0.03	0.03	0.03	0.00	0.00
FeO	18.50	18.70	18.40	17.60	17.62	18.78	20.80	17.67	18.21	9.71	9.64	16.74	16.60	16.62
MgO	41.60	41.50	41.70	41.75	41.80	40.48	38.87	41.73	41.34	48.35	48.48	43.22	43.01	42.08
MnO	0.27	0.27	0.25	0.28	0.25	0.32	0.33	0.27	0.25	0.12	0.15	0.35	0.34	0.25
CaO	0.33	0.35	0.36	0.33	0.39	0.36	0.47	0.36	0.36	0.08	0.07	0.00	0.00	0.20
Cr_2O_3	0.00	0.30	0.16	0.00	0.00	0.30	0.31	0.23	0.00	0.23	0.00	0.15	0.22	0.00
NiO	0.16	0.20	0.15	0.18	0.17	0.18	0.13	0.18	0.19	0.40	0.37	0.00	0.00	0.15
total	99.27	99.77	99.93	99.02	99.02	99.03	99.02	99.02	99.04	99.04	99.32	99.51	98.93	99.21
Si	0.99	0.99	0.99	0.99	1.00	0.99	0.99	0.99	0.99	0.99	1.00	0.99	0.99	1.02
Ti	0.00	0.00	0.00	0.00	0.00	0.01	0.01	0.00	0.01	0.00	0.00	0.00	0.00	0.00
Al	0.00	0.00	0.00	0.00	0.00	0.00	0.00	0.00	0.00	0.00	0.00	0.00	0.00	0.00
Fe	0.40	0.40	0.39	0.38	0.38	0.41	0.46	0.38	0.39	0.20	0.20	0.36	0.36	0.35
Mg	1.60	1.59	1.59	1.60	1.60	1.56	1.52	1.60	1.59	1.79	1.78	1.64	1.65	1.60
Mn	0.01	0.01	0.01	0.01	0.01	0.01	0.01	0.01	0.01	0.00	0.00	0.01	0.01	0.01
Ca	0.02	0.02	0.02	0.02	0.02	0.02	0.03	0.02	0.02	0.00	0.00	0.00	0.00	0.01
Cr	0.00	0.00	0.00	0.00	0.00	0.00	0.00	0.00	0.00	0.00	0.00	0.00	0.00	0.00
Ni	0.00	0.00	0.00	0.00	0.00	0.00	0.00	0.00	0.00	0.01	0.01	0.00	0.00	0.00
total	3.01	3.01	3.01	3.00	3.00	3.00	3.00	3.01	3.01	3.00	3.00	3.00	3.00	2.98
Fo%	80.0	79.8	80.2	80.9	80.9	79.4	76.9	80.8	80.2	89.9	90.0	82.2	82.2	81.9

Sample #	R102-ol1-c	R102-ol2-c	R129-ol1-c	R129-ol2-c	R129-ol3-c	R129-ol3-c	R92-ol8-c	R92-ol8-r	R129-ol1-c	R129-ol2-c	R129-ol3-c	R36-ol2-r	R82-ol1-c	R92-ol9-c
SiO_2	39.90	39.87	39.10	37.90	39.20	39.50	39.50	39.50	40.30	37.50	39.70	40.00	39.10	39.50
TiO_2	0.06	0.03	0.04	0.11	0.00	0.03	0.00	0.03	0.03	0.04	0.05	0.11	0.04	0.00
Al_2O_3	0.70	0.00	0.00	0.50	0.00	0.00	0.00	0.00	0.00	0.00	0.00	0.20	0.00	0.00
FeO	17.70	13.20	19.00	26.00	18.30	17.20	18.80	17.40	18.50	17.20	19.20	20.30	19.00	18.80
MgO	40.70	45.38	41.80	35.10	41.50	42.40	42.50	43.40	43.70	38.60	42.60	42.20	41.80	42.50
MnO	0.27	0.22	0.28	0.43	0.26	0.24	0.26	0.24	0.27	0.26	0.28	0.30	0.28	0.26
CaO	0.40	0.25	0.30	0.54	0.30	0.35	0.30	0.35	0.45	0.53	0.40	0.33	0.30	0.30
Cr_2O_3	0.00	0.00	0.00	0.00	0.00	0.00	0.00	0.00	0.00	0.02	0.02	0.00	0.00	0.00
NiO	0.20	0.00	0.17	0.00	0.16	0.19	0.16	0.19	0.19	0.18	0.20	0.00	0.00	0.00
total	99.95	99.00	100.69	100.60	99.72	99.92	101.52	101.12	103.44	94.35	102.45	103.44	100.52	101.36
Si	1.01	1.00	0.99	0.99	1.00	1.00	0.99	0.99	0.99	1.01	0.99	0.99	0.99	0.99
Ti	0.00	0.00	0.00	0.00	0.00	0.00	0.00	0.00	0.00	0.00	0.00	0.00	0.00	0.00
Al	0.02	0.00	0.00	0.02	0.00	0.00	0.00	0.00	0.00	0.00	0.00	0.01	0.00	0.00
Fe	0.38	0.28	0.40	0.57	0.39	0.36	0.40	0.37	0.38	0.39	0.40	0.42	0.40	0.40
Mg	1.54	1.70	1.58	1.37	1.58	1.60	1.59	1.62	1.60	1.55	1.58	1.56	1.58	1.59
Mn	0.01	0.00	0.01	0.01	0.01	0.01	0.01	0.01	0.01	0.01	0.01	0.01	0.01	0.01
Ca	0.02	0.01	0.02	0.03	0.02	0.02	0.02	0.02	0.02	0.03	0.02	0.02	0.02	0.02
Cr	0.00	0.00	0.00	0.00	0.00	0.00	0.00	0.00	0.00	0.00	0.00	0.00	0.00	0.00
Ni	0.00	0.00	0.00	0.00	0.00	0.00	0.00	0.00	0.00	0.00	0.00	0.00	0.00	0.00
total	2.98	3.00	3.01	3.00	3.00	3.00	3.01	3.01	3.01	2.99	3.01	3.00	3.01	3.01
Fo%	80.4	86.0	79.7	70.6	80.2	81.5	80.1	81.6	80.8	80.0	79.8	78.8	79.7	80.1

Sample #	R36-ol2-i	R92-ol9-c	R92-ol9-r	R92-ol10-c	R92-ol10-r	R92-ol11-c	R129-ol1-c	R129-ol2-c	R129-ol3-c	R67-ol7-xenolith	R67-ol6-xenolith	R67-ol5-xenolith	R67-ol4-xenolith	R67-ol3-xenolith
SiO_2	39.20	39.50	37.90	39.10	39.50	39.50	39.70	40.30	37.50	40.60	40.80	41.10	41.40	41.20
TiO_2	0.06	0.03	0.11	0.04	0.00	0.03	0.05	0.03	0.04	0.00	0.00	0.00	0.00	0.00
Al_2O_3	0.21	0.00	0.50	0.00	0.00	0.00	0.00	0.00	0.00	0.00	0.00	0.00	0.00	0.00
FeO	19.69	17.40	26.00	19.00	18.80	17.40	19.20	18.50	17.20	10.90	13.30	12.20	14.00	11.80
MgO	41.36	43.40	35.10	41.80	42.50	43.40	42.60	43.70	38.60	45.90	44.90	46.20	44.50	46.00
MnO	0.29	0.24	0.43	0.28	0.26	0.24	0.28	0.27	0.26	0.29	0.29	0.28	0.26	0.28
CaO	0.33	0.35	0.54	0.30	0.30	0.35	0.40	0.45	0.53	0.20	0.00	0.20	0.20	0.20
Cr_2O_3	0.00	0.00	0.21	0.00	0.00	0.00	0.00	0.04	0.00	0.00	0.00	0.00	0.00	0.05
NiO	0.00	0.00	0.00	0.00	0.00	0.00	0.00	0.00	0.00	0.32	0.29	0.30	0.35	0.29
total	101.13	100.93	100.81	100.52	101.36	100.93	102.23	103.29	94.15	98.21	99.58	100.28	100.71	99.82
Si	0.99	0.99	0.99	0.99	0.99	0.99	0.99	0.99	1.01	1.02	1.02	1.01	1.02	1.02
Ti	0.00	0.00	0.00	0.00	0.00	0.00	0.00	0.00	0.00	0.00	0.00	0.00	0.00	0.00
Al	0.01	0.00	0.02	0.00	0.00	0.00	0.00	0.00	0.00	0.00	0.00	0.00	0.00	0.00
Fe	0.42	0.37	0.57	0.40	0.40	0.37	0.40	0.38	0.39	0.23	0.28	0.25	0.29	0.24
Mg	1.56	1.63	1.37	1.58	1.59	1.63	1.59	1.60	1.55	1.71	1.67	1.70	1.64	1.70
Mn	0.01	0.01	0.01	0.01	0.01	0.01	0.01	0.01	0.01	0.01	0.01	0.01	0.01	0.01
Ca	0.02	0.02	0.03	0.02	0.02	0.02	0.02	0.02	0.03	0.01	0.00	0.01	0.01	0.01
Cr	0.00	0.00	0.00	0.00	0.00	0.00	0.00	0.00	0.00	0.00	0.00	0.00	0.00	0.00
Ni	0.00	0.00	0.00	0.00	0.00	0.00	0.00	0.00	0.00	0.01	0.01	0.01	0.01	0.01
total	3.00	3.01	3.00	3.01	3.01	3.01	3.01	3.01	2.99	2.98	2.98	2.99	2.98	2.98
Fo%	78.9	81.6	70.6	79.7	80.1	81.6	79.8	80.8	80.0	88.2	85.8	87.1	85.0	87.4

Sample #	R67-ol2-xenolith	R67-ol1-xenolith	R66-ol9-xenolith	R66-ol7-xenolith	R66-ol6-xenolith	R66-ol5-xenolith	R66-ol4-xenolith	R66-ol3-xenolith	R66-ol2-xenolith	R66-ol12-xenolith	R66-ol11-xenolith	R66-ol10-xenolith	R66-ol1-xenolith	R66-ol1-xenolith
SiO_2	41.74	41.30	41.40	41.60	41.00	41.90	41.90	41.60	41.40	42.00	41.00	41.20	41.00	41.40
TiO_2	0.00	0.00	0.00	0.00	0.00	0.00	0.00	0.00	0.00	0.00	0.04	0.00	0.00	0.00
Al_2O_3	0.00	0.00	0.00	0.00	0.00	0.00	0.00	0.00	0.00	0.00	0.00	0.00	0.00	0.00
FeO	10.51	10.20	10.00	10.50	9.60	9.70	8.90	8.60	9.60	11.00	12.20	12.20	11.50	10.50
MgO	46.36	47.60	47.20	47.40	47.80	48.30	48.40	48.40	48.60	47.00	46.10	45.10	45.70	47.50
MnO	0.20	0.19	0.24	0.23	0.19	0.18	0.14	0.12	0.15	0.19	0.21	0.23	0.31	0.23
CaO	0.29	0.00	0.30	0.00	0.00	0.00	0.00	0.00	0.00	0.10	0.00	0.00	0.30	0.00
Cr_2O_3	0.00	0.00	0.00	0.00	0.00	0.00	0.00	0.00	0.00	0.15	0.00	0.00	0.00	0.00
NiO	0.30	0.25	0.23	0.33	0.37	0.31	0.42	0.38	0.30	0.31	0.20	0.25	0.21	u.32
total	99.40	99.54	99.38	100.06	98.96	100.39	99.76	99.10	100.05	100.76	99.75	98.99	99.04	99.95
Si	1.03	1.02	1.02	1.02	1.01	1.02	1.02	1.02	1.01	1.02	1.02	1.03	1.02	1.02
Ti	0.00	0.00	0.00	0.00	0.00	0.00	0.00	0.00	0.00	0.00	0.00	0.00	0.00	0.00
Al	0.00	0.00	0.00	0.00	0.00	0.00	0.00	0.00	0.00	0.00	0.00	0.00	0.00	0.00
Fe	0.22	0.21	0.21	0.22	0.20	0.20	0.18	0.18	0.20	0.22	0.25	0.25	0.24	0.22
Mg	1.70	1.75	1.73	1.73	1.76	1.75	1.76	1.77	1.77	1.71	1.70	1.68	1.69	1.74
Mn	0.00	0.00	0.01	0.00	0.00	0.00	0.00	0.00	0.00	0.00	0.00	0.00	0.01	0.00
Ca	0.02	0.00	0.02	0.00	0.00	0.00	0.00	0.00	0.00	0.01	0.00	0.00	0.02	0.00
Cr	0.00	0.00	0.00	0.00	0.00	0.00	0.00	0.00	0.00	0.00	0.00	0.00	0.00	0.00
Ni	0.01	0.00	0.00	0.01	0.01	0.01	0.01	0.01	0.01	0.01	0.00	0.01	0.00	0.01
total	2.97	2.98	2.98	2.98	2.99	2.98	2.98	2.98	2.99	2.97	2.98	2.97	2.98	2.98
Fo%	88.7	89.3	89.4	88.9	89.9	89.9	90.7	90.9	90.0	88.4	87.1	86.8	87.6	89.0

Sample #	R64-ol9-xenolith	R64-ol8-xenolith	R64-ol7-xenolith	R64-ol6-xenolith	R64-ol5-xenolith	R64-ol4-xenolith	R64-ol3-xenolith	R64-ol2-xenolith	R64-ol16-xenolith	R64-ol15-xenolith	R64-ol14-xenolith	R64-ol13-xenolith	R64-ol12-xenolith	R64-ol11-xenolith
SiO_2	40.70	40.50	40.30	40.70	40.60	41.30	40.40	39.70	40.80	41.00	40.40	40.70	40.70	40.00
TiO_2	0.00	0.00	0.00	0.04	0.00	0.00	0.00	0.00	0.00	0.00	0.00	0.00	0.00	0.00
Al_2O_3	0.00	0.00	0.00	0.00	0.00	0.00	0.00	0.00	0.00	0.00	0.00	0.00	0.00	0.00
FeO	14.10	14.40	14.70	14.20	13.50	12.30	13.60	16.40	13.50	12.80	13.20	13.00	15.40	13.80
MgO	43.40	43.80	43.60	44.50	44.50	45.70	45.20	42.20	45.10	45.50	44.50	44.50	43.70	43.80
MnO	0.44	0.48	0.38	0.38	0.39	0.30	0.35	0.41	0.34	0.33	0.37	0.33	0.44	0.41
CaO	0.30	0.30	0.30	0.20	0.20	0.00	0.00	0.30	0.00	0.00	0.20	0.20	0.30	0.30
Cr_2O_3	0.00	0.00	0.00	0.00	0.00	0.00	0.00	0.07	0.00	0.06	0.00	0.00	0.00	0.00
NiO	0.28	0.31	0.24	0.30	0.31	0.36	0.37	0.28	0.33	0.27	0.34	0.28	0.34	0.33
total	99.22	99.79	99.52	100.33	99.50	99.96	99.92	99.36	100.07	99.96	99.01	99.01	100.90	98.67
Si	1.02	1.01	1.01	1.01	1.02	1.02	1.01	1.01	1.02	1.02	1.02	1.02	1.01	1.01
Ti	0.00	0.00	0.00	0.00	0.00	0.00	0.00	0.00	0.00	0.00	0.00	0.00	0.00	0.00
Al	0.00	0.00	0.00	0.00	0.00	0.00	0.00	0.00	0.00	0.00	0.00	0.00	0.00	0.00
Fe	0.30	0.30	0.31	0.30	0.28	0.25	0.28	0.35	0.28	0.27	0.28	0.27	0.32	0.29
Mg	1.63	1.64	1.63	1.65	1.66	1.69	1.68	1.60	1.67	1.68	1.67	1.66	1.62	1.65
Mn	0.01	0.01	0.01	0.01	0.01	0.01	0.01	0.01	0.01	0.01	0.01	0.01	0.01	0.01
Ca	0.02	0.02	0.02	0.01	0.01	0.00	0.00	0.02	0.00	0.00	0.01	0.01	0.02	0.02
Cr	0.00	0.00	0.00	0.00	0.00	0.00	0.00	0.00	0.00	0.00	0.00	0.00	0.00	0.00
Ni	0.01	0.01	0.00	0.01	0.01	0.01	0.01	0.01	0.01	0.01	0.01	0.01	0.01	0.01
total	2.98	2.99	2.99	2.99	2.98	2.98	2.99	2.99	2.98	2.98	2.98	2.98	2.99	2.99
Fo%	84.6	84.4	84.1	84.8	85.5	86.9	85.6	82.1	85.6	86.4	85.7	85.9	83.5	85.0

Sample #	R64-ol10-xenolith	R64-ol1-xenolith	R40-ol6-xenolith	R40-ol5-xenolith	R40-ol4-xenolith	R40-ol3-xenolith	R40-ol2-xenolith	R40-ol1-xenolith	R106-ol2-xenolith	R102-ol2-xenolith
SiO_2	40.90	40.40	39.90	40.44	40.13	40.50	40.15	40.11	41.10	39.16
TiO_2	0.00	0.00	0.00	0.00	0.00	0.00	0.00	0.00	0.00	0.05
Al_2O_3	0.00	0.00	0.00	0.00	0.00	0.00	0.00	0.00	0.00	0.00
FeO	13.50	15.20	16.30	15.51	15.29	14.72	13.71	14.87	14.10	19.29
MgO	44.40	43.60	42.40	42.80	42.76	43.36	44.65	43.24	44.80	40.03
MnO	0.37	0.40	0.21	0.24	0.21	0.26	0.26	0.22	0.20	0.48
CaO	0.20	0.20	0.20	0.29	0.19	0.30	0.20	0.29	0.30	0.00
Cr_2O_3	0.00	0.00	0.00	0.00	0.05	0.00	0.00	0.00	0.08	0.00
NiO	0.28	0.27	0.19	0.23	0.19	0.28	0.24	0.28	0.19	0.00
total	99.67	100.09	99.20	99.51	98.83	99.41	99.22	99.02	100.77	99.03
Si	1.02	1.01	1.01	1.02	1.02	1.02	1.01	1.01	1.02	1.01
Ti	0.00	0.00	0.00	0.00	0.00	0.00	0.00	0.00	0.00	0.00
Al	0.00	0.00	0.00	0.00	0.00	0.00	0.00	0.00	0.00	0.00
Fe	0.28	0.32	0.35	0.33	0.32	0.31	0.29	0.31	0.29	0.42
Mg	1.65	1.63	1.61	1.61	1.62	1.63	1.67	1.63	1.65	1.54
Mn	0.01	0.01	0.00	0.01	0.00	0.01	0.01	0.00	0.00	0.01
Ca	0.01	0.01	0.01	0.02	0.01	0.02	0.01	0.02	0.02	0.00
Cr	0.00	0.00	0.00	0.00	0.00	0.00	0.00	0.00	0.00	0.00
Ni	0.01	0.01	0.00	0.00	0.00	0.01	0.00	0.01	0.00	0.00
total	2.98	2.99	2.99	2.98	2.98	2.98	2.99	2.99	2.98	2.99
Fo%	85.4	83.6	82.3	83.1	83.3	84.0	85.3	83.8	85.0	78.7

Table A3.2
Pyroxene Analyses

sample #	R 25-px7-r	R25-px-r	R25-px3-c	R25-px3-r	R25-px5-c	R25-px5-i	R25-px5-r	R25-px6	R25-px6	R25-px6	R25-px6-c	R25-px6-c	R25-px6-c	R25-px6-r
SiO_2	50.37	49.89	47.57	48.74	48.59	48.54	45.68	50.20	49.99	50.03	50.64	49.24	49.10	50.57
TiO_2	1.37	0.97	1.84	1.57	1.54	1.74	2.70	1.08	1.27	1.37	0.98	1.48	1.47	0.98
Al_2O_3	2.25	2.81	3.40	1.09	5.02	5.43	6.96	3.55	3.53	2.23	1.62	4.81	4.80	2.84
FeO	15.39	15.57	16.93	21.66	10.34	10.76	13.62	14.00	13.92	15.28	20.60	11.89	11.86	15.78
MnO	0.88	0.87	0.98	1.09	0.35	0.32	0.44	0.00	0.00	0.88	0.92	0.00	0.00	0.88
MgO	7.64	7.35	5.93	3.94	10.74	10.46	7.97	7.79	7.75	7.59	4.88	8.95	8.92	7.45
CaO	19.89	20.02	21.21	18.02	22.09	21.73	20.98	20.71	20.38	19.75	17.04	21.72	21.66	20.29
Na_2O	2.65	2.03	1.84	3.55	0.92	0.96	1.42	2.66	1.96	2.62	2.84	1.77	1.76	2.06
Cr_2O_3	0.00	0.00	0.00	0.00			0.00		0.00	0.00	0.00	0.00	0.00	0.00
total	100.45	99.50	99.70	99.65	99.59	99.94	99.76	99.99	98.80	99.77	99.50	99.85	99.57	100.84
Si	1.82	1.826	1.912	1.561	1.647	1.752	1.747	1.738	1.746	1.752	1.676	1.749	1.568	1.703
Ti	0.056	0.079	0.025	0.182	0.143	0.086	0.086	0.092	0.09	0.081	0.136	0.091	0.173	0.126
Al	0.224	0.201	0.099	0.495	0.393	0.311	0.319	0.319	0.324	0.314	0.379	0.314	0.499	0.334
Cr	0.014	0	0.026	0.003	0.003	0	0	0.005	0.003	0.007	0.001	0.002	0.004	0.002
Fe	0.193	0.257	0.128	0.263	0.259	0.216	0.212	0.217	0.21	0.213	0.244	0.22	0.254	0.254
Mn	0.003	0.006	0.001	0.002	0.005	0.002	0.006	0.001	0.003	0.004	0	0.003	0.002	0.005
Mg	0.784	0.718	0.916	0.565	0.637	0.714	0.719	0.714	0.703	0.718	0.636	0.714	0.574	0.644
Ca	0.903	0.897	0.888	0.918	0.903	0.901	0.897	0.901	0.899	0.9	0.905	0.891	0.914	0.916
Na	0.017	0.018	0.013	0.038	0.04	0.049	0.043	0.04	0.05	0.038	0.042	0.034	0.04	0.036
total	4.014	4.003	4.008	4.027	4.031	4.03	4.029	4.028	4.026	4.026	4.019	4.018	4.027	4.02
Ja	0.017	0.018	0.013	0.038	0.04	0.049	0.043	0.04	0.05	0.038	0.042	0.034	0.04	0.036
Ti-tesh	0.056	0.079	0.025	0.182	0.143	0.086	0.086	0.092	0.09	0.081	0.136	0.091	0.173	0.126
Ca-tesh	0.095	0.025	0.036	0.093	0.067	0.09	0.104	0.095	0.094	0.114	0.065	0.098	0.113	0.046
Wo	0.752	0.793	0.827	0.643	0.693	0.725	0.707	0.714	0.715	0.705	0.704	0.702	0.628	0.744
En	0.784	0.718	0.916	0.565	0.637	0.714	0.719	0.714	0.703	0.718	0.636	0.714	0.574	0.644
Fs	0.196	0.263	0.129	0.265	0.264	0.218	0.218	0.218	0.213	0.217	0.244	0.223	0.256	0.259

sample #	R25-px7-c	R25-px7-i	R36-px1-c	R36-px1-c	R36-px1-i1	R36-px1-i2	R36-px1-i3	R36-px1-r	R36-px1-r1	R36-px13-c	R36-px14-c	R36-px15-c	R36-px2-c	R36-px2-i1
SiO_2	49.88	51.00	46.98	46.27	46.75	46.93	44.71	41.52	47.03	40.98	43.52	46.97	45.08	46.55
TiO_2	1.08	1.30	3.09	3.26	3.20	2.88	4.82	6.08	3.27	6.35	5.04	3.08	4.45	3.21
Al_2O_3	3.53	3.60	7.28	7.20	7.36	7.13	8.57	11.21	7.16	11.03	8.82	7.06	7.50	7.23
FeO	13.92	14.20	6.81	6.92	6.71	6.82	7.77	8.05	7.06	8.26	8.17	6.91	8.03	6.90
MnO	0.00		0.19	0.04	0.08	0.13	0.01	0.05	0.08	0.05	0.17	0.06	0.16	0.07
MgO	7.74	7.90	12.97	12.76	12.63	12.91	11.38	10.20	12.88	9.95	11.28	12.83	11.44	12.82
CaO	20.58	20.80	22.53	22.40	22.46	22.51	22.54	22.58	22.37	22.49	22.27	22.53	22.63	22.83
Na_2O	2.65	2.00	0.60	0.55	0.69	0.52	0.58	0.54	0.47	0.51	0.55	0.68	0.49	0.50
Cr_2O_3	0.00		0.00	0.17	0.11	0.23	0.04	0.12	0.08	0.11	0.09	0.00	0.07	0.10
total	99.37	100.80	100.45	99.57	99.99	100.06	100.42	100.35	100.40	99.73	99.91	100.12	99.85	100.21
Si	1.74	1.72	1.70	1.72	1.77	1.80	1.68	1.81	1.83	1.88	1.84	1.86	1.82	1.92
Ti	0.09	0.12	0.11	0.09	0.08	0.07	0.12	0.06	0.05	0.04	0.05	0.04	0.06	0.03
Al	0.32	0.33	0.35	0.36	0.29	0.23	0.38	0.25	0.25	0.18	0.22	0.17	0.23	0.12
Cr	0.00	0.00	0.00	0.00	0.01	0.00	0.00	0.01	0.01	0.01	0.02	0.01	0.02	0.03
Fe	0.22	0.25	0.22	0.21	0.20	0.22	0.24	0.17	0.17	0.16	0.16	0.16	0.17	0.13
Mn	0.00	0.01	0.01	0.01	0.00	0.00	0.00	0.00	0.00	0.00	0.00	0.00	0.00	0.00
Mg	0.71	0.66	0.69	0.69	0.73	0.74	0.65	0.75	0.77	0.82	0.78	0.82	0.78	0.84
Ca	0.91	0.91	0.93	0.91	0.92	0.93	0.93	0.92	0.90	0.89	0.91	0.92	0.93	0.90
Na	0.04	0.03	0.04	0.04	0.03	0.03	0.04	0.03	0.03	0.03	0.03	0.03	0.03	0.03
total	4.03	4.02	4.03	4.03	4.02	4.02	4.03	4.01	4.01	4.00	4.01	4.02	4.02	3.99
Ja	0.04	0.03	0.04	0.04	0.03	0.03	0.04	0.03	0.03	0.03	0.03	0.03	0.03	0.03
Ti-tesh	0.09	0.12	0.11	0.09	0.08	0.07	0.12	0.06	0.05	0.04	0.05	0.04	0.06	0.03
Ca-tesh	0.10	0.06	0.09	0.15	0.11	0.06	0.11	0.09	0.11	0.08	0.10	0.07	0.09	0.04
Wo	0.72	0.73	0.72	0.67	0.74	0.80	0.70	0.77	0.74	0.77	0.76	0.82	0.78	0.83
En	0.71	0.66	0.69	0.69	0.73	0.74	0.65	0.75	0.77	0.82	0.78	0.82	0.78	0.84
Fs	0.22	0.25	0.22	0.22	0.20	0.22	0.24	0.17	0.17	0.16	0.16	0.16	0.17	0.14

sample #	R36-px2-i2	R36-px2-i3	R36-px2-r	R38 -5a core	R38 5b rim	R38-px2-c	R38-px3-c	R38-px5-c	R38-px5-r	R42-px1-c	R42-px1-r	R42-px1-r	R42-px1-rim	R42-px2-c
SiO_2	45.67	45.60	45.62	45.90	49.00	41.65	42.14	46.16	49.58	49.20	48.30	48.61	45.10	49.90
TiO_2	3.94	3.04	4.20	3.00	1.80	3.87	3.44	3.02	1.82	2.32	2.80	2.67	4.10	1.71
Al_2O_3	7.99	8.10	7.46	6.20	4.50	12.47	12.05	6.23	4.55	5.70	6.80	5.25	8.60	5.15
FeO	6.90	6.58	7.85	14.10	13.80	17.40	18.81	14.18	13.96	5.50	6.50	7.03	7.60	5.25
MnO	0.16	0.21	0.18			0.38	0.47	0.00	0.00	0.10	0.13	0.12	0.10	0.00
MgO	12.35	12.32	11.70	7.00	7.80	9.66	9.71	7.04	7.89	13.60	13.30	13.46	11.60	14.26
CaO	23.23	22.41	22.55	20.00	19.70	11.43	10.37	20.11	19.93	23.40	23.50	23.36	23.20	22.97
Na_2O	0.51	0.53	0.45	2.80	2.10	2.95	2.65	2.82	2.13	0.41	0.47	0.35	0.48	0.44
Cr_2O_3	0.05	0.03	0.00			0.00	0.00	0.00	0.00	0.32	0.22	0.00	0.06	0.75
total	100.80	98.82	100.01	99.00	98.70	99.80	99.64	99.55	99.85	100.55	102.02	100.85	100.84	100.42
Si	1.81	1.81	1.75	1.74	1.88	1.75	1.74	1.85	1.82	1.85	1.90	1.84	1.84	1.98
Ti	0.06	0.06	0.08	0.09	0.04	0.08	0.08	0.04	0.06	0.05	0.04	0.05	0.05	0.00
Al	0.25	0.24	0.33	0.31	0.17	0.34	0.34	0.22	0.29	0.17	0.13	0.21	0.23	0.05
Cr	0.01	0.01	0.00	0.00	0.02	0.00	0.01	0.02	0.02	0.01	0.02	0.03	0.01	0.07
Fe	0.18	0.19	0.20	0.21	0.17	0.25	0.20	0.15	0.16	0.18	0.14	0.16	0.20	0.10
Mn	0.00	0.00	0.01	0.00	0.00	0.01	0.00	0.00	0.00	0.00	0.00	0.00	0.00	0.00
Mg	0.75	0.76	0.71	0.70	0.79	0.63	0.69	0.81	0.74	0.81	0.83	0.78	0.73	0.90
Ca	0.92	0.93	0.90	0.93	0.91	0.93	0.93	0.89	0.89	0.94	0.94	0.93	0.91	0.82
Na	0.03	0.03	0.03	0.04	0.03	0.04	0.03	0.03	0.04	0.02	0.02	0.02	0.04	0.07
total	4.01	4.02	4.02	4.03	4.00	4.02	4.02	4.00	3.99	4.02	4.00	4.00	4.01	3.99
Ja	0.03	0.03	0.03	0.04	0.03	0.04	0.03	0.03	0.04	0.02	0.02	0.02	0.04	0.07
Ti-tesh	0.06	0.06	0.08	0.09	0.04	0.08	0.08	0.04	0.06	0.05	0.04	0.05	0.05	0.00
Ca-tesh	0.10	0.09	0.14	0.08	0.06	0.13	0.14	0.12	0.13	0.05	0.04	0.09	0.10	-0.02
Wo	0.76	0.77	0.68	0.75	0.81	0.72	0.71	0.73	0.69	0.84	0.86	0.79	0.77	0.84
En	0.75	0.76	0.71	0.70	0.79	0.63	0.69	0.81	0.74	0.81	0.83	0.78	0.73	0.90
Fs	0.18	0.19	0.21	0.21	0.17	0.26	0.21	0.15	0.16	0.18	0.14	0.16	0.21	0.11

sample #	R42-px2-c	R42-px3-c	R42-px3-c	R42-px3-i1	R42-px3-i2	R42-px3-r	R42-px3-r	R56-px1-c	R56-px1-r	R56-px2-c	R64-px-c	R64-px1-c	R64-px1-r	R64-px2-c
SiO_2	49.40	48.90	50.63	49.39	51.84	48.80	49.00	46.93	46.70	51.20	46.73	50.39	49.20	50.30
TiO_2	1.70	1.68	1.46	1.97	1.02	2.31	2.12	2.97	3.20	1.53	2.97	1.35	2.13	1.80
Al_2O_3	5.10	5.05	3.98	5.29	2.84	5.78	5.50	7.62	7.70	4.00	7.62	5.15	6.60	3.90
FeO	5.19	5.14	5.34	5.39	4.31	5.78	6.00	6.53	6.40	5.40	6.53	4.85	5.10	5.70
MnO	0.00	0.00	0.00	0.11	0.06	0.00	0.09	0.17	0.13	0.11	0.07	0.08	0.00	0.06
MgO	14.11	13.97	14.94	14.11	15.29	13.62	13.80	12.87	12.00	14.50	12.38	14.75	13.40	14.70
CaO	22.74	22.51	23.38	23.42	22.64	23.23	23.40	22.57	22.20	23.10	23.36	22.57	22.40	23.80
Na_2O	0.43	0.43	0.35	0.42	0.34	0.38	0.38	0.44	0.52	0.42	0.41	0.37	0.49	0.22
Cr_2O_3	0.74	0.74	0.35	0.52	0.93	0.32	0.34	0.00	0.07	0.59	0.20	0.83	0.50	0.43
total	99.41	98.42	100.42	100.63	99.27	100.23	100.63	100.10	98.92	100.85	100.27	100.34	99.82	100.91
Si	1.80	1.78	1.78	1.78	1.66	1.72	1.68	1.75	1.68	1.75	1.79	1.84	1.81	1.83
Ti	0.07	0.07	0.08	0.08	0.14	0.10	0.12	0.08	0.13	0.10	0.08	0.06	0.08	0.07
Al	0.26	0.28	0.29	0.28	0.38	0.36	0.39	0.33	0.37	0.29	0.26	0.21	0.22	0.21
Cr	0.01	0.01	0.01	0.00	0.00	0.00	0.00	0.00	0.00	0.00	0.01	0.00	0.00	0.01
Fe	0.18	0.19	0.22	0.22	0.25	0.23	0.23	0.24	0.25	0.24	0.24	0.24	0.24	0.23
Mn	0.00	0.00	0.00	0.00	0.00	0.00	0.00	0.01	0.01	0.00	0.00	0.01	0.00	0.00
Mg	0.74	0.73	0.71	0.72	0.65	0.67	0.65	0.66	0.65	0.69	0.72	0.73	0.73	0.73
Ca	0.93	0.92	0.91	0.90	0.91	0.91	0.92	0.91	0.91	0.91	0.90	0.89	0.91	0.90
Na	0.03	0.03	0.03	0.03	0.04	0.04	0.03	0.05	0.04	0.03	0.03	0.04	0.03	0.03
total	4.02	4.02	4.01	4.01	4.03	4.02	4.02	4.02	4.03	4.02	4.02	4.01	4.02	4.01
Ja	0.03	0.03	0.03	0.03	0.04	0.04	0.03	0.05	0.04	0.03	0.03	0.04	0.03	0.03
Ti-tesh	0.07	0.07	0.08	0.08	0.14	0.10	0.12	0.08	0.13	0.10	0.08	0.06	0.08	0.07
Ca-tesh	0.11	0.11	0.11	0.08	0.07	0.13	0.13	0.11	0.08	0.07	0.07	0.05	0.04	0.05
Wo	0.76	0.74	0.72	0.74	0.70	0.69	0.67	0.71	0.71	0.75	0.75	0.78	0.79	0.79
En	0.74	0.73	0.71	0.72	0.65	0.67	0.65	0.66	0.65	0.69	0.72	0.73	0.73	0.73
Fs	0.18	0.19	0.23	0.23	0.26	0.24	0.24	0.24	0.26	0.25	0.24	0.24	0.24	0.23

sample #	R64-px2-l	R64-px2-r	R64-px2c	R64-px4-c	R65-px1-c	R66-px1-c	R67-px1-c	R67-px2-c	R74-px1-c	R74-px1-l	R74-px1-r	R74-px2-c	R74-px2-r	R74-px3-c
SiO_2	51.58	50.00	46.45	49.50	54.30	48.50	48.10	47.60	47.72	47.70	44.30	46.20	44.90	46.90
TiO_2	1.40	1.84	2.94	1.82	0.09	2.15	2.31	2.49	2.67	3.00	4.80	3.50	4.10	3.00
Al_2O_3	2.97	4.85	7.55	5.30	1.20	5.70	6.00	6.40	6.53	6.30	8.60	8.20	8.90	7.40
FeO	4.46	5.15	7.94	6.50	3.40	6.60	5.80	6.00	7.13	7.10	8.10	7.50	7.40	7.60
MnO	0.00	0.00	0.18	0.10	0.05	12.90	0.00	0.08	0.10	0.10	0.07	0.09	0.09	0.20
MgO	15.05	14.16	11.27	13.10	16.60	0.08	13.20	13.00	12.67	12.90	11.60	12.10	11.60	11.90
CaO	23.76	23.56	23.03	23.00	21.10	22.90	23.30	22.80	22.67	22.50	22.70	22.90	22.90	22.60
Na_2O	0.21	0.27	0.59	0.48	0.93	0.45	0.39	0.45	0.42	0.40	0.50	0.48	0.44	0.68
Cr_2O_3	0.64	0.92	0.00	0.39	2.40	0.27	0.49	0.40	0.19	0.00	0.00	0.00	0.00	0.00
total	100.06	100.74	99.94	100.19	100.07	99.55	99.59	99.22	100.10	100.00	100.67	100.97	100.33	100.28
Si	1.72	1.72	1.73	1.74	1.78	1.75	1.72	1.76	1.72	1.72	1.80	1.82	1.83	1.85
Ti	0.10	0.11	0.11	0.09	0.09	0.09	0.10	0.08	0.10	0.11	0.06	0.06	0.05	0.06
Al	0.35	0.33	0.31	0.31	0.28	0.31	0.34	0.30	0.33	0.32	0.25	0.22	0.21	0.19
Cr	0.00	0.01	0.00	0.00	0.00	0.00	0.00	0.00	0.00	0.00	0.02	0.02	0.02	0.01
Fe	0.24	0.26	0.26	0.23	0.22	0.20	0.21	0.21	0.22	0.22	0.18	0.17	0.16	0.19
Mn	0.00	0.00	0.01	0.00	0.00	0.01	0.00	0.00	0.00	0.00	0.00	0.00	0.00	0.00
Mg	0.66	0.66	0.68	0.68	0.71	0.71	0.69	0.71	0.68	0.70	0.76	0.78	0.79	0.78
Ca	0.91	0.91	0.91	0.94	0.90	0.93	0.93	0.93	0.94	0.92	0.93	0.91	0.93	0.91
Na	0.04	0.04	0.04	0.03	0.04	0.03	0.03	0.03	0.03	0.04	0.03	0.03	0.02	0.02
total	4.02	4.03	4.03	4.03	4.01	4.02	4.03	4.03	4.03	4.03	4.02	4.01	4.01	4.00
Ja	0.04	0.04	0.04	0.03	0.04	0.03	0.03	0.03	0.03	0.04	0.03	0.03	0.02	0.02
Ti-tesh	0.10	0.11	0.11	0.09	0.09	0.09	0.10	0.08	0.10	0.11	0.06	0.06	0.05	0.06
Ca-tesh	0.10	0.08	0.06	0.09	0.07	0.10	0.11	0.12	0.11	0.06	0.09	0.08	0.08	0.04
Wo	0.71	0.73	0.75	0.76	0.74	0.74	0.72	0.73	0.73	0.75	0.78	0.77	0.80	0.81
En	0.66	0.66	0.68	0.68	0.71	0.71	0.69	0.71	0.68	0.70	0.76	0.78	0.79	0.78
Fs	0.25	0.26	0.26	0.23	0.22	0.21	0.22	0.22	0.22	0.23	0.18	0.17	0.16	0.19

sample #	R81-px1-c	R81-px1-c	R81-px1-i1	R81-px1-i3	R81-px1-i4	R81-px1-i5	R81-px1-r	R81-px1-r	R81-px1i2	R92-px1-c	R92-px1-r	R92-px2-c	R92-px2-r	R92-px3-c
SiO_2	48.50	49.00	46.70	47.90	49.20	45.82	44.90	46.20	45.70	48.80	48.90	53.30	49.20	50.10
TiO_2	2.68	2.43	3.40	2.80	2.28	3.61	4.50	3.80	3.80	1.98	1.90	0.33	0.00	0.59
Al_2O_3	5.03	4.88	6.55	5.83	4.78	7.80	8.27	6.93	7.48	5.10	5.10	1.30	4.80	3.50
FeO	7.57	7.20	7.70	7.60	7.60	7.72	8.00	8.20	8.10	6.20	6.10	5.50	6.20	6.10
MnO	0.12	0.08	0.13	0.10	0.15	0.11	0.16	0.15	0.07	0.09	0.09	0.22	0.08	0.11
MgO	13.05	13.10	12.40	13.00	13.20	11.73	11.60	12.10	11.70	14.10	14.30	16.10	14.50	15.20
CaO	22.61	22.60	22.60	22.40	22.20	22.56	22.80	22.80	22.70	22.60	22.50	22.10	22.80	22.50
Na_2O	0.45	0.41	0.46	0.43	0.49	0.57	0.49	0.48	0.51	0.23	0.22	0.32	0.20	0.18
Cr_2O_3	0.00	0.33	0.15	0.20	0.11	0.08	0.10	0.08	0.21	0.46	0.40	0.12	0.16	0.37
total	100.01	100.03	100.09	100.26	100.01	100.00	100.82	100.74	100.27	99.56	99.51	99.29	97.94	98.65
Si	1.70	1.81	1.84	1.84	1.77	2.00	1.87	1.96	1.88	1.94	1.93	1.93	1.94	1.61
Ti	0.11	0.06	0.05	0.04	0.08	0.03	0.06	0.05	0.04	0.03	0.03	0.04	0.04	0.11
Al	0.36	0.27	0.24	0.22	0.32	0.08	0.16	0.05	0.22	0.13	0.16	0.16	0.10	0.57
Cr	0.00	0.01	0.00	0.00	0.00	0.00	0.00	0.00	0.00	0.00	0.00	0.00	0.00	0.00
Fe	0.25	0.21	0.34	0.34	0.44	0.68	0.56	0.73	0.38	0.51	0.45	0.45	0.50	0.56
Mn	0.00	0.00	0.01	0.01	0.02	0.03	0.03	0.04	0.00	0.03	0.00	0.00	0.03	0.01
Mg	0.67	0.72	0.59	0.61	0.46	0.29	0.35	0.24	0.51	0.43	0.45	0.45	0.44	0.56
Ca	0.92	0.92	0.88	0.90	0.87	0.72	0.90	0.78	0.89	0.83	0.85	0.85	0.82	0.47
Na	0.02	0.03	0.07	0.07	0.11	0.22	0.14	0.28	0.13	0.15	0.20	0.15	0.20	0.22
total	4.03	4.01	4.03	4.04	4.05	4.04	4.06	4.11	4.04	4.04	4.06	4.02	4.07	4.11
Ja	0.02	0.03	0.07	0.07	0.11	0.22	0.14	0.28	0.13	0.15	0.20	0.15	0.20	0.22
Ti-tesh	0.11	0.06	0.05	0.04	0.08	0.03	0.06	0.05	0.04	0.03	0.03	0.04	0.04	0.11
Ca-tesh	0.12	0.12	0.07	0.07	0.05	-0.20	-0.09	-0.32	0.00	-0.08	-0.10	-0.06	-0.18	0.12
Wo	0.69	0.74	0.76	0.79	0.74	0.89	0.93	1.05	0.84	0.89	0.92	0.87	0.96	0.24
En	0.67	0.72	0.59	0.61	0.46	0.29	0.35	0.24	0.51	0.43	0.45	0.45	0.44	0.56
Fs	0.25	0.21	0.35	0.35	0.46	0.71	0.59	0.76	0.38	0.54	0.45	0.45	0.53	0.57

sample #	R92-px3-r	R92-px4-c	R94-px1-c	R94-px2-c	R94-px4-c	R94-px5-c	R94-px5-r	R94-px6-c	R94-px7-c	R94-px7-c	R94-px7-c	R94-px7-r	R94-px7-r	R102-px1-c
SiO_2	48.10	46.70	46.73	47.72	47.12	46.13	47.32	45.96	49.10	49.59	49.69	45.67	48.31	47.54
TiO_2	2.28	0.72	3.37	3.17	3.17	3.56	2.77	3.53	1.99	1.94	2.24	3.92	2.26	2.43
Al_2O_3	5.40	6.40	7.03	6.44	7.03	7.82	6.83	7.55	5.00	4.80	4.31	7.25	5.59	6.19
FeO	6.30	6.60	7.23	7.03	6.53	6.83	6.83	6.96	5.49	5.10	6.08	7.06	5.68	6.88
MnO	0.09	0.08	0.00	0.14	0.16	0.10	0.07	0.09	0.07	0.06	0.09	0.13	0.00	0.08
MgO	14.00	13.30	12.28	12.77	12.77	12.38	12.87	12.25	14.11	14.41	14.01	12.54	13.72	13.56
CaO	22.70	22.70	23.66	22.47	23.27	23.27	23.27	23.42	22.93	23.42	22.83	22.83	23.42	22.59
Na_2O	0.19	0.21	0.45	0.52	0.41	0.44	0.40	0.37	0.35	0.32	0.30	0.55	0.37	0.53
Cr_2O_3	0.44	0.27	0.00	0.00	0.00	0.00	0.08	0.00	0.80	0.58	0.18	0.00	0.66	0.20
total	99.50	96.98	100.73	100.26	100.46	100.52	100.44	100.13	99.84	100.21	99.73	99.95	100.02	99.99
Si	1.63	1.79	1.90	1.95	1.93	1.79	1.90	1.88	1.94	1.93	1.93	1.94	1.97	1.82
Ti	0.10	0.09	0.05	0.05	0.05	0.09	0.05	0.04	0.03	0.03	0.04	0.04	0.03	0.05
Al	0.55	0.29	0.21	0.08	0.08	0.29	0.21	0.22	0.13	0.16	0.16	0.10	0.10	0.22
Cr	0.00	0.00	0.00	0.00										0.01
Fe	0.61	0.46	0.45	0.47	0.47	0.46	0.45	0.38	0.51	0.45	0.45	0.50	0.64	0.19
Mn	0.02	0.00	0.00	0.02	0.02	0.00	0.00	0.00	0.03	0.00	0.00	0.03	0.04	0.00
Mg	0.56	0.41	0.45	0.49	0.50	0.41	0.45	0.51	0.43	0.45	0.45	0.44	0.23	0.80
Ca	0.43	0.84	0.82	0.82	0.83	0.84	0.82	0.89	0.83	0.85	0.85	0.82	0.84	0.90
Na	0.20	0.21	0.16	0.18	0.18	0.21	0.16	0.13	0.15	0.20	0.15	0.20	0.15	0.02
total	4.09	4.08	4.03	4.05	4.07	4.08	4.03	4.04	4.04	4.06	4.02	4.07	4.02	4.01
Ja	0.20	0.21	0.16	0.18	0.18	0.21	0.16	0.13	0.15	0.20	0.15	0.20	0.15	0.02
Ti-tesh	0.10	0.09	0.05	0.05	0.05	0.09	0.05	0.04	0.03	0.03	0.04	0.04	0.03	0.05
Ca-tesh	0.15	-0.10	-0.06	-0.19	-0.20	-0.10	-0.06	0.00	-0.08	-0.10	-0.06	-0.17	-0.12	0.10
Wo	0.18	0.85	0.82	0.97	0.98	0.85	0.82	0.84	0.89	0.92	0.87	0.96	0.93	0.74
En	0.56	0.41	0.45	0.49	0.50	0.41	0.45	0.51	0.43	0.45	0.45	0.44	0.23	0.80
Fs	0.62	0.46	0.45	0.49	0.49	0.46	0.45	0.38	0.53	0.45	0.45	0.52	0.69	0.19

sample #	R102-px1-i2	R102-px1-r	R102-px1-r	R102-px1-r	R102-px2-c	R102-px2-r	R106-px1-c	R106-px2-c	R106-px3-c	R106-px4-c	R106-px5-c	R107-px1	R107-px1	R107-px3-c
SiO_2	49.30	49.40	48.81	49.90	48.02	48.50	48.50	49.90	45.60	50.29	49.50	50.19	50.00	49.60
TiO_2	1.89	1.96	1.97	1.90	2.47	2.38	2.56	1.97	3.40	1.28	1.92	1.67	1.70	1.10
Al_2O_3	4.95	4.75	5.25	5.05	6.04	6.10	5.10	5.90	7.50	3.96	4.40	1.77	1.80	2.20
FeO	5.94	5.45	5.84	5.94	6.63	6.90	6.90	5.80	7.50	4.85	7.40	14.35	14.60	19.30
MnO	0.10	0.00	0.00	0.07	0.10	0.07	0.00	0.12	0.00	0.00	0.00	0.68	0.70	1.30
MgO	14.06	14.06	13.66	14.26	13.76	13.30	14.80	13.10	12.10	16.34	13.60	8.44	8.60	3.90
CaO	22.67	23.07	23.17	22.67	22.77	23.10	22.50	23.20	22.90	22.77	22.50	19.74	20.10	19.80
Na_2O	0.40	0.38	0.41	0.40	0.43	0.45	0.40	0.47	0.31	0.59	0.60	2.36	2.40	2.00
Cr_2O_3	0.39	0.65	0.62	0.67	0.23	0.20	0.00	0.38	0.00	0.00	0.00	0.00		
total	99.69	99.71	99.72	100.85	100.44	101.00	100.76	100.84	99.31	100.08	99.92	99.20	99.90	99.20
Si	1.86	1.88	1.80	1.80	1.78	1.84	1.83	1.84	1.82	1.83	1.78	1.79	1.83	1.79
Ti	0.00	0.02	0.06	0.02	0.07	0.05	0.05	0.06	0.06	0.05	0.07	0.07	0.05	0.07
Al	0.21	0.16	0.24	0.29	0.27	0.21	0.22	0.21	0.23	0.22	0.26	0.27	0.26	0.22
Cr	0.01	0.01	0.01	0.01	0.01	0.02	0.01	0.02	0.02	0.02	0.01	0.01	0.01	0.00
Fe	0.20	0.19	0.20	0.21	0.22	0.18	0.19	0.17	0.18	0.18	0.21	0.21	0.18	0.21
Mn	0.00	0.00	0.00	0.00	0.00	0.00	0.00	0.00	0.00	0.00	0.00	0.00	0.00	0.00
Mg	0.82	0.85	0.78	0.76	0.76	0.78	0.78	0.78	0.76	0.78	0.76	0.73	0.72	0.82
Ca	0.92	0.91	0.91	0.94	0.90	0.90	0.90	0.92	0.93	0.89	0.91	0.91	0.91	0.89
Na	0.02	0.01	0.01	0.02	0.04	0.03	0.03	0.03	0.03	0.03	0.03	0.03	0.03	0.03
total	4.04	4.03	4.02	4.04	4.04	4.01	4.01	4.01	4.02	4.01	4.03	4.02	4.00	4.04
Ja	0.02	0.01	0.01	0.02	0.04	0.03	0.03	0.03	0.03	0.03	0.03	0.03	0.03	0.03
Ti-tesh	0.00	0.02	0.06	0.02	0.07	0.05	0.05	0.06	0.06	0.05	0.07	0.07	0.05	0.07
Ca-tesh	0.20	0.11	0.10	0.23	0.10	0.08	0.08	0.07	0.09	0.09	0.10	0.10	0.11	0.05
Wo	0.73	0.78	0.75	0.68	0.74	0.78	0.77	0.79	0.78	0.75	0.74	0.75	0.75	0.77
En	0.82	0.85	0.78	0.76	0.76	0.78	0.78	0.78	0.76	0.78	0.76	0.73	0.72	0.82
Fs	0.20	0.19	0.20	0.22	0.22	0.18	0.19	0.17	0.18	0.18	0.21	0.22	0.18	0.21

sample #	R129-px10	R129-px11	R129-px12	R129-px2-c	R129-px3-c	R129-px7-c	R129-px8-c	R129-px9-c	R66-px-xenolith	R66-px-xenolith	R66-px-xenolith	R66-px-xenolith	R66-px-xenolith	R66-px-xenolith
SiO_2	51.28	49.60	49.60	49.70	46.80	43.90	48.81	52.60	54.40	58.40	55.20	54.10	55.30	55.40
TiO_2	1.49	1.74	1.82	0.14	0.07	4.54	2.82	0.91	0.35	0.00	0.20	0.48	0.22	0.25
Al_2O_3	2.97	4.36	4.85	5.00	7.00	8.50	4.55	2.30	1.80	0.70	1.00	1.30	1.10	0.90
FeO	5.15	5.25	5.45	6.20	6.60	8.60	8.22	4.20	2.70	5.70	3.30	3.10	3.10	3.20
MnO	0.08	0.07	0.03	0.09	0.08	0.08	0.19	0.04	16.70	34.10	17.60	17.10	17.50	17.30
MgO	15.94	14.85	14.95	14.60	13.40	11.90	12.87	16.90	0.00	0.17	0.00	0.06	0.16	0.09
CaO	23.27	23.27	22.97	23.50	23.40	22.60	22.37	22.80	21.80	1.10	20.60	22.60	20.50	21.20
Na_2O	0.16	0.19	0.22	0.22	0.23	0.26	0.25	0.19	0.77	0.07	0.73	0.34	0.71	0.71
Cr_2O_3	0.35	0.82	0.74	0.09	0.31	0.00	0.00	0.92	1.53	0.34	1.62	1.13	1.38	1.53
total	100.68	100.14	100.62	99.54	97.89	100.38	100.08	100.86	100.05	100.58	100.25	100.21	99.97	100.58
Si	1.85	1.85	1.84	1.83	1.88	1.85	1.79	1.66	1.97	2.00	1.99	1.96	2.00	2.00
Ti	0.04	0.05	0.05	0.05	0.04	0.00	0.00	0.13	0.01	0.00	0.01	0.01	0.01	0.01
Al	0.17	0.19	0.19	0.21	0.13	0.22	0.32	0.38	0.08	0.03	0.04	0.06	0.04	0.04
Cr	0.00	0.00	0.02	0.02	0.01	0.00	0.01	0.00	0.04	0.01	0.05	0.03	0.04	0.04
Fe	0.15	0.23	0.16	0.17	0.16	0.19	0.21	0.27	0.08	0.16	0.10	0.09	0.09	0.10
Mn	0.00	0.00	0.00	0.00	0.00	0.00	0.00	0.00	0.00	0.01	0.00	0.00	0.01	0.00
Mg	0.90	0.76	0.82	0.82	0.87	0.81	0.76	0.67	0.90	1.73	0.95	0.92	0.94	0.93
Ca	0.90	0.90	0.92	0.91	0.91	0.94	0.96	0.91	0.85	0.04	0.80	0.88	0.79	0.81
Na	0.04	0.04	0.01	0.02	0.01	0.02	0.02	0.02	0.05	0.01	0.05	0.02	0.05	0.05
total	4.05	4.02	4.02	4.02	4.02	4.04	4.06	4.04	3.99	3.98	3.98	3.99	3.98	3.98
Ja	0.04	0.04	0.01	0.02	0.01	0.02	0.02	0.02	0.05	0.01	0.05	0.02	0.05	0.05
Ti-tesh	0.04	0.05	0.05	0.05	0.04	0.00	0.00	0.13	0.01	0.00	0.01	0.01	0.01	0.01
Ca-tesh	0.06	0.04	0.08	0.09	0.04	0.20	0.29	0.10	0.01	0.03	-0.02	0.01	-0.02	-0.02
Wo	0.80	0.80	0.79	0.76	0.84	0.74	0.66	0.68	0.83	0.01	0.82	0.86	0.81	0.83
En	0.90	0.76	0.82	0.82	0.87	0.81	0.76	0.67	0.90	1.73	0.95	0.92	0.94	0.93
Fs	0.15	0.23	0.16	0.17	0.16	0.20	0.21	0.27	0.08	0.17	0.10	0.09	0.10	0.10

sample #	R106-px-xenolith	R106-px-xenolith	R102-px-xenolith	R102-px-xenolith	R64-px-xenolith	R64-px-xenolith	R64-px-xenolith	R64-px-xenolith	R64-px-xenolith
SiO_2	45.10	57.40	53.00	55.10	50.60	49.60	46.90	47.70	48.30
TiO_2	4.40	0.73	0.48	0.09	1.79	2.07	2.80	2.69	2.60
Al_2O_3	8.50	13.90	2.40	0.50	4.80	6.00	7.20	6.90	6.80
FeO	7.30	5.20	6.10	5.20	5.80	6.00	6.50	7.00	5.60
MnO	11.60	6.20	14.90	16.00	14.10	13.60	12.50	12.30	12.60
MgO	0.07	0.08	0.17	0.39	0.11	0.06	0.10	0.13	0.13
CaO	23.00	12.40	21.80	22.50	23.20	22.70	23.10	23.20	23.60
Na_2O	0.35	3.28	0.44	0.88	0.30	0.37	0.40	0.49	0.46
Cr_2O_3	0.00	0.00	0.07	0.17	0.06	0.12	0.00	0.09	0.26
total	100.32	99.19	99.36	100.83	100.76	100.52	99.50	100.50	100.35
Si	1.69	1.99	1.96	2.01	1.86	1.83	1.76	1.77	1.79
Ti	0.12	0.02	0.01	0.00	0.05	0.06	0.08	0.08	0.07
Al	0.37	0.57	0.10	0.04	0.21	0.26	0.32	0.30	0.25
Cr	0.00	0.00	0.00	0.01	0.00	0.00	0.00	0.00	0.01
Fe	0.23	0.15	0.19	0.16	0.18	0.18	0.21	0.22	0.17
Mn	0.00	0.00	0.01	0.01	0.00	0.00	0.00	0.00	0.00
Mg	0.65	0.32	0.82	0.87	0.77	0.74	0.70	0.68	0.69
Ca	0.92	0.46	0.86	0.88	0.91	0.90	0.93	0.93	0.94
Na	0.03	0.22	0.03	0.06	0.02	0.03	0.03	0.04	0.03
total	4.01	3.88	3.99	4.01	4.00	4.00	4.02	4.02	4.01
Ja	0.03	0.22	0.03	0.06	0.02	0.03	0.03	0.04	0.03
Ti-tesh	0.12	0.02	0.01	0.00	0.05	0.06	0.08	0.08	0.07
Ca-tesh	0.10	0.31	0.04	-0.03	0.09	0.12	0.14	0.12	0.07
Wo	0.70	0.13	0.80	0.90	0.77	0.72	0.72	0.74	0.80
En	0.65	0.32	0.82	0.87	0.77	0.74	0.70	0.68	0.69
Fs	0.23	0.15	0.20	0.17	0.18	0.18	0.21	0.22	0.17

Table A3.3
Titanomagnetite Analyses

	R129-mt1	R129-mt2	R129-mt3	R25-mt2	R25-mt3	R25-mt4	R25-mt5	R36-mt1	R36-mt2	R36-mt3	R64-mt1	R64-mt2	R67-mt1
SiO_2	0.30	0.20	0.20	0.30	0.30	0.30	0.20	0.26	0.26	0.26	0.30		
TiO_2	26.50	25.80	25.80	10.20	9.90	6.16	7.70	19.41	19.61	19.80	1.53	0.37	0.37
Al_2O_3	3.40	4.10	3.80	0.30	0.20	0.60	0.40	5.91	5.97	6.03	18.60	23.30	23.10
FeO	63.80	63.30	63.50	79.90	80.60	84.90	83.50	62.10	62.72	63.34	26.90	22.50	22.70
MgO	2.80	2.90	3.00	0.30	0.30	0.20	0.20	7.16	7.23	7.31	12.70	11.40	11.30
MnO	0.70	0.65	0.64	1.72	1.71	1.41	1.51	0.34	0.35	0.35			
CaO	0.17	0.16	0.21		0.22			0.04	0.04	0.04			
Na_2O								0.06	0.06	0.06		0.02	
K2O	0.03	0.03							0.00	0.00			
Cr_2O_3	0.03	0.09	0.05	0.09	0.04	0.04	0.04	0.42	0.42	0.42	37.00	40.00	39.70
NiO		0.06							0.00	0.00	0.17	0.16	0.13
total	97.71	97.34	97.17	92.79	93.24	93.54	93.56	95.60	96.65	97.61	97.10	97.75	97.29

	R67-mt3	R106-mt1	R106-mt2	R106-mt3	R74-mt1	R74-mt2	R74-mt3	R40-mt1	R40-mt2	R-40-mt3	R94-mt1	R94-mt2	R94-mt2
SiO_2	0.30				0.50	0.51	0.51	0.40	0.30	0.50	0.30	0.20	
TiO_2	14.00	48.40	7.70	14.40	17.90	18.08	18.26	5.00	5.06	4.95	19.30	14.30	17.70
Al_2O_3	7.70	0.50	6.70	3.10	6.60	6.67	6.73	9.20	9.30	9.11	5.80	7.10	6.90
FeO	52.30	42.40	50.20	71.40	62.40	63.02	63.65	42.10	42.56	41.68	61.50	57.20	62.30
MgO	5.50	5.20	4.50	2.80	6.40	6.46	6.53	4.70	4.75	4.65	7.70	7.90	6.20
MnO		1.00		0.86	0.35	0.35	0.36				0.35	0.15	0.37
CaO													
Na_2O								0.03	0.03	0.03	0.03		
K2O									0.00	0.00			
Cr_2O_3	15.60		25.60	0.15	0.90	0.91	0.92	34.70	35.08	34.35	0.40	9.20	2.60
NiO	0.16				0.16	0.16	0.16	0.07	0.07	0.07	0.15	0.17	0.11
total	95.52	97.52	94.69	92.71	95.28	96.16	97.11	96.27	97.15	95.34	95.44	95.96	96.14

	R56-mt1	R56-mt2	R42-mt1	R42-mt2	R78-mt1	R78-mt2	R25-mt6	R107-mt1	R107-mt2	R107-mt3
SiO_2	0.30	0.40	0.30	0.20		0.70			0.40	0.30
TiO_2	21.40	21.80	17.80	17.90	49.10	25.40	10.40	12.4	12.30	12.50
Al_2O_3	5.30	5.60	6.60	6.30	0.50	4.60		0.6	0.20	0.60
FeO	61.50	61.50	62.90	63.70	40.70	58.30	79.80	78.1	78.38	78.20
MgO	5.70	6.20	6.50	6.20	4.90	3.60				
MnO	0.57	0.50	0.23	0.41	0.96	1.00	1.60	2.6	2.78	2.41
CaO							0.30		0.28	
Na_2O			0.03			0.02				
K2O		0.03								
Cr_2O_3	0.06	0.27	1.02	0.83						
NiO			0.07							
total	94.89	96.39	95.41	95.60	96.13	93.65	92.02	93.73	93.94	93.71

Table A3.4
Hornblende Analyses

sample #	R56-hrn1	R56-hrn2	R56-hrn3	R56-hrn4	R56-hrn5	R56-hrn6	R56-hrn7	R56-hrn8	R56-hrn9	R56-hrn10	R56-hrn11	R56-hrn12	R56-hrn13	R56-hrn14
SiO_2	38.80	38.70	38.80	39.10	38.20	38.41	38.31	39.19	39.49	37.82	39.18	37.93	38.80	38.70
TiO_2	7.90	7.90	7.90	7.50	7.70	7.82	7.82	7.98	7.58	7.62	7.98	7.74	7.90	7.42
Al_2O_3	13.70	13.50	13.60	13.50	13.00	13.56	13.37	13.74	13.64	12.87	13.83	13.23	13.60	13.36
FeO	11.30	11.80	10.70	10.60	14.80	11.19	11.68	10.81	10.71	14.65	11.41	11.57	10.70	10.49
MgO	10.80	11.30	11.60	11.50	8.90	10.69	11.19	11.72	11.62	8.81	10.91	11.08	11.60	11.38
MnO	0.15	0.18	0.13	0.09	0.18	0.15	0.18	0.13	0.09	0.18	0.15	0.18	0.13	0.09
Cao	12.40	12.20	12.20	12.40	12.00	12.28	12.08	12.32	12.52	11.88	12.52	11.96	12.20	12.27
Na_2O	2.19	2.21	2.24	2.13	2.18	2.17	2.19	2.26	2.15	2.16	2.21	2.17	2.24	2.11
K_2O	1.45	1.49	1.37	1.44	1.62	1.44	1.48	1.38	1.45	1.60	1.46	1.46	1.37	1.43
total	98.69	99.28	98.54	98.26	98.58	97.70	98.29	99.53	99.24	97.59	99.66	97.30	98.53	97.26
Si	5.98	5.95	5.97	6.03	6.00	5.98	5.95	5.97	6.03	6.00	5.98	5.95	5.97	6.03
Ti	0.92	0.91	0.91	0.87	0.91	0.92	0.91	0.91	0.87	0.91	0.92	0.91	0.91	0.87
Al	2.49	2.44	2.47	2.45	2.41	2.49	2.44	2.47	2.45	2.41	2.49	2.44	2.47	2.45
Fe	1.46	1.52	1.38	1.37	1.94	1.46	1.52	1.38	1.37	1.94	1.46	1.52	1.38	1.37
Mg	2.48	2.59	2.66	2.64	2.08	2.48	2.59	2.66	2.64	2.08	2.48	2.59	2.66	2.64
Mn	0.02	0.02	0.02	0.01	0.02	0.02	0.02	0.02	0.01	0.02	0.02	0.02	0.02	0.01
Ca	2.05	2.01	2.01	2.05	2.02	2.05	2.01	2.01	2.05	2.02	2.05	2.01	2.01	2.05
Na	0.65	0.66	0.67	0.64	0.66	0.65	0.66	0.67	0.64	0.66	0.65	0.66	0.67	0.64
K	0.29	0.29	0.27	0.28	0.32	0.29	0.29	0.27	0.28	0.32	0.29	0.29	0.27	0.28
total	16.33	16.39	16.35	16.34	16.38	16.33	16.39	16.35	16.34	16.38	16.33	16.39	16.35	16.34

Table A3.5
Feldspar Analyses

sS	R56-plag-c	R56-plag-c	R78-plag-c	R78-plag-c	R78-plag-c	:R78-plag-c	R107-plag-c	R107-plag2-c	R107-plag2-i	R107-plag2-r	R107-plag3-c	R107-plag3-i	R107-plag3-r	R107-plag4-c
SiO_2	51.30	50.80	48.90	50.10	49.70	51.30	65.10	64.80	64.10	65.10	63.50	64.90	64.10	64.30
TiO_2	0.13	0.08	0.07	0.09	0.04	0.10	0.00	0.00	0.00	0.00	0.00	0.06	0.00	0.00
Al_2O_3	30.90	31.40	32.20	30.70	31.60	30.80	21.20	21.10	22.20	21.00	21.60	21.70	21.90	21.50
FeO		0.40	0.40	0.40	0.40	0.00	0.20	0.27	0.26	0.56	0.23	0.28	0.25	0.23
MgO	0.00	0.00	0.00	0.00	0.00	0.00	0.02	0.00	0.00	0.02	0.00	0.23	0.00	0.00
MnO	0.00	0.00	0.00	0.00	0.06	0.00	0.00	0.00	0.00	0.00	0.00	0.00	0.00	0.00
Cao	14.80	14.70	16.20	15.80	15.30	14.80	1.30	1.10	1.40	1.20	1.60	1.30	1.40	1.20
Na_2O	3.15	3.10	2.53	2.50	2.73	3.13	7.40	7.20	7.90	8.00	8.80	6.80	7.70	7.80
K_2O	0.29	0.35	0.12	0.21	0.25	0.36	5.25	6.05	4.81	4.22	4.97	4.64	5.40	5.33
total	100.57	100.83	100.42	99.8	100.08	100.49	100.47	100.52	100.67	100.1	100.7	99.91	100.75	100.35
Si	9.21	9.21	8.85	9.01	9.00	9.22	11.59	11.58	11.50	11.60	11.37	11.55	11.48	11.49
Ti	0.02	0.01	0.01	0.01	0.01	0.01	0.00	0.00	0.00	0.00	0.00	0.01	0.00	0.00
Al	6.75	6.71	7.08	6.93	6.96	6.73	4.45	4.44	4.55	4.41	4.56	4.55	4.55	4.53
Fe	0.00	0.06	0.06	0.06	0.06	0.00	0.03	0.04	0.04	0.08	0.03	0.04	0.04	0.03
Mg	0.00	0.00	0.00	0.00	0.00	0.00	0.01	0.00	0.00	0.01	0.00	0.06	0.00	0.00
Mn	0.00	0.00	0.00	0.00	0.01	0.00	0.00	0.00	0.00	0.00	0.00	0.00	0.00	0.00
Ca	2.85	2.85	3.14	3.04	2.97	2.85	0.25	0.21	0.26	0.23	0.31	0.25	0.26	0.23
Na	1.10	1.09	0.89	0.87	0.96	1.09	2.55	2.49	2.67	2.76	3.05	2.35	2.63	2.70
K	0.07	0.08	0.03	0.05	0.06	0.08	1.19	1.38	1.07	0.96	1.13	1.05	1.21	1.22
total	19.98	20.01	20.06	19.97	20.02	19.99	20.06	20.14	20.09	20.05	20.45	19.86	20.17	20.20
An	71	71	77	77	74	71	6	5	7	6	7	7	6	6
Ab	27	27	22	22	24	27	64	61	67	70	68	64	64	65
Or	2	2	1	1	1	2	30	34	27	24	25	29	30	29

sS	R107-plag4-i1	R107-plag4-r	R107-plag5-c	R107-plag5-i	R107-plag5-i2	R107-plag5-r	R107-plag6	R107-plag7	R129-plag	R129-plag	R129-plag	R131-plag	R131-plag2	R131-plag3
SiO_2	65.60	64.90	65.50	65.30	64.80	64.60	64.80	68.30	50.40	50.81	52140	51.70	49.80	49.50
TiO_2	0.00	0.00	0.00	0.00	0.00	0.00	0.00	0.00	0.00	0.00	0.00	0.00	1.29	1.92
Al_2O_3	20.80	21.30	21.00	21.20	20.90	20.60	22.00	19.70	31.70	30.87	30.80	0.00	4.00	4.40
FeO	0.17	0.22	0.14	0.18	0.13	0.23	0.26	0.32	0.56	0.64	0.49	4.30	4.90	7.40
MgO	0.00	0.29	0.00	0.00	0.00	0.00	0.00	0.00	0.08	0.12	0.06	17.00	16.50	13.60
MnO	0.00	0.00	0.00	0.00	0.00	0.00	0.00	0.00	0.00	0.00	0.00	0.00	0.00	0.00
Cao	0.90	1.10	1.10	0.90	1.10	0.80	1.60	0.40	12.30	12.67	13.30	22.70	23.00	22.50
Na_2O	7.60	7.80	7.90	8.20	7.20	7.10	7.00	4.60	4.60	3.76	3.50	0.50	0.60	0.60
K_2O	5.90	5.19	5.16	4.58	6.46	7.07	4.56	7.47	0.57	0.51	0.50	0.00	0.02	0.11
total	100.97	100.8	100.8	100.36	100.59	100.4	100.22	100.79	100.21	99.38	100.05	96.2	100.11	100.03
Si	11.70	11.58	11.67	11.65	11.59	11.66	11.56	12.05	9.56	9.32	9.44	10.53	9.88	9.85
Ti	0.00	0.00	0.00	0.00	0.00	0.00	0.00	0.00	0.00	0.00	0.00	0.00	0.19	0.29
Al	4.31	4.41	4.34	4.39	4.40	4.31	4.56	4.10	6.45	6.67	6.54	0.00	0.92	1.03
Fe	0.02	0.03	0.02	0.03	0.02	0.03	0.04	0.05	0.08	0.10	0.07	0.73	0.80	1.23
Mg	0.00	0.08	0.00	0.00	0.00	0.00	0.00	0.00	0.02	0.03	0.02	5.16	4.78	4.03
Mn	0.00	0.00	0.00	0.00	0.00	0.00	0.00	0.00	0.00	0.00	0.00	0.00	0.00	0.00
Ca	0.17	0.21	0.21	0.17	0.21	0.15	0.30	0.08	2.27	2.49	2.57	4.95	4.79	4.79
Na	2.59	2.66	2.69	2.79	2.50	2.45	2.38	1.57	1.54	1.34	1.22	0.20	0.23	0.23
K	1.32	1.16	1.15	1.03	1.47	1.60	1.02	1.68	0.13	0.12	0.11	0.00	0.00	0.03
total	20.11	20.13	20.08	20.06	20.19	20.21	19.86	19.53	20.05	20.02	19.96	21.57	21.59	21.48
An	4	5	5	4	5	4	8	2	58	63	66	96	95	95
Ab	63	66	66	70	60	58	64	47	39	34	31	4	5	5
Or	32	29	29	26	35	38	28	50	3	3	3	0	0	1

sS	R131-plag4-c	R131-plag4-r	R131-plag5
SiO_2	50.30	48.60	51.20
TiO_2	0.14	0.10	0.15
Al_2O_3	31.00	31.90	31.00
FeO	0.47	0.56	0.48
MgO	0.02	0.00	0.00
MnO	0.00	0.00	0.00
Cao	14.20	15.50	14.40
Na_2O	3.30	2.60	3.40
K_2O	0.29	0.19	0.21
total	99.73	99.57	100.76
Si	9.22	8.97	9.27
Ti	0.02	0.01	0.02
Al	6.69	6.94	6.62
Fe	0.07	0.09	0.07
Mg	0.01	0.00	0.00
Mn	0.00	0.00	0.00
Ca	2.79	3.06	2.79
Na	1.17	0.93	1.19
K	0.07	0.04	0.05
total	20.04	20.04	20.02
An	69	76	69
Ab	29	23	30
Or	2	1	1

Table 3.6
Nepheline Analyses

sample	R25-neph1	R25-neph2	R25-neph3-c	R25-neph3-r	R25-neph3-i	R25-neph4	R25-neph5	R25-neph6	R25-neph7	R25-neph8	R25-neph9	R38-neph1	R38-neph1	R38-neph1
SiO_2	47.54	47.14	45.30	43.65	45.69	45.11	45.20	45.30	43.68	50.10	53.30	45.01	46.70	46.26
TiO_2	0.00		0.00	0.00	0.00	0.00			0.00		0.60	0.00		0.00
Al_2O_3	32.65	32.75	34.14	33.95	32.98	32.85	32.30	34.40	33.41	31.10	25.90	32.69	33.90	32.83
FeO	0.59	0.78	0.58	0.58	0.58	0.49	0.54		0.00	2.20	2.10	0.87	0.70	0.78
CaO	0.00	0.49	0.00	0.00	0.00	0.00			0.00		0.90	0.00		0.00
Na_2O	15.68	15.48	14.55	17.65	16.78	16.85	17.65	16.30	18.14	11.00	15.10	16.49	16.30	15.68
K_2O	3.82	4.02	4.95	5.04	4.75	4.85	4.75	4.80	4.90	5.00	0.30	5.04	5.00	4.70
total	100.28	100.66	99.52	100.88	100.78	100.14	100.44	100.80	100.13	99.40	98.20	100.10	102.60	100.25
Si	8.90	8.83	8.59	8.31	8.63	8.59	8.60	8.51	8.36	9.38	9.98	8.59	8.64	8.74
Ti	0.00	0.00	0.00	0.00	0.00	0.00	0.00	0.00	0.00	0.00	0.08	0.00	0.00	0.00
Al	7.20	7.23	7.63	7.62	7.34	7.37	7.25	7.62	7.54	6.86	5.72	7.35	7.39	7.31
Fe	0.09	0.12	0.09	0.09	0.09	0.08	0.09	0.00	0.00	0.34	0.33	0.14	0.11	0.12
Ca	0.00	0.10	0.00	0.00	0.00	0.00	0.00	0.00	0.00	0.00	0.18	0.00	0.00	0.00
Na	1.42	1.41	1.34	1.63	1.54	1.55	1.63	1.48	1.68	1.00	1.37	1.52	1.46	1.44
K	0.23	0.24	0.30	0.31	0.29	0.29	0.29	0.29	0.30	0.30	0.02	0.31	0.30	0.28
total	17.85	17.92	17.95	17.95	17.88	17.88	17.85	17.90	17.88	17.89	17.68	17.91	17.90	17.89

sample	R38-neph1	R38-neph1	R38-neph2	R38-neph2	R38-neph2	R38-neph3	R38-neph4	R38-neph4	R38-neph5	R38-neph5	R38-neph5	R38-neph6	R38-neph7	R38-neph7
SiO_2	46.83	46.45	46.06	48.00	45.77	46.16	45.77	44.81	46.46	46.46	47.60	49.30	46.10	46.80
TiO_2	0.00	0.00	0.00		0.00	0.00	0.00	0.00	0.00	0.00				
Al_2O_3	32.77	32.93	33.22	33.40	32.44	32.83	32.73	32.98	33.37	32.50	32.40	32.10	33.10	32.70
FeO	1.19	0.98	1.47	1.00	1.27	0.88	0.69	0.87	1.07	0.78	1.20	2.50	0.80	0.80
CaO	0.00	0.00	0.00		0.00	0.00	0.00	0.00	0.00	0.00		0.70		
Na_2O	15.15	14.99	15.48	14.30	15.97	16.27	15.88	16.49	14.16	15.13	14.50	11.70	16.00	14.90
K_2O	4.75	5.10	4.61	4.40	4.61	4.70	4.80	4.85	4.85	4.75	4.60	4.20	4.80	4.90
total	100.68	100.45	100.84	101.10	100.06	100.84	99.86	100.01	99.91	99.62	100.30	100.50	100.80	100.10
Si	8.80	8.76	8.67	8.90	8.70	8.70	8.70	8.55	8.77	8.81	8.94	9.16	8.68	8.83
Ti	0.00	0.00	0.00	0.00	0.00	0.00	0.00	0.00	0.00	0.00	0.00	0.00	0.00	0.00
Al	7.26	7.32	7.37	7.30	7.27	7.29	7.33	7.41	7.42	7.26	7.17	7.03	7.34	7.27
Fe	0.19	0.15	0.23	0.16	0.20	0.14	0.11	0.14	0.17	0.12	0.19	0.39	0.13	0.13
Ca	0.00	0.00	0.00	0.00	0.00	0.00	0.00	0.00	0.00	0.00	0.00	0.14	0.00	0.00
Na	1.38	1.37	1.41	1.29	1.47	1.49	1.46	1.52	1.29	1.39	1.32	1.05	1.46	1.36
K	0.28	0.31	0.28	0.26	0.28	0.28	0.29	0.30	0.29	0.29	0.28	0.25	0.29	0.29
total	17.91	17.91	17.96	17.90	17.92	17.89	17.89	17.92	17.94	17.88	17.89	18.02	17.90	17.88

sample	R38-neph8	R38-neph8-	R38-neph9	R38-neph10	R107-neph1	R107-neph1	R107-neph2	R107-neph33	R107-neph4	R107-neph5	R107-neph6	R107-neph7	R107-neph8	R107-neph9
SiO_2	48.60	50.90	45.50	46.20	67.43	67.12	65.48	66.22	66.14	66.20	68.21	67.03	67.33	68.00
TiO_2						0.00	0.58	0.60	0.50		0.00	0.00	0.00	
Al_2O_3	33.20	31.60	32.67	32.17	18.52	19.30	21.53	21.61	21.85	21.80	20.45	19.89	21.17	21.30
FeO	0.80	2.40	1.20	0.70		0.58	0.00				0.00	0.00	0.00	
CaO	0.50	0.30				0.00	1.07	0.90	1.60	1.40	0.69	0.49	0.69	0.60
Na_2O	12.80	11.00	16.40	16.10	3.30	5.43	7.47	7.70	7.90	8.10	8.04	7.94	7.64	7.20
K_2O	4.90	3.70	4.90	4.70	11.30	7.76	3.88	3.90	2.90	3.10	3.43	4.02	3.72	3.80
total	100.80	99.90	100.67	99.87	100.55	100.20	100.01	100.93	100.89	100.60	100.81	99.37	100.55	100.90
Si	9.01	9.41	8.63	8.78	12.12	11.99	11.59	11.61	11.57	11.62	11.91	11.92	11.80	11.85
Ti	0.00	0.00	0.00	0.00	0.00	0.00	0.08	0.08	0.07	0.00	0.00	0.00	0.00	0.00
Al	7.25	6.89	7.30	7.20	3.92	4.07	4.49	4.47	4.51	4.51	4.21	4.17	4.37	4.37
Fe	0.12	0.37	0.19	0.11	0.00	0.09	0.00	0.00	0.00	0.00	0.00	0.00	0.00	0.00
Ca	0.10	0.06	0.00	0.00	0.00	0.00	0.20	0.17	0.30	0.26	0.13	0.09	0.13	0.11
Na	1.15	0.99	1.51	1.48	0.29	0.47	0.64	0.65	0.67	0.69	0.68	0.68	0.65	0.61
K	0.29	0.22	0.30	0.28	0.65	0.44	0.22	0.22	0.16	0.17	0.19	0.23	0.21	0.21
total	17.92	17.94	17.92	17.86	16.98	17.06	17.22	17.20	17.28	17.26	17.12	17.09	17.16	17.15

sample	R107-neph10	R107-neph11	R107-neph12	R107-neph13	R107-neph14	R107-neph15
SiO_2	67.82	67.23	68.50	66.10	66.40	67.03
TiO_2	0.00	0.00	0.00			0.00
Al_2O_3	20.58	20.48	20.48	21.70	21.70	19.31
FeO	0.00	0.00	0.00			0.59
CaO	0.69	0.69	0.59	1.40	1.60	0.39
Na_2O	7.64	8.04	7.94	7.60	7.30	6.96
K_2O	3.72	3.14	3.23	3.00	3.50	6.57
total	100.45	99.57	100.74	99.80	100.50	100.84
Si	11.89	11.87	11.94	11.66	11.66	11.91
Ti	0.00	0.00	0.00	0.00	0.00	0.00
Al	4.25	4.26	4.21	4.51	4.49	4.04
Fe	0.00	0.00	0.00	0.00	0.00	0.09
Ca	0.13	0.13	0.11	0.26	0.30	0.07
Na	0.65	0.69	0.67	0.65	0.62	0.60
K	0.21	0.18	0.18	0.17	0.20	0.37
total	17.13	17.13	17.11	17.26	17.27	17.09

Appendix 4
Mineral Analyses. Trace Elements.

A4.1 Methodology.

Trace element concentrations in minerals were determined using a inductively coupled plasma- mass spectrometer- laser probe (ICP-MS) housed at Memorial University of Newfoundland. An outline of the procedure used in this study is similar to that described by Jenner et al. (1993) and is briefly outlined below.

The system uses a Q-switched NdYAG laser operating at the fundamental wavelength of 1064 nm which has been modified by the introduction of frequency-quadrupling hardware resulting in a laser beam with a wavelength of 266 nm (Jackson et al., 1992). The 266 nm laser pulses were attenuated to the working energy of 1mJ/pulse by using a ratable half-wave plate and thin glass laser calcite polarizer. Ablated material was flushed in a continuous flow of argon into the torch of an ICP-MS. For runs one through five a SCIEX ELAN model 250 ICP-MS was used. Instrumentation, optimization, and operating conditions were described by Jackson et al. (1992). For runs six through eight a Fisons PQ2 was used. Data on up to 22 elements were determined using rapid peak jumping with dwell times of between 8 ms and 17ms for each element. Instrument background levels were established by acquiring data for approximately 20s prior to commencing ablation for each analysis.

For calibration purposes, spiked silicate glass reference material NIST610 was analyzed twice for approximately 20s before and after each run. Correction for differences in ablation yield between standard and sample was achieved by use of Ca (for pyroxene and olivine) and Ti (magnetite) as internal standards, based on electron microprobe analyses. Part of the time resolved signal for each analysis was then isolated (Figure A4-1) for calculation of concentrations using the procedure outline in Jackson et al., 1992.

Table A4.1
Trace element concentrations of the titanaugites

sample#	R36-px1-c	R36-px1-r	R36-px2-r1	R36-px2-i1	R36-px2 c	R36-px2-i2	R36-px3-r	R36-px3-c	R36-px4-c	R36-px5-c	R36-px6-c	R36-px7-c	R36-px8-c	R36-px-8r
Run #	1	1	1	1	1	1	1	1	2	2	2	2	3	3
V	277.99	355.51	289.36	380.56	394.65	364.98	268.87	338.90	270.09	284.80	315.56	304.58	299.7	283.7
Rb	0.2	0.9	3.8	3.1	3.4	0.3	1.1	1.1						
Sr	92.2	113.2	113.6	114.3	115.1	118.3	105.9	103.7					85.9	83.6
Y	10.5	14.7	14.2	13.7	12.5	14.9	13.1	12.4	10.89	12.26	10.41	12.23	14.3	11.9
Zr	63.0	90.3	88.9	87.5	84.7	100.3	78.6	83.2	69.7	80.1	56.3	66.5	89.0	79.9
Nb	0.4	0.5	0.6	0.5	0.4	0.4	0.8	0.6	0.5	0.6	0.4	0.4	1.9	0.4
Cs	0.1	0.0	0.0		0.1	0.0		0.0					0.7	
Ba	0.8	0.7	2.8	2.8	2.4	1.1	0.5	1.7	0.1	0.1	0.3	0.1	2.1	1.3
La	3.4	5.0	4.9	4.7	4.6	5.6	4.3	4.5	3.4	3.9	2.6	3.2	3.6	3.7
Ce	16.1	21.6	20.8	24.9	23.6	24.1	22.0	20.9	14.9	17.1	11.1	13.9	16.2	15.0
Pr	2.6	3.8	4.0	3.6	3.6	4.1	3.5	3.7					3.6	2.4
Nd	13.9	19.3	21.4	19.1	17.0	21.7	17.9	19.2	12.3	14.8	10.4	13.5	12.9	14.2
Sm	3.1	6.2	6.3	5.7	6.2	6.5	5.4	5.5					4.6	4.5
Eu	1.6	2.3	1.7	1.9	2.2	2.2	2.6	1.7					1.8	1.5
Gd	4.5	5.5	5.1	4.4	5.2	5.0	5.7	4.4					0.8	4.4
Dy	3.6	3.7	3.6	3.7	4.0	4.3	4.1	3.3					1.5	3.7
Er	0.9	0.9	1.5	0.9	2.0	1.5	1.3	1.5	1.0	1.0	1.1	1.1	0.8	1.3
Yb	0.7	0.9	1.1	1.1	1.1	1.1	0.3	0.8					-0.3	0.5
Hf	3.0	4.1	4.7	3.7	3.4	4.0	3.0	2.8	2.7	2.7	2.2	3.0	2.7	2.3
Ta	0.1	0.1	0.1	0.1	0.3	0.1	0.0	0.1	0.1	0.1	0.1	0.1	0.0	0.1
Th	0.0	0.1	0.1	0.0	0.0	0.1	0.0	0.1	0.0	0.1	0.0	0.0	0.0	0.1

sample#	R36-px9-c1	R36-px9-c2	R36-px9-r1	R36-px10-r1	R36-px10-r2	R36-px10-i1	R36-px10-c	R36-px10-i2	R81-px1-r1	R81-px1-i	R81-px1-c	R81-px1-r2	R81-px2-c	R81-px2-r
Run #	3	3	3	3	3	3	3	3	5	5	5	5	5	5
V	297.7	278.0	317.5	303.2	289.36	380.56	394.65	364.98	252.24	322.82	486.16	328.44	362.69	724.51
Rb	2.2	1.5			3.8	3.1	3.4	0.3						2.3
Sr	88.5	85.9	100.2	105.5	113.6	114.3	115.1	118.3	101.6	106.2	110.7	113.5	100.1	121.4
Y	14.3	10.4	14.6	15.7	14.2	13.7	12.5	14.9	11.0	13.4	13.9	15.0	11.3	15.6
Zr	97.1	76.1	91.2	96.6	88.9	87.5	84.7	100.3	69.9	90.1	90.7	99.1	79.5	122.9
Nb	0.6	0.6	0.6	0.5	0.6	0.5	0.4	0.4	0.2	0.4		0.9	0.5	0.8
Cs					0.0		0.1	0.0						
Ba		2.0				2.8	2.4	1.1			1.2			3.0
La	4.5	2.6	4.5	4.2	4.9	4.7	4.6	5.6	4.0	4.9	5.0	4.7	2.9	5.8
Ce	16.2	10.9	16.7	18.1	20.8	24.9	23.6	24.1	16.7	17.2	17.7	23.9	15.4	26.7
Pr	3.3	2.5	3.5	3.4	4.0	3.6	3.6	4.1	3.1	3.3	3.7	3.9	2.9	4.0
Nd	18.7	9.8	17.4	20.4	21.4	19.1	17.0	21.7	17.2	21.7	22.0	22.7	13.5	22.2
Sm	4.2	6.0	5.0	6.0	6.3	5.7	6.2	6.5	4.9	8.1	4.8	6.2	3.0	3.2
Eu	1.7	1.0	2.1	2.0	1.7	1.9	2.2	2.2	1.9	1.6	1.4	2.2	1.4	2.3
Gd	4.7	2.8	5.0	6.9	5.1	4.4	5.2	5.0	5.4	2.7	4.2	6.5	3.5	3.5
Dy	4.0	4.8	3.7	4.1	3.6	3.7	4.0	4.3	2.6	2.9	2.2	3.6	2.1	4.6
Er	0.9	1.2	1.3	1.1	1.5	0.9	2.0	1.5	0.9	1.1	2.2	1.5	1.6	
Ybb	2.0	0.0	1.0	1.6	1.1	1.1	1.1	1.1		0.8	2.6	0.7		
Hf	3.6	4.8	4.5	3.4	4.7	3.7	3.4	4.0	2.6	3.7	5.1	4.0	2.3	3.6
Ta	0.1	0.1	0.1	0.2	0.1	0.1	0.3	0.1	0.1		0.2	0.1		0.5
Th	0.3	0.0	0.0	0.0	0.1	0.0	0.0	0.1					0.1	

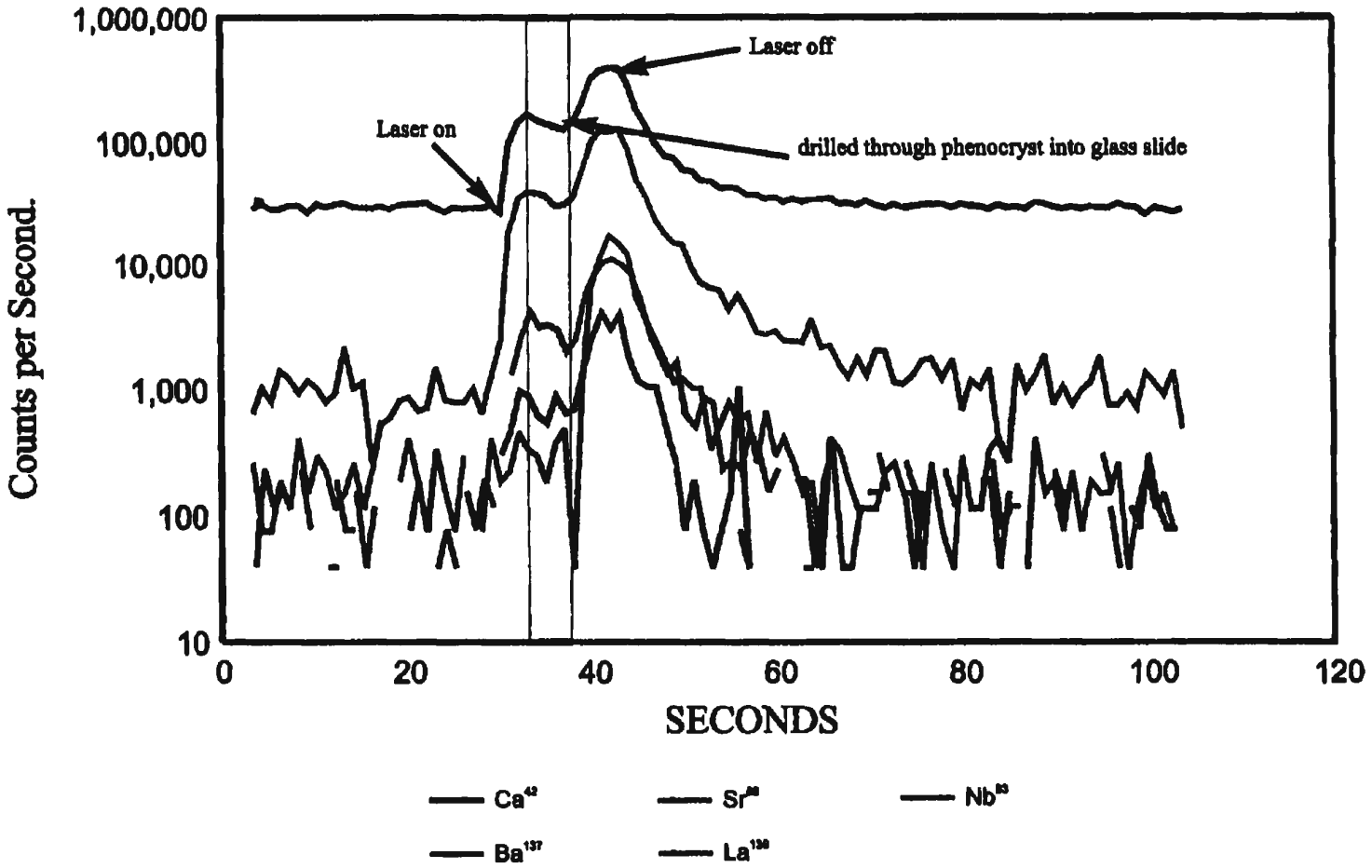

Figure 4A-1: A sample spectrum of the data collected during analysis of a pyroxene (JA24e04). From 0 to *ca.* 30 seconds background count rates are collected while from *ca.* 32-36 seconds (shown by yellow band) data were acquired on the pyroxene. Between *ca.* 36 and 42 seconds data acquisition continued but the beam had drilled through into the glass slide, as shown by the jump in concentrations of all the elements.

Table A4.2
Trace element concentrations of diopside-augites

sample#	R94-px1-r	R94-px1-c	R94-px2-c	R42-px1-c	R42-px2c
Run #	6	6	6	4	4
V	175.86	183.69	171.69	151.89	184.61
Rb			0.37		
Sr	95.23	92.05	87.96	77.29	98.7
Y	8.99	9.44	8.22	5.63	6.94
Zr	50.06	49.66	44.28	24.83	30.88
Nb	0.44	0.32	0.30		
Ba	1.33		0.52		
La	3.38	3.05	2.97	2.34	2.81
Ce	11.61	11.94	11.28	6.98	9.89
Pr	2.24	2.69	2.06	1.42	1.7
Nd	11.03	11.50	10.10	6.12	9.67
Sm	3.35	3.55	3.08	2.21	
Eu	1.16	1.43	1.06	0.54	0.5
Gd	3.18	3.07	3.22		
Dy	2.02	2.19	2.04		
Er	0.81	0.71	0.90		
Yb	0.54	0.61	0.38		
Hf	2.77	2.63	2.02		
Ta	0.07	0.08	0.07		2.33
Th		0.03	0.02		

Table A4.3
Trace element concentrations of POPPs

sample #	R94-pxl-c1	R94-pxl-c2	R94-pxl-c3	R94-pxl-c4	R94-pxl-c5	R94-pxl-c6	R94-pxl-r1	R94-pxl-r2	R94-pxl-r3	R74-pxl-c1	R74-pxl-c2	R74-pxl-c3	R74-pxl-r	R74-pxl-i3
Run #	6	6	6	6	6	6	6	6	65	7	7	7	7	7
V	204.16	219.09	197.12	206.44	170.60	169.12	320.53	343.96	377.77	160.82	163.75	178.19	340.52	301.27
Rb	1.97	9.97	1.28	2.59		1.42	1.06		10.58	0	0.02	0.61	-0.01	-0.01
Sr	78.75	89.37	80.81	75.95	83.38	80.68	117.35	114.09	152.27	70.24	71.78	69.46	93.85	97.96
Y	10.38	9.38	10.31	9.74	8.91	7.28	17.41	21.22	25.04	6.26	7.65	7.04	14.34	15.83
Zr	45.09	60.92	40.94	40.43	36.72	26.21	106.55	143.71	180.80	26.18	25.05	25.07	98.77	103.52
Nb		0.73		0.35	0.87	0.52	0.79	1.46	1.83		0.19	0.27	0.39	0.71
Cs		1.26								0.06	0.20			
Ba	6.67	62.66	7.82	9.55	12.51	8.02	9.16	2.28	55.75	2.02	2.76	1.15	0.14	0.47
La	2.13	2.68	2.11	2.18	2.67	1.92	5.95	6.79	10.78	1.43	1.69	1.50	4.66	4.88
Ce	7.03	9.64	8.92	8.46	9.04	7.81	21.50	23.80	39.67	5.33	5.36	5.14	14.99	17.19
Pr	1.38	2.03	1.74	1.82	1.79	1.38	4.26	4.88	7.88	0.99	1.23	1.03	2.70	3.68
Nd	8.26	9.79	8.53	8.57	8.96	7.98	21.13	25.30	34.80	6.31	6.62	5.34	13.72	19.17
Sm	3.06	2.91	3.32	2.90	2.43	1.40	5.88	6.39	11.28	1.56	2.33	2.24	5.13	5.37
Eu	0.66	1.20	0.94	0.79	1.06	0.85	2.45	2.51	3.13	0.66	0.93	0.91	1.44	1.59
Gd	2.20	3.26	4.06	3.13	2.42	2.61	5.22	6.42	8.45	1.13	1.86	2.69	3.93	4.57
Dy	2.50	2.88	2.43	2.11	2.13	2.11	4.23	5.09	6.52	1.89	1.86	0.81	3.29	3.42
Er	0.78	0.74	0.87	1.08	0.81	0.74	2.07	2.00	2.56	0.40	0.52	0.40	1.18	1.44
Yb		0.76	0.77	0.63	0.34	0.62	0.98	0.96	1.34	0.36	0.18	0.45	0.57	0.83
Hf	2.00	2.81	2.13	2.07	2.08	1.10	5.49	7.94	7.43	0.56	0.25	1.12	4.79	3.23
Ta		0.05	0.05	0.06	0.13		0.28	0.24	0.31	0.10	-0.02	0.05	0.16	0.06
Th		0.14	0.04	0.07	0.06	0.08	0.09	0.14	0.33	0.02	0.05	0.05	0.02	0.03

sample#	R74-px1-i2	R74-px1-i1	R66-px1-c1	R66-px1-c2	R66-px1-c3	R66-px1-c4	R66-px1-c5	R66-px1-r1	R66-px1-r2	R66-px1-r3	R66-px1-r3	R42-px1-c1	R42-px1-c3	R42-px1-c2
Run #	7	7	8	8	8	8	8	8	8	8	8	4	4	4
V	307.04	271.36	161.97	158.49	189.42	158.53	157.16	165.41	179.17	174.44	146.45	224.9	262.64	243.56
Rb			1		0.47		0.31		0.04	0.32	0.04	-		2.25
Sr	93.32	89.80	321.30	319.49	331.53	331.65	314.65	114.75	101.58	167.72	89.34	106.03	97.1	98.28
Y	15.30	13.11	22.24	20.61	22.88	19.79	20.00	9.94	8.63	12.48	7.41	8.49	9.56	6.98
Zr	94.52	85.70	338.78	294.99	316.39	303.19	296.76	95.60	52.20	116.07	42.53	33.58	57.47	35.35
Nb	0.49	0.44	3.61	2.87	2.74	2.21	2.39		0.57	1.26	0.36	-		
Cs	-0.01	0.08	1.00	0.15	0.08		0.02		0.08	0.04	0.03	-		
Ba	0.42	0.66	0.44	5.47	2.86	0.85	1.67	14.32	0.19	3.43	0.54	-		8.85
La	4.74	3.72	16.36	16.85	21.99	18.68	20.02	7.05	4.78	9.53	3.85	3.01	3.3	2.99
Ce	16.72	15.29	53.02	47.66	66.97	54.26	55.25	17.56	16.79	30.20	14.35	11.79	11.31	12.24
Pr	3.33	2.91	9.36	8.10	10.60	9.78	9.52	2.92	2.80	5.19	2.23	2.05	1.89	1.79
Nd	15.29	14.89	30.68	37.07	41.44	37.53	37.58	12.02	12.02	19.94	9.91	10.81	11.73	9.74
Sm	4.74	5.25	8.15	8.29	10.14	8.99	9.04	7.95	3.86	4.67	3.06	3.53	3.32	2.26
Eu	1.98	1.34	2.90	1.90	3.54	2.49	3.07	1.21	1.18	1.86	1.07	0.9		0.55
Gd	5.12	4.00	5.65	6.74	8.02	6.54	6.09	1.76	2.51	3.71	2.60			
Dy	3.26	2.34	4.66	4.46	5.20	5.04	5.16	1.73	1.81	2.95	1.48			
Er	1.15	1.30	2.08	1.10	2.17	2.16	1.24	0.43	0.68	0.93	0.66			
Yb	0.55	1.24	2.46	0.83	1.38	1.39	1.43	0.47	0.50	0.61	0.47	0.53		
Hf	3.71	4.02	15.59	8.27	11.77	12.09	12.53	6.66	2.61	5.14	2.03			
Ta	0.16	0.16	0.53	0.55	0.67	0.46	0.42	-0.09	0.12	0.25	0.05	1.96	3.29	1.48
Th	0.05	0.07	0.17	0.39	0.20	0.33	0.18	0.12	0.13	0.18	0.02	-		

sample#	R42-px1-c4	R42 - px1-r1	R42 - px1-r2
Run #	4	4	4
V	190.09	296.81	376.87
Rb		8.37	7.09
Sr	67.65	139.45	122.09
Y	7.25	25.93	26.37
Zr	32.15	265.47	217.41
Nb		30.67	14.33
Cs			
Ba		37.39	29.52
La	2.14	18.93	12.44
Ce	7.72	56.34	36.16
Pr	1.3	7.47	6.15
Nd	8	34.93	33.77
Sm	2.72	9.82	9.41
Eu	0.56	2.73	2.71
Gd			
Dy			
Er			
Yb		1.92	2.91
Hf			
Ta	1.92	10.43	9.45
Th		174	0.91

Tabble A4.5
Trace element concentrations of magnetites

SS	R36 - mt1	R36 - mt1	R36 - mt2	R36 - mt2	R36 - mt3	R36 - mt3	R36 - mt4	R36 - mt4	R36- mt5	R36mt6	R81- mt1	R81- mt2	R81- mt3
Run #	1	1	1	1	1	1	1	1	1	1	5	5	5
Y	0.36	0.13	0.31	0.34	0.12	0.3	0	0	0.27	0.11	0.6	0	0.3
Zr	35.7	32.4	51.7	81	28.1	54.6	24.6	23.8	41.47	19.77	28.2	29.3	30
Rb													3
Nb	8	6.3	8.3	10.9	6.3	7.1	6.8	6.8	7.54	1.53	7	7.4	8.1
Yb						0.2	0.3	0.3	0.25	0.03			0.3
Hf	1	0.9	1.3	1					1.06	0.19	2		1.7
Ta	0.8	0.6	0.6	0.6	0.6	0.4	0.9	0.8	0.65	0.18	1.7	0.4	

Table A4.6
Trace element concentration of glass

	R36- glass	R36- glass	R36- glass	R36- glass	R36- glass	R36- glass	R81 glass	R81 glass	R81 glass	R81 glass
Run #	1	1	1	1	1	5	5	5	5	5
Rb	93.09	96.12	92.01	96.09	88.88	98.62	35.88	21.01	34.92	48.49
Sr	475.87	420.25	455.02	530.20	368.83	459.78	857.09	1059.08	872.62	964.81
Y	24.91	23.70	25.63	21.17	20.73	20.14	24.51	21.30	24.05	27.58
Zr	367.05	314.05	356.15	303.86	309.81	269.47	273.72	220.58	272.04	293.83
Nb	97.12	82.34	84.47	84.13	93.40	72.61	55.72	39.20	57.80	62.85
Cs	0.95	0.57	0.82	1.04	0.16	1.18	0.92	0.43	0.49	1.66
Ba	614.15	144.40	90.39	135.49	229.57	200.78	453.49	468.03	388.31	510.50
La	44.28	44.70	40.41	43.63	37.09	41.53	45.91	35.67	44.50	50.94
Ce	95.86	110.42	96.13	93.64	88.16	114.42	98.66	71.79	91.70	105.63
Pr	11.41	10.68	11.23	11.51	10.39	11.18	13.08	9.29	12.53	12.69
Nd	41.46	45.86	47.33	45.95	41.75	44.65	56.27	44.10	52.51	59.53
Sm	8.94	7.46	8.99	9.03	7.54	9.08	13.17	8.96	8.51	14.16
Eu	2.64	2.46	2.41	2.66	2.49	2.44	3.42	4.14	3.62	3.97
Gd	7.19	6.55	6.66	7.26	6.61	6.73	8.76	8.97	8.89	8.51
Dy	5.51	5.28	4.78	5.56	5.34	4.83	6.20	5.89	5.28	6.18
Er	1.96	2.33	2.42	2.22	1.94	2.34	2.63	2.78	2.91	2.20
Yb	1.57	1.22	0.96	1.59	1.23	0.97	1.21	1.92	1.20	1.51
Hf	7.21	6.23	7.00	7.38	7.03	6.11	5.53	4.10	6.12	6.95
Ta	4.54	4.36	4.80	5.09	5.07	3.68	2.92	2.36	3.29	3.38
Th	5.06	4.34	4.29	4.97	4.79	4.27	5.01	3.50	4.78	5.46

Table A4.6
Detection Limits for Individual Runs
(nd-not determined)

Run	1	2	3	4	5	6	7	8
Rb	0.41	0.10	0.24	1.54	0.54	0.08	0.22	0.06
Sr	0.45	nd	0.18	0.44	0.09	0.09	0.24	0.07
Y	0.09	0.02	0.11	0.26	0.09	0.03	0.08	0.02
Zr	0.06	0.04	0.10	0.06	0.19	0.13	0.34	0.10
Nb	0.15	0.02	0.17	0.23	0.13	0.06	0.12	0.04
Cs	0.08	nd	0.11	0.09	nd	0.04	0.14	0.04
Ba	0.11	0.08	0.08	0.13	nd	0.20	0.72	0.24
La	0.25	0.01	0.26	0.65	0.06	0.02	0.06	0.02
Ce	0.04	0.01	0.08	0.06	0.06	0.01	0.03	0.01
Pr	0.08	nd	0.08	0.10	0.05	0.02	0.05	0.02
Nd	0.03	0.05	0.07	0.05	0.24	0.05	0.15	0.05
Sm	0.15	nd	0.18	0.24	0.26	0.09	0.28	0.11
Eu	0.19	nd	0.22	0.20	0.10	0.02	0.07	0.02
Gd	0.06	nd	0.10	0.06	0.32	0.03	0.12	0.04
Dy	0.21	nd	0.26	0.15	0.19	0.04	0.16	0.05
Er	0.09	0.06	0.18	0.13	0.21	0.05	0.17	0.05
Yb	0.12	nd	0.20	0.16	0.31	0.06	0.25	0.01
Hf	0.20	0.08	0.27	0.20	0.30	0.01	0.04	0.08
Ta	0.19	0.02	0.25	0.18	0.09	0.04	0.19	0.06
Pb	0.04	nd	0.10	0.06	nd	0.01	0.04	0.01
Th	0.10	0.03	nd	0.18	0.12	0.01	0.04	0.02
U	0.07	nd	0.12	0.10	nd	0.01	0.02	0.01

Appendix 5

Primary magma, mantle source and partial melting calculations

Table A5.1
Calculated primary magma compositions and ratio of ol:px:mt added (sample # followed by * recalculated to 13 MgO wt. %; ** recalculated to 14 MgO wt. %)

Type I mafic samples

	R54	R36*	R77*	R53*	R94*	R113*	R134*	R129*	R83*	R19*	R52*	R81*	R130*	R84*
ol:px:mt	16:79:5	23:70:7	33:55:17	35:62:5	35:61:4	23:71:6	30:67:3	25:65:10	22:70:8	25:67:8	30:62:8	25:66:9	30:61:9	20::73:7
SiO_2	44.24	42.98	44.14	43.63	44.00	43.94	44.24	43.95	44.07	43.92	43.74	43.99	43.98	43.97
TiO_2	2.80	4.32	3.04	3.30	3.68	3.34	3.14	3.58	3.50	3.47	3.55	3.59	3.34	3.24
Al_2O_3	10.76	10.12	10.08	11.43	10.93	10.61	10.86	10.68	10.37	10.63	10.99	10.40	10.72	10.02
FeO	11.53	13.76	12.84	12.16	12.06	12.61	11.50	12.44	12.51	12.48	12.39	12.47	12.51	12.62
MnO	0.20	0.21	0.32	0.23	0.21	0.23	0.21	0.21	0.24	0.24	0.23	0.23	0.23	0.25
MgO	12.93	12.93	12.93	12.93	12.93	12.93	12.93	12.93	12.93	12.93	12.93	12.93	12.93	12.93
CaO	12.70	14.57	13.02	13.34	12.90	13.11	12.64	13.04	12.97	13.11	13.27	13.06	13.02	13.24
Na_2O	2.41	1.75	1.60	1.90	1.65	1.92	1.90	1.84	1.94	2.14	1.91	2.07	1.62	2.92
K_2O	1.42	0.45	1.36	1.47	1.26	1.10	1.63	1.31	1.29	1.30	1.63	1.48	1.08	0.57
P_2O_5	0.49	0.30	0.44	0.48	0.43	0.54	0.63	0.35	0.50	0.53	0.47	0.81	0.48	0.60
Rb	30.52	20.84	26.83	35.43	27.55	20.83	37.27	30.58	26.55	33.33	39.13	21.59	26.69	42.82
Ba	624.07	294.46	499.05	593.02	397.45	414.00	755.65	404.73	457.84	463.64	659.93	314.03	585.53	534.13
Sr	676.61	462.00	651.66	638.84	672.81	691.99	892.33	566.97	731.75	820.32	742.82	590.31	616.01	722.49
Ta		2.05			2.78	3.54		2.58		3.48		2.36		0.00
Nb	50.41	33.47	49.75	66.71	44.40	55.37	69.34	40.81	54.55	58.17	63.98	38.94	47.53	66.55
Hf		5.31			5.80	7.49		5.02		6.40		5.27		0.00
Zr	214.51	169.87	233.71	241.39	211.38	257.36	285.27	171.33	281.76	238.35	232.99	191.63	230.93	288.77
Y	17.54	16.86	20.24	20.04	20.19	21.19	23.70	16.66	21.96	20.73	19.43	20.01	20.35	22.29
Th	4.23	2.99	4.79	4.22	3.77	6.07	5.75	4.72	5.44	6.87	6.40	3.38	4.73	6.37
U	2.24	0.69	0.39	0.77	0.84	1.28	1.63	0.99	0.45	1.39	0.61	0.71	1.11	1.68
La		25.72			33.33	44.46		32.05		48.62	0.00	30.22		
Ce	127.35	56.01	90.95	116.01	71.94	94.39	141.78	68.75	108.42	99.52	122.38	67.74	85.97	136.67
Pr		6.88			9.10	11.51		8.32		11.74		8.79		
Nd		30.49			38.07	46.47		33.75		46.16		37.47		
Sm		6.81			8.34	9.47		7.05		9.16		8.10		
Eu		2.15			2.54	3.00		2.26		2.85		2.68		
Gd		0.00			0.00	0.00		0.00		0.00		0.00		
Tb		0.69			0.84	0.86		0.63		0.79		0.72		
Dy		4.40			4.73	5.44		4.19		5.13		4.80		
Ho		0.61			0.71	0.73		0.56		0.67		0.63		
Er		1.67			1.97	2.14		1.68		2.10		1.95		
Tm		0.18			0.22	0.23		0.17		0.21		0.19		
Yb		1.28			1.43	1.70		1.33		1.54		1.37		

	R51*	R50*	R46*	R111*	R89*
ol:px:mt	30:63:7	30:65:5	31:61:6	30:65:5	32:62:6
SiO_2	43.79	43.77	43.91	44.03	43.97
TiO_2	3.51	3.57	3.62	3.50	3.49
Al_2O_3	10.67	10.96	10.79	10.61	10.59
FeO	12.45	12.39	12.41	12.48	12.48
MnO	0.22	0.24	0.20	0.24	0.24
MgO	12.93	12.93	12.93	12.93	12.93
CaO	13.28	13.23	13.07	12.96	13.05
Na_2O	2.63	1.96	1.79	1.38	2.06
K_2O	0.51	1.48	1.26	1.26	1.17
P_2O_5	0.42	0.42	0.40	0.63	0.43
Rb	50.91	32.97	25.46	24.66	23.91
Ba	657.70	509.31	383.29	379.26	385.96
Sr	746.07	622.28	630.61	603.93	886.65
Ta				2.58	
Nb	57.73	56.70	48.08	44.75	47.94
Hf				5.93	
Zr	214.53	206.99	215.76	217.80	239.12
Y	17.75	17.72	19.80	20.64	21.04
Th	6.42	5.39	4.20	4.18	3.53
U	0.41	0.72	1.76	1.01	0.61
La				35.46	
Ce	110.41	103.26	80.49	78.81	96.57
Pr				10.02	
Nd				42.59	
Sm				8.77	
Eu				2.72	
Gd				0.00	
Tb				0.74	
Dy				5.02	
Ho				0.65	
Er				2.06	
Tm				0.20	
Yb				1.53	

Type II mafic samples

	R47*	R128*	R40*	R17*	R119*	R33*	R133*	R76*	R56*	R80*	R55*	R78*
ol:px:mt	35:65:0	27:73:0	31:69:0	33:68:0	23:76:0	30:67:0	31:68:1	30:68:2	28:68:4	33:65:2	26:70:4	31:63:6
SiO_2	45.67	45.68	45.99	45.35	45.57	45.46	45.55	45.17	45.53	45.48	45.48	45.49
TiO_2	2.86	2.73	2.85	3.30	3.13	3.17	3.20	3.20	3.17	3.30	3.24	3.17
Al_2O_3	11.32	10.70	10.73	11.22	11.20	11.43	11.08	11.90	11.25	11.38	11.48	11.13
FeO	11.48	12.34	11.06	12.25	11.79	11.74	11.99	11.65	11.77	11.71	11.72	11.78
MnO	0.17	0.15	0.19	0.22	0.22	0.20	0.22	0.23	0.20	0.22	0.25	0.25
MgO	12.96	12.96	12.96	12.96	12.96	12.96	12.96	12.96	12.96	12.96	12.96	12.96
CaO	11.92	12.10	11.62	12.36	12.07	12.16	12.12	12.44	12.11	12.13	12.10	12.17
Na_2O	1.68	1.38	2.48	1.37	1.53	1.55	1.67	1.86	1.42	1.72	1.67	2.77
K_2O	0.95	0.83	0.45	1.34	1.40	1.36	1.31	1.28	1.54	1.36	0.80	0.71
P_2O_5	0.49	0.51	0.41	0.57	0.45	0.44	0.48	0.53	0.45	0.40	0.40	0.37
Rb	13.25	5.31	5.91	26.23	30.90	28.02	22.44	61.44	37.42	24.58	17.18	63.56
Ba	554.54	225.30	256.88	417.80	567.09	526.28	368.34	585.71	518.53	443.83	448.41	563.61
Sr	466.61	313.99	448.82	615.54	604.65	619.68	536.98	1527.1	589.59	676.06	748.97	867.69
Ta	2.31	0.00	1.59	2.77	0.00	0.00	2.51	3.43	3.02	0.00	2.45	0.00
Nb	36.37	25.00	29.13	49.44	51.23	49.50	43.44	73.17	66.49	46.63	40.89	52.31
Hf	5.35		4.03	6.61			6.03	5.36	5.07		4.90	
Zr	175.53	131.00	467.59	254.51	225.13	217.04	214.74	268.92	257.17	225.26	170.24	208.83
Y	17.40	13.58	15.49	19.43	18.87	19.24	19.69	23.48	21.31	20.48	17.53	16.55
Th	4.24	1.10	2.36	5.38	5.11	5.09	4.57	7.17	6.02	3.82	4.64	4.64
U	0.86	1.27	0.49	1.15	0.63	0.19	1.06	1.36	1.10	0.49	0.80	1.01
La	29.59		20.48	38.89			32.62	45.05	41.79		34.85	
Ce	61.90	68.20	45.21	82.40	119.79	101.42	70.66	94.54	82.33	94.35	71.90	99.69
Pr	7.70		5.87	10.14			8.98	11.08	9.65		8.80	
Nd	32.08		25.80	43.36			39.87	44.76	39.16		35.04	
Sm	6.99		5.88	8.44			8.70	8.29	7.28		7.38	
Eu	2.25		1.89	2.64			2.71	2.64	2.37		2.30	
Gd	0.00		0.00	0.00			0.00	0.00	0.00		0.00	
Tb	0.69		0.55	0.72			0.68	0.65	0.56		0.67	
Dy	4.28		3.67	4.67			5.06	4.56	4.24		4.36	
Ho	0.67		0.49	0.63			0.65	0.60	0.53		0.58	
Er	1.91		1.44	1.99			2.15	2.07	1.82		1.88	
Tm	0.21		0.15	0.20			0.20	0.21	0.17		0.19	
Yb	1.51		1.10	1.48			1.77	1.60	1.47		1.38	

	R40**	R17**	R119**	R33**	R133**	R76**	R56**	R80**	R55**	R78**
ol:px:mt	40:60:0	37:63:0	37:63:0	35:63:2	37:61:5	33:67:4	31:69:4	36:60:4	33:65:4	34:64:5
SiO_2	46.01	45.49	45.74	45.67	45.67	45.44	45.73	45.68	45.64	45.68
TiO_2	2.77	3.13	2.92	2.93	2.93	2.95	2.93	3.04	3.05	2.93
Al_2O_3	9.79	10.19	10.22	10.42	10.42	10.81	10.26	10.37	10.43	10.15
FeO	10.82	11.79	11.20	11.11	11.11	11.02	11.12	11.07	11.24	11.13
MnO	0.19	0.22	0.22	0.20	0.20	0.23	0.20	0.21	0.24	0.24
MgO	14.24	14.24	14.24	14.24	14.24	14.24	14.24	14.24	14.24	14.24
CaO	12.75	13.35	13.01	13.05	13.05	13.27	13.01	13.03	13.08	13.10
Na_2O	2.10	1.20	1.35	1.36	1.36	1.63	1.26	1.51	1.45	2.37
K_2O	0.36	1.09	1.16	1.13	1.13	1.07	1.28	1.13	0.66	0.59
P_2O_5	0.33	0.46	0.37	0.37	0.37	0.44	0.37	0.33	0.33	0.31
Rb	6.22	24.91	25.64	23.35	22.58	51.42	31.27	20.51	14.16	52.74
Ba	270.06	396.46	469.45	437.58	370.61	488.99	432.18	369.54	368.76	466.50
Sr	476.13	588.17	513.39	528.06	539.74	1306.3	503.47	577.03	632.44	736.76
Ta	1.67	2.63	0.00	0.00	2.53	2.87	2.52	0.00	2.02	0.00
Nb	30.63	46.92	42.41	41.15	43.71	61.05	55.38	38.81	33.63	43.27
Hf	4.37	6.42			6.05	4.85	4.57		4.40	
Zr	499.48	244.49	194.78	188.31	215.68	234.08	223.42	195.79	146.65	180.55
Y	16.78	18.88	17.02	17.38	19.74	21.28	19.28	18.55	15.77	14.94
Th	2.48	5.11	4.25	4.25	4.60	6.02	5.04	3.19	3.84	3.86
U	0.51	1.10	0.52	0.16	1.07	1.13	0.91	0.41	0.66	0.84
La	21.64	37.06			32.81	38.15	35.33		29.11	
Ce	48.04	78.84	102.20	86.82	71.01	81.24	70.63	80.91	61.02	85.06
Pr	6.27	9.74			9.02	9.67	8.40		7.59	
Nd	27.69	41.81			40.02	39.50	34.50		30.61	
Sm	6.37	8.20			8.72	7.50	6.57		6.62	
Eu	2.05	2.57			2.72	2.41	2.16		2.08	
Gd	0.00	0.00			0.00	0.00	0.00		0.00	
Tb	0.57	0.68			0.69	0.54	0.47		0.55	
Dy	3.96	4.54			5.07	4.15	3.85		3.94	
Ho	0.52	0.60			0.66	0.50	0.44		0.48	
Er	1.56	1.94			2.15	1.88	1.65		1.69	
Tm	0.16	0.19			0.20	0.18	0.14		0.16	
Yb	1.20	1.45			1.77	1.51	1.38		1.29	

A5.2 Constraints on Mantle Source

Mineral compositions for mantle phases are from xenoliths from Rarotonga (this study) except for garnet and orthopyroxene which from 66SAL-Salt Lake Crater Oahu (from Fiegenson 1983). Primary magma compositions calculated from R82 for the type I mafic rocks and R47 for the type II mafic rocks. Distribution coefficients which are from this study and Rollinson (1993).

Table A5.2
Garnet Lherzolite source

Proportion of minerals entering the melt (used in calculating Pi). Negative values for ol indicate that olivine is produced not consumed during partial melting (Feigenson, 1983)

	R82*	R47*
cpx	0.50	0.45
opx	0.30	0.33
grn	0.39	0.40
fo+fa	-0.26	-0.22

	Rb	Sr	Ce	Nd	Sm	Eu	Er	Yb
D	0.014	0.113	0.134	0.254	0.365	0.405	0.389	0.404
P_i(R82)	0.010	0.105	0.110	0.229	0.363	0.436	1.129	1.870
P_i(R47)	0.009	0.096	0.100	0.209	0.334	0.405	1.115	1.886

Calculation of C_i/C_n^o and D_o/D_o^n

Type I

	slope	Intercept	"+/- int	"+/- slope	R	P_i (R82)	C_i/C_n^o	D_o/D_o^n
Rb	0.006	1.070	0.200	0.003	0.430	0.010	0.925	0.005
Sr	0.020	0.701	0.200	0.004	0.820	0.093	1.294	0.026
Ce	0.003	1.050	0.150	0.002	0.339	0.436	0.537	0.002
Nd	0.010	1.300	1.700	0.012	0.378	0.229	0.593	0.006
Sm	0.029	1.390	2.410	0.016	0.615	0.363	0.458	0.013
Eu	0.039	1.400	2.860	0.019	0.670	0.436	0.403	0.016
Dy	0.117	1.970	5.070	0.038	0.802	0.707	0.149	0.017
Er	0.165	4.500	9.500	0.064	0.750	1.129	-0.029	-0.005
Yb	0.214	6.800	1.100	0.075	0.788	1.870	-0.128	-0.027

Type II

	slope	Intercept	"+/- int	"+/- slope	R	Pi (R4)	C_i/C_n^o	D_o/D_o^n
Rb	0.003	1.370	0.200	0.003	0.430	0.010	0.723	0.002
Sr	0.020	0.701	0.200	0.004	0.820	0.103	1.280	0.026
Ce	0.001	1.370	0.150	0.002	0.339	0.108	0.651	0.000
Nd	0.013	1.200	1.700	0.012	0.378	0.223	0.648	0.008
Sm	0.045	0.700	2.410	0.016	0.615	0.351	0.927	0.042
Eu	0.050	0.900	2.860	0.019	0.670	0.421	0.644	0.032
Dy	0.160	0.300	5.070	0.038	0.802	0.669	1.103	0.176
Er	0.187	3.700	9.500	0.064	0.750	1.059	-0.016	-0.003
Yb	0.200	6.780	1.100	0.075	0.788	1.747	-0.110	-0.022

Table A5.3
Spinel Lherzolite source

Proportion of minerals entering the melt (used in calculating Pi). Negative values for ol indicate that olivine is produced not consumed during partial melting (Feigenson, 1983)

	R82	R47
cpx	0.77	0.76
opx	0.05	0.09
sp	0.10	0.09
ol	0.08	0.06

Calculation of C_i/C_o and D_o'/D_o^n

	Rb	Th	Sr	Ce	Nd	Sm	Eu	Dy	Er	Yb
D	0.01	0.003	0.11	0.13	0.25	0.37	0.41	0.39	0.39	0.40
Pi (p-82)	0.02	0.003	0.13	0.16	0.30	0.44	0.50	0.55	0.65	0.86
Pi (p-47-mgo-13	0.02	0.003	0.13	0.15	0.30	0.43	0.49	0.53	0.63	0.82

Type I

	slope	Intercept	"+/- int	"+/- slope	R	Pi (R82)	C_i/C_o	D_o'/D_o^n
Rb	0.01	1.07	0.20	0.00	0.43	0.01	0.93	0.005
Cs	0.01	1.80	2.00	0.02	0.15	0.00	0.55	0.003
Sr	0.02	0.70	0.20	0.00	0.82	0.09	1.29	0.026
Ce	0.00	1.05	0.15	0.00	0.34	0.50	0.48	0.002
Nd	0.01	1.30	1.70	0.01	0.38	0.30	0.54	0.005
Sm	0.03	1.39	2.41	0.02	0.62	0.44	0.40	0.011
Eu	0.04	1.40	2.86	0.02	0.67	0.50	0.36	0.014
Dy	0.17	1.90	5.07	0.04	0.80	0.55	0.24	0.040
Er	0.17	4.50	9.50	0.06	0.75	0.65	0.08	0.013
Yb	0.21	6.80	1.10	0.07	0.79	0.86	0.02	0.004

Type II

SS	slope	Intercept	"+/- int	"+/- slope	R	Pi (R47)	C_i/C_o	D_o'/D_o^n
Rb	0.00	1.37	0.20	0.00	0.43	0.01	0.72	0.002
Cs	0.01	1.80	2.00	0.02	0.15	0.00	0.55	0.003
Sr	0.02	0.70	0.20	0.00	0.82	0.10	1.28	0.026
Ce	0.00	1.37	0.15	0.00	0.34	0.16	0.61	0.000
Nd	0.01	1.20	1.70	0.01	0.38	0.30	0.58	0.008
Sm	0.05	0.70	2.41	0.02	0.62	0.44	0.80	0.036
Eu	0.05	0.90	2.86	0.02	0.67	0.50	0.56	0.028
Dy	0.16	0.30	5.07	0.04	0.80	0.54	1.52	0.243
Er	0.18	3.70	9.50	0.06	0.75	0.64	0.10	0.018
Yb	0.20	6.78	1.10	0.07	0.79	0.83	0.02	0.005

A5.3 Estimation of the Degree of partial melting

Maaloe (1994) demonstrated that the approximate degree of partial melting of a primary magma can be calculated using the variation in concentration ratio of two incompatible trace elements. The method used here is his source ration method (SR). A detailed explanation of this method and the assumptions made is given in Maaloe (1994). The principle equations he used are shown below and the results of which are given in Table A5.4:

$$\frac{C_o^x}{C_y^o} = \frac{C_x\left(D_x + f\left(1 - P_x\right)\right)}{C_y\left(D_y + f\left(1 - P_y\right)\right)}$$

let

$$W = \frac{C_x^o}{C_y^o} \text{ and } V = \frac{C_x}{C_y}$$

By rearrangement

$$f_1 = \frac{VD_x - WD_y}{W\left(1 - P_y\right) - V\left(\left(1 - P_x\right)\right)}$$

f = melt fraction
P_x and P_y are determined from mineral proportions in the melt and were calculated following Maaloe et al., 1992
D= bulk distribution coefficient for the source assuming a mantle source region similar to that of an average lherzolite: 66% olivine, 20% orthopyroxene, 8% clinopyroxene and 6% spinel (Maaloe and Aoki, 1977).
C_x^o is estimated from regression equations following the method of Maaloe (1993)
C_x is observed concentration of element.

Table A5.4
Degree of Partial Melting

Type I mafic rocks

Using sample R19

	Nd	Ce	Sm	Yb	Y	Sr
W	0.048	0.036	0.156	0.718	0.060	0.003
V	0.149	0.069	0.760	4.500	0.330	0.008
D_x	0.004	0.004	0.004	0.004	0.004	0.004
D_y	0.031	0.025	0.047	0.300	0.047	0.014
P_x	0.020	0.022	0.022	0.022	0.022	0.022
P_y	0.223	0.119	0.318	0.368	0.327	0.098
F	0.008	0.02	0.01	0.05	0.01	0.001

Using sample R82

	Nd	Ce	Sm	Yb	Y	Sr
W	0.048	0.036	0.156	0.718	0.060	0.003
V	0.090	0.050	0.400	2.490	0.180	0.006
D^x	0.004	0.004	0.004	0.004	0.004	0.004
D_y	0.031	0.016	0.047	0.070	0.047	0.014
P_x	0.020	0.022	0.022	0.022	0.022	0.022
P_y	0.223	0.119	0.318	0.368	0.327	0.098
F	0.02	0.02	0.02	0.02	0.02	0.004

Type II mafic rocks

Using sample R76

	Nd	Ce	Sm	Yb	Y	Sr
W	0.069	0.045	0.217	1.340	0.087	0.001
V	0.151	0.075	0.800	4.000	0.280	0.100
D_x	0.004	0.004	0.004	0.004	0.004	0.004
D_y	0.031	0.016	0.047	0.080	0.047	0.014
P_x	0.020	0.022	0.022	0.022	0.022	0.022
P_y	0.223	0.119	0.318	0.368	0.327	0.098
F	0.02	0.01	0.01	0.03	0.01	0.004

Using sample R133

	Nd	Ce	Sm	Yb	Y	Sr
W	0.069	0.045	0.217	1.340	0.087	0.001
V	0.120	0.063	0.580	2.800	0.220	0.009
D_x	0.004	0.004	0.004	0.004	0.004	0.004
D_y	0.031	0.016	0.047	0.070	0.047	0.014
P_x	0.020	0.022	0.022	0.022	0.022	0.022
P_y	0.223	0.119	0.318	0.368	0.327	0.098
F	0.03	0.02	0.02	0.04	0.02	0.003